Generation and characterisation of tissue-engineered Pseudoislet models for the study of diabetes

AJILE ABDULHUSEIN JASSIM ELTTAYEF

Submitted for Degree of Philosophy

School of Postgraduate Medicine
Institute of Science and Technology in Medicine
Keele University

June 2018

Abstract

The islets of Langerhans are multicellular aggregates within the pancreas containing beta cells that sense changes in blood glucose level and respond by secreting insulin. The cells within the islets communicate with each other through gap junctions. The 3D structure of the islets is crucial for their metabolic function. Artificial reconstruction of isolated beta cells into 3D cell aggregates has led to the generation of Pseudoislets (PIs) which mimic islets of Langerhans and can produce insulin. However, the lifespan of PIs is generally a few days in culture after which, central cell death occurs. The overall aim of this project was to improve PI viability and biofunction through development of two new techniques. The first technique being developed was a series of coating solutions consisting of Pluronic F127 (F127) and gelatin type A (Gelatin), which systematically altered the substrate properties of cell culture plates where PIs were formed by suspension culture. The second technique was generation of gelatin beads, functioning as microchannels inside of PIs, and drug carriers when loading with anti-inflammation agents to reduce inflammation and central necrosis. The beta cell line, BRIN-BD11, was used to form PIs.

Coating solutions with different ratios of gelatin and F127 (90%, 95%, 98% and 100% of Gelatin in the mixture) have been designed. Surfaces coated with these coating solutions generated different ATR-FTIR spectra, contact angle (CA) values and protein adsorption capacities and the changes were dependent on the original substrate chemistry. The coating of suspension culture plates with gelatin alone failed to generate suspended PIs, while coating with F127 alone resulted in the generation of large, irregular PIs. On the other hand, coating suspension culture plates with a combination of gelatin and F127 solutions formed suspended PIs of differing sizes. The lower the percentage of gelatin in the mixture for the coating, the higher the size

of PIs. The higher the F127 content, the more hydrophilic the surface was, which led to lower CA values of the substrate. Coating solutions containing 95-98% Gelatin produced homogenous and smaller PIs than on F127 coating. PIs formed on 98% Gelatin coated plates had larger size but more homogenous morphology (268 ± 10 μm) than PIs produced on ULA plate (235 ± 30 μm). These larger PIs exhibited comparable cell viability, the same level of insulin expression in GSIS and Western blotting assays and higher gene expression of key beta cell markers than smaller PIs formed on ULA plates. Furthermore the larger PIs expressed more of the gap junction protein, connexin 36, in comparison to PIs generated on ULA plates, revealing the optimised configuration of cells in these PIs. Altogether, regulating the hydrophicility of suspension culture plates by F127 and gelatin ratio in the coating solution changed the physical properties of PI and altered the expression of key beta cell markers.

Gelatin beads (GBs) of 30-40 μm sizes were produced by Water/Oil emulsion techniques. The degree of swelling and stability of GBs was controlled by crosslinking with 5% glutaraldehyde (GA) vapour for 6 hours. The incorporation of 40 μm GBs into PIs (25-50 GB/per PI) significantly increased the proliferation and cellular viability of the PIs for both large and small sized PIs. Loading of anti-inflammatory cytokines, IL-10 and anti-IL-1β into GBs allowed for sustained release of these agents over time. Incorporation of IL-10 and anti-IL-1β loaded GBs to PIs revealed a synergetic effect in the improvement of the proliferation/viability of PIs regardless of PIs size (large or small). LDH release from the PIs was decreased dramatically and insulin release was increased significantly. Thus GBs played active roles as microchannels and drug carriers which improved the viability and function of PIs.

Table of contents

List of Figures

List of table

List of Scheme

Acknowledgement

Firstly, I would like to express sincere gratitude to my lead supervisor Professor Ying Yang for continuous support throughout of my PhD study and related research for her advice, patient, motivation and for allowing me to grow as a research scientist. Also, my deep thank goes to my co-supervisor Dr Catriona Kelly for making my PhD full of knowledge and for help and guidance me from my first day in the UK. I would also like to thank my advisor Dr Alan Harper for his supportive comments.

I am grateful to my family. Words cannot express how grateful I am to my father, my mother, my siblings, my wife and sons and daughters who have provided me with moral and emotional support in my life. I am also grateful to my other family members and friends who have supported me along the way. I would like to thank my both brothers Mardan and Adan who gone from this life, and I pray for them. I would like to thank my wife Dr Buthainah for being helpful and making my PhD and our time enjoyable.

I am also grateful to Dr Ruslan Dmitriev from University College Cork for his unfailing support and assistance

To my PhD colleagues both past and present, thank you for making my time here a blast. To my group, both past and present especially postdoc Dr Lanxin Lyu, thank you for being gathering helping each other. To GHRC staff, thank you for being always helpful

My final thanks go to my sponsor the Ministry of higher education and scientific research in Iraqi for this wonderful opportunity to study aboard.

Poster presentation

1. **TCES (Tissue and Cell Engineering Society) 2016**: Ajile Elttayef, Catriona Kelly, Ying Yang. Improving the viability of Pseudoislets for better treatment of diabetes.
2. **UKSB UK (Society for Biomaterials) 2106.** Ajile Elttayef, Catriona Kelly, Ying Yang. The effect of substrate coating on Pseudoislet formation.
3. **UKSB UK (Society for Biomaterials) 2017.** Ajile Elttayef, Catriona Kelly, Ying Yang. The effect of gelatin beads in the Pseudoislets on the section of insulin

Oral presentation

1. **ISTM postgraduate symposium 2016:** Ajile Elttayef, Catriona Kelly, Ying Yang. Generation and characterisation of tissue-engineered model for diabetes treatment
2. **ISTM postgraduate symposium 2017:** Ajile Elttayef, Catriona Kelly, Ying Yang. Fabrication and characterisation of Pseudoislets with different sizes, 3D morphology and cell-cell contacts.
3. **TCES (Tissue and Cell Engineering Society) 2017**: Ajile Elttayef, Ruslin Dmitriev, Catriona Kelly, Ying Yang. Fabrication and characterisation of Pseudoislets with different sizes, 3D morphology and cell-cell contacts

Abbreviations

2D	Tow dimensional
3D	Three dimensional
AFM	Atomic force microscopy
Anti-GAD	Anti-glutamic acid decarboxylase
Anti-IL-1β	Ani-interleukin-1beta
ATP	Adenosine triphosphate
ATR	Attenuated total reflectance
CA	Contact angle
CCK-8	Cell count kit-8
Cx	Connexin
DM	Diabetes mellitus
DMSO	Dimethyl sulfoxide
DPBS	Dulbecco's phosphate buffer saline
E-CAD	E-cadherin
ECM	Extra cellular matrix
ELISA	Enzyme-linked immunosorbent assay
FBS	Fetal bovine serum
FTIR	Fourier transformed infrared
GA	Glutaraldehyde
GBs	Gelatin beads
GLUT2	Glucose transporter 2
GSIS	Glucose-stimulated insulin secretion
HPLC	High performance liquid chromatography
IL-10	Interleukin-10
kD	Kilo Dalton
LDH	Lactate dehydrogenase
MTT	3-(4,5-dimethylthiazol-2yl)-2,5-diphenyltetrazolium bromide
NCAM	Neural cell adhesion molecule
PBS	Phosphate buffered Saline
PDMS	Polydimethyl siloboxane
PEO	Polyethylene oxide
PIs	Pseudoislets
PP	Polypeptide
PPO	Polyprolylene oxide
PtPFPP	Pt(II)-tetrakis (pentafluorophenyl) porphyrin
RIA	Radioimmunoassay
RINm5F	Pancreatic beta cells and transformed
RPMI	Roswell Park Memorial Institute
SA	Cellular self-assembly
SEM	Scanning electron microscopy
SGP	Suspension culture green product

SOP	Suspension culture old product
T1DM	Type 1 diabetes mellitus
T2DM	Type 1 diabetes mellitus
TCP	Tissue culture plate
ULA	Ultra-low attachment
XPS	X-ray photoelectron spectroscopy
α-cells	Alpha-cells
β-cells	Beta cells

Chapter 1

Introduction

1.1 Pancreas

The pancreas is an organ situated in the abdomen. It has an important role in the breakdown of large molecules of the food to produce cellular fuel. It has two main functions: an exocrine function which helps in digestion and an endocrine function that regulates blood glucose levels.[1]

1.1.1 Anatomy of Pancreas

The pancreas is an endocrine organ and lies in the upper left abdomen. It is located behind the stomach, with the head of the pancreas encircling the duodenum as shown in Figure 1.1.[2]

Figure 1.1 The image illustrating the location of the Pancreas in the human body[3]

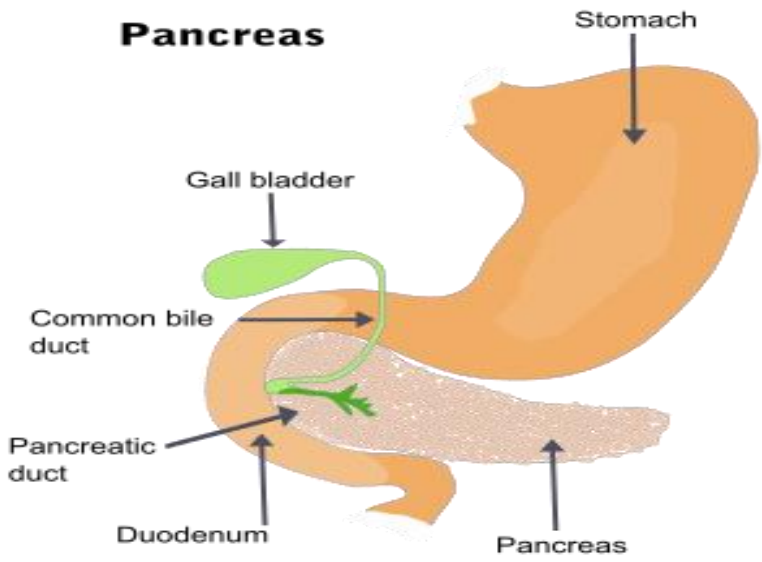

This figures shows the location of Pancreas within the gastrointestinal tract.

The pancreas is classified as a heterocrine gland because it contains both endocrine and exocrine glandular tissue. The exocrine tissue accounts for about 99% of the pancreas by weight with the endocrine portion accounting for the remaining 1%. The exocrine cells

in the acini produce digestive enzymes, which enter the ducts. The ducts of many acini connect to form larger and larger ducts, which feed into the large pancreatic duct.[1]

On the other hand, the endocrine portion of the pancreas comprises tiny bundles of cells called islets of Langerhans.[2] The islets contain five different types of cells; alpha cells, beta cells, delta cells, F or polypeptide (PP) cells and epsilon cells as shown in Figure 1.2. A capillary network transports secreted islet hormones around the body. Alpha and beta cells account for the vast majority of islet cells. Alpha cells (~10-15% of total islet cells) produce glucagon, which increases blood glucose levels. Beta cells (~80-85% of total islet cells) produce insulin, which decreases blood glucose levels.[4]

Figure 1.2 Diagram of pancreatic islets and surrounding acini[5]

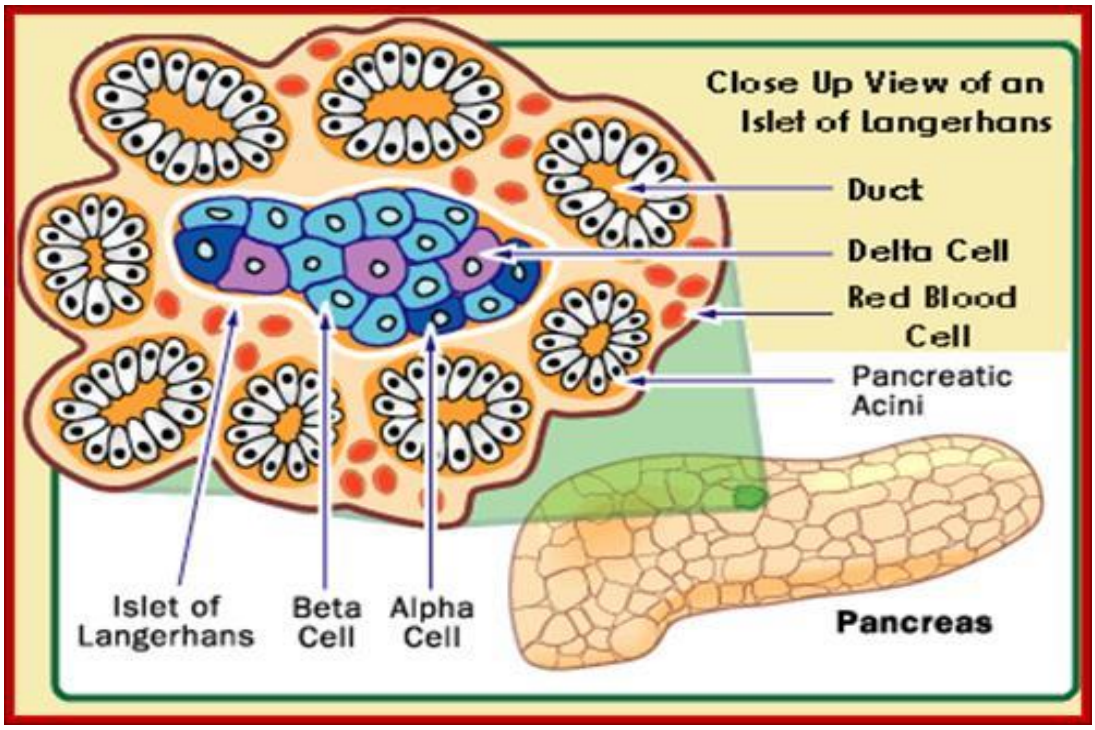

The diagram illustrates the distribution of pancreatic cells in islets.

1.1.2 Physiology of Pancreas

The exocrine gland secretes digestive enzymes such as amylase, lipase and trypsin to the gut, which aid break down protein, lipids, carbohydrates, and nucleic acids. While the endocrine gland that consists of approximately 1 million islets of Langerhans that secrete many hormones including:[5]

a. Insulin produced by beta cells
b. Glucagon produced by alpha cells.
c. Somatostatin produced by delta cells.
d. A pancreatic polypeptide produced by F or polypeptide cells.
e. Ghrelin produced by Epsilon cells.

Islets of Langerhans cells work as a micro-organ to maintain glucose homeostasis. The beta cell is the most plentiful cell in the islet and senses circulating glucose concentrations in the blood. The beta cell responds to elevated glucose concentrations by secreting appropriate levels of insulin.[6] Beta cell function and proliferation are controlled by regulatory signals from both the pancreatic and non-pancreatic environment.[7] Firstly, a dense vascular network exists within the islets, which facilitates the transport of oxygen and nutrients to the islet to maintain cellular health, while transporting secreted insulin away from the islet. Beta cells interact with the endothelial cells of the capillary network via the vascular basement membrane. It has been known that beta cells secrete vascular endothelial growth factors to stimulate vascular development. Whereas, the endothelial cells produce a basement membrane rich with laminin, which supports and promotes insulin gene expression and beta cells proliferation.[8] Secondly, cell-cell communication between beta cells through many transmembrane receptors (via circulation factors) which have an important effect on insulin gene expression and glucose-stimulated insulin

secretion (GSIS) via circulation of beta cells with other cells which might be endocrine and non-endocrine cells for example of vascular neuronal or haematopoietic origin.[9] Thirdly, there is reciprocal communication between alpha cells and beta cells to maintain glucose homeostasis.[10] The mechanism by which nutrients stimulate insulin secretion is related to ATP messenger and ATP-sensitive potassium channel. Homeostasis of blood glucose is maintained by insulin that is secreted from beta cells. Also, it has been found that at glycolytic intermediate and principal substrate of mitochondria stimulate glucagon secretion from alpha cells.[11] Glucagon secretion was decreased and insulin release was increased when the concentration of glucose was elevated.[11] Fourthly, islets are rich with neurons from the sympathetic and parasympathetic nervous system as shown in Figure 1.3. The parasympathetic nervous system and sympathetic nervous system have contrasting influence on insulin secretion from beta cells, for instance; feeding induces parasympathetic neural activity to pancreas, which stimulates insulin secretion, Whereas, induce sympathetic neural system activation by stress for example, will inhibit insulin secretion and increase glucagon secretion.

Figure 1.3 Summary of beta cells interactions with the pancreatic environment[14]

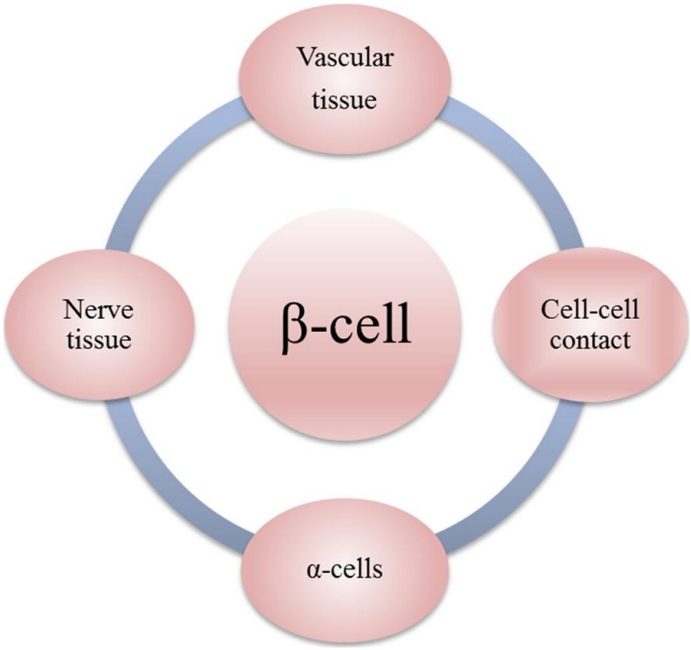

This figures outlines the factors, which regulated beta cells secretion including the communication between cells, alpha cells, nerves tissue and vascular tissues.
Islet cells exert autocrine and paracrine effects on neighbouring cells.

Autocrine signalling may modulate their activities through by-products of their function.[8,12] For example, the secretion of insulin negatively affects glucagon secretion. Insulin inhibits glucagon and somatostatin. While somatostatin also negatively affects insulin and glucagon secretion. Also, glucagon induces somatostatin secretion.[13] It has been shown through an examination of functional areas of the rat pancreas that ventral and dorsal islets exist. They found glucagon production from dorsal islets contained 10 times as much glucagon as ventral islets, even though insulin and total protein contents were similar. While basal rates of insulin secretion and proinsulin biosynthesis were observed in both dorsal and ventral islets.[8]

1.2 Pancreatic beta cells function

1.2.1 Metabolic function of insulin

Insulin is a peptide hormone secreted by beta cells in the pancreas. It normalises carbohydrate and fat metabolism. Insulin regulates the absorption of glucose from the blood to skeletal muscles and adipose tissue.

The human insulin protein is composed of 51 amino acids and has a molecular weight of 5.8 kD. It is a dimer of an A-chain and B-chain, which are connected by disulphide bonds.[14] Although insulin from animal sources differs somewhat in strength from that of humans, porcine insulin is nearly similar to human insulin and was often administered to diabetic patients in the past.[12] Insulin is synthesized from a single chain precursor called preproinsulin, which is converted to proinsulin in the endoplasmic reticulum. Proinsulin is composed of three fragments: a carboxylic terminal (A- chain), an amino-terminal (B-chain) and C-peptide, which is located between the A and B-chains.[15] Proinsulin is packed into small granules within the Golgi complex, which then moves to the cell surface. As the granules mature, proteases spilt proinsulin into equal amounts of insulin and c-peptide, allowing the insulin molecule which comprises the A and B chains linked by disulphide bridges as illustrated in Figure 1.4, to adopt its active configuration.[16]

Figure 1.4 Stages of insulin synthesis[16]

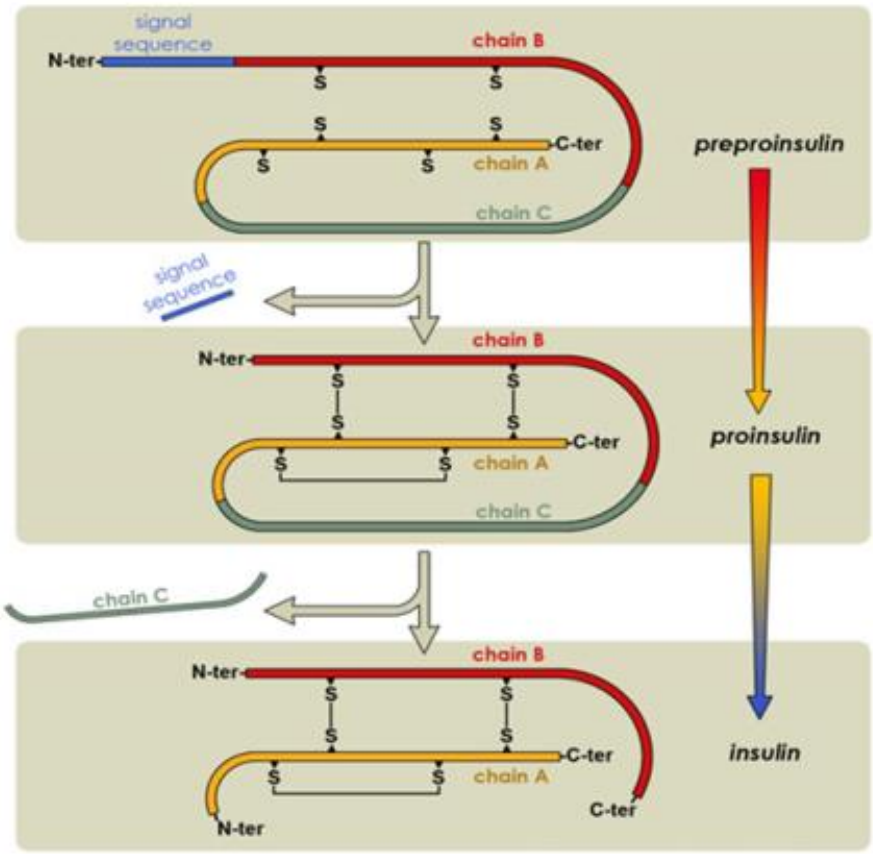

This Figure illustrates the steps by which insulin hormones are synthesised from polypeptide chain preproinsulin then proinsulin and active insulin plus C-chain are formed.

1.2.2 Molecular regulation of insulin secretion from beta cells

The complex architecture of pancreatic islets cell-cell communication has been confirmed to be crucial for normal islet function.[13,17–19] The vital role of homologous contact between beta cells is supported by observations in rodents in which islets were dissociated into a single cell suspension, and the ability of beta cells from these islets to respond to glucose was decreased.[20] Thus researchers suggest that intercellular contact coordinates the function of beta cells by synchronising activities.[21] This interaction is mediated by cell adhesion molecules and gap-junction proteins. Beta cells are interconnected by gap junctions, which form channels across the extracellular space. The channels allow direct exchange of small cytoplasmic molecules such as glucose from one cell to another. This

ensures electrical coupling and promotes insulin secretion. Several adhesion molecules such as integrins and cadherins are known to be expressed in islets and to have an important role in the maintenance of islet architecture.[8,18]

Recent studies have examined in detail the cytoarchitecture of human islets.[8,18,22] Comparing with animal models has proved that the pattern of distribution of islets cells is unique in that the different endocrine cell types are distributed uniformly through the islets and not sorted into central and peripheral compartments.[23] Heterogeneity regarding insulin secretion also exists between human beta cells and implies that insulin secretion is affected by cell-cell contact. To this end, homologous and heterologous intercellular communication in beta cells have a crucial influence on insulin secretion, and this may be related to the particular hierarchical of human islets.[8] The secretion of insulin from single beta cells and aggregated cells pairs in comparison with beta and non-beta cells have been studied. It has been demonstrated that insulin secretion from the aggregates of beta cells is higher than non-beta cells.[8]

The secretion of islet hormones is highly regulated and coordinated to ensure maintenance of glucose homeostasis through actions on peripheral tissues including the liver, muscles and adipose tissue. Insulin provokes glucose uptake by peripheral tissues. While glucagon causes the liver to convert stored glycogen to glucose which releases into bloodstream when blood glucose levels fall.[24]

The mechanism of insulin secretion is complicated, and the signal transduction is different from other extracellular stimuli. It starts with taking glucose into the cell by glucose transporter 2 (GLUT2) which will flip inside the cells and provoke insulin

secretion. While in most other extracellular stimuli, they start with binding to plasma membrane receptor then activation of intracellular secondary signals.[23]

1.2.3 Role of ATP and calcium ion

Incretins are gut hormones which secreted from endocrine cells into blood within short time after oral nutrients. Two types of incretins have been known; glucose-dependent insulinotropic peptide (GIP) and glucagon-like peptide-1 (GLP-1). The incretins help common actions of pancreas via potent enhancers of glucose-stimulated insulin release. Dipeptidyl peptidase rapidly-4 (DPP-4) is enzyme deactivated the action of both incretins. A lack of incretins secretion or a rise in their clearance are pathogenic factors in diabetes.[25

The insulin secretion pathway starts with glucose entry into beta cells. This is mediated through glucose transports proteins (GLUTs). There are 12 types of GLUT with GLUT2 facilitating glucose entry into the beta cell. The entrance of glucose into beta cell increases the ATP/ADP ratio due to the metabolism of glucose via the glycolysis pathway and oxidative phosphorylation.[26] The elevated ATP/ADP ratio leads to closure of the ATP-dependent K^+ channel (K_{ATP}) leading to depolarisation of the plasma membrane. After that, the voltage-gated calcium channels opens allowing entry of calcium ions into the beta cell. The entrance of calcium causes subsequent insulin exocytosis. Also, other stimuli that may also regulate insulin secretion include neurotransmitters, amino acids and fatty acids which regulated by hormones such as growth hormone, cortisol, epinephrine and glucagon.[27–29] Through the accumulation of positive charge of cationic amino acid in the presence of glucose inside of the cell because of more ATPs are formed. Thus, depolarisation of cell membrane which leads to open voltage-gated Ca^{+2} channel and Ca+2 stimulates insulin exocytosis as shown in Figure 1.5.[29]

The relation between protein ingestion and insulin secretion has been studied *in vitro* using beta cells; some studies confirm that amino acid like arginine, leucine, and phenylalanine have a strong insulinotropic effects.[26] In addition to that Randle's work confirms that in fasting state the rate of fatty acids oxidation will be increased leading to the suppression of glucose oxidation and activation of gluconeogenesis which will affect insulin secretion.[27]

Figure 1.5 The flowchart showing the mechanism of insulin production[29]

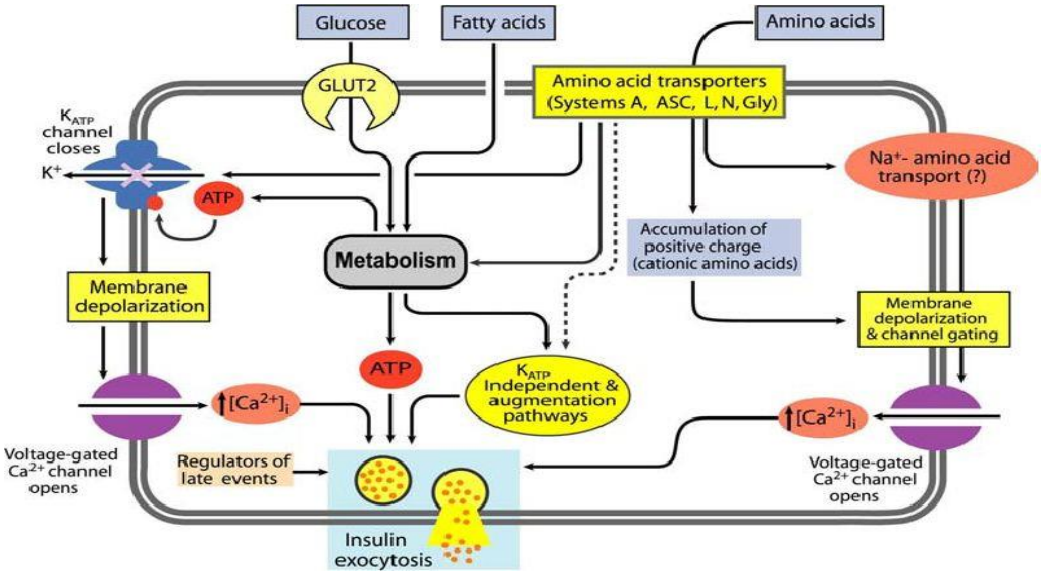

This flowchart demonstrates the mechanisms by which insulin release is stimulated by nutrients and amino acids. There are two mains mechanisms. (A) The direct depolarisation of plasma membrane through cationic amino. (B) Metabolism of amino acids such as alanine, glutamine and leucine. Both of them depend on the cellular content of ATP inside of the beta cell.

1.2.4 Cell-cell contact

Cell-cell interactions are indispensable for initiation of insulin secretion in response to glucose. Primary beta cells connect with each other through adhesion molecules including N-, R-, E-cadherin and neural cell adhesion molecule (NCAM).[2,30] The extracellular domain of E-cadherin (E-CAD) produces calcium-dependent homodimers with cadherins of neighbouring cells, hence facilitating cell-cell adhesion. The essential role of E-CAD on aggregation of beta cells has been investigated using a mouse model.[31] It has been

shown that ectopic expression of a dominant negative E-cadherin substituted with type N- and E-CAD in the beta cells of mouse embryos transiently interfered with clustering of beta cells.[30,31]

Some researchers have suggested that E-CAD brings beta cells close and helps in secretion of insulin via intra-islets signalling *in vivo*.[32] It has been demonstrated that both E-CAD and NCAM play essential roles in the cellular organisation of pancreatic islets. Also, studies showed that a loss of E-CAD in beta cells led to impaired insulin secretion and reduction of beta cell size.[32] E-CAD and NCAM are present in both beta cells and non-beta cells in rat islets, although NCAM expression level is much higher in non-beta cells.[33] E-CAD is responsible for homotopic interactions which are necessary for cell type segregation.[33] While cell-cell interaction is essential for survival and function improvements of beta cells, these issues have not been observed in alpha cells.[34]

1.2.4 Connexins

Connexins (Cx) are channels on cell membranes resulting from the opposition of two transmembrane structures. Two connexions, in particular, Cx43 and 36, play a crucial role in regulating pancreatic function.[35] Previous studies have investigated the contribution of connexin 36 (Cx36) in beta cell function. Cell-cell communication between beta cells by Cx36 is involved in controlling insulin secretion.[35] It was found that Cx36-dependent signalling plays a physiological role in the regulation of beta cell function and the expression of Cx36 is correlated to insulin secretion through intercellular synchronisation of Ca^{2+} transients induced during stimulation. Therefore, the alteration in the Cx36 level has an impact on the development and maintenance of the dysfunction of beta cells that will end with diabetes.[35]

1.3 Diabetes Mellitus

Diabetes Mellitus (DM) is a group of metabolic disorders characterised by hyperglycaemia with metabolic disorders of carbohydrates, fats and proteins resulting from defects in insulin secretion, insulin action or both. The hyperglycaemia can be defined as a condition of increase of glucose level in blood plasma to above of 11.1 mmol/L (200 mg/dL) called 'fasting plasma glucose'. The symptom of diabetes is not easy to diagnosis at an early stage, but the symptom of DM can be noticeable when the level of glucose 15-201 mmol/L (~ 250-300 mg/dL). The levels of glucose which are measured to be hyperglycaemia could be different from person to another, because of the person's renal threshold of glucose and overall glucose tolerance.

There are two major types of diabetes, Type 1 diabetes where the body can't form insulin (the hormone responsible for glucose metabolism) and Type 2 diabetes in which the insulin is either absent or not functioning well. A condition is known as pre-diabetes in which the blood glucose level is higher than normal, but not high enough to be called diabetes. Diabetes warning signs can be mild especially with Type 2 diabetes, polyuria, polydipsia and polyphagia are the main symptoms for diabetes, there are several tests that help in diabetes diagnosis like blood glucose test, oral glucose tolerance test, urine glucose test and ketone bodies in urine.

The complications of DM include coronary heart disease, kidney failure, blindness, limb amputation and premature death. Besides, the complications of DM include long-term damage, dysfunction and insufficiency of the various organs. These range from autoimmune destruction of the pancreatic cells that result in insulin deficiency to abnormalities in the production of insulin. The symptoms of hyperglycaemia include polyuria, polydipsia, weight loss, sometimes with polyphagia and blurred vision.[36] It has

estimated that 415 million people are suffering from DM in 2015, which is 1 in 11 of the world population,[19] and the number of people with DM will reach to 642 million by 2040.

1.3.1 Types of Diabetes

The commonest types of diabetes are type 1 diabetes (T1DM) and type 2 diabetes (T2DM).[37] T2DM is the most common form of DM and is characterised by disorders of insulin action and insulin secretion; either of which may be the predominant feature. Not all patients have insulin resistance and impaired insulin secretion at clinical presentation.[38]

The long-term effects of DM include progressive development of specific complications of retinopathy with potential blindness. The end-stage of DM complications include impaired wound healing will be the risk of foot ulcers may lead to a risk for lower limb amputations; renal failure since the blood vessels in the kidneys are injured and cannot clean the blood properly with accumulating of waste materials in the blood.[38] The direct and indirect effects on the human vascular tree are the main source of morbidity and mortality in both T1DM and T2DM.

1.3.2 Type 1 diabetes and current treatments

Type 1 diabetes mellitus (T1DM) results from beta cell destruction in the pancreas and is characterised by an absolute absence of insulin production. T1DM accounts for 5-10% of all types of diabetes. It is caused by autoimmune, genetic, and environmental factors. T1DM was previously referred to as insulin-dependent diabetes mellitus (IDDM) or juvenile onset diabetes as it presents relatively early in life, and frequently before the age of thirty.[39,40] It has been known that T1DM is characterised by the presence of anti-

glutamic acid decarboxylase (anti-GAD) or insulin antibodies in islet cells, which triggers autoimmune processes leading to beta cell destruction.[41,42]

Current treatment for T1DM depends on exogenous insulin injection therapy. It includes many daily injections and insulin pump therapy (chronic subcutaneous injection). Insulin pump therapy could lead to lipodystrophy which results from long-term injection at the same place. Although insulin therapy allows a monitor of the control level of blood glucose through daily glucose monitoring, strict blood glucose control could be difficult because of environmental variation, for instance, age, diet exercise or pregnancy. The complication of the exogenous insulin injection therapy may lead to long-term complications of DM for example retinopathy, neuropathy and nephropathy.[43] Therefore, looking for alternative management of T1DM is crucial. Cell therapy represents one of the new treatment methods and is a promising technique to be used widely in the future.[44]

1.4 Cell therapy

The number of patients with diabetes mellitus in the world is steadily increasing. Looking for new methods to prevent or cure this disease has been a crucial medical issue. Effective treatment is required to prevent the long-term complications of T1DM. One of the alternative methods of treatment for T1DM is islet transplantation in which islets are transferred from a donor pancreas to a T1DM patient. The newly implanted islets start to make and release insulin helping T1DM patients to avoid daily injection of insulin. However, since the 1970s most of the attempts to reproduce a success in human islets transplantation ended with disappointment mainly due to islet rejection and the limited supply of islets for transplantation.[45]

In 2000s researchers at the University of Alberta in Edmonton (Canada) established a new procedure for islet transplantation by increasing the number of transplanted islets which had been typically used, shortening the time between isolation of islets from a donor pancreas and transplantation into the recipient, and the use of a new immunosuppressive protocol.(46) This protocol used three different types of immunosuppressive drug. By the end of the 1st year post-transplantation, 50-68% of patients did not need insulin supplement. However, after five years only 10% of patients are free of daily insulin injection mainly due to islets rejection. So, in order to protect these cells from attack by the immune system, several methods have been developed including encapsulation of islets with a coating to protect them from the immune system while allowing them to release insulin.

The bioreactor ßAir has already developed one of the immune protection methods. Beta-O_2 Technologies Company uses "bioreactor ßAir, a proprietary implantable bioartificial pancreas". The reactive ßAir adapts a new chamber system containing islets of Langerhans in which cells have high viability and immunoprotection to produce insulin. This new device was applied for human transplantation in 2012 in Dresden's Technical University (Germany) with follow-up for 10 months. The outcome was positive. After that, the experts at Uppsala University (Sweden) checked the blood glucose level and βAir implanted patients. They found this device is effective for the treatment of the patients with diabetes if the oxygen is fed daily through a needle to the device.(46)

1.5 Generation and characterisation of tissue-engineered Pseudoislets

1.5.1 The principle of Pseudoislets

Due to a large number of animals needed to perform DM studies, researchers looked for alternative methods that may help to reduce the number of animals needed for initial experiments, and for better cell therapy. As such, pseudoislets (PIs) are considered a replacement for the real islets for research purposes.

Pseudoislets (PIs) are three-dimensional islet cell clusters. It is hoped to recapitulate the function of native islets by PIs. The use of PIs in research began in the 1980s. Researchers discovered that the digestion of dog pancreas with trypsin formed a single cell suspension, which could re-aggregate in 4-8 days in rotational cultures.[47] PIs could include all islet cell types and were stable for about 28 days. These PIs also could release hormones in response to appropriate stimuli.[47]

The principles and functions of PIs have been described and discussed in the past. Intensive research continues to maximise their insulin secretion, viability and transplantation potential. There are a few factors regulating to PI's structure including cell source (species source), cell types, single or multiple cell types and methods to generate PIs.

1.5.2 Pseudoislets structure

PI generation should mimic native islets. Research has been conducted on the effect of a few factors, such as cell sources, single or multiple pancreatic cells types in the PIs, additional cell type in PIs on bio-functional PI's structure.

The first selection of islet cells for PIs generation is from animals, i.e. primary cells. There are a wide variety of islet species used in the research including, rat, mouse, dog,[48,49] monkeys,[50] cats[51] and pig.[52] Recently, another method of generating islet aggregates have been reported.[53] This method relies on methylcellulose/particles to control the number of polystyrene microsphere in PIs. This aggregation took place within less than half an hour, and the aggregation of cells can be altered to allow different arrangements when different cell types are used in the same PIs.[54,55] Other sources of PIs have been used from neonatal pig islets,[56] neonatal rats,[35,57] cadaveric pancreas from children[58] and neonatal human tissue.[59]

To gain more information regarding insulin secreted through *in vitro* study, insulin-producing cell lines have been used to generate and study PI formation. Many rodent insulinoma cell lines have been established from transgenic animals expressing the SV40 antigenic oncogene from the insulinoma gene promoter. These cell lines include the MIN6, βHC, βTC cell lines.[60,61] These cell lines retain many of the characteristics of fully differentiated beta cells. The RINm5F cell line was produced from a transplantable rat insulinoma,[60] and several derived cell lines have been generated from their clones. For example, the BRIN-BD11 cell lines[60] was generated via electrofusion of RINm5F clone and normal rat islets.[60] Likewise, the INS-1 cell line was derived from the original radiation tumour, which can produce a high level of insulin secretion and can maintain insulin secretory responsiveness over a prolonged period of culture.[60] Human insulin-releasing cell lines including 1.1B4. 1.4E7 and 1.1E7 have been generated by electrofusion of freshly isolated human pancreatic beta cells with the immortal human PANC-1 epithelial cell line.[60] A novel human electrofusion-derived beta cell line with stable features similar to those of primary pancreatic beta cell in terms of structure and function has been reported.[60]

The effect of including other islets cell types into PIs on insulin production has been investigated. It has been found that using different ratios of alpha cells to beta cells of 1:2, 1:1, 2:1 would produce different levels of insulin.[62] It has been reported that PIs comprising 8,000 cells in a 1:8 alpha/beta cell ratio, produced more insulin with enhancement by 3 times compared with PIs formed from beta cells only. Furthermore, Kelly *et al.* have investigated heterotypic PIs composed of alpha, beta and delta cells. The PIs can produce normal pattern insulin release in response to different types of stimulation.[63] They found that PIs generated from mixed three types of cell lines (insulin (MIN6), glucagon (αTC 1.9) and somatostatin (TGP52) produce more insulin than PIs formed from MIN6 only *in vitro* after 7 days of culture.[63]

Researchers compared PIs produced from a mixture of original pancreatic beta cells and transformed (RINm5F) cells. [64]They found that the native beta cells occupied the centre of the PI surrounded by zones of non-beta cells, while RINm5F cells were located in the peripheral region. They revealed that RINm5F cells might not share the same surface features of native beta cells completely.[64]

Nikolova *et al.* have found that pancreatic beta cells *in vitro* do not form a basement membrane. They used VEGF-A to attract endothelial cells which form capillaries with vascular basement membranes next to the beta cells.[65]

The formation of PIs involves engineering approaches; various tissue-engineering methods have been developed, which will affect cell-cell contact and the architecture of PIs which is crucial for function.

1.5.3 Established techniques for formation of Pseudoislets

1.5.3.1 Cellular self-assembly

Cellular self-assembly is one of the common techniques used for the production of PIs. Self-assembly mimics natural processes which happen during embryogenesis, morphogenesis and organogenesis.[66] It is a spontaneous and reversible association of small molecular units into big organised structure design by non-covalent interactions.[67] For example, the re-aggregation of pancreatic cells has shown a spontaneous fusion *in vitro* into clusters, which mimic the native islets. Some studies suggested that differential adhesion could be the reason behind the self-assembly behaviour. For instance, Hauge-Evans *et al.* have found that culturing MIN6 cells on gelatin coated plates for 7 days elicited the formation of PIs.[20] This process was dependent upon the presence of E-CAD as it could be inhibited in the presence of an anti-CAD antibody or absence of Ca^{+2} needed for E-CAD binding. These PIs had improved functionality as they showed a greater glucose-stimulated secretion of insulin when compared to a monolayer of MIN6 cells.[20,68] Therefore, regulation of the cell-cell adhesion through alterations in the extracellular matrix (ECM) could be a useful strategy to improve the success of islets transplantation. For example, Liu *et al.*[69] in 2015 showed that beta cells and ECM interaction improved cell self-assembling techniques which may be used to develop treatment efficacy of transplantation of islets.[69]

1.5.3.2 Hanging drops

The hanging drop method has been used to crystallise proteins, achieve embryonic body formation by stem cells and evaluate tumour invasion.[70] Hanging drop cultivation depends on microgravity forces in the droplet, which stimulates cellular interactions. The classic hanging drop technique depends upon culturing a small drop of cells, which allows

cells to grow and the spheroid islets formed as shown in Figure 1.6. The hanging drop technique was also used to study the microbiology of bacteria in confined and controlled environments. This technique has allowed cell drops to be maintained without spreading the culture. Moreover, the hanging drop technique has been used to genetically modify the function in islet spheroids with controlled size and morphology.[71–73]

Figure 1.6 The hanging drop sizes is optimised by the diameter of plateau on the bottom of plate[74]

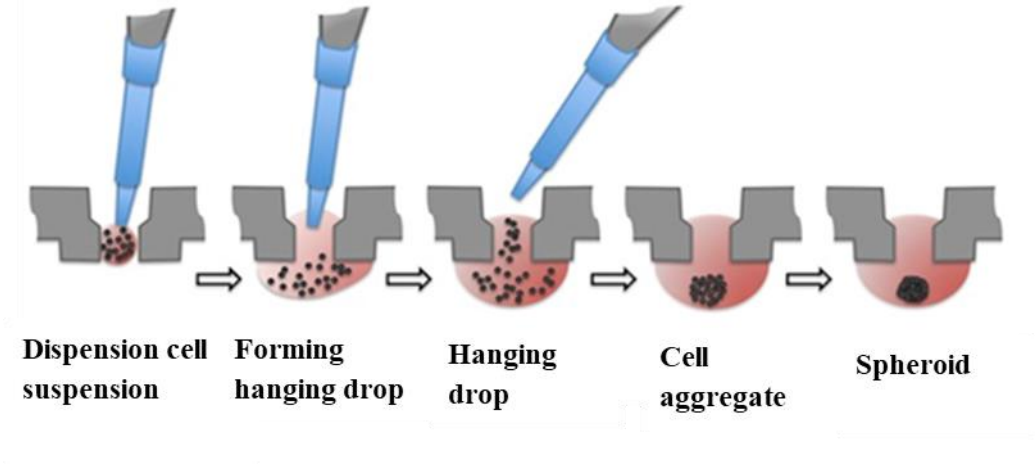

This Figure shows the way by which the hanging drop is confined by the diameter of the plateau on the bottom surface of the plate.

1.5.3.3 Suspension culture

The simplest method used to promote the formation PIs is to grow the beta cells in suspension. The surface characteristics of suspension culture containers induce beta cells attaching to each other rather than to the surface of the culture containers. In general, many cell types differentiate and lose their normal phenotype when grown under 2D cell attachment culture conditions.[75] The suspension culture is used to prevent this problem in pancreatic islets culture, helping islets to maintain their functional properties. However, beta cells display different morphologies based on the surface properties of the materials on which they are cultured. For example, beta cells cultured in a low cell attachment

microenvironment formed PIs with an islet-like structure after 7 days of culturing.[76,77] While the use of bacterial petri dish formed PIs with a smaller size compared to those formed on ultra-low attachment culture plates.[78] Both PIs formed on the ultra-low attachment, and bacterial petri dish displayed improved abilities to secrete insulin.[75,78] Several studies have used treated tissue culture plastic for the production of suspension cultures.[79,80]

On the other hand, human mesenchymal stem cells have been used to generate insulin-producing cells and combine with pellet suspension culture to induce them to differentiate into beta cell type.[81] Lin *et al.* [81] have found that suspension culture and stem cells could be stimulated by adding ECM such as laminin and fibronectin.[81]

Lehmann *et al.* have reported that the smaller sized PIs have better biological function since small islets display superiority in human islets transplantation clinically.[82] Also, Yang and colleagues have found that the treatment of the surface of the plastic dish with collagen, Lipidure and type IV collagen impacted on PIs sizes, viability and insulin secretion. They found that Lipidture gave the best viability as shown Figure 1.7.[83]

Figure 1.7 Live/dead staining images showing the cell viability of MIN6 cells grown on different substrates[83]

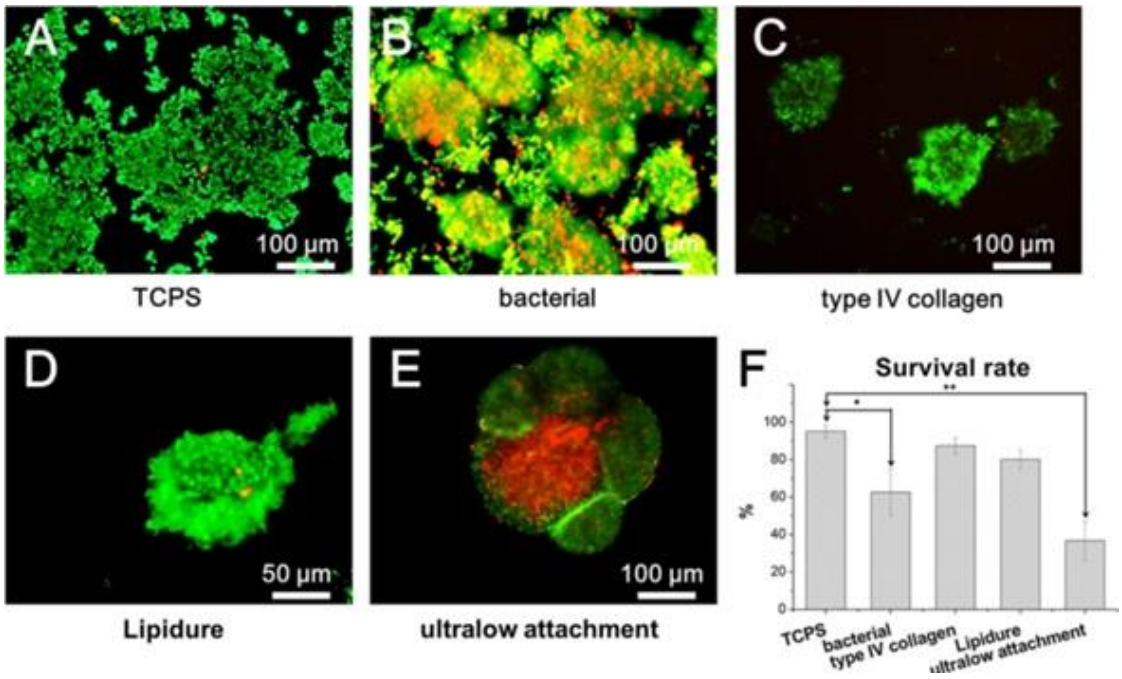

This figure illustrates live/dead staining MIN 6 monolayer cells and PIs. The survival rate (F) of each group is shown.

1.5.4 Functional assessment

1.5.4.1 Morphology

The component and hierarchical structure of islets play a crucial role in beta cell physiology.[34] The morphology of PIs can be visualised initially through using light microscopy to get live images for PIs. For further details of PIs morphology, thin section of PIs could be observed by light microscopy after PIs stained with Hematoxylin and eosin.[84] The cell-cell connection/arrangement within PI, which relate to PI morphology, can be assessed by immunofluorescence methods as well.[85,86]Key protein and hormone expressions from the pancreatic beta cells in PIs can be illustrated by staining with specific antibodies, for instance, insulin, GLUT2 and Cx36. The expression can be quantified or qualified using fluorescence microscopy and/or confocal microscopy.[60,83]

Immunofluorescence staining of cell types in PIs revealed that alpha cells tend to be peripherally distributed, while beta cells form the core of the PIs.[87] Electron microscopy has been used to study intracellular components of PIs, which revealed well-preserved cell ultrastructure and intracellular membrane connection in PIs (Figure 1.8)

It has been found that beta cell functionality was enhanced when the cell-cell communication is formed in 3D PIs. The PI structure is shown in Figure 1.8 confirming improvements in insulin release in comparison to 2D culture.[87] Also, researchers have found that insulin production is altered in relation to the expression of E-cadherin and gap junction proteins between the cells.[88] The pancreatic cell lines can be grown into 2D monolayer configuration or reconstituted to 3D aggregates depending on the types of cell culture substrate. Beta cells have formed PIs when cultured in low cell attachment surfaces[75,89] or bacterial Petri dishes, but generate 2D monolayer when culturing in tissue culture plates.[83]

Figure 1.8 Images of a pancreatic beta PIs (BRIN-BD11) by different microscopic techniques[87]

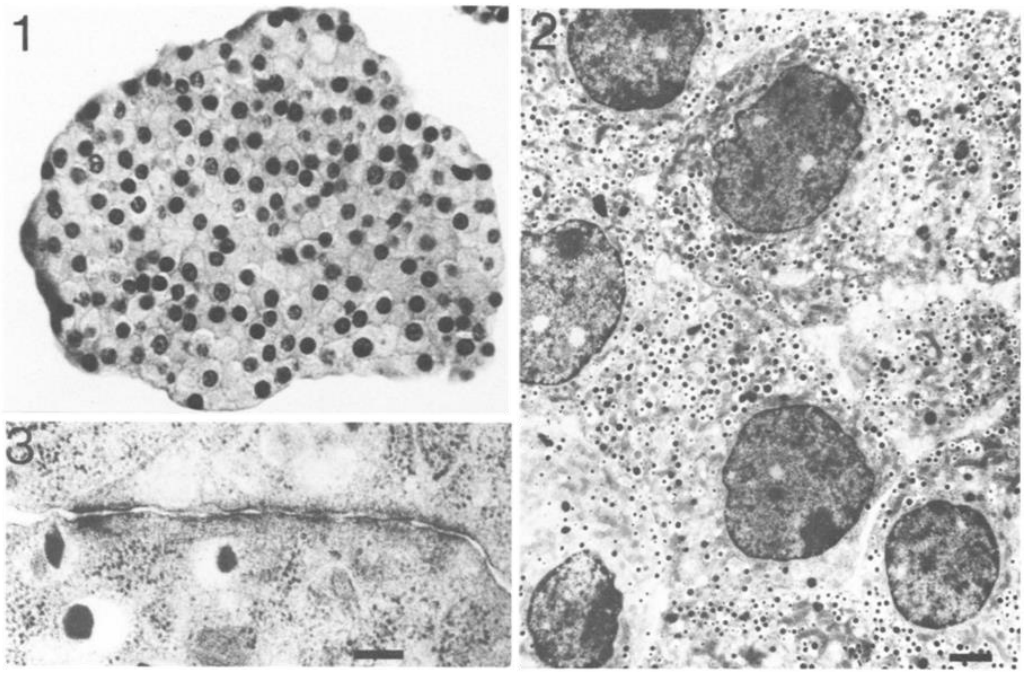

(This figure shows (1) section stained with Hematoxylin and eosin, imaged by light microscopy, X400. (2) Thin section electronic microscopy of PIs, X660. The scale bar = 1.0 μm. (3) Thin section electronic microscopy showing membrane features of two components in PIs, X78,000. The scale bar = 1.0 μm.

1.5.4.2 Immunohistochemistry

Immunohistochemistry (IHC) is a powerful process using the principle of antibodies binding specifically to antigens in biological tissues to detect the antigens, e.g. proteins or enzymes in cells of a tissue section. It combines immunological and biochemical techniques to visualise specific proteins in tissues or cells via using suitable antibodies to bind specifically to their target antigen in the specimens.[90] Any immunohistochemistry method aims to detect the maximum amount of antigen with the least possible background which maximises the signal to noise ratio. Many methods have been used to detect the amount of antigen present, and each one depends on the level of sensitivity required and the technical capabilities in the laboratory.[91] IHC staining is widely used to determine specific molecular markers such as proliferation or cell death.[92]

IHC has been used to detect the expression of E-cadherin, Cx43, Cx36, GLUT2 and insulin in pancreatic beta cell studies.[34,83,93] It has been seen that these key protein expressions were greater when cells were arranged in a 3D configuration rather than in 2D monolayer culture. Additionally, the expression of insulin and GLUT2 were higher in small PIs compared with large PIs.[27,83,94]

1.5.4.3 Insulin production

Insulin release starts with glucose which is the main simulator. The action of insulin occurs in a biphasic pattern. The first phase takes only a few minutes, followed by a sustained second phase as shown in Figure 1.9. The first phase of the release includes the plasma membrane fusion of a small, freely releasable pool of granules. The granules discharge their contents in response to nutrients and non-nutrient secretagogues. On the other hand, second-phase insulin secretion is triggered by nutrients. So, the shape of the glucose-insulin dose-response curve determines mainly by the activity of glucokinase, which represented the rate-limiting step for glucose metabolism in pancreatic beta cells. Blood glucose level below 5 mmol/L does not affect insulin release, and half-maximal stimulation occurs at ~8 mmol/L.[95]

Figure 1.9 Phases of normal insulin secretion [95]

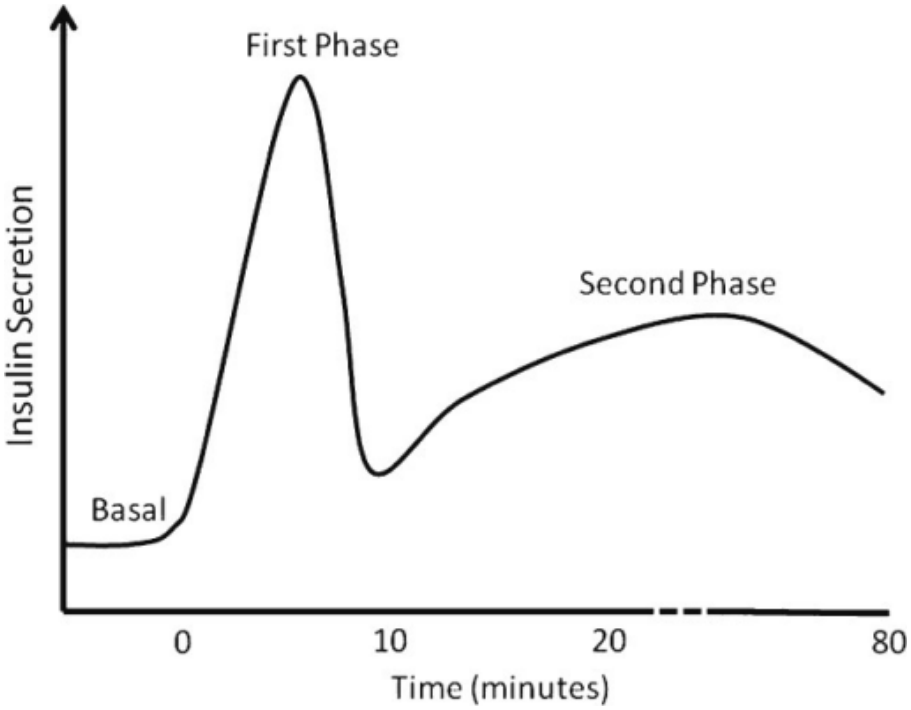

The figure shows the mechanism by which glucose regulates insulin release

The ability of isolated islets to secreted insulin has been established in static cultures, which showed that the dynamics of insulin release significantly increase when cells are configured as PIs when compared with monolayer cells.[21,34,85] It has reported that PIs formed from rat pancreatic islets revealed clear biphasic dose-dependent insulin responses after half an hour glucose stimulation over the range from 5.5 to 30 mM. The data indicated that islets cells reaggregated into 3D structures with close morphologic similarities for native islets.[87] The dynamics of insulin secretion from PIs is similar to that of primary mouse islets, although the amount of insulin secreted from PIs has been reported to be less than primary islets. [75] Bereton and co-workers have reported that cellular interaction among beta cells are sufficient to preserve the normal pattern of insulin release which is different from *in vivo* islets in that regulation is achieved through glucagon and somatostatin.[62] It has been studied that MIN6 monolayer and PIs cultures possess similar levels of insulin release in response to basal glucose concentration.[20]

Glucose-induced insulin production from MIN6 PIs is significantly higher than that of MIN6 monolayer cells.[20] Furthermore, the use of perfusion technique showed similar insulin response.[20,21]

Many techniques have been applied to determine insulin level. The first method is named as bioassays to measure insulin-like activity (serum insulin) which have been used for detection of the ability of human or animals to produce insulin after oral or intravenous injection with glucose. The level of insulin is measured at different time points of the injection.[98] Although the bioassays methods are used for *in vitro* and *in vivo* cases, the low sensitivity of this method to insulin antagonist and insulin substance its limited to use in routine clinical laboratory.

The second method is through chromatography procedures, particularly high performance liquid chromatography (HPLC). HPLC has been widely used in the measurement of insulin, proinsulin and C-peptide level in biological fluids. The C-peptide produced from cleavage of proinsulin is equal to the amount of insulin.[97] So, the C-peptide level could be used as a marker of insulin release and an assessment of beta cell function..

The third technique is immunoassays composed of the radioimmunoassay (RIA).and the enzyme-linked immunosorbent assay (ELISA) which are widely used. RIA was first used in 1959 by Yalow *et al*.[98] However, this methodology is restricted by potential safety concerns due to the presence of radiolabelled antigen, the instability of the reagents and

need for a long time incubation and washing steps.[99] ELISA involves fluorescence, in which the insulin in samples is determined by binding to insulin antibody labelled with fluorescence.[100] The advance of ELISA assay enables to detection of insulin with highly sensitivity.[100] Recently a new approach has been established to be a rapid insulin assay, which depends on homogenous time-resolved fluorescence with more beneficial due to more rapid and cost-effective than other used methods. This method has been applied in an insulin secreting cell line in INS-1E cells and pancreatic islets.[101]

1.6 Parameters controlling Pseudoislets' viability and function

1.6.1 PI Size

The increment in the sizes of PIs leads to malnutrition and hypoxia which leads to necrosis and cell death in the centre of PIs.[26] Yang *et al.*[27] have reported that the diameters of PIs were inversely proportional to the amount of insulin secreted with PIs of 100 μm in diameter secreting more insulin than PIs of 280 μm in diameter. The reason for the increase of insulin secretion may be due to cell viability, which is higher in small-sized PIs. Several techniques have been applied to control PI size, which could consequently improve function.[35,83,93] The level of ATP has been measured within the production of different sizes of PIs, and the outcome showed that the larger the size of the PI, the lower the amount of ATP produced, which subsequently hindered mitochondrial membrane potential.[102]

The substrate types of culture plates have been found to affect the size and morphology of PIs. If the cells were cultured on a low cell attachment microenvironment, the cells would form cell aggregations with sizes ranging 50 to 300 μm after 7 days of

culture.[21,68,89] However, the size of PIs was modified to about 100 μm when the cells were cultured in bacterial culture Petri dishes after the same period. These researchers suggest that using an ultra-low attachment culture plate when culturing PIs could improve their ability to secrete insulin in comparison to those cultured on a more adhesive plate.[75,83]

Chawla *et al.*[102] report that the use of suspension bioreactors for culturing neonatal porcine tissue helped to produce islet-like structures. Other research groups have proved that PIs grown in Lipidure and type IV collagen-coated dishes have produced a diameter of 100-150 μm with better cell viability. The viability and size of PIs are crucial for their function.[21,68,89] Also, Liu has tried to increase the functionality of cells within PIs by selection of PI size. He found that beta cells in the spheroids of 200 μm exhibited largest insulin secretion based on glucose stimulus when compared to others with sizes of 100, 300, 400 and 500 μm.[103] Also, it has been shown that a reliable way to generate viable survival PIs from human islets whilst also controlling the size involves the use of agarose microwell platforms, which can form PIs with accuracy and with high similarity to native islets.[102]

1.6.2 Beta cell packing density

It is believed that controlling the density of PIs improves the viability and functionality of the beta cells. Previous studies have demonstrated that 50% of the transplanted cells had a reduced capability to secrete insulin. This is likely to be due to decreasing viability of cells in the centre of PIs.[105–107]

Halban and colleagues have studied the effect of beta cell density on cell aggregation.[35,108] They found that aggregations are resulting from mixing of the beta

cells with non-beta cells in cluster form generated larger units via gap junctions, in which beta cells where located in a core surrounded by non-beta cells. Such connections were vital to improving cells function especially insulin production. Their study showed an increase of 9-fold for insulin when fused of 21% beta cells with 79% of non-beta cells by raising glucose concentration from 50 to 300 mg/dl.[108]

The PIs model from pancreatic beta cell has been shown much improved 3D islet-like structure after incorporated with a glucagon-secreting cell line (alpha TC1). The model showed the ability to self-organise into the structure similar to native islets which is crucial for their function.[107,110]

Prior work has produced pseudoislets predominantly from the MIN6 insulin-secreting cell line. In the current study, we employed BRIN-BD11 for several reasons. Firstly, BRIN-BD11 cells have high expression of GLUT2 and glucokinase consistent with the MIN6 and βHC9 cell lines. Furthermore, the BRIN-BD11 cell line is glucose responsive consistent with cell lines including INS-1 and βHC.[111] Importantly; the BRIN-BD11 cell line proliferates at a much higher rate than MIN6, INS-1, or βTC1 cells. Therefore, the use of this cell line for the generation of pseudoislets would exacerbate the issues around large Pseudoislet size, e.g. central necrosis and allow an opportunity to address these issues fully.

However, the BRIN-BD11 cell line produces strong expression of hexokinase, which can promote higher sensitivity towards lower concentrations of glucose than βTC1, βHC. Another difficulty of using this cell lines is that it associates with the changing of characteristics over a period of continuous growth. For example, glucose responsiveness is largely lost after passage 55, and therefore all experiments in this project were

conducted below passage 40. The cells may have abnormal chromosomal content, other genetic mutations and another abnormal protein expression,[111] because this cell line culture has the ability to grow without limits which is related to their tumour origin.

1.6.3 ECM expression in the PIs

ECM in islets of Langerhans plays a crucial role in maintaining pancreatic beta cells and influences their physiology dramatically. Recently, it has been confirmed that the pancreatic ECM plays a vital role in beta cells viability and insulin secretion.[110] The ECM has roles during integrin-mediated cell adhesion, which affects the survival of beta cells and insulin secretion from beta cells. Therefore, to improve the viability of islets or generations of PIs, adding ECM components to PIs to re-build the native cellular matrix environment may be a beneficial strategy.[113]

It has been confirmed that ECM structure and composition are also involved in islet architecture and beta cell polarity. Researchers have found three ECM dependent structural regions on the surface of beta cells within the intact islet. These regions provide specific physiological functions of the transport of glucose molecules, cell adhesion and exocytosis.[113,114] They found that islets cells can sense the endothelial basement membrane enriched in protein laminin through integrin-dependent adhesion molecules, which is crucial to maintaining beta cell polarity and targeted secretion.[65]

The interactions between islets and ECM have been studied on the functionality of cells in the term of GSIS cultured in 2D, and 3D culture via ECM coated tissue culture surfaces under some conditions such as coated culture surfaces with collagen type IV and matrigel. It has been reported that beta cells cultured in gels containing collagen type IV secreted

more insulin when stimulated with glucose compared to beta cells cultured with collagen type I , laminin, fibronectin or fibrinogen.[87]

1.7 The effect of substrate chemistry on the formation of PIs by suspension culture

1.7.1 Substrate chemistry and cell adhesion

Cell attachment to the surface is through cell adhesion that occurs through a natural interaction process between the cell and the ECM. Cells adhere to the underlying ECM via cell-substratum bonds, which are typically receptor-ligand complexes formed between adhesion receptors (such as integrins) on the cell surface and their ligands in ECM.[113] The native ECM contains multiple ligands, which can interact with integrins. These include fibronectin, vitronectin, collagen and laminin.[116]

For *in vitro* cell culture, the substrates of cell culture containers have to have the strong capacity to adsorb proteins including fibronectin, vitronectin, collagen, laminin. Thus, such substrates can become an artificial ECM containing appropriate ligands which promote cell adhesion.[117,118

A good understanding of the relationships between the behaviour of cells and the physicochemical properties of the substrates such as the surface free energy, hydrophobicity, the presence of functional groups and surface charges is of prime importance to control cell adhesion, proliferation and spreading of cells.[119] Therefore, surface properties have a crucial influence on cell adhesion. To generate PIs on the culture containers, the cells must not anchor to surfaces. Blocking protein adsorption, i.e. any strategies to prevent ligand-integrin interaction occurring will promote PIs formation.

1.7.2 Substrate chemistry and cell aggregation

Many strategies have been used to generate cell aggregates *in vitro*, which prevent protein anchoring to the substrate. Therefore, survival through cell-cell adhesion which leads to cell aggregation. One of most common techniques in cell aggregation is changing substrate chemistry for suspension culture.[119]

Pluronic is a copolymer consisting of polyethylene oxide (PEO) and polypropylene oxide (PPO) segments. These segments can be adsorbed onto hydrophobic surfaces forming extremely hydrophilic environments on the surface, which can prevent protein adsorption and cell attachment. The amphiphilic behaviour of this molecule has been used in many biomedical applications for reduction of protein adsorption and cell adhesions.[120,122] Also, this polymer can be used to modify different types of surfaces, for instance, glass, polyethylene and polystyrene. In the same way, the properties of the surface can be modified by mixing small amounts of this block copolymer with other polymers.[122]

Previous studies have reported many methods to use PEO coating for surfaces in different protocols including physical adsorption,[1213 covalent grafting,[124] chemisorption and self-assembled monolayers (SAM).[124] The results from SAM and physical adsorption could produce unstable surfaces. Whereas, the other methods formed poor reproducibility.[125-126] Furthermore, it has been investigated that collagen type 1 with a hydrogel of PEO could improve the differentiation of precursor cell aggregation to generate mature, insulin-releasing and islet-like structures.[127]

1.7.3 Techniques to characterise substrate chemistry

1.7.3.1 Fourier transform infrared spectroscopy

Fourier transformed infrared spectroscopy (FTIR) is a common technique used to determine the molecular structure and chemical composition of given samples.[128] One of the strengths of FTIR is the ability to obtain spectra from a wide range of solids, liquid and gases. Nevertheless, in several cases, some form of specimen preparation is required to obtain a better spectrum. In FTIR traditionally IR spectrometers have been applied to analyse samples by transmitting IR radiation directly through samples where the sample is a liquid or solid. The intensity of spectrum features is influenced by the thickness of the sample, and typically the thickness is a few tens of microns.[128] FTIR spectroscopy techniques have also been applied in biological analyses. It relies on the non-perturbative function process, is capable of extraction of biological data and images in diagnosis and assessment of cell functionality.

1.7.3.2 X-ray photoelectron spectroscopy

The X-ray photoelectron spectroscopy (XPS) is a technique that measures the element composition at the parts of thousand range, chemical formula and electronic state by using surface-sensitive quantitative spectroscopy via irradiating beams.[129] XPS is used for detection of surface chemistry extensively. Recently researchers have used the XPS to prove that coating an amphiphilicity homopolymer on surfaces reduced nonspecific protein adsorption. The homopolymer was immobilised onto the substrate through which the interactions between the polymers and proteins and using XPS was studied to measure protein adsorption.[130]

1.7.3.3 Contact angle

A contact angle (CA) is the angle formed through the interface happening between liquid with a solid surface. It measures the quantities of wettability of the solid surface by a liquid. There is a unique CA for a given system of solid at a given temperature and pressure.[131] The CA has a crucial role in many industrial processes such as lubrication, liquid coating, printing.[132,133] As well as these, it has been applied in the academic field to measure special wettability, superior repellency and controlled adhesion of different types of surfaces.[133–135] Several studies have involved the measurement of the contact angles as primary data which specifies the degree of wetting when a solid and liquid interact.[135,137] The CA can be divided into two types; small CA and large CA. The small CA (angle value less than 90°), corresponds to high wettability and the associated surfaces are called hydrophilic. While the large CA (angle values greater than 90°) corresponds to low wettability, and the associated surfaces are named hydrophobic[137], as shown in Figure 1.9.[136] Thus the measurement of CA can predict the wettability of a surface and adhesion interactions among cells and different types of surfaces.

Figure 1.10 Classification of the surfaces of materials according to their CAs[138]

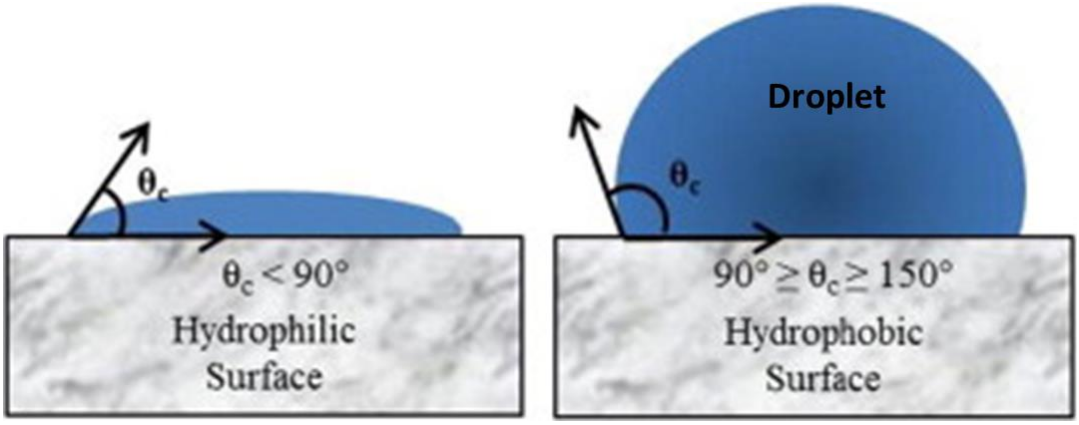

This figure illustrates the way by which contact angle is measured.

1.7.3.4 Scanning electron microscopy

A scanning electron microscope (SEM) is a kind of electron microscope, which produces images of a given specimen through scanning the surface with a focused beam of electrons. In the SEM the electrons interact with atoms in the specimen, generating several signals that bear information regarding the surfaces and the composition of the specimen.[139] The SEM technique illustrates the details for taken sample at magnifications, that would be hard to obtain under normal optical microscopic conditions.[138]

1.7.3.5 Atomic force microscopy

Atomic force microscopy (AFM) is a technique by which a very high-resolution type of scanning probe microscope is used with resolution at the order of fractions of a nanometer, more than 1000 times better than the optical diffraction limit. The AFM information is gathered by touching the surface with a mechanical probe. AFM has been used to investigate or explore the material surface of biological systems in order to collect new morphological, structural and mechanical information.[141]

1.8 Aims of the project

Central necrosis in Pseudoislets is the main challenge limiting the use of PIs for the study of diabetes. It is accepted that this central necrosis results from a shortage of nutrients and oxygen diffusing to the centre of PIs, especially those of 200 μm or more in diameter. Therefore, the aims of this project were:

- To develop two novel techniques to control the physical properties of PIs and enhance functionality via: (1) the development of a series of coating solutions for

cell suspension culture; (2) the generation of vents within PIs and drug carriers for PIs through use of micro-gelatin beads.

- To identify the optimal composition of the coating solution and define the impact on PI morphology and function.
- To synthesise and optimise micro-gelatin beads that could be incorporated into PIs to improve cell viability and insulin production

Chapter 2

Materials and Methods

2.1 Materials

Table 2.1 List of materials, catalogues number and supplier

Name	Catalogue number	Supplier
(3-(4,5-dimethylthiazol-2yl)-2,5diphenyltetrazolium bromide	M2128	Sigma-Aldrich, UK
10-20% SDS-PAGE gel	NT21-1020	Generon, UK
2,2′-Azino-bis(3-ethylbenzothiazoline-6-sulfonic acid)	A3219-100ml	Sigma-Aldrich, UK
3-isobutyl-1-methylxanthine (IBMX)	I7018	Sigma-Aldrich, UK
4′,6-Diamidino-2-phenylindole (DAPI)	D9542	Sigma-Aldrich, UK
4-20% Tris-HEPES gradient mini gel	NH21-420	Thermo- Fisher Scientific, UK
Acetone, for analysis	A/0600/PC21	Fisher Chemical, UK
Amersham Hybond P 0.45 PVDF	10600029	GE Healthcare Life Science, UK
Anti-Connexin 36 / GJA9 antibody for WB	ab139524	Abcam, UK
Anti-GAPDH antibody	ab8245	Abcam
Anti-mouse IgG, HRP-linked Antibody	7076P2	Cell Signaling Technology, UK

Anti-rabbit IgG, HRP-linked Antibody	7074P2	Cell Signaling Technology, UK
Anti-Rat IL-1β	500-P80	Peprotech, UK
Ascorbic acid phosphate	A8960	Sigma-Aldrich, UK
Boric acid	B0394-100G-D	Sigma-Aldrich, UK
Bovine serum albumin (BSA)	A2153-50G	Sigma-Aldrich, UK
BupH™ Tris-HEPES-SDS Running Buffer	28398	Thermo- Fisher Scientific, UK
Cell Counting Kit-8 (CCK-8)	96992	Sigma-Aldrich, UK
Cell Dissociation Buffer, enzyme-free, PBS	13151-014	Life Technologies, UK
Collagen from human placenta (type 4)	C5533-5MG	Sigma-Aldrich, UK
Connexin 36 primary antibody	SC-398063	Santa Cruz Biotechnology, UK
Corning ultra- low attachment surface culture dish, 6-well plate	EW-01835-26	Cole-Parmer, UK

Dimethyl sulfoxide (DMSO)	D2650	Sigma-Aldrich, UK
Donkey anti-goat polyclonal antibody	SC-45102	Santa Cruz Biotechnology, UK
Donkey anti-rabbit polyclonal antibody	SC-2089	Santa Cruz Biotechnology
Donkey anti-goat IgG-B	SC-2042	Santa Cruz Biotechnology, UK
Ethanol (absolute)	E0650/17	Thermo-Fisher Scientific, UK
FBS (fetal bovine serum)	DE14-801F	Lonza, UK
Fibronectin	F0895	Sigma-Aldrich, UK
Fluorescein isothiocyanate isomer I	F7250-250MG	Sigma-Aldrich, UK
gelatin from bovine skin type B	G9391-100G	Sigma-Aldrich, UK
gelatin from porcine skin, type A	G6144-100G	Sigma-Aldrich, UK
Glucose Powder	G7021	Sigma-Aldrich, UK

Anti-GLUT2	Sc-9117	Santa Cruz Biotechnology, UK
Glutaraldehyde grade I	G5882-10X1ML	Sigma-Aldrich, UK
Glutaraldehyde grade II	G6257-10X1ML	Sigma-Aldrich, UK
Goat anti-mouse monoclonal antibody	SC-16516	Santa Cruz Biotechnology, UK
Goat anti-mouse IgG	SC-2010	Santa Cruz Biotechnology, UK
Goat anti-Mouse IgG (H+L), Poly-HRP Secondary Antibody, HRP	32230	Thermo- Fisher Scientific, UK
Goat anti-Rabbit IgG (H+L), Secondary Antibody, Alexa Fluor® 594 conjugate	A-11037	Thermo-Fisher Scientific, UK
Halt™ Protease Inhibitor Cocktail (100X)	78429	Thermo- Fisher Scientific, UK
Hank Buffer saline solution (HBSS)	H9394-500ML	Sigma-Aldrich, UK
HEPES	H-3375	Sigma-Aldrich, UK
Human Laminin 5 full-length protein	ab42326	Abcam, UK

Insulin	I9278	Sigma-Aldrich, UK
Insulin (L6B10) Mouse for WB	mAb #8138	Cell Signaling Technology, UK
Lucifer Yellow CH, Lithium	L-453	Life Technologies, UK
Methanol	A4561	Thermo- Fisher Scientific, UK
Mouse anti-rabbit IgG-B	SC-2491	Santa Cruz Biotechnology, UK
Novex® Tris-Glycine SDS Running Buffer (10X)	LC2675	Thermo- Fisher Scientific, UK
NuPAGE® LDS Sample Buffer (4X)	NP0007	Thermo- Fisher Scientific, UK
NuPAGE® MES SDS Running Buffer (20X)	NP0002	Thermo- Fisher Scientific, UK
Optical Adhesive Cover	4360954	Invitrogen , UK
PageRuler™ Plus Prestained Protein Ladder, 10 to 250 KD	26619	Thermo- Fisher Scientific, UK
PageRuler™ Unstained Low Range Protein Ladder	26632	Thermo- Fisher Scientific, UK

Paraformaldehyde	P/0840/53	Fisher Scientific, UK
Penicillin, streptomycin,	BE17-745E	Lonza, UK
Phosphate buffered saline (PBS)	BE17-516F	Lonza, UK
Pierce BCA protein assay kit	23221	Thermo Fisher Scientific, UK
Pierce™ 20X TBS Tween™ 20 Buffer	28360	Thermo- Fisher Scientific, UK
Pierce™ ECL Western Blotting Substrate	32109	Thermo- Fisher Scientific, UK
Pierce™ LDH Cytotoxicity Assay Kit	88954	Thermo-Fisher Scientific, UK
PluriStrainer 20 µm	43-50020-03	Cambridge Bioscience Ltd
PluriStrainer 30 µm	43-50030-03	Cambridge Bioscience Ltd
PluriStrainer 40 µm	43-50040-03	Cambridge Bioscience Ltd
Potassium phosphate	PHR 1330	Sigma-Aldrich, UK
Quantifast SYBR green RT-PCR kit	204154	Qiagen, UK
Rabbit polyclonal anti-insulin	SC-9168	Santa Cruz biotechnology

Rat-insulin ELISA	80-INSRT-E0l-ALP	Stratech Scientific Ltd
Rabbit anti-Goat IgG (H+L) Secondary Antibody, Alexa Fluor® 568 conjugate	A-11079	Thermo- Fisher Scientific, UK
Recombinant Murine IL-10	210-10	Peprotech, UK
Radioimmunoprecipitation assay buffer (RIPA)	R0278	Sigma-Aldrich, UK
Radioimmunoprecipitation assay buffer ((RIPA) Lysis and Extraction Buffer	89900	Thermo- Fisher Scientific, UK
Rnase zap	R2020-250ML	Sigma-Aldrich, UK
RNeasy Mini Kit	74104	Qiagen, UK
Rosewell Park Memorial Institute (RPMI1640)	12-918F	Lonza, UK
RPMI1640 with L-glutamine	BE12-702F/12	Lonza, UK
Sudan Black	199664-25G	Sigma-Aldrich, UK
Tip gel, 30mm, 200µl, sterile	5002306428	VWR, UK
Tris Buffered Saline with Tween® 20 (TBST-10X)	SRE0031-500ML	Sigma-Aldrich, UK
Triton X-100	9002-93-1	Sigma-Aldrich, UK
Trypan Blue Stain (0.4%)	T10282	Thermo Fisher Scientific, UK

Trypsin/EDTA10X	LZBE02-007E	Lonza, UK
Tween 20	P2287	Sigma-Aldrich, UK
Ultra-Low Attachment, polystyrene, round bottom, sterile, 96-well plate	CLS7007-24EA	Sigma-Aldrich, UK
UptiLight US WBlot HRP Chemilum. ECLmax Substrate	58372A	Interchim, UK

2.2 Methods

2.2.1 BRIN-BD11 cell culture

The BRIN-BD11 cell line is a hybrid cell line that is produced from the electrofusion of primary rat pancreatic islets with the RINm5F cell line, which is derived from the NEDH rat insulinoma. BRIN-BD11 cells were a generous gift from Ulster University.

The cells were cultivated as a monolayer for less than forty passages. The cells were grown in a T25 flask with 4-5 mL of warm Roswell Park Memorial Institute (RPMI) 1640 media supplemented with 10% fetal bovine serum (FBS) (Lonza, UK) and 1% Penicillin-Streptomycin (Lonza, UK). The cells were examined daily using a microscope (Olympus CKX41, Japan), which was attached to a CCD camera (1X 2-SLP, Micropublisher S-ORTV, Japan). The cells attached to the bottom of the plate surface and deflected light around their membrane.

The cells were passaged when they reached 80-90% confluence through discarding old media and washing the cells twice with 4 mL phosphate buffer saline (PBS) (Lonza, UK). Pre-warmed trypsin/EDTA 1X (2 mL) (Lonza, UK) was added to the flask and incubated at 37 °C and 5% CO_2 for 2-4 minutes. The flask was checked microscopically for cell detachment. Once detached, 4 mL of media was added to the flask to inactivate the trypsin. The cell suspension solution was transferred into a 15 mL falcon tube, and the tube was centrifuged at 900 rpm for 5 minutes. The supernatant was aspirated, and the pellet was re-suspended in 1 mL media. After that, the cells were counted using a hemocytometer (Counting Chamber; Thomas Scientific, UK), prior to use in experiments. Cells between passage number 21 and 30 were employed in the current study.

For prolonged storage, cells were detached from the flask with trypsin/EDTA and resuspended in 80% FBS, 10% RPMI and 10% DMSO (Dimethyl sulfoxide 99%, Fisher Scientific, UK). The cell suspension was immediately transferred to cryovials and placed in isopropanol filled in Mr Frosty freezing container for controlled cooling at -80 °C before being transferred to liquid nitrogen storage dewars.

2.2.2 Generation of coating solution

Coating solutions

Pluronic F127 (Polyethene oxide (PEO)-polypropylene oxide (PPO)) polyethene oxide is a block copolymer with an average molecular structure of $(PEO)_{99}$-$(PPO)_{65}$-$(PEO)_{99}$ and a molecular weight of 12.600 KD. A solution of 2% F127 was prepared in deionized water with gentle shaking at 4 °C for 20-30 minutes to aid dissolution of the polymer. A 1% solution of gelatin type A (Sigma-Aldrich, UK) was prepared in deionized water with heating at 65°C for 15 minutes.

Preparation of the culture plates

Three different types of culture plates were used in this study. The first was Ultra-low attachment 6-well plates and 24-well plates, which are commercially available from Corning Inc. NY. The second type of culture plate was a 24-well flat-bottomed suspension cell culture plate (SARSTEDT, USA) coated with five different coating solutions as outlined below. The third type of plate used was a standard 24-well cell culture plate (SARSTEDT, UK) coated with the same five types of the coating solution.

The five coating solutions used in this study comprised mixes of gelatin

and F-127 in varying ratios as follows:

1. Pure gelatin type A (1% (w/v))
2. Pure F127(2% (w/v)
3. A mixture of 90% (w/v) gelatin type A solution and 10% (w/v) F127 solution.
4. A mixture of 95% (w/v) gelatin type A solution and 5% (w/v) F127 solution.
5. A mixture of 98%(w/v) gelatin type A solution and 2% (w/v) F127 solution.

All the coating solutions were sterilized by filtering the solution using a 0.2 µm filter prior to use. 1 mL of the above coating solution per well was added, and the coated plates were incubated at 37 °C and 5% CO_2 overnight. The coating solution was then aspirated, and the plates were allowed to dry inside a laminar flow hood for 2 hours

2.2.3 Generation of PIs by suspension culture

Inside a laminar flow hood, cells were seeded at a density of 2×10^5 cells/well in Ultra-low attachment 6-well plates. A total of 7 mL of media was added to each well. PIs were generated in 24-well plates using two different cells seeding densities: 8×10^3 and 32×10^3 cells/well, with 3 mL media added to each well. Following seeding, the plates were incubated for seven days at 37°C and 5% CO_2. Media was not changed during the culture period. Images for cell aggregates were taken on day 3 and day 7 with a light microscope (Olympus CKX41, Japan) which was attached to a CCD camera (1X 2-SLP, Micropublisher S-ORTV, Japan).

2.2.4 Rotary culture approaches for the generation of PIs

To assess the role of movement in assisting the formation of PIs, plates were agitated for 3 days after seeding inside an incubator using a Shaker (model R100 Rotates shaker, Luckham) at 32 rotations per minute and incubated at 37°C and 5% CO_2. From day 4 to

day 7, plates were placed in an incubator without agitation. Media was not changed during the incubation period.

2.2.5 Measuring the morphology and size of PIs

Approximately 4-50 PIs were formed in each well. On day 7 of culture, the morphology of the PIs was assessed by light microscopy using a light microscope attached to a CCD camera. Diameters of PIs cultured on different substrates were compared using ImageJ software.

2.2.6 Measuring cell number

Measuring of cell number was started from dissociation of PIs with HBSS free calcium for 4 hours in an incubator at 37 °C and 5% CO_2. The suspension cells were transferred to 1.5 Eppendorf tubes and centrifuged for 5 minutes at 900 rpm. Then, the old media was discarded and the pellet suspended with 990 µL of fresh media and mixed of 10 µL of trypan blue and counted by using the Countess® Automated Cell Counter Invitrogen ((MP10227). Cell counting Chamber slide is a plastic disposable which holds the sample in two separated chambers for duplication. The sample was mixed, and 10 µL of sample was used on each side of the chamber to be counted.

2.2.7 Measuring PI proliferation by MTT assay

MTT reagent (3-(4,5-dimethylthiazol-2yl)-2,5 diphenyltetrazolium bromide can be used to assess the proliferation of PIs as a function of redox potential. MTT is reduced via mitochondrial enzymes to an insoluble product which is dissolved using a detergent and read at 570 nm. Briefly, the PIs were examined and compared with corresponding monolayer cultures using the MTT assay. For monolayer cells, trypsin (150 µL per well)

was added to detach cells. After that 300 µL of media was added to stop the action of trypsin, the mixture then was transferred to a 1.5 mL Eppendorf tube and centrifuged at 1000 rpm for 3 minutes. In the case of PIs, the cells were collected and directly transferred to 1.5 mL Eppendorf tubes and centrifuged for 3 minutes at 3000 rpm. Supernatants were removed, and the cells were washed once with 1 mL of phosphate buffered saline (PBS). This was followed by the addition of 100 µL of media to each Eppendorf, followed by 10 µL of 12 mM MTT reagent (3-(4,5-dimethylthiazol-2yl)-2,5 diphenyltetrazolium bromide) (Sigma-Aldrich, UK). The Eppendorf tubes were incubated at 37 °C and 5% CO_2 for 2 hours. Eppendorf tubes were then centrifuged for 3 minutes at 3000 rpm and 85 µL of solution discarded. Finally, 220 µL of DMSO (Dimethyl sulfoxide 99%, Fisher Scientific, UK) was added, and the solution was placed at 37 °C for 45 minutes and the absorbance measured at 570 nm using a microplate reader (BioTek Instruments, USA).

2.2.8 Measuring PI viability using Cell count kit-8

The Cell count kit-8 (CCK-8) kit was used to measure the viability of the PIs incorporating gelatin beads as the CCK-8 assay allows cells to be recovered afterwards, whilst the MTT assay does not. The kit's action depends on the presence of water-soluble tetrazolium salt (2-(2-methoxy -4-nitrophenyl)-3- (4-nitrophenyl-5- (2,4-disulfophenyl 2-tetrazolium monosodium salt, WST-8) reagent, which is reduced by the dehydrogenase of cells to formazan dye. Consequently, the amount of formazan generated corresponds to the number of viable cells. Briefly, PIs were transferred from tissue culture plates into 0.5 mL Eppendorf tubes. The medium was discarded after centrifuging for 5 minutes at 1000 rpm. The PIs were washed once with duplicate sterilised PBS (DPBS, Lonza, UK). A working solution was prepared to comprise 10 µL CCK-8 (Cell Counting Kit-8, Sigma-Aldrich; UK) plus 100 µL media, and 110 µL working solution was added to each Eppendorf and gently mixed by pipetting. The Eppendorf tubes were then incubated at

37 °C and 5% CO_2 for 4-5 hours. The Eppendorf tubes were centrifuged for 5 minutes at 1000 rpm and supernatants transferred into a 96-well plate. The intensity of colour was measured at 450 nm using a microplate reader.

2.2.9 Measuring cytotoxicity by lactate dehydrogenase assay

A lactate dehydrogenase (LDH) assay kit was used to assess cytotoxicity in PI cultures based on the fact that LDH is an oxidoreductase enzyme that catalyses the interconversion of lactate and pyruvate inside the cells as shown in Figure 2.1. Therefore, if cells are dead LDH will be found in a high amount in the media.

Figure 2.1 Mechanism of LDH cytotoxicity assay

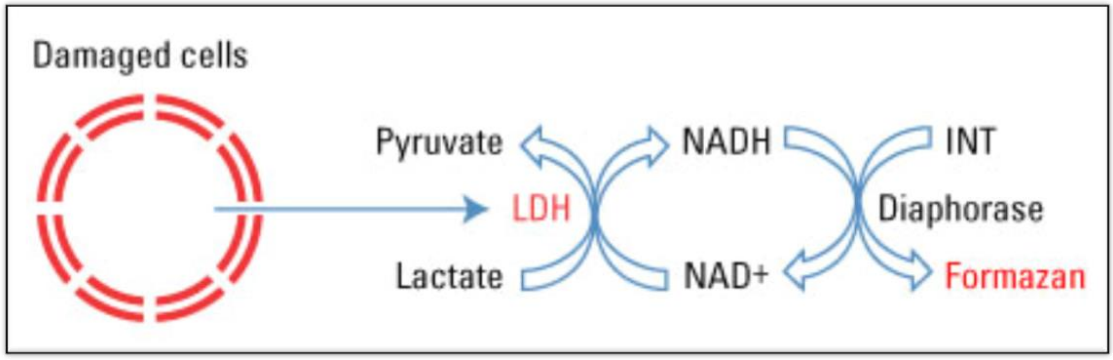

The assay is dependent on the detection of LDH released from the damaged cells to media as a biomarker for cellular cytotoxicity.

The determination of LDH value was conducted according to the manufacturer's instructions. The procedure started with LDH assay working solution which was prepared by dissolving one vial of substrate mix (lyophilization) with 11.4 mL of ultrapure water in a 15 mL conical tube. It was mixed well by inverting gently and enveloped with Aluminium foil to protect the reagent from light. The reaction solution was prepared from the reaction mix by combining 0.6 mL of assay buffer with 11.4 mL of substrate pipetting the solution gently. A spontaneous LDH activity control was prepared by adding 10 µL

of sterile, ultrapure water to PIs in triplicate. A maximum LDH activity control was prepared by adding 10 µL of Lysis Buffer (10x) to PIs in triplicate.

The spontaneous LDH activity control and maximum LDH activity control were kept in the incubator at 37 °C, 5% CO_2 overnight. An LDH positive control was diluted with 1% (w/v) BSA in PBS in a 1:10000 ratio. Then, 50 µL of 1x LDH positive control, and RPMI, which served as a negative control, was placed in a 96-well flat-bottom plate in triplicate. Also, 50 µL of the reaction mix was transferred to each sample well and mixed carefully. The samples in the plate were incubated at room temperature for 30 minutes in the dark. Next, 50 µL of stop solution was added to each well and mixed thoroughly. Absorbance was measured at 490 nm and correction at 689 nm using a microplate reader.

2.2.10 Glucose-stimulated insulin secretion

PIs were transferred to Eppendorf tubes carefully and centrifuged gently at 900 rpm for 5 minutes to create a small cell pellet before aspiration of media. The pellets were washed twice with 250 µL of Hank's Buffered Saline Solution 1X (HBSS 1X) (Sigma-Aldrich, UK) supplemented with 1 mM calcium. The cells were primed with 250 µL of 1.1 mM glucose and incubated for 40 minutes at 37 °C and 5% CO_2. After that, the 1.1 mM glucose was removed following gentle centrifugation (900 rpm for 5 minutes), and 250 µL of 16.7 mM glucose was added. PIs were incubated for a further 20 minutes at 37 °C and 5% CO_2. Finally, centrifugation was performed, and supernatants were transferred to 1.5 mL Eppendorf tubes and stored at -20°C for subsequent determination of insulin secretion by ELISA. A standard curve of insulin was calculated using the standards provided with the kit and ranged from 0 ng/mL to 5.5 ng/mL. Insulin concentration (ng/mL) released from test samples was estimated depending on the equation of the standard curve.

The remaining PI pellets were transferred to the ice after adding 60 µL of 0.5% RIPA buffer (Sigma-Aldrich, UK) and allowed to lyse for 20 minutes. The Eppendorf tubes were centrifuged at 4 °C for 20 minutes, and the supernatant transferred to a fresh Eppendorf tube, which was then stored at -80 °C until needed.

Total protein was quantified using the BCA protein assay (Thermo-Fisher, UK) according to manufacturer's instructions. In brief, working solution was prepared using 1 parts A, 5 parts B. A standard curve was prepared using protein solution with concentrations ranging from 0 µg/mL to 2 µg/mL using standard protein (2 mg/mL) provide with the kit. Next,10 µL sample and standard were taken, and 100 µL of buffer solution was added to each sample and standards in each well of a 96-well plate. The mixture was incubated at 37 °C and 5% CO_2 for 30 minutes before reading at 570 nm using microplate reader.

2.2.11 RNA extraction from Pseudoislets

PIs were collected and transferred to Corning 15 mL tube and centrifuged at 1200 rpm for three minutes. The media was discarded from tubes, and 1 mL of DPBS was added. After that, the PIs with DPBS were transferred into 1.5 mL Eppendorf tubes and centrifuged at 2000 rpm for 3 minutes, and the pellets were kept in ice for subsequent RNA extraction. For the monolayer cells, which were used as a control, the media was aspirated from the well and the cells washed once with DPBS, followed by addition of 150 µL of 1x trypsin/EDTA and incubated for 2 minutes at 37 °C and 5% CO_2. Next, the wells were examined under a microscope to check all cells were detached. After this, 250 µL of media was added to each well and transferred to 1.5 mL Eppendorf tubes. The tubes were centrifuged at 2000 rpm for three minutes. After discarding the media, the tubes were washed once with 1 mL DPBS. After discarding the DPBS, the pellet was kept at -80 °C for subsequent RNA extractions.

Total RNA was extracted from cells using the Qiagen RNAeasy Mini Kit which was adjusted according to cell number. Briefly, 350 µL of 90% lysis buffer was mixed with 10% beta-mercaptoethanol and added gently to the PIs. Following lysis and homogenization, the lysate buffer was transferred to a 1.5 mL Eppendorf tube, and 350 µL of 70% ethanol was added. The sample was transferred to the RNeasy Mini spin column and centrifuged at 14000 rpm for 15 seconds. The supernatant was discarded, and the total RNA remained bound to the membrane of the Mini spin column. The membrane was washed with 700 µL RW1 buffer and centrifuged at 14000 rpm for 15 seconds. After discarding of the supernatant, further washing with 500 µL of RPE was carried out and centrifuged at 14000 rpm for 15 seconds. The membrane was washed a final time with 500 µL of RPE and centrifuged for 2 minutes at 14000 rpm. The RNeasy Mini spin column was placed in a fresh 2 mL collection tube and centrifuged at 14000 rpm for 1 minute to remove any residual fluid. The RNA was eluted from the membrane using 30 µL of RNase free water. RNA concentration was measured using a Nanodrop 200 spectrophotometer (Thermo Scientific, UK) and stored at -80 °C until used.

2.2.12 Quantitative real-time reverse transcription polymerase chain (qRT-PCR)

One-step quantitative real-time reverse transcription polymerase chain (qRT-PCR) was conducted on PI samples using QuantiFast SYBR® Green RT-PCR Kit (Qiagen, UK). SYBR green is a fluorescent dye that can bind to the double strand DNA and emit light that can be detected by the thermocycler. Briefly, the RNA extracts were diluted using nuclease free distilled water to reach a final concentration of 100 ng/mL, in a final volume of 25 µL /well. A master mix was prepared for each well comprising 12.5 µL of SYBR Green, and 1 µL of the appropriate primer (10 µM). Finally, 0.25 µL of dNTP mix RT(enzyme) was added just before the transfer to the PCR machine. Cycling conditions were as follows 50 °C for 10 minutes to convert RNA to cDNA; denaturation of cDNA

at 95 °C for 5 minutes; 40 cycles of denaturation at 95 °C for 1 second, annealing (at various temperatures) for 30 seconds, and extension at 60 °C for 30 seconds. Primers sequences (Table 2.2) were designed using rat gene sequences from NCBI map viewer and PCR primer design software. The primers were bought from (Invitrogen, Thermo Fisher Scientific, UK). All the primers were evaluated in NCBI primer-blast.

Table 2.2 Primer sequences for RT-PCR Primer sequences for RT-PCR

Primers	Sequence		Product size
Rat E-Cadherin	F	GGGTTGTCTCAGCCAATGTT”	185
	R	“CACCAACACACCCAGCATAG ”	
Rat Cx36	F	“TAACCAGGCCTGCTATGACC”	163
	R	“CAGGGCTAGGAAGACAGTCG”	
Rat Insulin	F	“GTACCTGGTGTGTGGGGAAC”	200
	R	“CCAGTTGGTAGAGGGAGCAG”	
GAPDH_EXONE	F	“C AA GGT CAT CCA TGA CAA CT”	301
	R	“GAT ACA TTG GGG TAG GAA AC”	

2.2.13 Immunological staining

PIs were transferred into 1.5 mL Eppendorf tube, and the medium was discarded after centrifuging at 2000 rpm for three minutes. The PIs were washed with PBS twice. Three PIs in each Eppendorf tube were fixed with 500 µL of 4% PFA (Paraformaldehyde) (Thermo Fisher Scientific, UK) and placed in the cold room for 90 minutes. The PIs were then permeabilized with 300 µL of 0.3% (v/v) Triton X-100 (Sigma, UK) in PBS for 60

minutes at room temperature. Following, 300 µL blocking solution (5% (w/v) BSA (Sigma-Aldrich, UK), 0.15% Triton X-100 in PBS)) was added to each Eppendorf.

The primary and secondary antibodies were diluted with buffer solution (1% BSA (w/v), 0.2% (v/v) Triton X-100) as shown in Table 2.3. Primary antibodies were applied overnight at 4 °C. After which, the primary antibodies were removed, and the PIs were washed with the buffer solution three times for 5 minutes each using a centrifuge for 3 minutes at 2000 rpm. Then the PIs were incubated with the secondary antibody for 4 hours at room temperature. After that, the PIs were washed three times with PBS for 10 minutes each, and the PIs were incubated in the presence of DAPI (diluted 1:100 with PBS) at room temperature for 60 minutes. This was followed by three washes with PBS for 20 minutes each. The PIs were examined using laser scanning confocal microscope (Olympus, Japan) sequential narrow band filter accounts for spectral bleed-through (FITC excitation set at 473 nm and DAPI).

Semiquantitative analysis of fluorescence intensity was measured BIO file for Z-stack images generated by confocal microscopy. The BIO file for each sample was analyzed using ImageJ images to calculate the intensity of fluorescence per μm^2.

Table 2.3 Antibody dilutions for immunostaining of PIs

Immunogen	Primary antibody name	Primary dilution	Secondary antibody name	Secondary antibody name
GLUT2	Rabbit polyclonal IgG anti-GLUT2	1:200	Donkey anti-Rabbit IgG	1:500
Cx36	Mouse monoclonal anti-connexin 36	1:500	Goat anti-Mouse IgG	1:500
Insulin	Rabbit polyclonal IgG anti-Isnulin	1:100	Donkey anti-Rabbit polyclonal	1:200
Rabbit anti-Goat IgG (H+L)			Secondary Antibody, Alexa Fluor® 568 conjugate	1:1000

2.2.14 Western blotting

Total protein was extracted and quantified from monolayer and PI cell pellets as described in Section 2.2.12.

The expression of Cx36,[83] GLUT2[75] and insulin[75] were detected by using western blot analysis. The dilution factors for Cx36, GLUT2 and insulin were 1:1000. Protein lysates (50 µg) were mixed in 0.5 mL Eppendorf tube using a 5 µL of a mixture agent consisting of 150 µL NUPAGE®LDS sample buffer (4x) (Thermo Fisher Scientific, UK) and 7.5 µL 2-Mercaptoethanol (Sigma-Aldrich, UK). Next, the samples were heated to 90 °C for 15 minutes and then centrifuged for 30 seconds at 12000 rpm. The samples were loaded

into a 12 % SDS-PAGE gel (Generon, UK) gently to avoid the formation of bubbles. The gel was immersed in the tank containing 500 mL of 1x NuPAGE® MES SDS Running Buffer (Thermo-Fisher Scientific, UK) and the proteins were separated on a 12% polyacrylamide gel at 70 V for 2 hours and 30 minutes.

An additional layer of filter paper was soaked in transfer buffer and placed on top of the gel. All air bubbles were removed after placing on the transfer apparatus. A small strip of PVDF membrane was soaked in methanol and transfer buffer for about 10 minutes. The SDS-PAGE gel was washed with cold deionized water for 10 minutes with gentle shaking. After that, the gel was removed and placed directly on PVDF membrane. Finally, another sheet of filter paper was soaked in the transfer buffer and placed at the top of the gel. Separated protein was transferred from gel to the PVDF membrane in a wet western blotting assembly as shown in Figure 2.2.

Figure 2.2 Protein transferring set-up

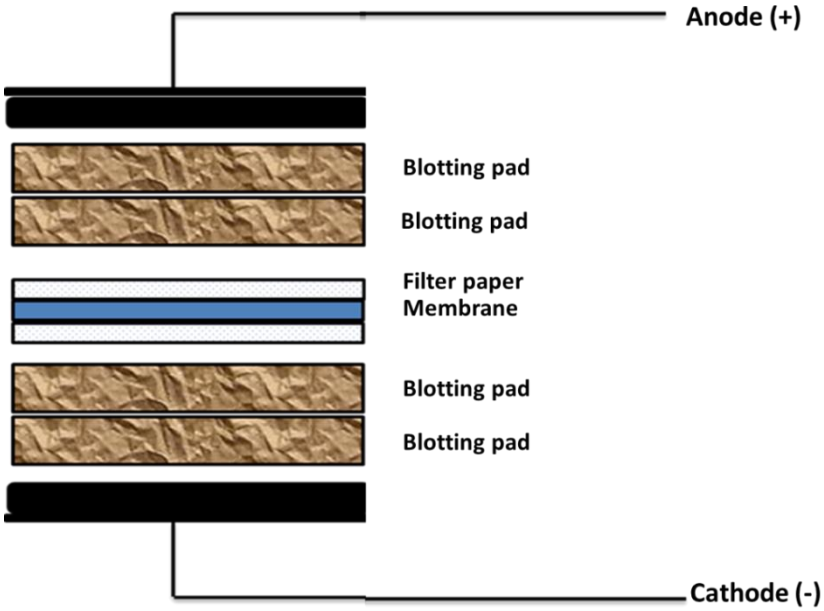

Assembly of wet type western blot proteins in gel migrates into the membrane where they are adsorbed and bound in semi-dry western blotting.

Proteins were transferred on the ice at 30 V (240 Ω) for two hours using transfer buffer 1x Tris-glycine SDS Running buffer (Thermo-Fisher Scientific). The non-specific binding sites on the membrane were blocked using 5% (w/v) non-fat dried milk for 1 hour at room temperature with shaking. The membrane was washed four times six minutes each with 1x Tris Buffered Saline with Tween®20 (TBST-20x; Thermo-Fisher Scientific). The primary antibodies were diluted with 5% (w/v) milk solution for Insulin (Cell Signaling Technology UK) of a concentration 1:1000. The membranes were added to the membrane four times for 6 minutes each with tris buffer saline with tween 20 Tris Buffered Saline with Tween® 20 (TBST) (Thermo-Fisher Scientific, UK). The membranes were incubated with appropriate Goat anti-Mouse horseradish peroxidase (HRP) (Abcam, UK) for 1h at room temperature to overnight at 4°C. After washing the membranes three times for ten minutes, signals were visualised using the FluorChem system (Bio-Techne (NASDAQ, TECH). Semi-quantitative measurement for Cx36, GLUT2 and insulin expression using western blot was determined using Alphapheiw software.[142]

2.2.15 Oxygen expression

To study the cell tissue oxygenation and bioenergetics metabolism, cell permeable phosphorescent probes need to be inserted or mixed to enable to follow the change in this tissue. Some of such probes have been used recently such as a dye called Pt(II)-tetrakis (pentafluorophenyl) porphyrin (PtPFPP) which is impregnated with dye named poly (9,9-diheptylfluorene) (PA2). The PA2 is non-toxic to cells, so the dye was mixed with cells from the day 0 before forming PIs. Phosphorescence lifetimes were measured in air-saturated and deoxygenated (5 mg/mL KH_2PO_4, 5 mg/mL Na_2SO_3) conditions. Large size nanoparticles (NPs) bearing PtPFPP and PFO dyes (135 nm) were produced.

At day 3 and day 7 the PIs were transferred to 12-well micro-chambers (Ibidi, Germany), pre-coated with a mixture of collagen IV and Poly-D-lysine. Staining with compound 1 (PA2) was achieved by adding it in regular growth medium to cells (10–20 µM), incubation for 16 h and washing in the medium before imaging. The 3D spheroid culture was generated as described in (Section 2.2 and Section 2.3). Live cells were analysed on widefield fluorescence Axiovert 200 (3D culture TXRed-4040 (Semrock) emission filters) and one-photon excited confocal Axio Examiner Z1 (subcellular localisation, imaging of spheroids; using 540 nm excitation, 565–605 nm emission filters) microscopes essentially. This work was in collaboration with Dr Ruslan Dmitriev in University College Cork, Ireland.

2.2.16 Water contact angle measurement

The water contact angle (CA) measurement is a determination of the wettability of substrate which is crucial in terms of identifying its biocompatibility. The hydrophobic materials show high contact angles with less wettability because of minimal spreading of the water droplet in comparison to hydrophilic material that displays a low contact angle with greater wettability as a result of spreading of the water droplet over time. To find out the wettability of different plastic plates which were used to generate the PIs, contact angle measurement was taken using the sessile drop technique.

The contact angle on a flat solid could be determined from the profile of a sessile drop described as the angle. Measured through liquids, especially water, where a liquid interface meets a solid surface. It has been used to study the wettability of surfaces, especially after coating. The equilibrium contact angle reveals the relative strength of liquid, solid and vapours molecular interaction. In this study different surfaces, were used to examine the measurement of contact angle on them.

Three types of 24-well culture plate were used in this study; cell adhesive (denoted as TCP), suspension culture (Sarstedt, USA, old product, denoted as SOP) and suspension culture (Sarstedt, USA, new product, green colour code, denoted as SGP). The bottom surfaces of all these plates were cut as shown in Figure 2.3 and coated with different solutions using the same procedure described in the Section 2.2.2.

Figure 2.3 The bottom surface of the plates for FTIR, protein adsorption and CA measurements

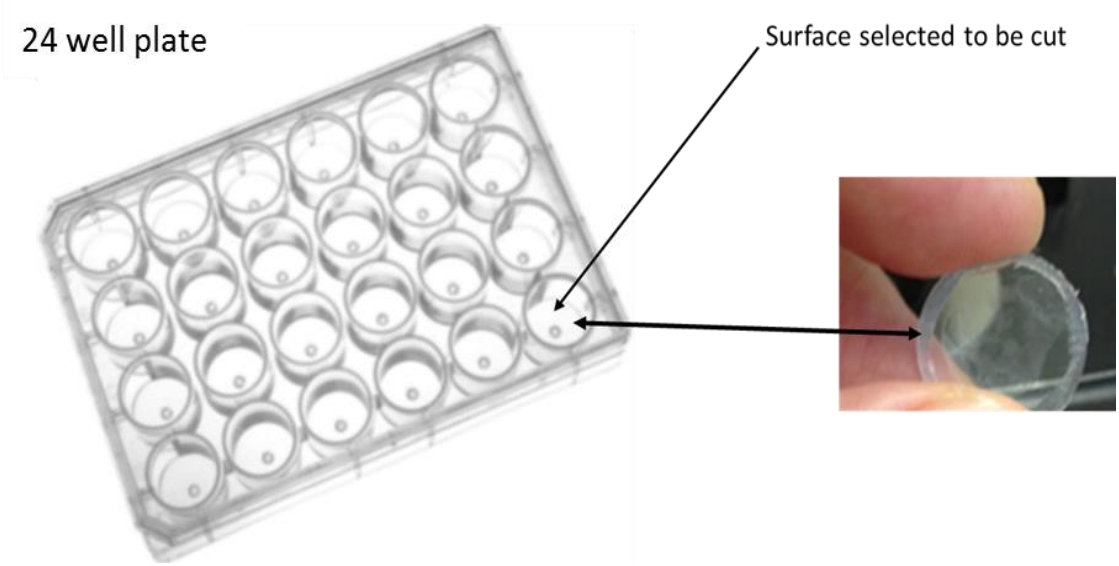

All the surfaces coated were incubated in the incubator at 37 °C overnight, and the coating solutions were discarded. The surfaces were placed inside of the hood for two hours to dry and kept at 4 °C until used.

A Hamilton syringe was used (as shown in Figure 2.4). 1 µL of ultrapure H_2O was placed onto the sample in vertical distance using Attention instrument with a CCD camera. Three samples from each group were measured to obtain mean CA values.

Figure 2.4 Image illustrating contact angle set-up

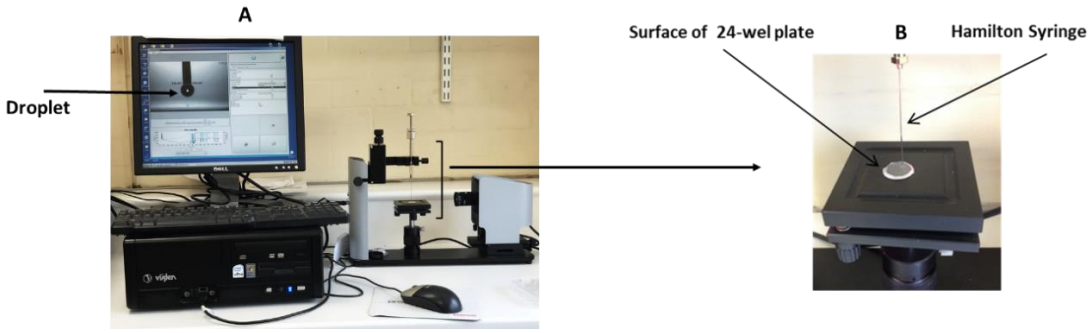

A: A microscope was connected to the CCD camera to take water droplet's images; B: Hamilton syringe and sample on the sampling stage during contact angle measurement.

2.2.17 Protein adsorption

To understand the capacity of surfaces used to produce the PIs we measured the protein adsorption for different surfaces that were used to form the PIs. Briefly, each surface was coated with 100 µL of 2% (w/v) BSA and incubated at 37°C for 2 hours. The BSA was then removed, and 0.1% (w/v) Coomassie Brilliant Blue Dye (500 µL) was added to each of the material surfaces and incubated for 4 hours. The stain solution was removed, and the stained surfaces were observed and imaged by light microscopy.

2.2.18 Attenuated Total Reflectance Fourier Transform Infrared Spectroscopy

A Fourier transform infrared (FT-IR) spectroscopy is widely used to determine the chemical structure for a sample of interest. It uses the IR light illumination due to the energy range of vibration and waging between chemical bonds. The FTIR allows giving specific information for each function group or any bonds among the chemical structure. Attenuated total reflectance (ATR) technique is a valuable measurement mode for identification of surface chemical structure and concentration of solid samples. ATR technique uses a crystal which produces total internal reflection, resulting in an evanescent wave. When a beam of infrared light is passed through the ATR crystal, the

resulted evanescent wave extends into the samples a few times and reaches the detector. It is very suitable for the analysis of a wide range of paints, coatings and reflective materials on surfaces (Figure 2.5).[143]

Figure 2.5 Multiple reflection ATR systems

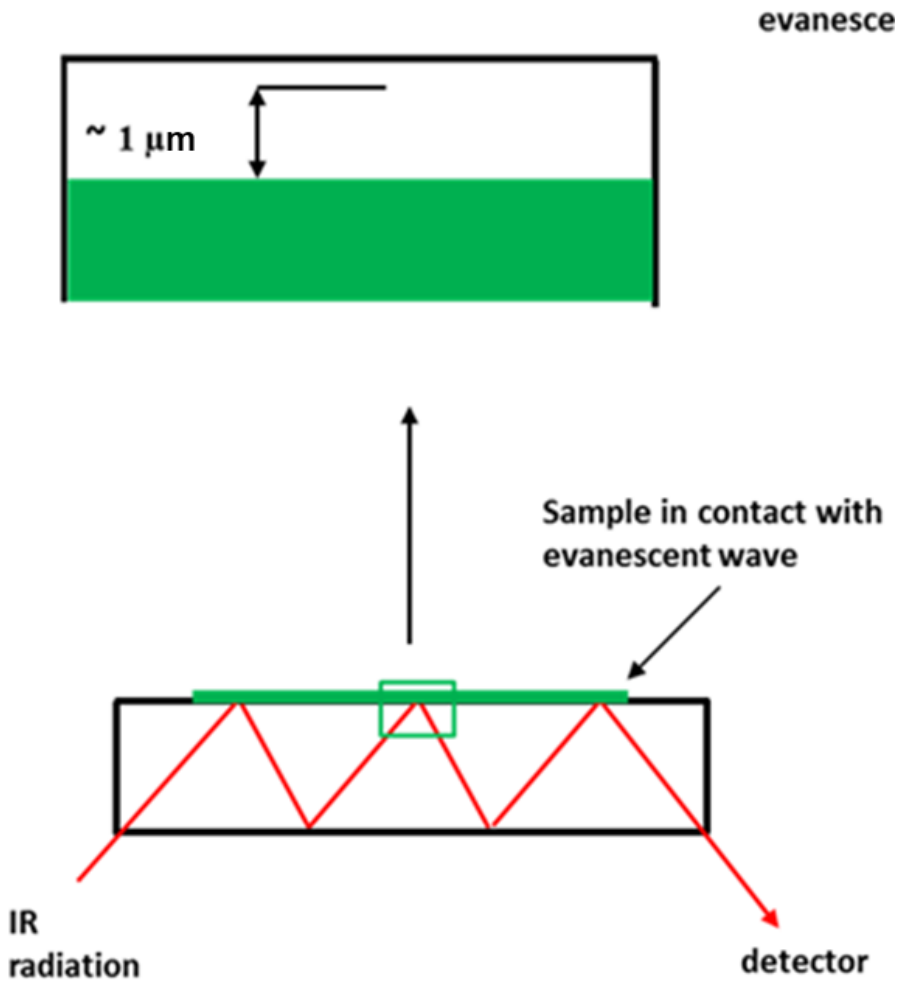

The figure shows the path of IR radiation in the sample for ATR-FTIR measurements.

A FT-IR spectrometer (Nicolet iS50, Thermo-Fisher, UK) (Figure 2.6) was used in this study with a diamond ATR crystal attachment. The samples were prepared in the same way described in section 2.2.17. FT-IR spectra were recorded over the wavenumber range 4000-500 cm^{-1}, co-adding of 256 scans with 4 cm^{-1} resolutions.

Figure 2.6 The photos of FT-IR spectrometers (Nicolet iS50)

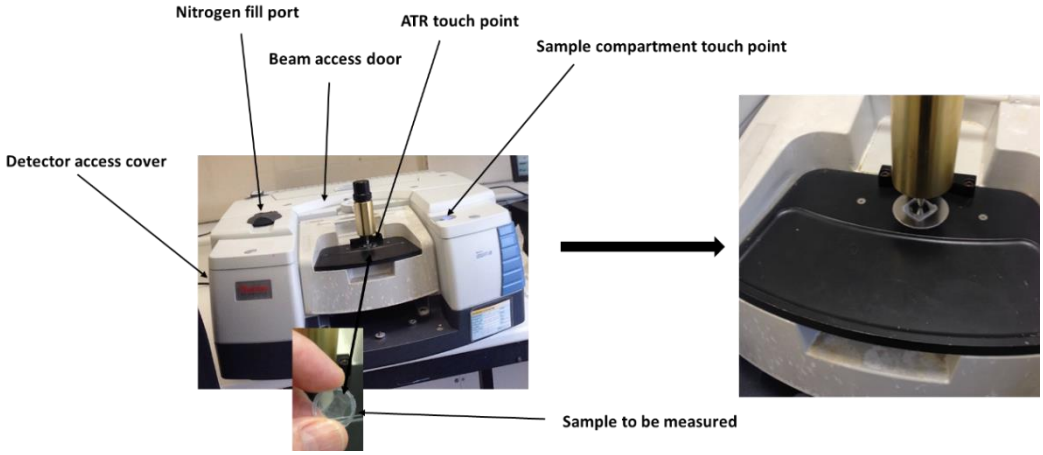

The figure shows the sample with Nicolet iS50 spectrometer used for ATR-FTIR measure.

2.2.19 Generation and characterisation of gelatin beads

Beads synthesis

Gelatin beads were optimised using the method of Iwanaga *et al.*[144] Briefly, a 15% (w/v) of gelatin type A (Sigma-Aldrich, UK) with 5% (w/v) glucose (Sigma-Aldrich) was added to 5 mL deionised water and heated to 70 °C. Meanwhile, 100 mL of olive oil was preheated to 70 °C with a magnetic stirrer. The aqueous solution of gelatin was added dropwise to olive oil with stirring at 420 rpm for 10 minutes to yield a water/oil emulsion. The temperature of the emulsion was directly decreased to 10°C with continued stirring for 30 minutes. Then, 75 mL of pre-cold acetone was added to the emulsion solution, followed by further stirring for 1 hour. The emulsion solution was then centrifuged at 4200 rpm at 5°C for 6 minutes. The formed pellets were washed three times with acetone and centrifuged at 4200 rpm. The formed gelatin beads were washed three times with acetone and centrifuged at 4200 rpm for 6 minutes each time.

Beads separation

The washed beads were passed through 30 µm or 40 µm sieves (PluriStrainer, Cambridge Bioscience Ltd, UK) and stored in acetone until use gelatin beads generated by different methods were imaged using an optical microscope. The sizes of beads were measured and analysed using ImageJ software.

Beads crosslinking using gaseous phase reaction

The gelatin beads (GBs) were crosslinked with 5% and 10% Glutaraldehyde (GA) (Sigma- Aldrich, UK) in the gas phase. Briefly, one mL of GA was placed in a small vial, the beads (30 µm and 40µm) were placed with 5 mL acetone in another vial. These vials were all placed in a glass petri dish, to allow for gaseous crosslinking (CL) for a period of 6 hours or 12 hours. Then the GBs were transferred to 2 mL Eppendorf tubes and washed three times with 1mL of distilled water by centrifugation at 4200 rpm for 3 minutes. The GB was then washed once with 1x DPBS (Dulbecco's Phosphates-Buffered Saline) by centrifugation at 4200 rpm for 3 minutes. Then a 1 mL of distilled water was mixed with the GBs, and the GBs aqueous solution was stored in an incubator at room temperature for maximum 7 days.

Beads swelling and degradation

The effects of crosslinking (CL) duration on the GBs swelling were assessed at high temperature (65°C). The GBs were crosslinked for 6 hours or 12 hours, placed in a 96-well plate with 200 µL distilled water, and incubated at 65°C for 20 minutes. The swelling of GBs (40µm and 30µm) were assessed by light microscopy. The bead images were taken, and size analysis was undertaken through ImageJ.

Beads washing and sterilisation

For sterilisation of beads, the beads were taken out from acetone and washed with Industrial methylated spirit 99% (IMS) three times, followed by centrifugation at 4200 rpm and 4 °C for 6 minutes each. Then, one mL of cold deionized water was added to wash beads three times at 4200 rpm and 4 °C for 6 minutes each. The crosslinked beads were also washed 3 times with 1x DPBS saline (1x DPBS; Sigma-Aldrich, UK) by centrifugation at 4200 rpm and 4 °C for 6 minutes each time.

2.2.20 Incorporation of beads into PI

The incorporated of beads was performed by three different methods. In general, about 25 GBs beads were mixed with 32,000 cells and 45 beads for 64,000 cells. The first method incorporating GBs into PIs was using ULA 96 well flat bottom plate. The second method was forming cell pellets in Eppendorf tube. Briefly, the cells were transferred into 1.5 mL Eppendorf tube. The GBs with cells were added to the same Eppendorf tube. The Eppendorf tubes were centrifuged at 1000 rpm for 4 minutes. After that, all tubes were placed in the incubator at 37 °C and 5% CO_2 for overnight. Next day, the pellet was transferred to suspension plate. The third method was using ULA 96 well round bottom plate. BRIN-BD11 cells were mixed with the beads in 300 µL of media and centrifuged using plate centrifuge (ALC PK 120, DJB Labcare Ltd, UK) at 900 rpm for 6 minutes. The plate was incubated at 37 °C and 5% CO_2. The images were taken every day.

2.2.21 Optimization of cytokines' concentrations in culture media on PIs' viability

In order to identify the optimum concentration of each cytokine on PIs' viability, series of IL-10 concentrations from 1 ng/mL to 1000 ng/mL in the culture media were assessed on PI's viability. Similarly, the optimum concentration of anti-IL-1β was estimated using series of anti-IL-1β concentrations from 0 µg/mL/ to 10 µg/mL in culture media for PI's

viability assessment. 32,000 cells/well were cultured by using ULA 96-well round bottom flask (Corning@Costar, USA). The plate was centrifuged for 6 minutes at 900 rpm to produce a single PI per well. The plate was incubated at 37°C and 5% CO_2 for 7 days. The viability of PIs in the presence of the cytokines was assessed at day 7 through using CCK-8 assay.

2.2.22 Incorporation of a mock drug into beads

Alexa Fluor® 568 conjugated antibodies, as a mock drug, was used to test the incorporation technique and drug release form GBs. The gelatin beads (GBs) 40 µm were crosslinked with 5% (v/v) GA for 6 hours. The GBs were transferred into 1.5 mL Eppendorf tubes, and they were washed 3 times with acetone, then three times with deionized water and 3 times with PBS at 4000 rpm for 5 minutes each.

The GBs were covered with aluminium foil and freeze dried for 2 hours using Benchtop freeze dryer. Dried gelatin beads were sterilised using UV radiation for 90 seconds. The GBs were incorporated with 10 µL of different concentrations of Alexa Fluor® 568 conjugated antibody (Thermo-Fisher). The concentrations were 0 µg/mL, 0.56 µg/mL, 1.25 µg/mL, 2.5 µg/mL, 5 µg/mL, 10 µg/mL. After the antibody was absorbed into the beads completely, the release of the antibody from the gelatin beads was measured by incubating the beads in PBS at 37°C. 100 µL of the solution were taken at various sampling time points, and fluorescence was measured at excitation/emission 565/625 from day 1 to day 7.

2.2.23 Incorporation of cytokines into beads

To load cytokines into GBs, the protocols of Nakase *et al*.[145] have been adapted and modified. The optimum concentration of each cytokine was determined by investigation of the improvement of the PIs' viability using CCK-8. The 100 ng/mL of IL-10 and 5 µg/mL of the anti-IL-1β were found optimal concentrations for the PIs respectively. The 10 µl of 100 ng/mL of IL-10 was incorporated into 25-50 GBs (for single PI) which had been freeze dried for two hours. The same procedure was applied to anti-IL-1β: 10 µl of 5 µg/mL of anti-IL-1β were incorporated into GBs (25-50 GBs/PI) which had freeze dried for two hours.

The BRIN BD-11 cells were placed into Ultra-low attachment 96-well plate round bottom (Corning@Costar, USA) with the beads incorporated with 100 ng/mL IL-10 or 5 µg/mL anti-IL-1β. Two types of cell densities in PIs were used in this experiment. One was 32,000 cells/well and the second was 64,000 cells/well. Following 300 µL media of cells and GBs were mixed and the plate was shaken using a plate shaker at 900 RPM for 6 minutes.

2.2.24 Assessment of drugs released

The release of incorporated mock drug from GBs was measured due to their fluorescence. Briefly, 100 µL of the culture media from each concentrate was taken and tested using the plate reader. The fluorescence intensity was measured at excitation 565 nm.

IL-10 concentration was measured using ELISA assay (PeproTech, USA). Standard serial dilutions in triplicate were loaded into an overnight pre-coated surface with a capture antibody specific to IL-10 and blocked for 1 hour by blocking buffer, followed by 2 hours

incubation with a diluted detection antibody mixture and 30 minutes with diluted Avidin-HRP. Each step was accompanied by discarding the contents forcibly and four times of washing with diluted detergent buffer. Finally, an enzymatic reaction initiated by addition of an ABTS-substrate (2,2′-Azino-bis (3-ethylbenzothiazoline-6-sulfonic acid)) (Sigma.Aldric) leading to bluish-green colour development within 5-15 minutes during which a visible signal was detected at 405 nm via plate reader.

2.2.25 Statistical analysis

ImageJ software version 1.4.3.67 was used for measuring the diameter of PIs. The diameters of fifteen PIs were counted to obtain the mean value. Comparisons between groups were performed using unpaired Student's t-test. Different comparisons of mean values were analysed using GraphPad Prism 7 with t-test and one-way ANOVA with multiple comparisons. P-values were considered as a significant as compared to control ($P < 0.05$ - $P < 0.0001$).

Chapter 3

Development of new techniques to enhance Pseudoislets biofunction

3.1 Introduction

The islets of Langerhans are multicellular aggregates within the pancreas containing beta cells that sense changes in the blood glucose level and respond by secreting insulin. The cells within the islets communicate with each other through gap junctions. The 3D structure of the islets is crucial for their metabolic functions.[28,146] Artificial reconstruction of isolated beta cells into islets of Langerhans through 3D cell aggregation has led to the generation of Pseudoislets (PIs), which can produce insulin in a physiologically responsive manner.[75]

There are many strategies to generate spherical aggregates from dissociated cells of primary tissues or differentiated stem cells. Hanging in drop culture[75] and suspension culture[145] have been widely used to generate cell aggregates. However, the aggregate size can be difficult to control using these methods. Another promising technique, microwell culture, has been used to generate size-controllable PIs from embryonic stem cells.[148–150] GSIS was greater when pancreatic beta cells were configured as 3D cell aggregates, similar in size and appearance to pancreatic islets.[85,151]

The simplest method used to promote the formation of PIs is to grow the beta cells in suspension. The method causes the beta cells to attach to each other rather than the surface of the culture container due to the non-adhesive property of the surface. Many cell types differentiate and lose their normal phenotype when grown under 2D cell culture conditions.[75] Suspension culture prevents this problem, thereby helping cells to maintain their function. Some studies have shown that beta cells display different morphologies based on the surface properties of the materials in which they are cultured.[83] Beta cells cultured in a low attachment microenvironment formed PIs with an islet-like structure.[75] The substrates commonly used to generate PIs by suspension culture are bacterial Petri

dishes which form small PIs,[83] and ultra-low attachment (ULA) culture plates in which larger PIs are usually formed.[152] The larger sized PIs formed on the ultra-low attachment plates displayed an improved ability to secrete insulin, but they suffered from central necrosis after 7 days of culturing.[75,153] Yang and colleagues have developed other surface treatments for the formation of PIs and found that the treatment of the surface with collagen, Lipidure and type IV collagen has an impact on PIs size, viability and insulin secretion.[83] They claimed that the PIs formed on the Lipidture surface had the best viability and insulin secretion.[83]

It is a huge challenge to maintain PI functionality including insulin secretion, gap junction communication, cell-cell communication and viability. PI size links to cell viability and sensitivity to glucose challenge.[83,95,154] It is already known that ULA culture plate leads to heterogeneous sizes of PIs. Thus, it is desirable to develop a material coating system which changes the cell attachment capacity of cell culture plates, to allow the study of the relationship between the physical properties of PIs (size and cell packing density) and their function. The end goal is to characterise better substrates, which could generate a large number of PIs of homogenous sizes and high viability.

3.2 Aim

This study aimed to develop two new techniques to control PIs' physical properties and improve their viability. The first technique was to develop a series of coating solutions consisting of a mixture of gelatin and Pluronic F127 that would be used for suspension cultures. This would allow determination of the effect of the chemical properties of the substrate on the size of cell aggregates. The chemical and physical properties of the coating surfaces were characterised in this chapter and formed the foundation to interpret the biological performance of PIs formed on these surfaces (Chapter 4). The second

technique involved the production of gelatin beads with a suitable size enabling swelling and incorporating into PIs. The stability, physical properties (size and shape) and the capacity to of the beads to carry drugs were investigated, which provided evidence for the biological performance on the modified PIs as detailed in Chapter 5.

3.3 Materials and Methods

3.3.1 Materials

Chemicals, cell culture plate types and reagent used in this chapter were listed in chapter 2 Section 2.1.

3.3.2 Generation of coating solution

The coating of suspension plates was described in Chapter 2 Section 2.2.2.

3.3.3 Generation of gelatin bead

The generation of GBs from gelatin solution was outlined in Chapter 2 Section 2.2.19.

3.3.4 Crosslinking of gelatin beads

The GBs were separated into sizes (30 µm and 40 µm) and crosslinked for 6 and 12 hours using gaseous reaction as described in Chapter 2 Section 2.2.19.

3.3.5 Characterisation of gelatin beads

The gelatin beads were characterised as outlined in Chapter 2 Section 2.2.19

3.3.6 Water contact angle measurement

The contact angle measurement for different type surfaces was outlined in Chapter 2 Section 2.2.16.

3.3.7 Protein adsorption

Protein adsorption on different culture surfaces coated with different coating solutions was described in Chapter 2 Section 2.2.17.

3.3.8 Attenuated total reflectance

A Fourier transform infrared (FT-IR) spectroscopy used for measurement of different types of surface chemistry was described in Chapter 2 Section 2.2.18.

3.4 Results

3.4.1 Characterisation of the effects of coating solutions on the substrate's chemical properties

Five coating solutions (F127, gelatin type A and three mixtures of F127 and gelatin, (98%, 95%, 90% of gelatin type A) have been used to coat three types of cell culture plates. Suspension culture plate 1 (old product (SOP)); suspension culture plate 2 (green product (SGP)); and tissue culture plate 3 (TCP). We hypothesised that the variation of F127 percentage in the coating solutions would change the chemical properties of cell culture plates and that this change is dependent on the substrate chemistry of the original plates. Figure 3.1 summarises the coating groups. Three characterisation techniques have been used to demonstrate the changes: ATR-FTIR spectroscopy has been used to identify changes in chemical properties; contact angle measurement revealed any changes in hydrophilicity; while Brilliant blue staining displayed the protein adsorption capacity of the surface.

3.4.1.1 Attenuated total reflection-Fourier transform infrared spectroscopy (ATR-FTI study

ATR-FTIR spectroscopy is a method used to determine the molecular structure and chemical composition of samples.[155] Our initial investigations examined the change of chemical properties of the culture substrates after coating by ATR-FTIR spectroscopy. The spectra shown in the following sections are the representative data from each group. Each spectrum was collected through 256 scans and experiments were repeated 3-5 times by duplicated samples.

Figure 3.1 The experimental variables used for coating plates

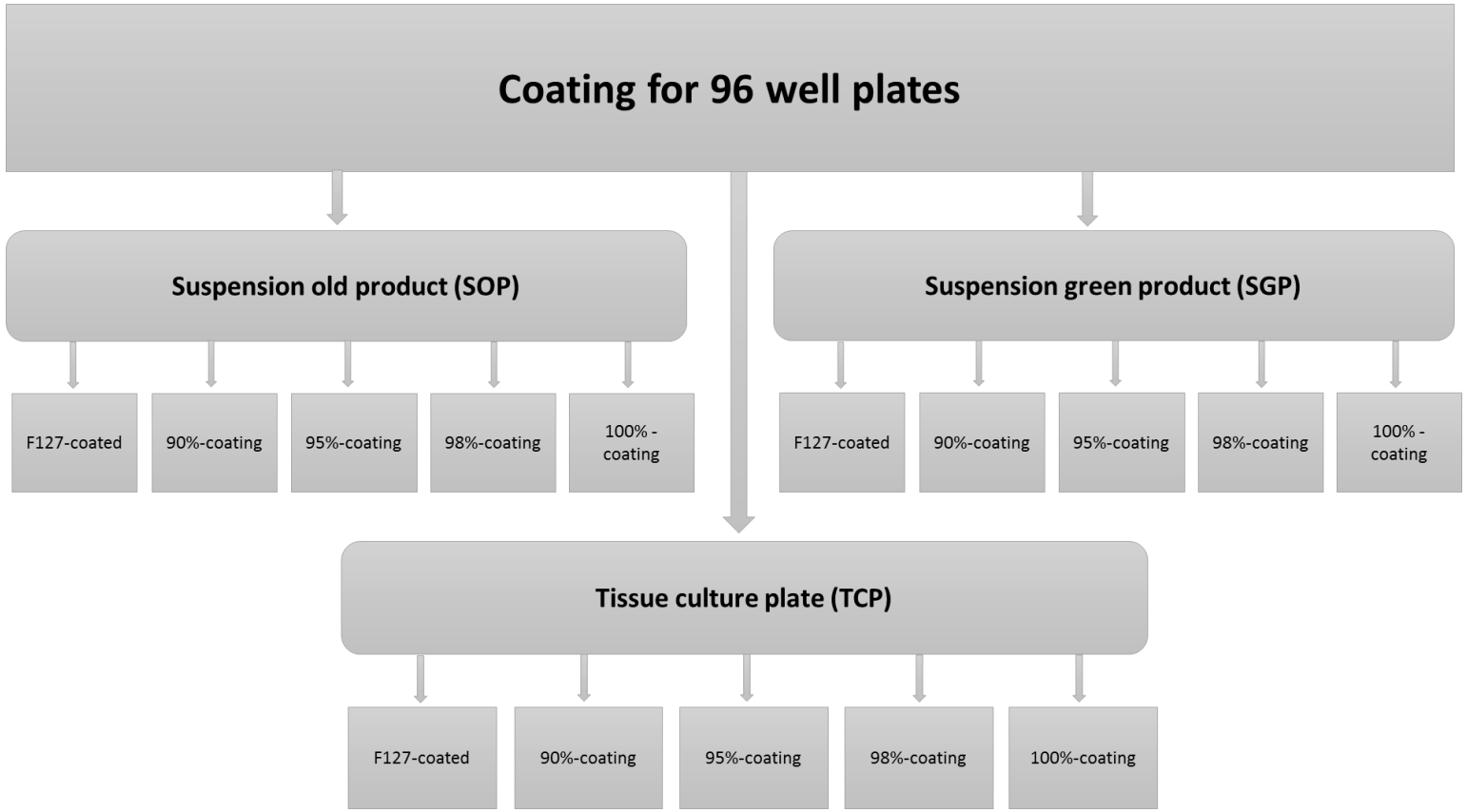

The design was used for generating different types of tissue culture plates through coating with gelatin A solution and F127 solution and mixture of both solutions. The concentrations of F127/gelatin in the mixtures are 100%/0%, 10%/90%, 5%/95%, 2%/98% and 0%/100%

3.4.1.1.1 Effect of coating solution on SOP plate

3.4.1.1.1.1 Uncoated SOP surface

Figure 3.2 is the ATR-FTIR spectrum of the uncoated suspension surfaces (SOP). Bands of the IR spectrum showed typical groups of polystyrene substance.[156] The peak at 3081 cm^{-1} - 3001 cm^{-1} region was assigned to C-H aromatic stretching; 2923 cm^{-1} and 2850 cm^{-1} bands were due to CH_2 asymmetric and symmetric tension; the bands in 1601 cm^{-1} and 1493 cm^{-1} were associated with arenes C=C stretching.[156] The IR band at 1069 cm^{-1} was for flexion C-H in the plane.[156] Another sharp band at 680 cm^{-1} was for arenes C-H bending. There was a weak band around 3400 cm^{-1}, which could be the result of special surface treatment for the suspension plate.

Figure 3.2 The ATR-FTIR spectrum of uncoated SOP surface

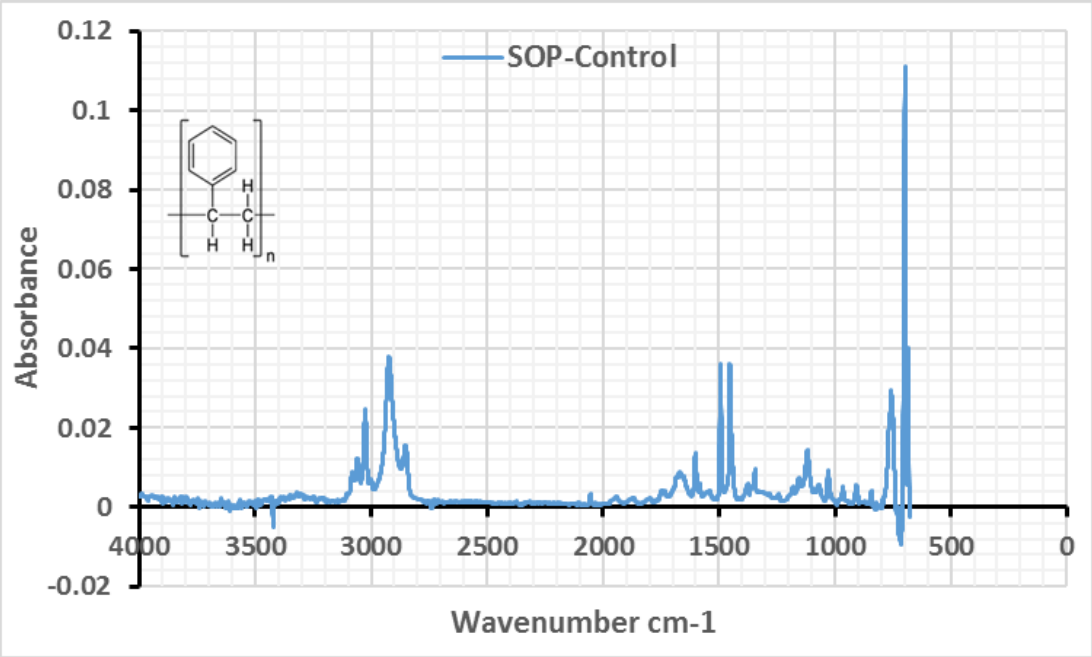

ATR-FTIR spectrum shows the characteristic peaks. Data are presented as 4-5 independent experiments conducted in duplicate.

3.4.1.1.1.2 SOP surface coated with F127

Coating the suspension surface with F127 solution resulted in a dramatic change of the spectrum (Figure 3.3). The decoration of F127 on the polystyrene substrate presented medium strength bands at 2980-2880 cm^{-1} which were due to CH_2 and CH_3 stretching. Another weak band at 1454 cm^{-1} was commonly related to methyl, methylene groups in PEO and PPO blockers. Furthermore, the strong band at 1100 cm^{-1} was C-O stretching. It was noticed that the characteristic bands of the uncoated plate at 3081 cm^{-1}-3001 cm^{-1} were not clear. These results demonstrate that the PEO and PPO blockers of F127 substance have covered the SOP surface.

Figure 3.3 The ATR-FTIR spectrum of F127coated SOP surface

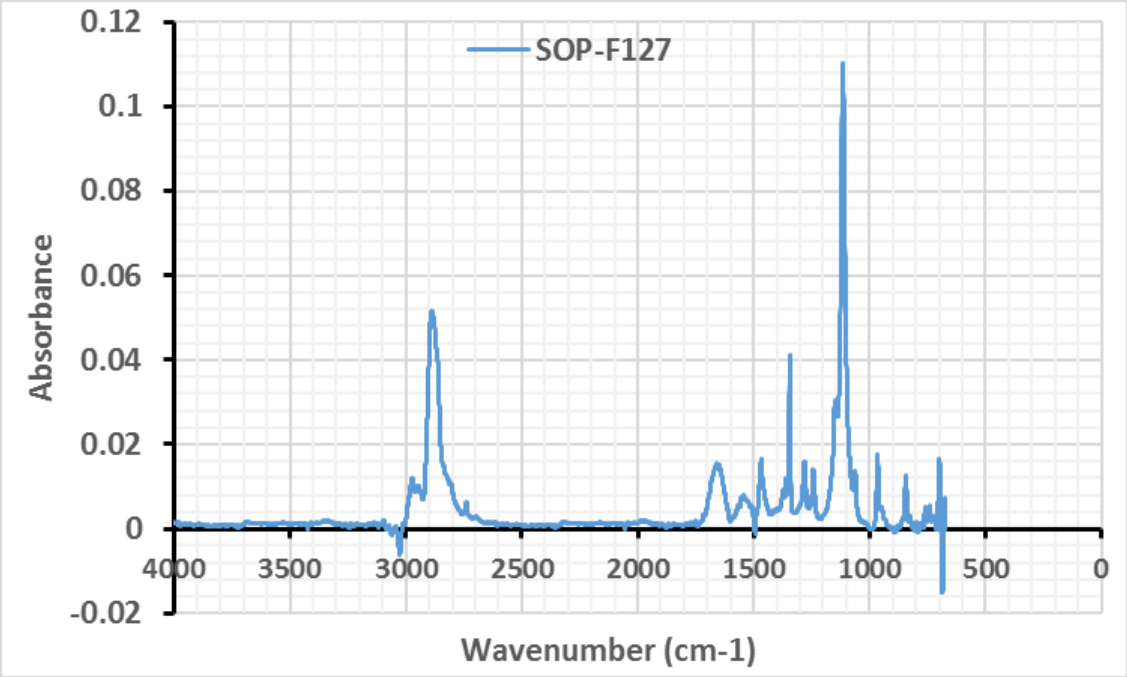

ATR-FTIR spectrum shows the characteristic peaks. Data are presented as 4-5 independent experiments conducted in duplicate.

3.4.1.1.1.3 SOP surface coated with 100% gelatin

The SOP plate coated with 100% gelatin showed a characteristic protein spectrum (Figure 3.4). There were five individual band regions. The strong bands at 3200-3500 cm^{-1} were for amide A, O-H and N-H stretching.[158,159] The bands at 2900 cm^{-1} were for CH_2 and CH_3 stretching.[158,159] The strong band at 1650 cm^{-1} was for Amide I (C=O stretching), 1500 cm^{-1} for amide II (NH bending), and the weak band (Amide III) at 1229 cm^{-1} for NH stretching.[160,161] It was also noticed that the characteristic bands of the uncoated plate at 3081-3001 cm^{-1} were not clear. These results again demonstrate that the gelatin has covered the SOP surface.

Figure 3.4 The ATR-FTIR spectrum of 100% gelatin coated SOP surface

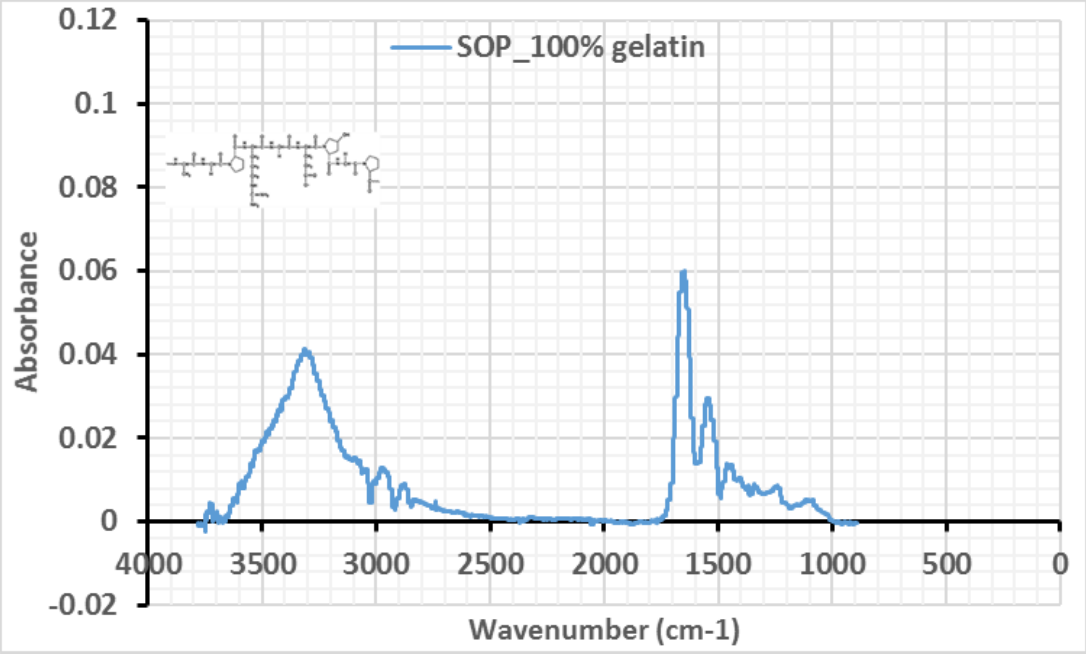

ATR-FTIR spectrum shows the characteristic peaks. Data are presented as 4-5 independent experiments conducted in duplicate.

3.4.1.1.1.4 SOP surface coated with 98% gelatin

The ATR-FTIR spectrum for the surface coated with 98% gelatin is displayed in Figure 3.5. Overall, the spectrum was very similar to that of the gelatin coated spectrum (Figure 3.4). The characteristic and strong bands of amide A, I and II at 3200-3500 cm^{-1}, 1650 cm^{-1} and 1547 cm^{-1}, respectively, were observed. However, there were three additional peaks appearing more clearly than with the 100% gelatin coated surface: a peak at 3100-3000 cm^{-1} region, a peak at 2900 cm^{-1} 1400 cm^{-1} region, and 1150 cm^{-1} region which may result from the F127 component of the coating solution.

Figure 3.5 The ATR-FTIR spectrum of 98% gelatin coated SOP surface

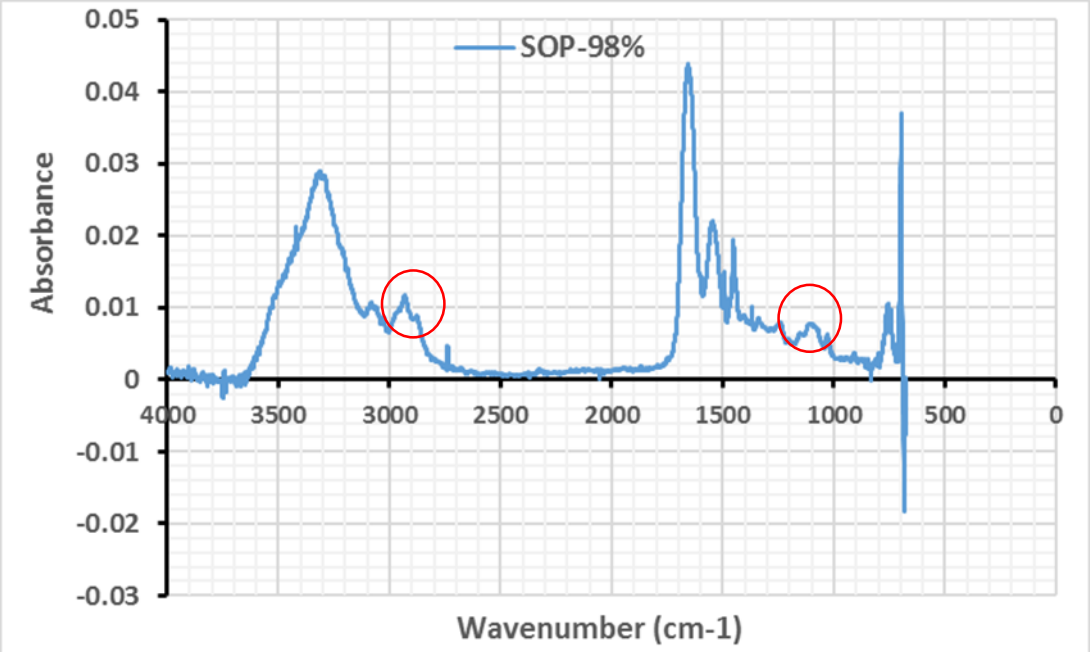

ATR-FTIR spectrum shows the characteristic peaks. Data are presented as 4-5 independent experiments conducted in duplicate. The circled peaks refer to methyl and methylene groups stretching at 3000-2950 cm^{-1} and C=O stretching at 1100 cm^{-1}

3.4.1.1.1.5 SOP surface coated with 95% gelatin

The ATR-FTIR spectrum of surface coated with 95% gelatin (Figure 3.6) demonstrated further differences between that of 98% gelatin coating, pure gelatin coating and F127 coating. Again, the spectrum was very similar to the 100% gelatin coated spectrum (Figure 3.4). The characteristic and strong bands of amide A, I and II at 3200-3500 cm^{-1}, 1650 cm^{-1} and 1547 cm^{-1} respectively were again clearly observed. However, the intensity of the three peaks at 3100 cm^{-1} regions, at 2900 cm-1 and 1400 cm-1 regions and 1150 cm^{-1} became stronger and more obvious than in the spectrum of surfaces coated with 98% gelatin. This is consistent with the increase of the F127 component in the coating mixture solution.

Figure 3.6 The ATR-FTIR spectrum of 95% gelatin coated SOP surface

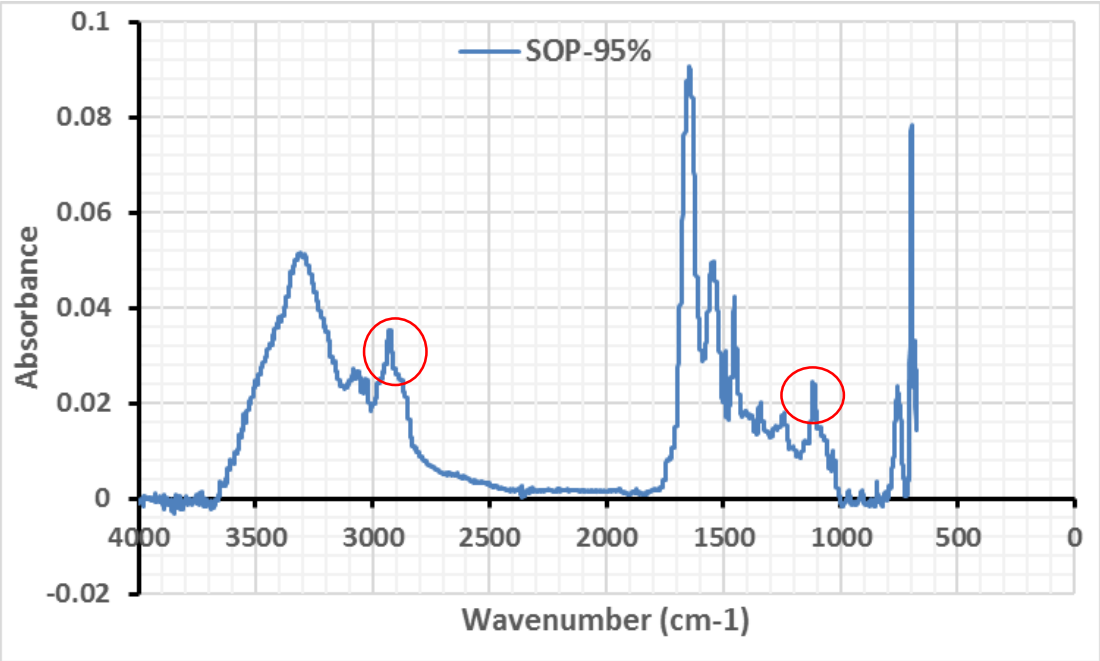

ATR-FTIR spectrum shows the characteristic peaks. Data are presented as 4-5 independent experiments conducted in duplicate. The circled peaks refer to methyl and methylene groups stretching at 3000-2950 cm^{-1} and C=O stretching at 1100 cm^{-1}

3.4.1.1.1.6 SOP surface coated with 90% gelatin

The coated SOP surface had quite a different spectrum when a solution of 90% gelatin and 10% F127 was applied (Figure 3.7), First, the intensity ratio of amide A to amide I and II reduced in comparison to the spectrum of the surface coated with a 100% gelatin solution. Secondly, the intensity of the three new peaks: the peak at 2950 cm^{-1} region, the peak at 2900 cm^{-1} region, 1400 cm^{-1} region and 1150 cm^{-1} became stronger and more obvious than the spectrum of 98% and 95% gelatin coated surfaces (Figure 3.6). The strong peak at 1100 cm^{-1} was from C=O stretching of PPO or PPE group, indicating the strong F127 component is appearing on the surface.

Figure 3.7 The ATR-FTIR spectrum of 90% gelatin coated SOP surface

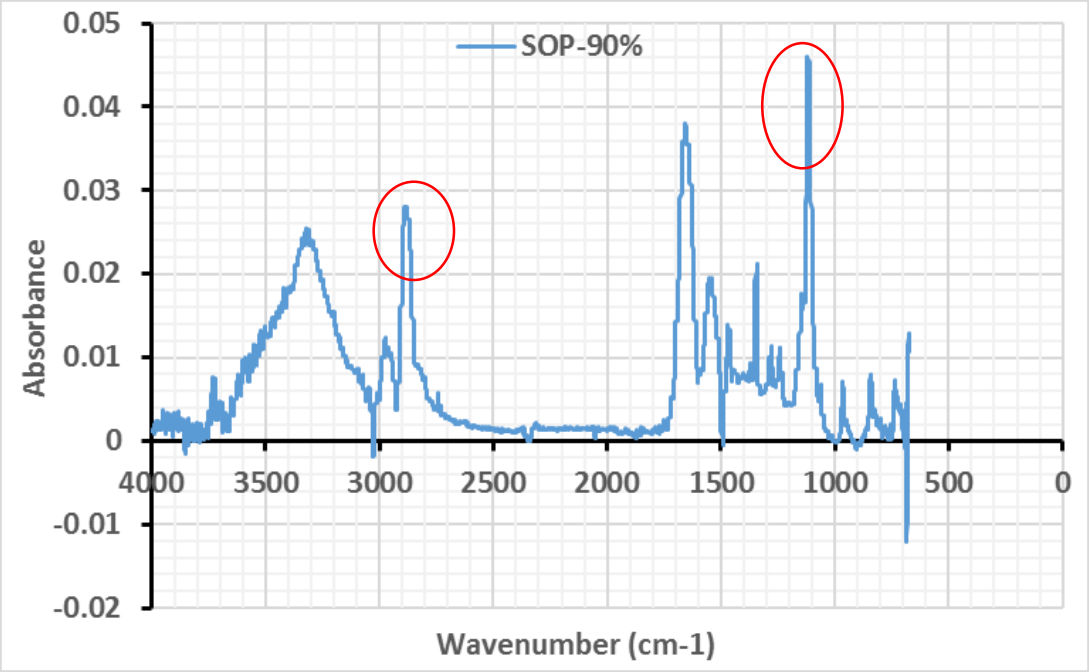

ATR-FTIR spectrum shows the characteristic peaks. Data are presented as 4-5 independent experiments conducted in duplicate. The circled peaks refer to methyl and methylene groups stretching at 3000-2950 cm^{-1} and C=O stretching at 1100 cm^{-1}

3.4.1.1.2 Effect of coating solution on TCP plate

3.4.1.1.2.1 Uncoated TCP surface

For adhesive tissue culture plate (TCP), ATR-FTIR spectra were also found to be dependent on the coating solution used. Bands of uncoated TCPs pronounced typical groups in polystyrene substance.[156] Peaks were observed at 3100-2900 cm^{-1} which were assigned to C-H aromatic stretching (alkenyl C-H stretching), and 2850 cm^{-1} bands were due to CH_2 asymmetric and symmetric tension. The bands at 1601 cm^{-1} and 1493 cm^{-1} were associated with arenes C=C stretching.[157] while another sharp band at 680 cm^{-1} was for arenes C-H bending (Figure 3.8).

Figure 3.8 The ATR-FTIR spectrum of uncoated TCP

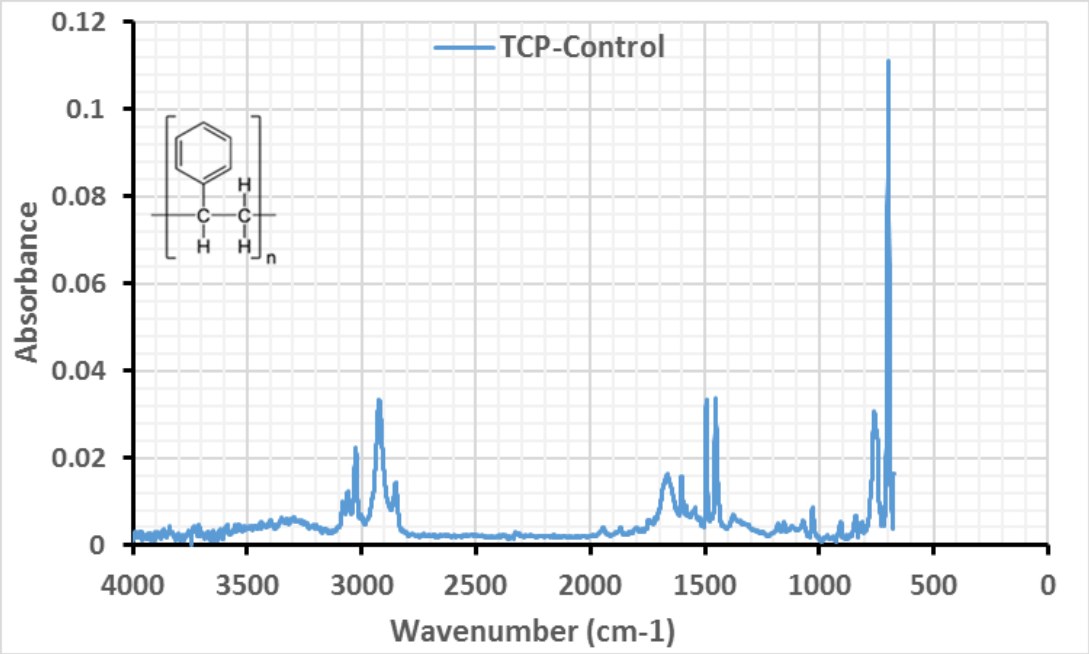

ATR-FTIR spectrum shows the characteristic peaks. Data are presented as 4-5 independent experiments conducted in duplicate.

3.4.1.1.2.2 TCP surface coated with F127

After coating the adhesive surface with the F127 solution, peaks observed at 3010-2900 cm^{-1} were due to CH_2 and CH_3 stretching, and peaks observed at 1640 cm^{-1} resulting from the stretching vibration of C=O stretching. Another band was observed at 1500 cm^{-1}, which is commonly related to methyl, methylene groups in PEO and PPO blocker. Also, the strong band at 1150 cm^{-1} was C=O stretching as a result of the PPO blocker. A sharp peak in the 1389 cm^{-1} region resulted from C-H bending, and the weak absorbance at 680 cm^{-1} was for arenes C-H bending, which related to the surface of polystyrene (Figure 3.9). The results demonstrated that the PEO and PPO blockers in F127 had coated the TCP surface.

Figure 3.9 The ATR-FTIR spectrum of F127 coated TCP surface

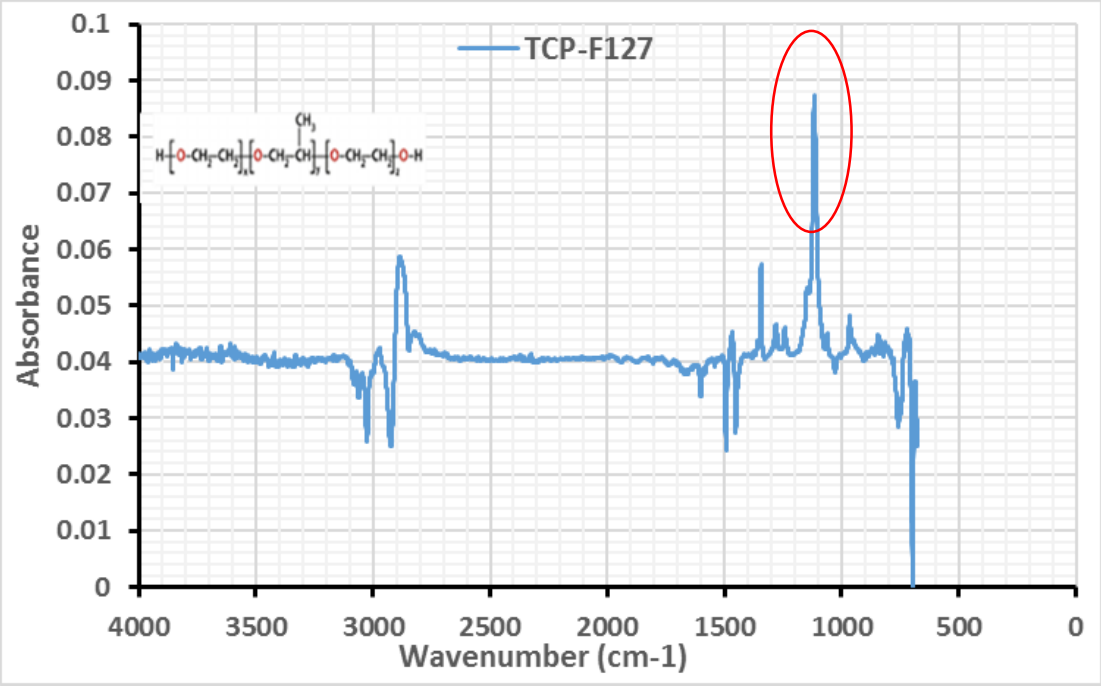

ATR-FTIR spectrum shows the characteristic peaks. Data are presented as 4-5 independent experiments conducted in duplicate. The circled peak refers to the peak of C=O stretching at 1150 cm^{-1}.

3.4.1.1.2.3 TCP surface coated with 100% gelatin

The TCP surface coated with 100% gelatin showed a characteristic protein spectrum (Figure 3.10). There were five individual band regions. The strong bands at 3500-3200 cm^{-1} reflected amide A (N-H stretching); the second band at 2900 cm^{-1} was for CH_2 and CH_3 stretching. The third sharp band at 1650 cm^{-1} resulted from Amide I, with the fourth band at 1547 cm^{-1} for amide II, and the fifth band at 1229 cm^{-1} for N-H stretching. It was also shown that the characteristic bands of the uncoated plate at 3081-3001 cm^{-1} and 1600-1400 cm^{-1} were largely absent. These results demonstrate that the gelatin has covered the TCP surface (Figure 3.10).

Figure 3.10 The ATR-FTIR spectrum of 100% gelatin coated TCP surface

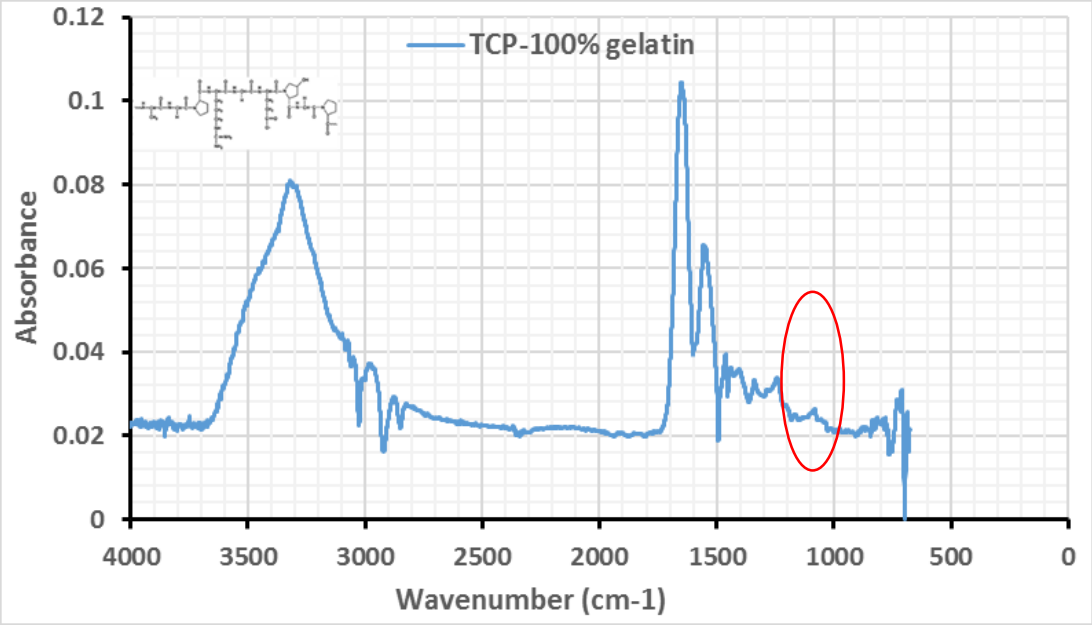

ATR-FTIR spectrum shows the characteristic peaks. Data are presented as 4-5 independent experiments conducted in duplicate. The circled peak refers to the peak of C=O stretching at 1150 cm^{-1}.

3.4.1.1.2.4 TCP surface coated with 98% gelatin

ATR-FTIR spectrum for the TCP surface coated with 98% gelatin (Figure 3.11) exhibited similarity to the spectrum of TCPs coated with 100% gelatin coating (Figure 3.10).

However, the intensity of the bands at 3200-3500 cm $^{-1}$, 1650 cm^{-1} and 1547 cm^{-1} representing amide A, I and II[158,159] respectively, were less pronounced in the spectrum of TCPs coated with 100% gelatin. Furthermore, the peaks at 680-860 cm $^{-1}$ were for arenes C-H bending for polystyrene appeared at low intensity to indicated the surface is likely to be coated with gelatin only and poorly absorbed F127 except there was a weak band at region 1150 cm^{-1} for C=O stretching in PPO. [160,161]

Figure 3.11 The ATR-FTIR spectrum of 98% gelatin coated TCP surface

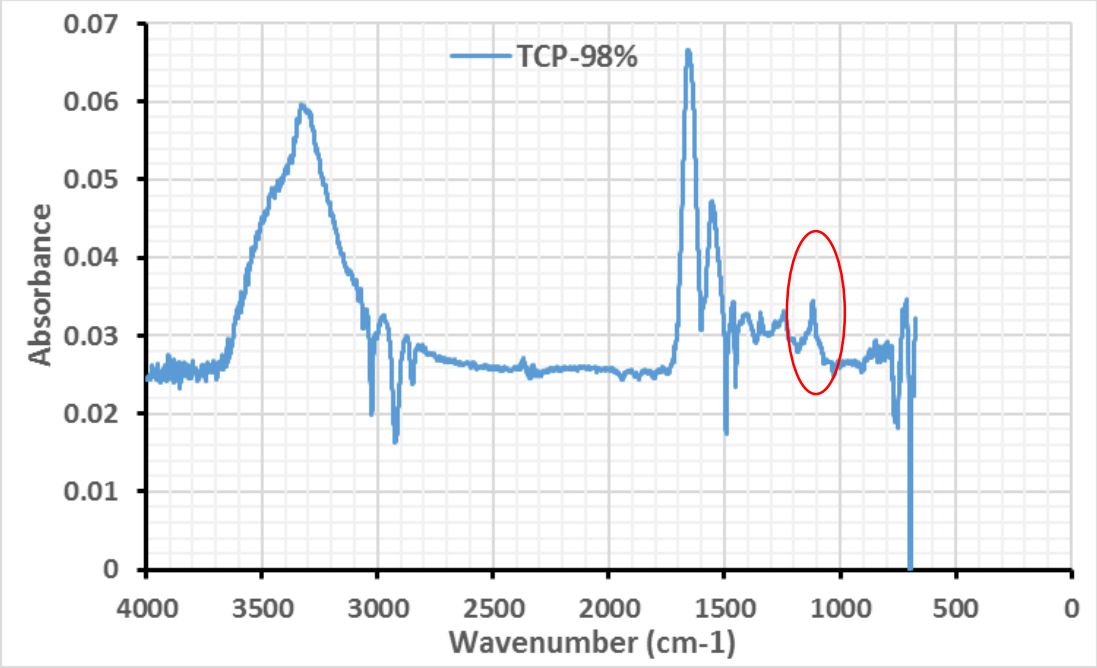

ATR-FTIR spectrum shows the characteristic peaks. Data are presented as 4-5 independent experiments conducted in duplicate. The circled peak refers to the peak of C=O stretching at 1150 cm^{-1}.

3.4.1.1.2.5 TCP surface coated with 95% gelatin

The ATR-FTIR spectrum for TCP surface coated with 95% gelatin (Figure 3.12) displayed similarity to the spectrum of 98% gelatin coating. However, the characterisation and spectrum of amide A, I and II at 3500-3200 cm $^{-1}$, 1650 cm^{-1} and 1547 cm^{-1}, respectively, were slightly decreased when compared with those generated by a coating of 98% gelatin (Figure 3.11). Furthermore, the region at 1100 cm $^{-1}$ was more

intense than in 98%, which could relate to C-O-C stretching in F127.[162-164] Overall, the ATR-FTIR results suggested that the TCP surface was coated with gelatin.

Figure 3.12 The ATR-FTIR spectrum of 95% gelatin coated TCP surface

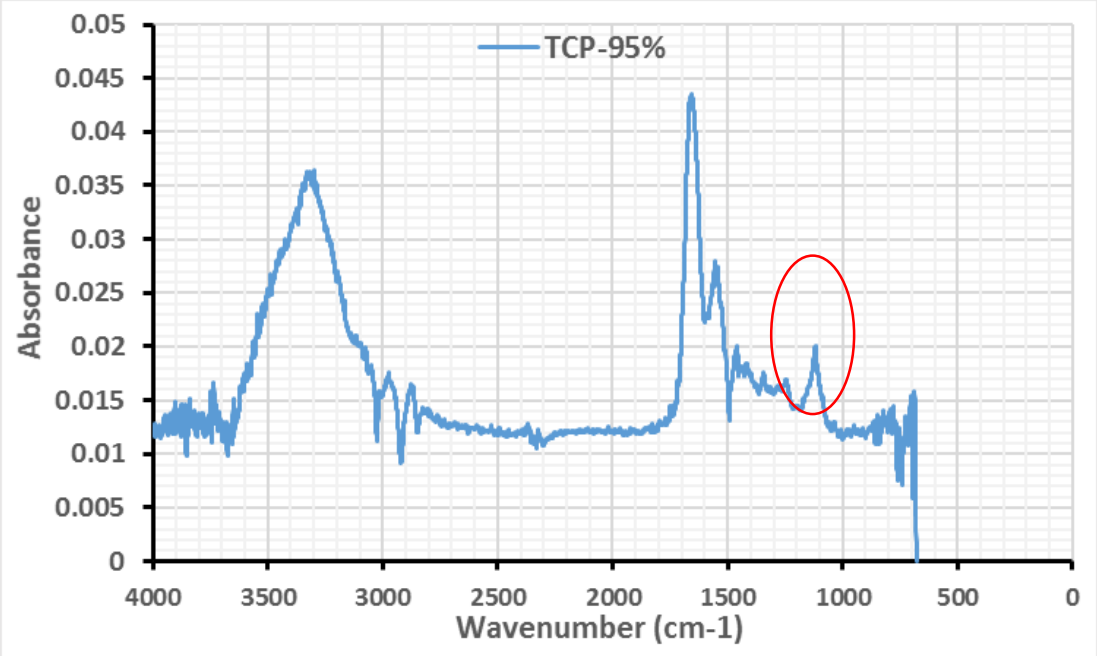

ATR-FTIR spectrum shows the characteristic peaks. Data are presented as 4-5 independent experiments conducted in duplicate. The circled peak refers to the peak of C=O stretching at 1150 cm^{-1}.

3.4.1.1.2.6 TCP surface coated with 90% gelatin

The ATR-FTIR spectrum of TCPs following coating with a solution of 90% gelatin is shown in Figure 3.13 and was largely comparable to that of TCPs coated with a 95% gelatin solution. However, the spectrum at 3500-3200 cm^{-1} for amide A, the region at 1650 cm^{-1} for amide I and the region at 1550 cm^{-1} for amide II were slightly less pronounced as the gelatin concentration was reduced. The increase in the percentage of F127 resulted in unclear spectrums for PEO or PPO.

Figure 3.13 The ATR-FTIR spectrum of 90% gelatin coated TCP surface

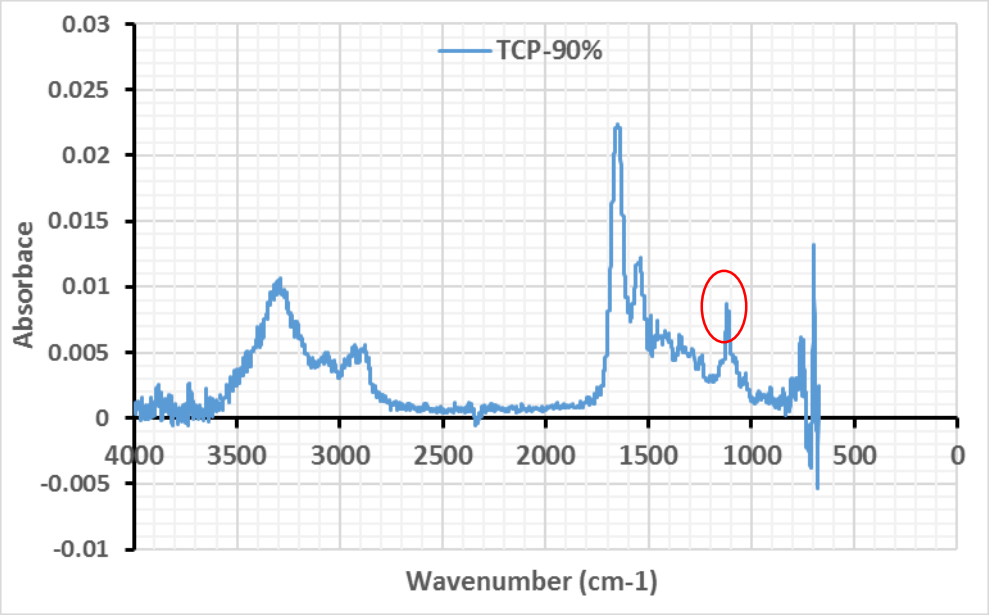

ATR-FTIR spectrum shows the characteristic peaks. Data are presented as 4-5 independent experiments conducted in duplicate. The circled peak refers to the peak of C=O stretching at 1150 cm^{-1}.

3.4.1.1.3 Effect of coating solution on SGP surface

3.4.1.1.3.1 Uncoated SGP surface

The ATR-FTIR spectra for SGP also varied according to the type of coatings but were most closely related to the spectra of TCPs as shown in Figure 3.8. Peaks at 3081 cm^{-1} - 3001 cm^{-1} were assigned to C-H aromatic stretching; 2923 cm^{-1} and 2850 cm^{-1} bands were due to CH_2 asymmetric and symmetric tension; the bands in 1600-1400 cm^{-1} were associated with arenes C=C stretch. Another sharp band at 680 cm^{-1} was for arenes C-H bending. There was a weak band around 3320 cm^{-1}, which could be the result of special surface treatment for the suspension plate (Figure 3.14).

Figure 3.14 The ATR-FTIR spectrum of uncoated SGP surface

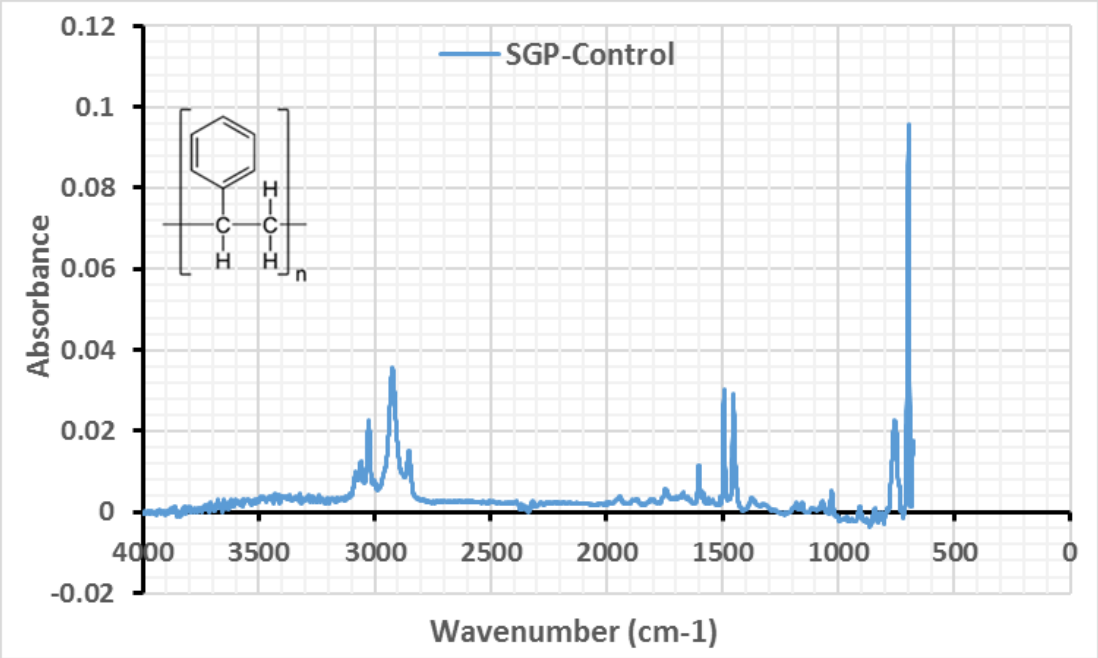

ATR-FTIR spectrum shows the characteristic peaks. Data are presented as 4-5 independent experiments conducted in duplicate.

3.4.1.1.3.2 SGP surface coated with F127

After coating the SGP surface with the F127 solution, it was seen that a clear change in the spectrum had been formed (Figure 3.15). The decoration of the F127 on the polystyrene peaks presented medium strength bands at 2980--2880 cm^{-1} which were due to CH_2 and CH_3 stretching. Another weak band at 1454 cm^{-1} was commonly related to methyl and methylene groups in PEO, PPO blockers. Furthermore, the strong band at 1100 cm^{-1} was C=O stretching. It was noticed that the characteristic bands of the uncoated plate at 3081-3001 cm^{-1} and 1601 and 1400 cm^{-1} for C=O stretching did not show clearly. These results proved that the PEO and PPO blockers have covered on the SGP surface (Figure 3.15).

Figure 3.15 The ATR-FTIR spectrum of F127 coated SGP surface

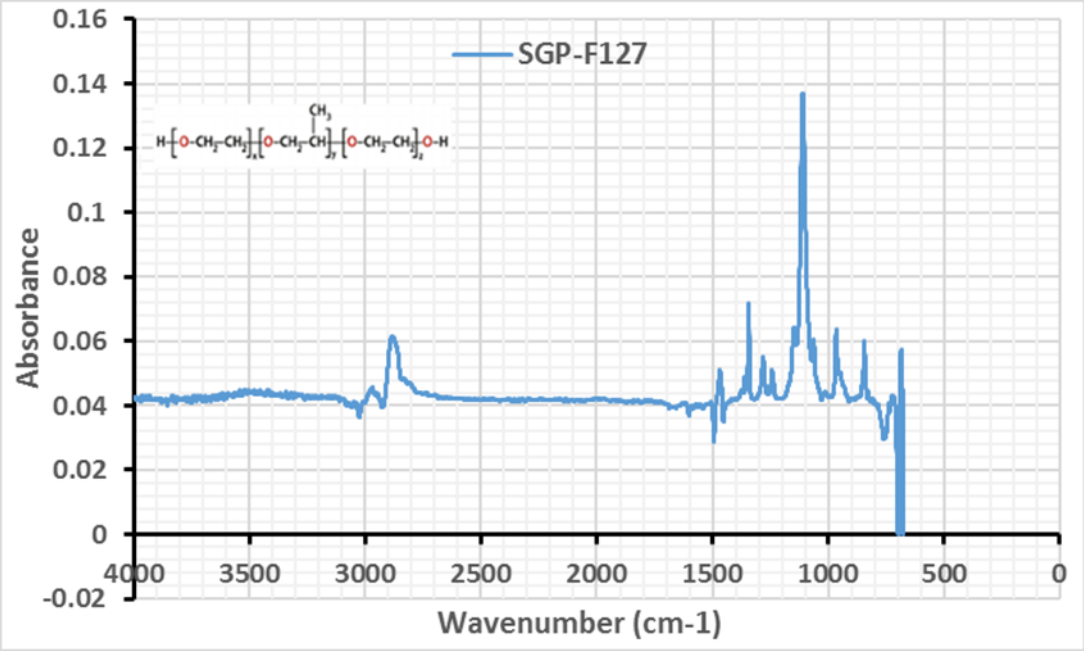

ATR-FTIR spectrum shows the characteristic peaks. Data are presented as 4-5 independent experiments conducted in duplicate.

3.4.1.1.3.3 SGP surface coated with 100% gelatin

Gelatin showed a characteristic protein ATR-FTIR spectrum (Figure 3.16). Similarly. The spectrums of gelatin-coating on the SGP surface displayed five individual band regions. The strong bands at 3500-3200 cm $^{-1}$ were for amide A, O-H and N-H stretching;[158,159] the band at 2900 cm^{-1} was for CH_2 and CH_3 stretching. The strong band at 1650 cm^{-1} was for Amide I, 1547 cm^{-1} for amide II, C=O stretching and the band at 1115 cm^{-1} for stretching C=O.[160,162] It was also observed that the characteristic bands of the uncoated plate at 3081-3001 **c**m^{-1} and 1600-1400 cm^{-1} were not observed. These results demonstrate that the gelatin has covered the SGP surface. (Figure 3.16).

Figure 3.16 The ATR-FTIR spectrum of 100% gelatin coated SGP surface

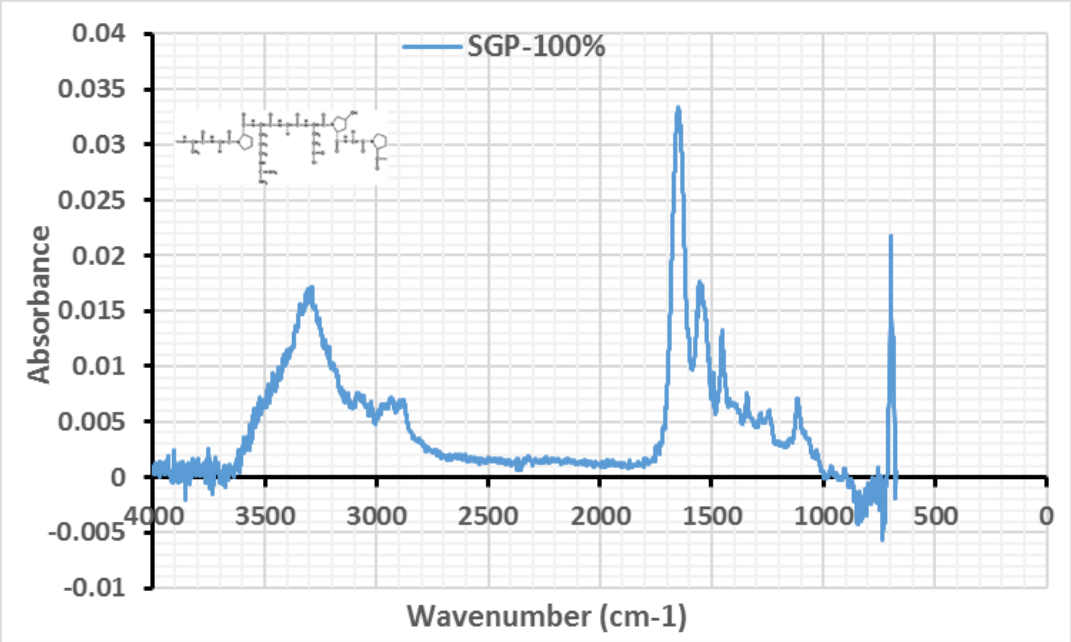

ATR-FTIR spectrum shows the characteristic peaks. Data are presented as 4-5 independent experiments conducted in duplicate.

3.4.1.1.3.4 SGP surface coated with 98% gelatin

ATR-FTIR spectrum for SGP coated with 98% gelatin solution was shown in Figure 3.17. In general, the spectrums were very similar to 100% gelatin coating (Figure 3.16). What it peaked at 3329 cm^{-1} was for Amine A, N-H stretching and O-H stretching. Also, pronounced a peak at 1639 cm^{-1} was for Amide I, C=O stretching, 1534 cm^{-1} for Amide II, N-H, and C-H vibration (Figure 3.17).

Figure 3.17 The ATR-FTIR spectrum of 98% gelatin coated SGP surface

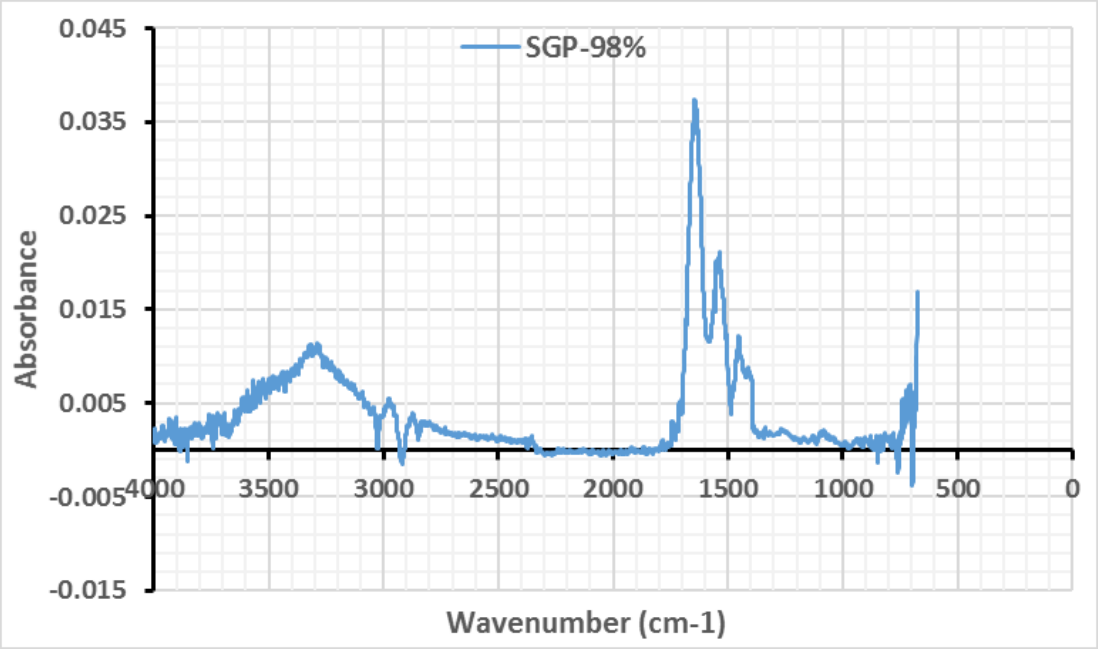

ATR-FTIR spectrum shows the characteristic peaks. Data are presented as 4-5 independent experiments conducted in duplicate.

3.4.1.1.3.5 SGP surface coated with 95% gelatin

The spectrum of surface coating with 95% gelatin (Figure 3.18) confirmed the additional difference between that of 98% gelatin coating, pure gelatin coating and F127 coating. Once more, the spectrum was very similar to gelatin coated spectrum. The characteristic and strong bands of amide A, I and II at 3200-3500 cm^{-1}, 1650 cm^{-1} and 1547 cm^{-1}, respectively, were presented clearly. However, the intensity of the three new peaks: a shoulder peak at 3100 cm^{-1} regions, a small peak at 2900 cm^{-1} region and 1400 cm^{-1} was reduced on the surface.

Figure 3.18 The ATR-FTIR spectrum of 95% gelatin coated SGP surface

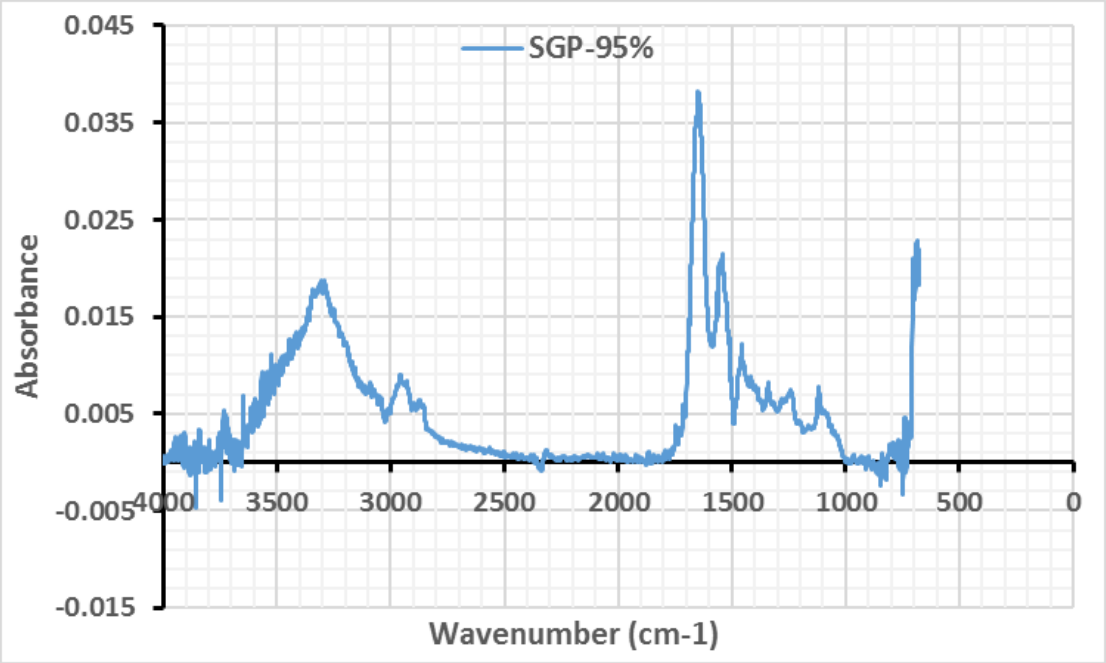

ATR-FTIR spectrum shows the characteristic peaks. Data are presented as 4-5 independent experiments conducted in duplicate.

3.4.1.1.3.6 SGP surface coated with 90% gelatin

When F127 content increased to 10% in the coating mixture, i.e. a mixing solution with 90% gelatin and 10% F127, the coated SGP surface had quite a different spectrum than the surfaces with other coating solutions. First, the intensity ratio of amide A to aimed I and II reduced in comparison to pure gelatin coated sample. Secondly, the intensity of the three new peaks: a shoulder peak at 3100 cm^{-1} regions, a small peak at 2900 cm^{-1} region and 1400 cm^{-1} became stronger and more obviously than the spectrum in 95% gelatin coated surface (Figure 3.19).

Figure 3.19 The ATR-FTIR spectrum of 90% gelatin coated SGP surface

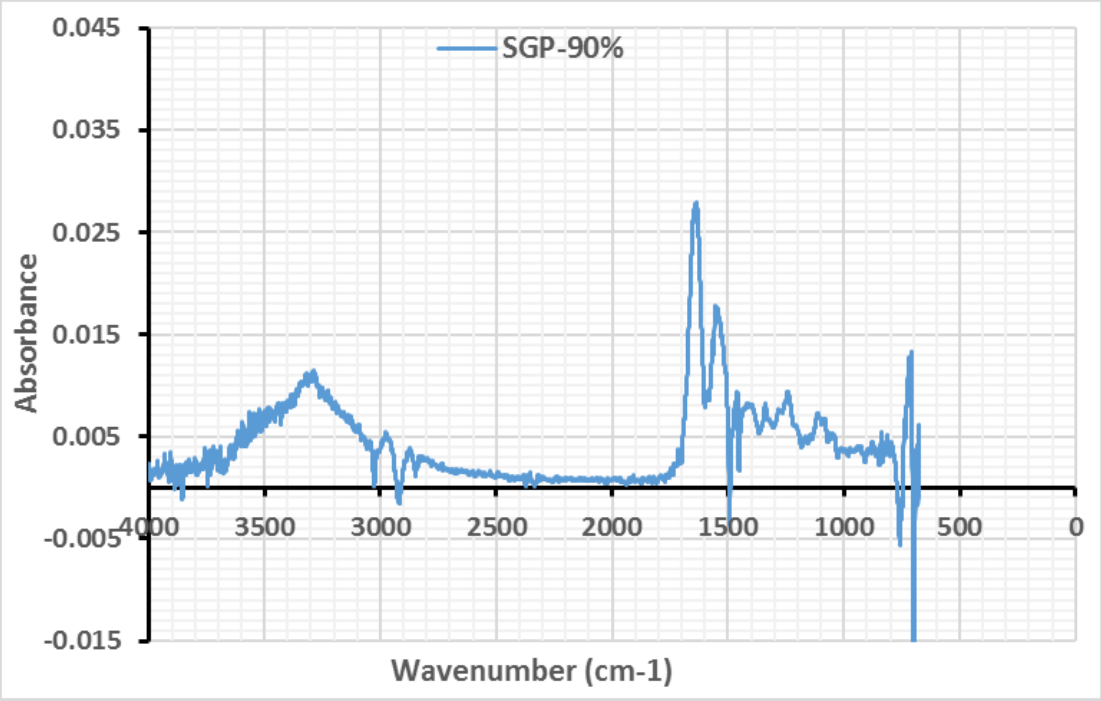

ATR-FTIR spectrum shows the characteristic peaks. Data are presented as 4-5 independent experiments conducted in duplicate.

3.4.1.2 Combinational analysis of the chemical properties of TCP, SOP and SGP plate surfaces

In order to find out the mechanisms of the coating effect on the properties of the surfaces (SOP, SGP and TCP), a combinational analysis of their FTIR spectra was undertaken. Figure 3.20 shows the ATR-FTIR spectra of uncoated surfaces of culture plates. The characteristic polystyrene spectrum was displayed for the three plates.[156] Compared with other surfaces (SGP and TCP), the aromatic C=C bending at 1700-1500 cm^{-1} was more intensity for TCP comparing to SGP. Furthermore, TCPs showed an increase in the intensity around 1150 cm^{-1}, which is flexion C-H in the plan, than in SOP. This did not appear in SGP. There was also a shoulder region around 3500-3200 cm^{-1} in TCP which did not appear clearly on other surfaces. SO, different surfaces, even uncoated, showed significant variation in their ATR-FTIR spectrum (Figure 3.20).

Figure 3.20 Comparison of ATR-FTIR spectra for uncoated surfaces (SOP, SGP and TCP)

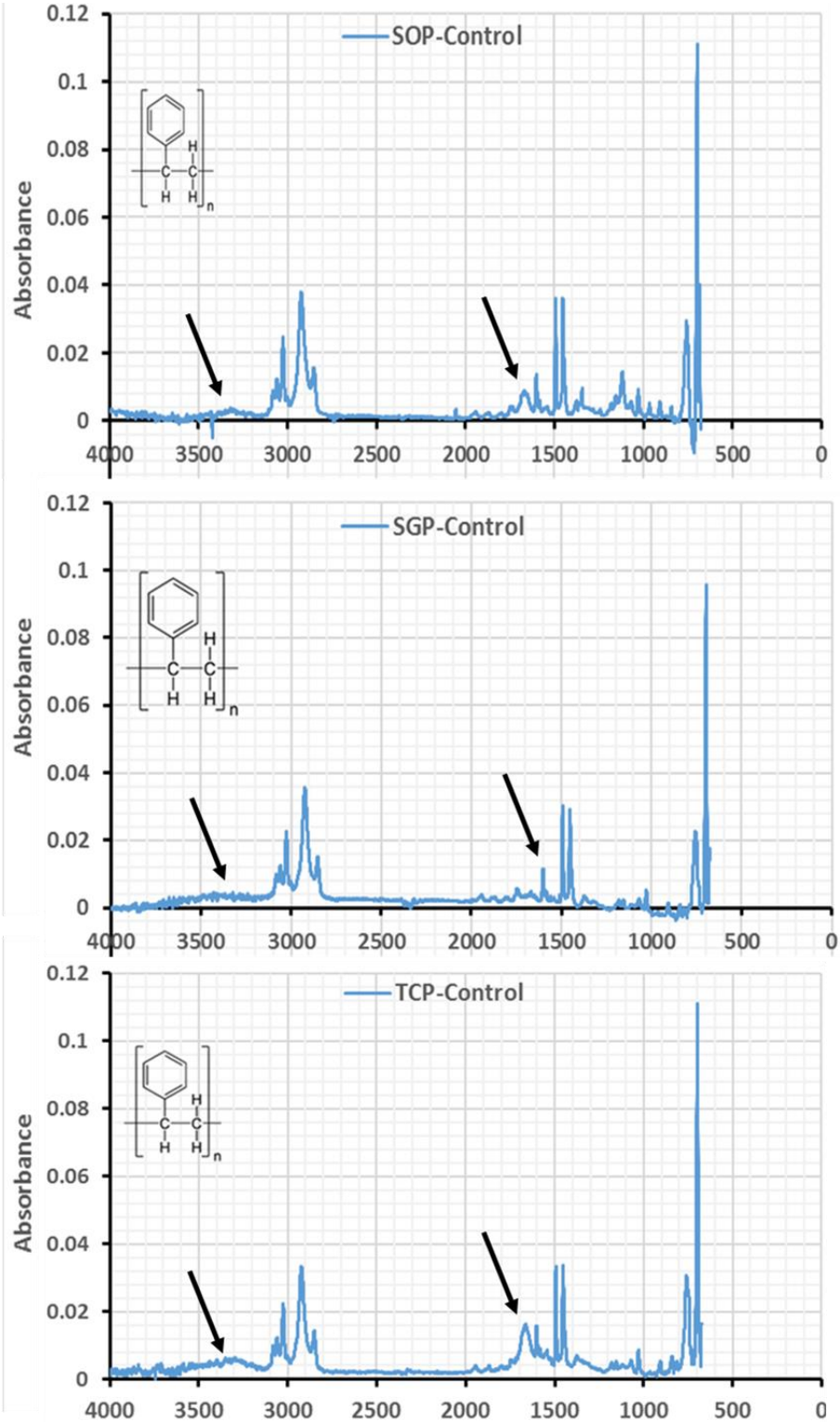

The arrows refer to amine A, N-H stretching and O-H stretching at 3500-3200 cm^{-1} and the aromatic C=C bending at 1700-1500 cm^{-1}.

3.4.1.3 Combinational analysis of single component coating solutions on SOP, TCP and SGP plate surfaces

As shown in Figure 3.21 it was seen that coating withF127 had displayed various absorbance intensity values for the three surfaces. The absorbance intensity ratio between the peak at 3060- 2900 cm^{-1} which were for CH_2 and CH_3 stretching, to peak at 1640 cm^{-1} for to C=O stretching in PEO and PPO was used for the comparison. This ratio was 2.2 for SOP surface, and the ratio was decreased slightly to 2.15 for another suspension plate (SGP), whereas, the ratio in TCP surface was declined to 1.5 (Table 3.1), indicating that the original surface property played an essential role to different IR spectra (Figure 3.21). This might result from the quantity of PEO-PPO-PEO molecules on the surfaces that might lead to different hydrophobicity on each surface. These results were close the previous studies.[165,166] The difference in the ATR-FTIR spectra of each type substrates coating with F127 was consistent with the trend of their CA value and protein staining. The CA values showed that the order of SOP < SGP < TCP after F127-coating. This might be because of higher PEO blocker adsorbed on TCP (Figure 3.24 and Figure 3.25).

Figure 3.21 Comparison of ATR-FTIR spectra for surfaces (SOP, SGP and TCP) coated with F127

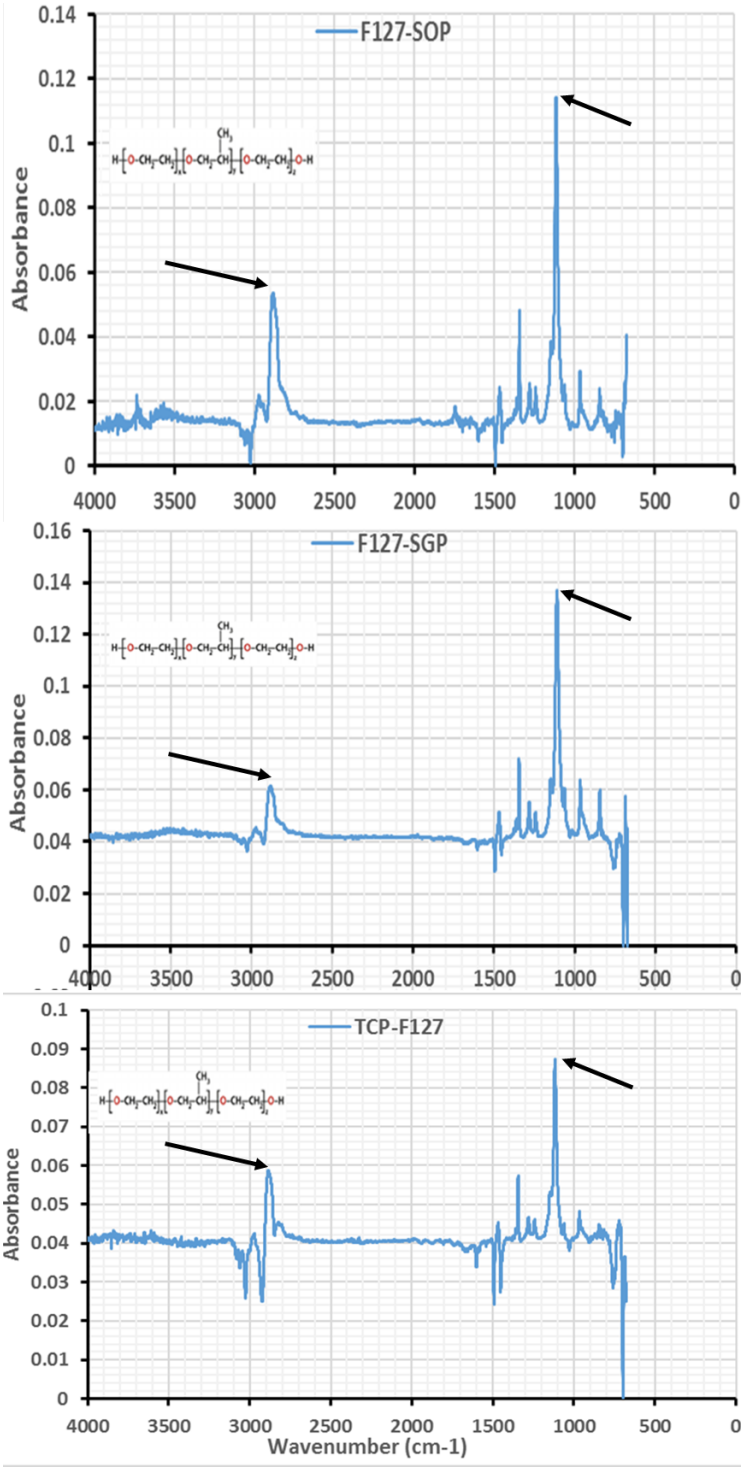

The arrows refer to bands of CH_2 and CH_3 stretching groups at 3000-2800 cm^{-1} and for C=O stretching at 1100 cm^{-1}.

Coating with 100% gelatin expressed different ATR-FTIR spectra for the surface. The major modification in the surface was shown in the absorbance intensity ratio of 3200-

2900 cm $^{-1}$ for amide A and O-H and N-H stretching, to 1650 cm^{-1} for C=O stretching. The ratio was 1.5, 2.2 and 1.5 for SOP, SGP and TCP respectively (Figure 3.22 and Table 3.1).

Figure 3.22 Comparison of ATR-FTIR spectra for surfaces (SOP, SGP and TCP) coated with 100% gelatin

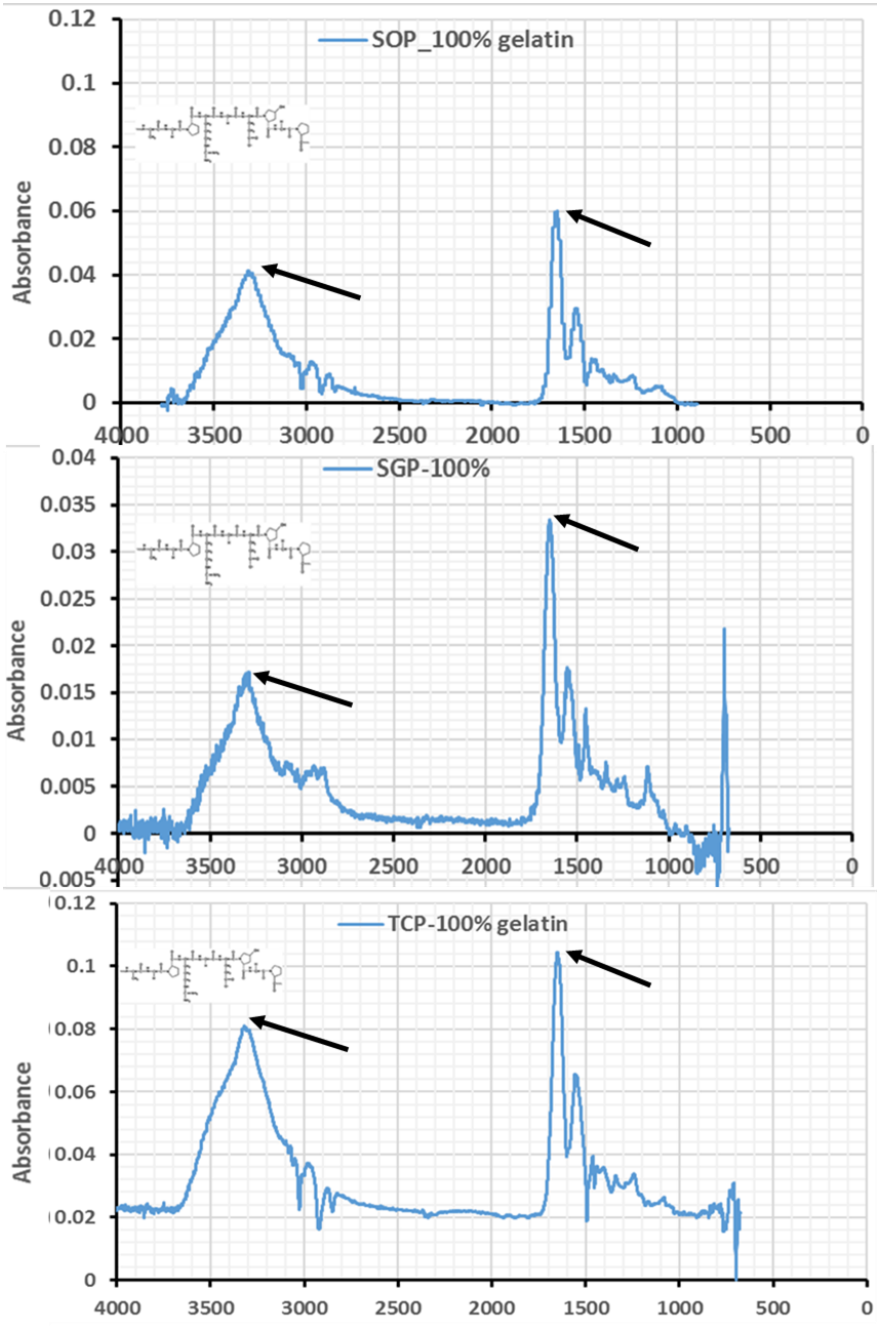

The arrows refer to bands of Amid A groups at 3200-2900 cm $^{-1}$ and for C=O at 1650 cm $^{-1}$.

Table 3.1 ATR-FTIR absorbance band ratio for SOP, SGP, and TCP surfaces coated with F127 and 100% gelatin

ATR-FTIR absorbance ratio	**SOP**		**SGP**		**TCP**	
	F127	100% gelatin	F127	100% gelatin	F127	100% gelatin
(3060- 2900 cm^{-1}) / 1640 cm^{-1}	2.2	1.5	2.15	2.2	1.5	1.5

3.4.1.4 The surface property changes depended on F127 percentage in the coating solution and the type of culture plates.

After coating of surfaces with a mixture of gelatin solution and F127 solution, the surfaces showed different ATR-FTIR spectrums depending on surface types as well as coating solution type (Figure 3.23). Two ratios of absorbance bands; 3500-3200 cm^{-1} for amide A stretching to absorbance 3000-2900 cm^{-1} for methyl stretching (Ratio 1), 1700-1600 cm^{-1} for amide I, II to absorbance 1200-1100 cm^{-1} for C-O, C-C (Ratio 2) were calculated from the spectra (Table 3.2). SOP surface was very sensitive to the percentage change of mixture components since the ratio 1 was 3 at 98% gelatin, decreased slightly to 1.25 at 95% gelatin and became 0.97 for 90% gelatin, indicating that the amount of gelatin was less on the surface compared to F127 coating.

While this phenomenon was different for TCP coating; the ratio 1 for the three coating solution was nearly the same, indicating that the surface (TCP) was covered with gelatin, and the percentage change of F127 in coating solution did not give a clear difference in the ATR results. Whereas, the SGP surface showed the similar trend of SOP surface which means that this surface also was sensitive to the difference in the coating mixture.

On the other hand, the ratio 2 produced a variety of information. The ratio 2 for SOP were 9, 3 and 0.04 for 98%, 95% and 98% respectively, indicating that PEO and PPO

molecules dominated the surface after 90% gelatin coating than other types. While, this ratio changed marginally for TCP (98%, 95%, 90% gelatin), illustrating that the PEO and PPO blockers had covered with gelatin. While the ratio 2 for SGP surface showed a large response to the coated mixture, declining from 9 in 98% coated to 3.7 but still higher than SOP, which was 0.97 (Figure 3.33 and Table 3.2). These data indicate that coated surfaces with F127, gelatin and mixtures of them led to different PEO or PPO or gelatin groups on the surface coated, which changed their hydrophobicity. The hydrophobicity and quantity of gelatin on the coating surface determined CA value and protein adsorption.(Figure 3.24 and Figure 3.25).

Figure 3.23 Comparison of ATR-FTIR spectra for SOP, SGP and TCP coated with F127 and 100% gelatin solutions in different ratios

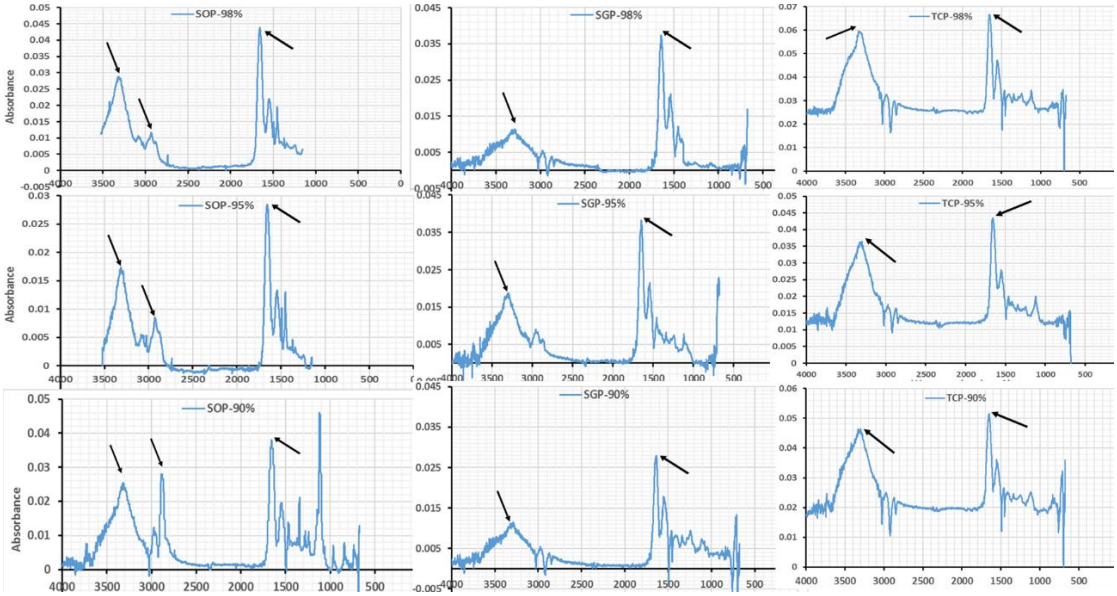

Arrows refer to ATR-FTIR absorbance selected for measurement of ratios.

Table 3.2 ATR-FTIR absorbance band ratio for SOP, SGP, and TCP surfaces coated with a mixture of F127 and gelatin solution at different ratios

	ATR-FTIR absorbance ratio	SOP			SGP			TCP		
		98%	95%	90%	98%	95%	90%	98%	95%	90%
(Ratio 1	**3500-3200)/(3000-2900)**Ratio 1	3	1.25	0.97	2.4	1.6	1	2	2.1	2.1
(Ratio 2	**(1700-1600)/(1200-1100)**	9	3	0.04	9	5.3	3.7	1.8	2.6	2.2

3.4.2 Effect of coating solution on contact angle measurements

Water contact angles of all surfaces were measured by the spreading degree of 1 µl water drop using a Hamilton Syringe. It was demonstrated that the contact angles (CA) of uncoated surfaces of the three types, TCP, SOP and SGP, were higher than all coated surfaces as shown in Figure 3.24, and 3.25. The highest CA was observed on the SOP surface, followed by the SGP surface. The lowest CA was observed on the TCP surface.

When coating with F127, gelatin and the mixture of the two components, the CA of the surfaces changed considerably and appeared to be dependent on the surface property of the original surface.

The CA values decreased dramatically ($P < 0.0001$) on surfaces coated with F127, 90% gelatin, 95% gelatin, 98% gelatin and 100% gelatin when compared with those of uncoated plates. However, the differences between the groups were not significant. The general order of CA on TCPs was as follows: Non-coated >> 100% gelatin > 98% gelatin > 95% gelatin > 90% gelatin and >100% F127. 100% gelatin coated showed the highest CA value in the TCP surfaces (Figure 3.24, and 3.25).

The coating reduced the CA on suspension surfaces, and significantly on SOP. While coating the surface with F127 showed the lowest reduction in CA. While coating with 100% gelatin resulted in a relatively large CA. Accordingly, the CA of the surface coatings was proportional to the percentage of F127. The order of CA in SOPs was as follows; 90% gelatin < 95% gelatin < 98% gelatin and <100% gelatin as shown in Figure 3.24, Figure 3.25. The CA in SGPs followed the same pattern (Figure 3.24, and Figure 3.25).

Figure 3.24 Water contact angle images for the substrates, TCP, SOP and SGP, coated with gelatin, F127and the mixture of the two components (90%, 95%, 98% of gelatin)

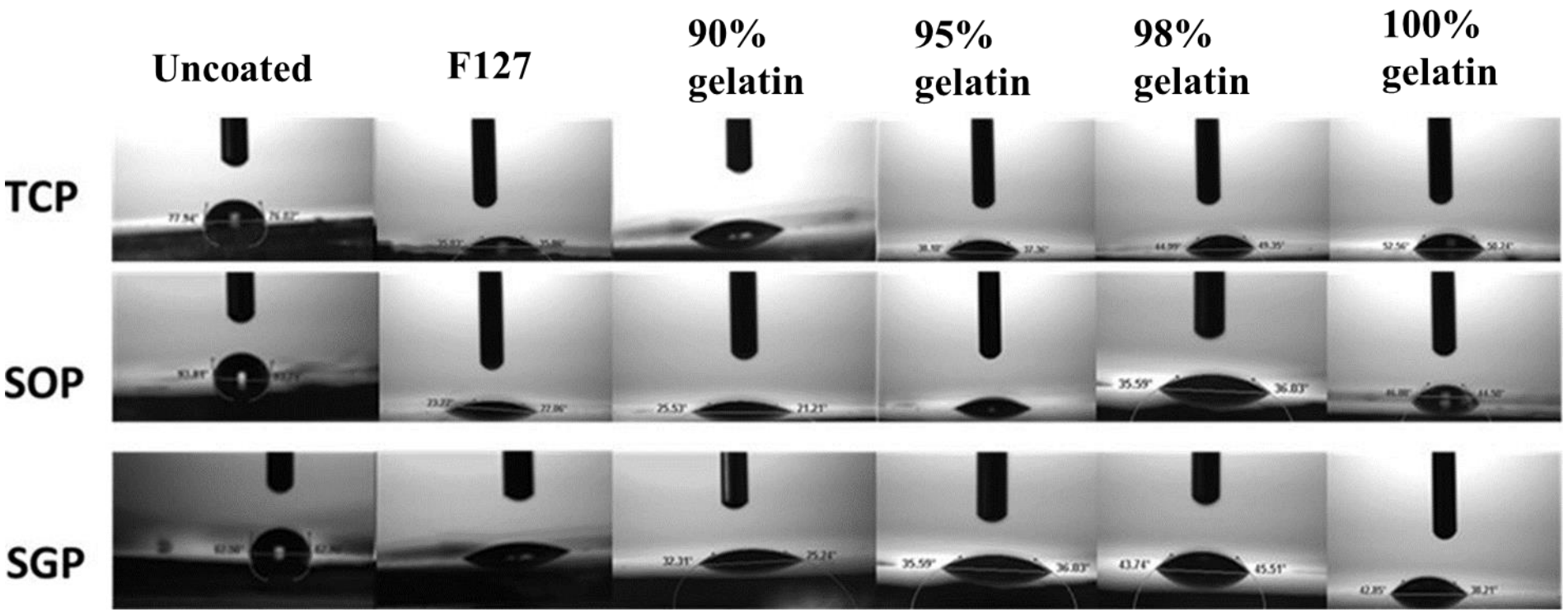

The representative-images of water contact angles on the surfaces of three type 24 well plates, TCP, SOP, SGP coating with different solutions, N=6.

Figure 3.25 Quantitative presentation of water contact angle of cell culture plates, TCP, SOP and SGP, coated with gelatin, F127 and the mixtures in comparison to uncoated surface

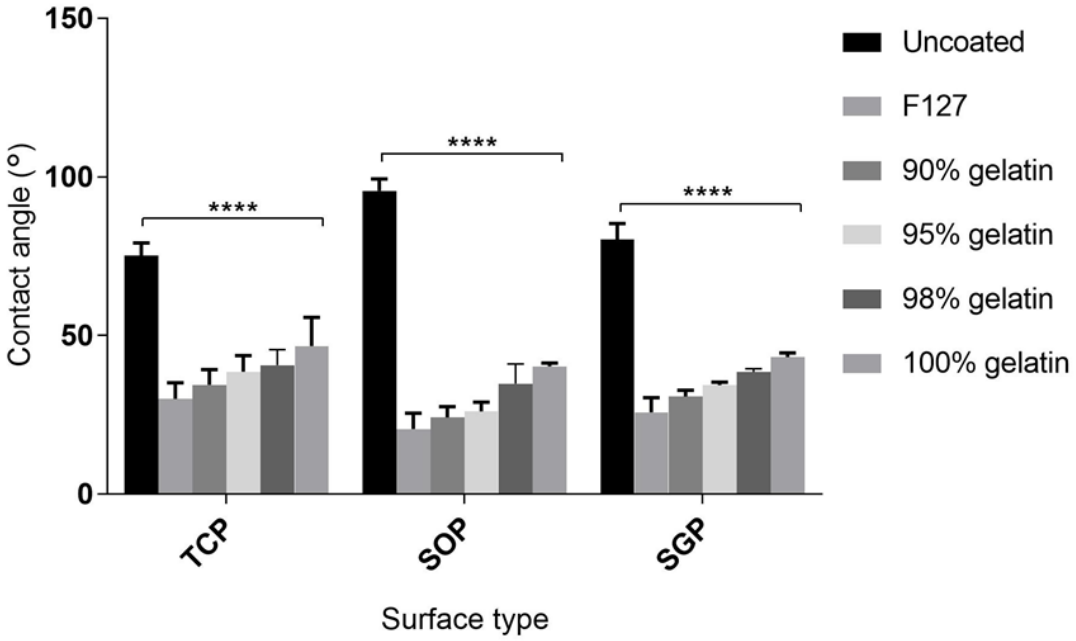

The effect of different coating types on three type surfaces of 24 well plates, TCP, SOP, SGP, on the contact angle value. Data are presented as mean ± SD from 6 independent experiments conducted in triplicate. **** < 0.0001 compared with uncoated as control.

3.4.3 Effect of coating solution on protein adsorption capacity

Protein adsorption on solid substrates depends on the properties of both the proteins and the substrate. Polarity, charge, surface energy, chemistry and morphology of protein are crucial for the interaction between surfaces and protein and the subsequent protein adsorption on it.[167] The adsorbed proteins on a surface can be visualized by Brilliant blue staining.

TCP surfaces showed more protein staining when compared with other surfaces regardless of coating type. It was observed that TCP surfaces coated with 100% gelatin displayed the highest staining and the surfaces coated with F127 showed the lowest

protein adsorption. Moreover, the staining intensity order of TCPs coated with a mixture of gelatin, and F127 was 90% <95% < 98 (Figure 3.26).

Protein adsorption on SOP surfaces was low for all groups. The uncoated surface and 100% gelatin surface showed the highest protein adsorption, although this was still poorly detected F127 coating showed no protein staining. The staining intensity order of SOPs coated with a mixture of gelatin, and F127 was 90% <95% < 98 (Figure 3.26). SGP data following a similar trend to that of SOP data (Figure 3.26).

Figure 3.26 The effect of surface coating on protein adsorption

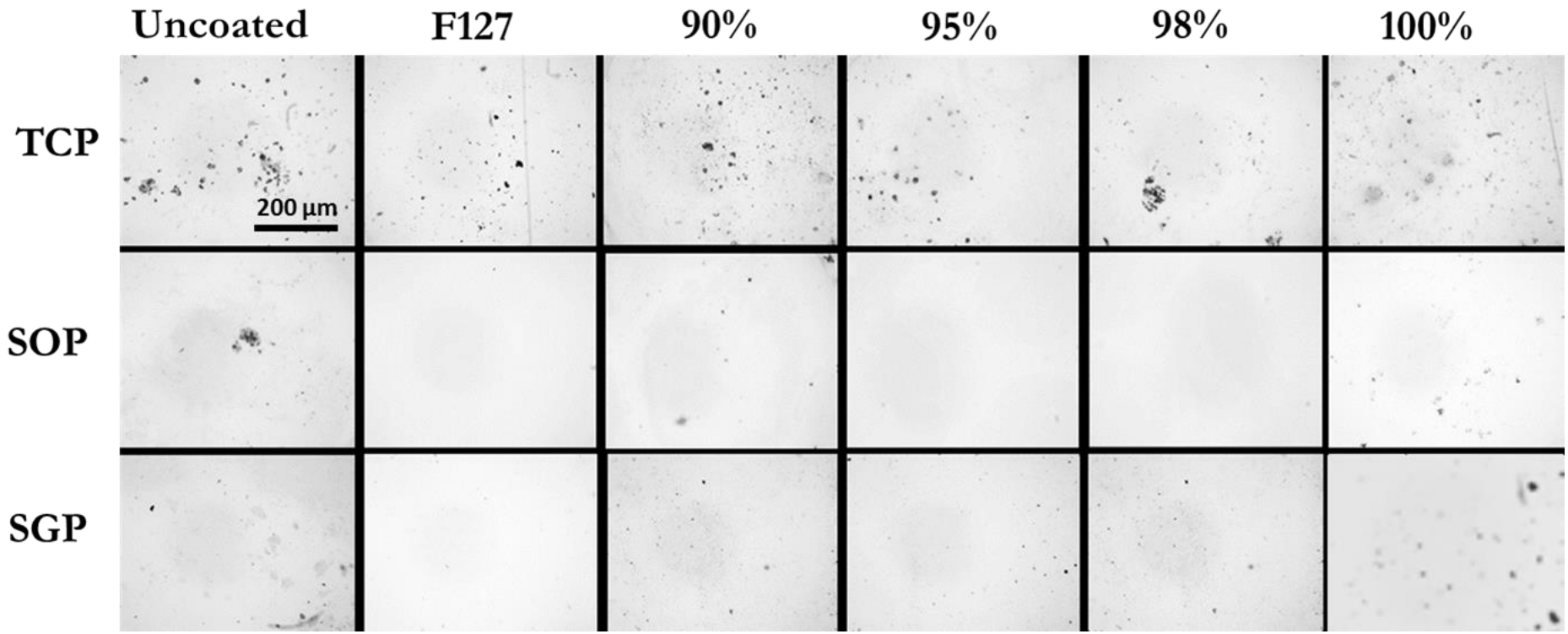

Protein adsorption was determined by staining with a Brilliant blue dye. Data were assessed by light microscopy using a 20X objective. Scale bars = 200 µm

3.4.4 Assessment of the effect of crosslinking reaction conditions and particle size on the stability of gelatin beads

3.4.4.1 The effect of crosslinking conditions on the concentration of 40 µm gelatin beads

Crosslinking with 5% glutaraldehyde

To prepare gelatin beads (GBs) of controlled size, 5% Glutaraldehyde (GA) was tested .d for crosslinking the protein.[168] GBs with a particle size < 40 µm were crosslinked with 5% GA using a vapour approach. The crosslinking reaction time varied from 1, 3, 6 and 12 hours denoted as, 1-hCL, 3-hCL. 6–hCL and 12-hCL, respectively. Figure 3.27A displays images of the crosslinked GBs incubating at 37°C for different periods. Light microscopy images showed that the CL time was crucial for swelling of the beads. GBs crosslinked for 1 hour and 3 hours showed more swelling during incubation, and they were degraded after 7 days' incubation (Figure 3.27A). GBs crosslinked with 5% GA for 6-hCL lasted until day 7 and displayed evidence of swelling (Figure 3.27A, B). However, crosslinking of GBs with 5% GA for 12 hours led to less/or non-swollen GBs.

Figure 3.27B is the quantitive presentation of the GBs size change with the incubation experiments at different reaction times (1-hCL, 3-hCL, 6–hCL and 12–hCL) with 5% GA by using ImageJ to determine the change in the size of GBs after incubation with PBS. The 40 µm GBs showed a significant increase in swelling ($P<0.05$-$P<0.0001$) following in for 1-hCL during incubation from day 1 incubation (day 1-IN) to day 7. The 40 µm GBs at 1 and 3-hCL had disappeared after 1 day incubation with PBS at 37 °C. Furthermore, long-time incubation (6-hCL or 12-CL) displayed a significant increase

(P<0.01-P<0.0001) in the swelling of 40 µm after 3 days and 7 days from the incubation with PBS GBs at 37 °C (Figure 3.27B).

Figure 3.27 Optical microscopy images of 40 µm GBs crosslinked with 5% GA for varying durations and incubated in PBS for up to one week

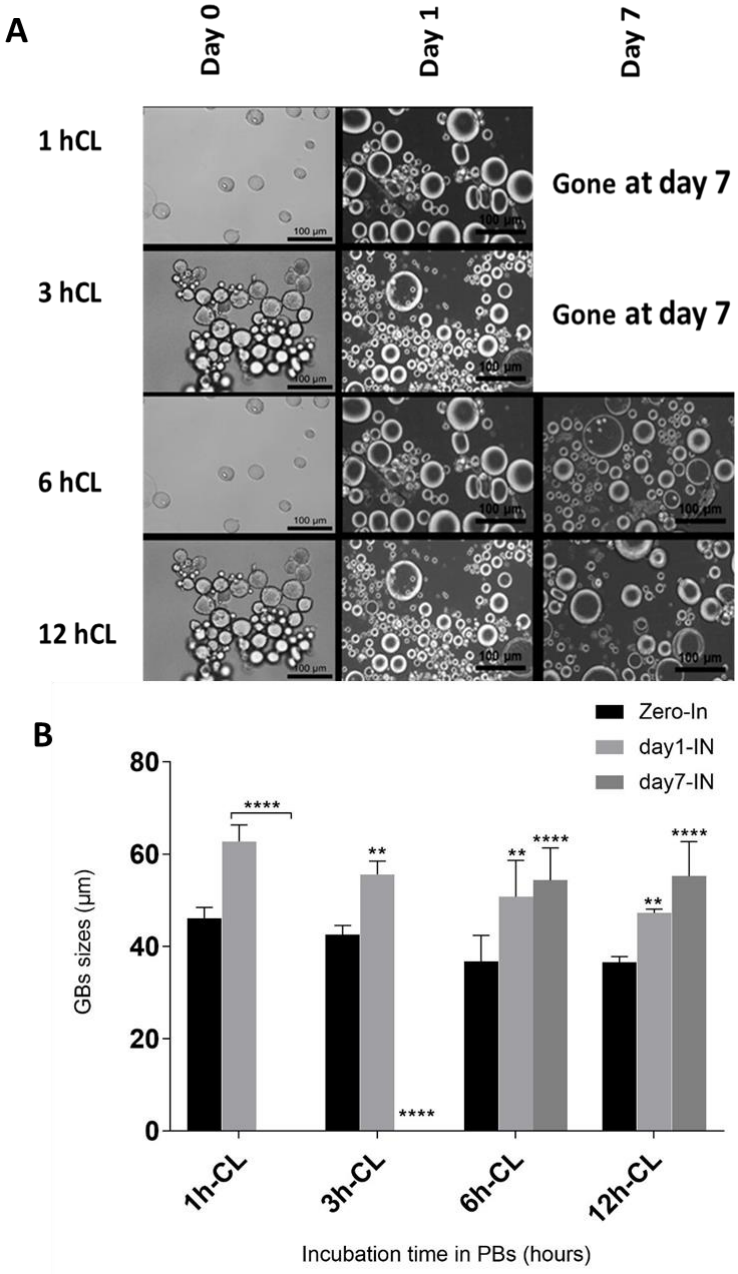

A. gelatin beads (40 µm) crosslinked (CL) with 5% GA for 1-h-CL; 3-hCL 6-hCL ,12-hCL and incubated in PBS at 37°C for 7 days. B: Quantitative calculation of the GBs sizes as a function of incubation time and crosslinking duration. Data are presented as mean ± SD from 7-8 independent experiments conducted in triplicate. **P<0.01, ***P<0.001 and ****P<0.0001 compared with GBs size at zero incubation (Zero-IN) using a 20X objective; Scale bar=100 µm.

Crosslinking with 10% glutaraldehyde

GBs (< 40 µm) were crosslinked with 10% GA using a vapour approach for 1, 3, 6, and 12 hours (1-hCL, 3-hCL, 6–hCL and 12–hCL) to check the effect of increasing the concentration of the crosslinking agent. Figure 3.28 shows images of the crosslinked GBs incubating at 37 °C for different periods. Light microscopy images show that the CL time is crucial for swelling of beads at 37 °C. GBs crosslinked for 1 hour showed more swelling during incubation time than 3–hCL even after 7 days. The GBs crosslinked with 10% GA for 3–hCL and 6–hCL showed swelling of GBs on day 7 (Figure 3.28A, B). Crosslinking of GBs with 10 % for 12 hours led to less formation of GBs or non-swelling.

Figure 3.28B is a quantitative presentation of the size change in GBs following crosslinking with 10% GA. ImageJ was used to determine the change in the size of GBs after incubation with PBS for 1-hCL, 3-hCL, 6–hCL and 12–hCL. Following 1-hCL, 40µm GBs displayed significant increases in swelling ($P<0.05$ and $P<0.0001$). Longer-term cross-linking (6-hCL or 12-hCL) did not elicit a significant increase in the swelling of 40 µm GBs for all incubation times at 37 °C. (Figure 3.28B).

Figure 3.28 Optical microscopy images of 40 µm GBs crosslinked with 10% GA for varying durations and incubated in PBS for up to one week

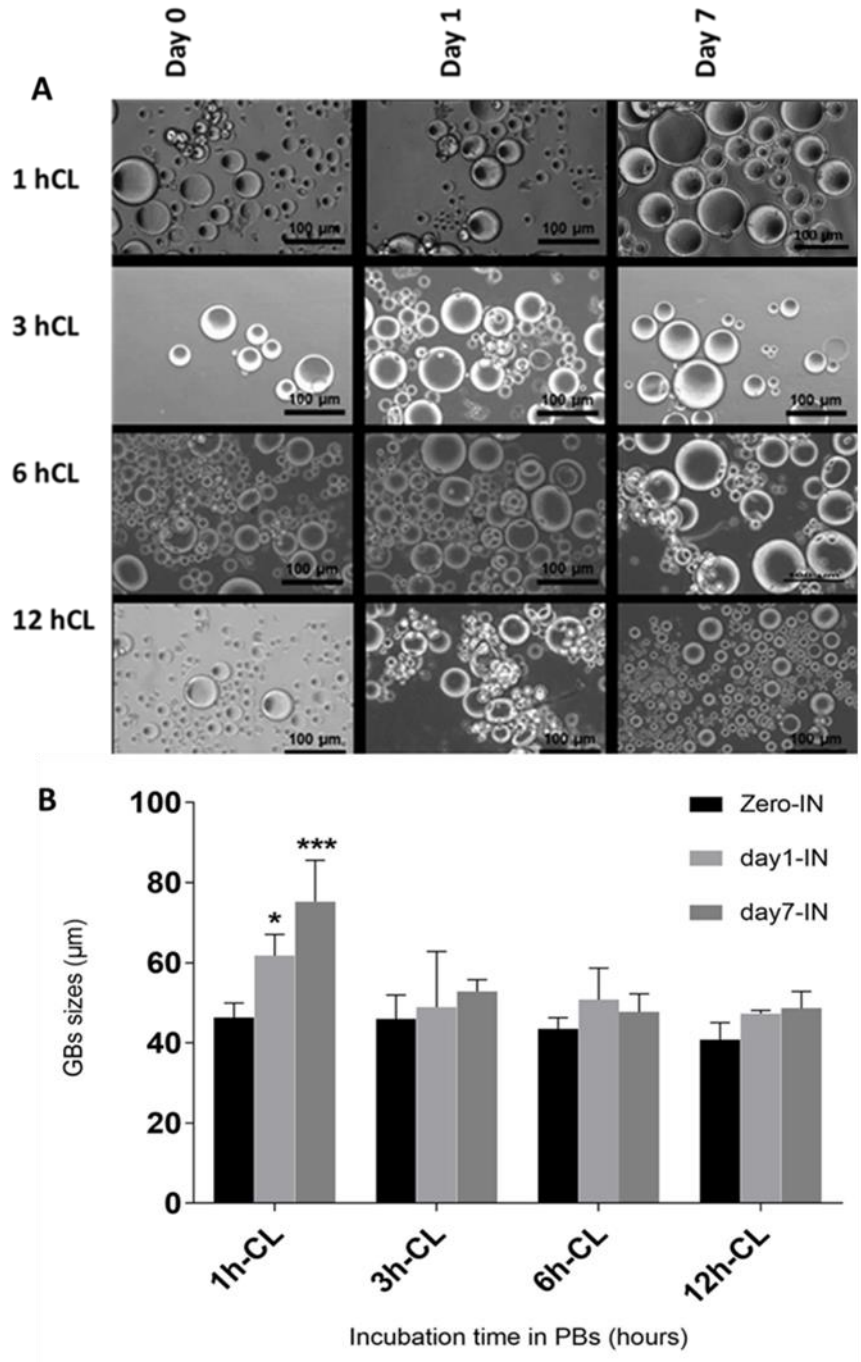

A: gelatin beads (40 µm) crosslinked with 10% GA for 1-hCL; for 3-hCL and 6-hCL for 12-hCL and incubated in PBS at 37°C for up to one week. B: Quantitative calculation of the GBs sizes as a function of incubation time and crosslinking duration. Data are presented as mean ± SD from 7-8 independent experiments conducted in triplicate. *P<0.05, ***P<0.001 compared with GBs size at Zero-IN using a 20X objective; Scale bar=100 µm.

3.4.4.2 The effect of crosslinking conditions on the generation of 30 µm gelatin beads

Crosslinking using 5% glutaraldehyde

GBs with a particle size < 30 µm were crosslinked with 5% GA using a vapour approach. The crosslinking reaction time varied from 1, 3, 6 and 12 hours denoted as, 1-hCL, 3-hCL. 6–hCL and 12-hCL respectively. Figure 3.29A displays images of the crosslinked GBs incubating at 37°C for different periods.

Figure 3.29B is a quantitative presentation of the GBs size change in the incubation experiments at different reaction times with 5% GA by using ImageJ to determine the change in the size of GBs after incubation with PBS following 1-hCL, 3-hCL, 6–hCL and 12–hCL. The 30 µm GBs crosslinked with 5% GA displayed significant swelling of GBs after 1-hCL ($P<0.05$) and following 7 days' incubation with PBS at 37 °C. Furthermore, 3-hCL also showed significant ($P<0.051$) increases in the diameter of GBs following 7 days' incubation at 37 °C. (Figure 3.29B). Other crosslinking periods (6-hCL and 12-hCL) did not display a significant change in particle size during the incubation period for 7 days (Figure 3.29B)

Figure 3.29 Optical microscopy images of 30µm GBs crosslinked with 5% GA for varying durations and incubated in PBS for up to one week.

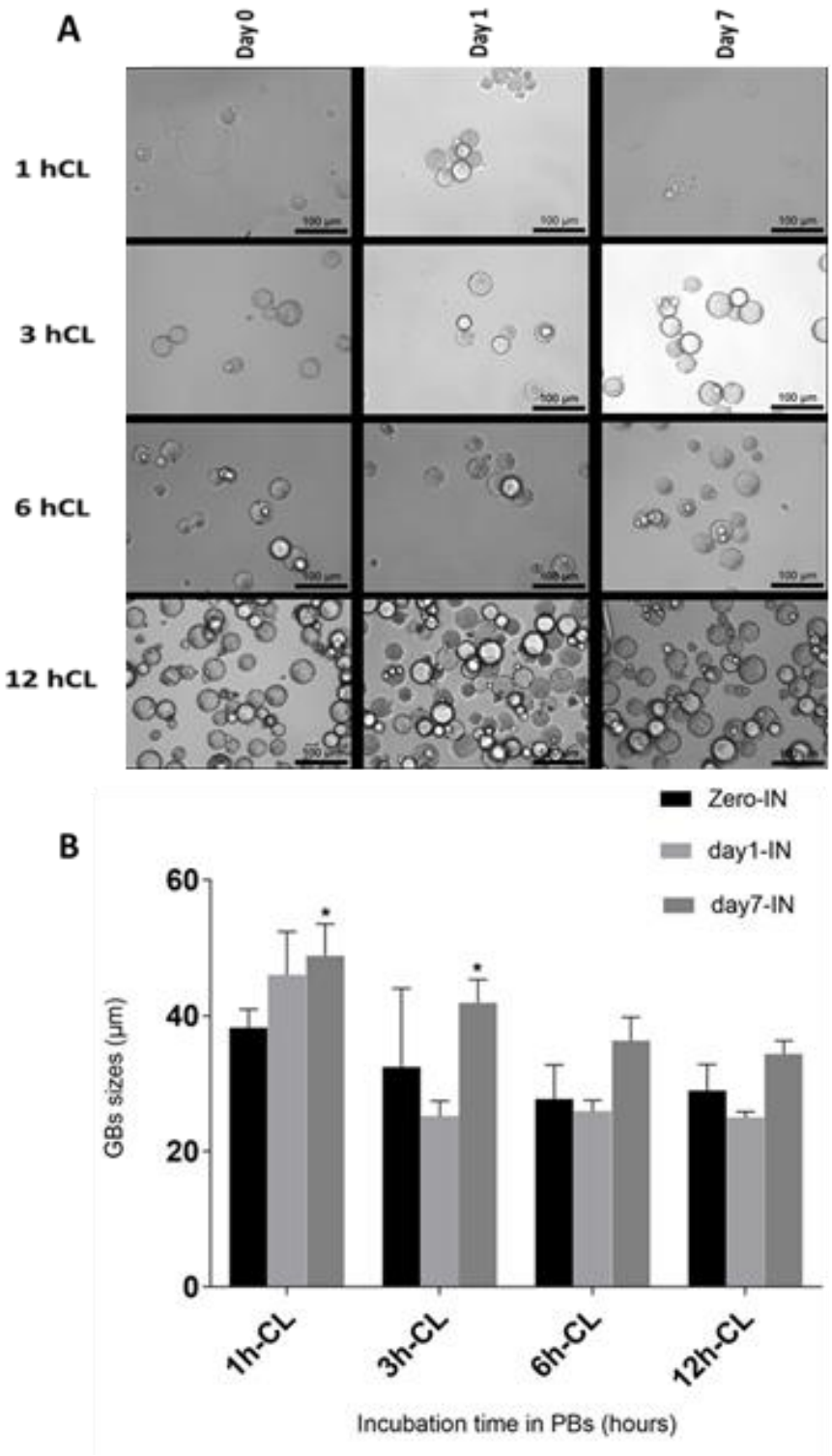

A: gelatin beads (30 µm) crosslinked with 5% GA for 1; 3 L and 12-hCL then incubated in PBS at 37°C for up to one week. B: Quantitative calculation of the GBs sizes as a function of incubation time and crosslinking duration. Data are presented as mean ± SD from 7-8 independent experiments conducted in triplicate. *P<0.05 compared with GBs size at Zero-IN using a 20X objective; Scale bar=100 µm.

Crosslinking using 10% glutaraldehyde

GBs with a particle size < 30 µm were crosslinked with 10% GA using a vapour approach. The crosslinking reaction time varied from 1, 3, 6 and 12 hours denoted as, 1-hCL, 3-hCL. 6–hCL and 12-hCL respectively. Figure 3.30A displays images of the crosslinked GBs incubating at 37°C for different periods. Light microscopy images showed that, in this instance, CL time did not affect GB swelling at any time point examined.

Figure 3.30B is a quantitative presentation of the GBs size change in the incubation experiments at different reaction times with 10% GA by using ImageJ to determine the change in the size of GBs after incubation with PBS 1-hCL, 3-hCL, 6–hCL and 12–hCL. Consistently, an effect of CL time on GB swelling was not observed**.**

Figure 3.30 Optical microscopy images of 30 µm GBs crosslinked with 10% GA for varying durations and incubated in PBS for up to one week

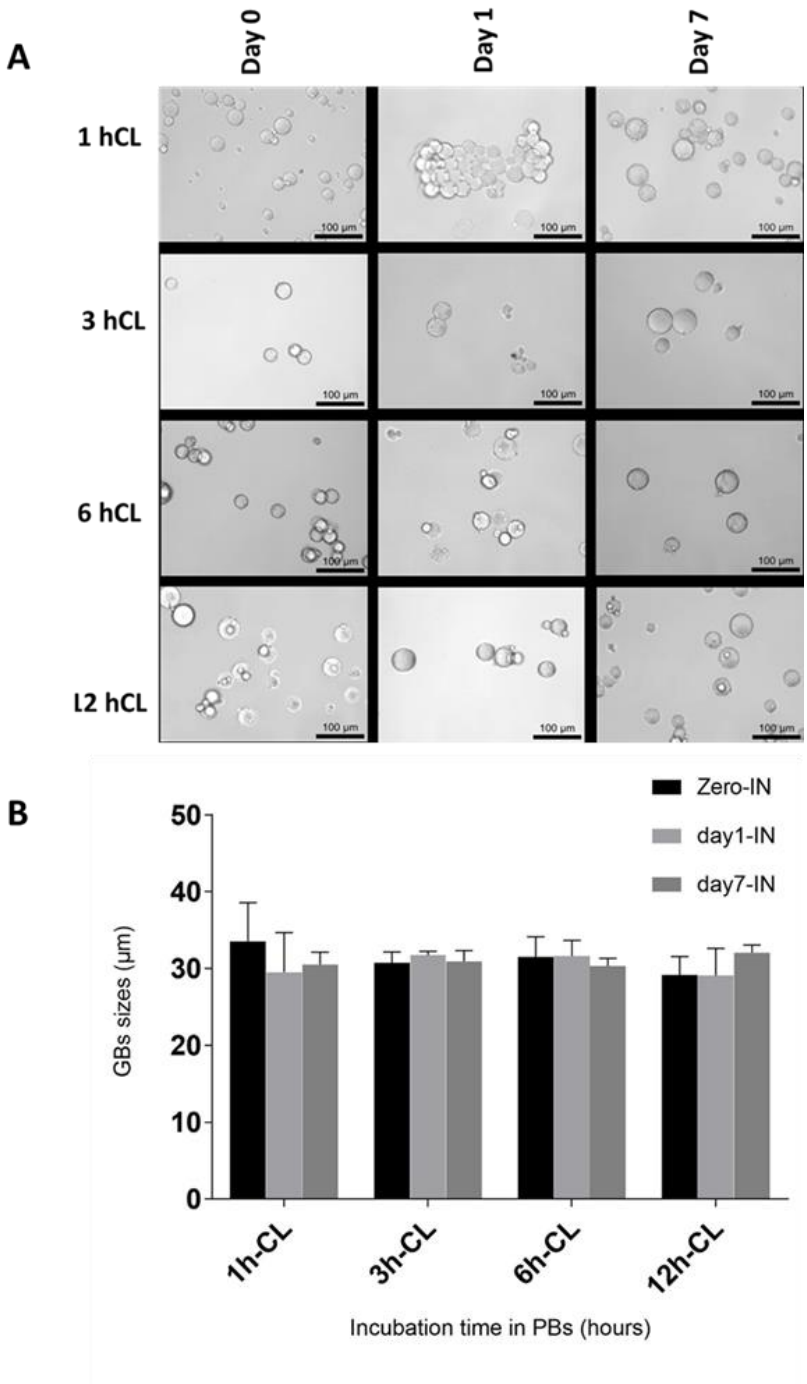

A: gelatin beads (30 µm) crosslinked with 10% GA for 1-h-CL; for 3-hCL and 6-hCL for 12-hCL and incubated in PBS at 37°C for up to one week. B: Quantitative calculation of the GBs sizes as a function of incubation time and crosslinking duration. Data are presented as mean ± SD from 7-8 independent experiments conducted in triplicate using a 20X objective; Scale bar=100 µm.

3.5 Discussion

The important issue for the study of the physiology of beta cells is to rebuild a three-dimensional structure *in vitro* known as Pseudoislets (PIs).[169] PIs present more native integrity of islets for beta cell culture enabling of biomimicking of beta cell function. The improvement of beta cells' activities in PIs is partially attributed to promoting cell-cell contact leading to enhanced glucose sensing, insulin production and insulin release.[20,94,109,170,171]

One of the most well-known technique to generate PIs is through suspension culture using ultra low attachment; which formed heterogeneous sizes of PIs and bigger PIs. Most of the PIs suffered from central necrosis after 7 days of culture. Thus, in this chapter, we developed a new coating solution strategy to generate cell culture substrates allowing better PI formation. The effects of gelatin solution, F127 and mixture of them on the surface property change when suspension and cell adhesion culture plates were being used for investigation.

3.5.1 The possible mechanisms which led the different treated surfaces

During the study, the production of our chosen suspension culture plate ceased, and we were therefore forced to choose an alternative product from the same supplier. Given this, we examined the properties of both old (SOP) and new products (SGP) and confirmed that the spectrums of ATR-FITR were different despite both products originating from the same supplier. Furthermore, a coating of the surface with gelatin solution, F127 and with a mixture of both significantly altered the hydrophobicity of culture plates, consistent with prior studies.[155,172–175] Similarly, the CA values and Protein adsorption varied according to the hydrophobicity of the surfaces which is again, consistent with the literature.[123,173,175–178] These differences may arise from the structure of F127 triblock

which is composed of two hydrophilic sides named PEO and a hydrophobic middle portion termed PPO (Scheme 3.1). Therefore, it would be expected that the PPO would attach to the surface allowing the free PEO chains to extend into the air.[179] PEO is highly hydrophilic and highly flexible chain. Once PEO molecules are on the outer surface, the surface becomes very hydrophilic and has a strong capacity to repel protein attachment.[180] Conversely, on a hydrophilic surface, such as that coated with F127, the opposite will take place. Furthermore, it has reported that the density and conformation of the adsorbed PEO-PPO-PEO vary depending on the chain length of the PEO and PPO blocks. [181] Based on these facts, we could explain the different surface properties, FTIR spectra, CA and protein adsorption capacity, after SOP, TCP, SGP plates were coated with different coating solutions and resulting change in these patterns when F127 or gelatin concentrations were increased or decreased. It is expected that F127 can reduce bimolecular adsorption[181] and for that reason, SOP surfaces coated with F127 showed the lowest CA value and no protein adsorption.

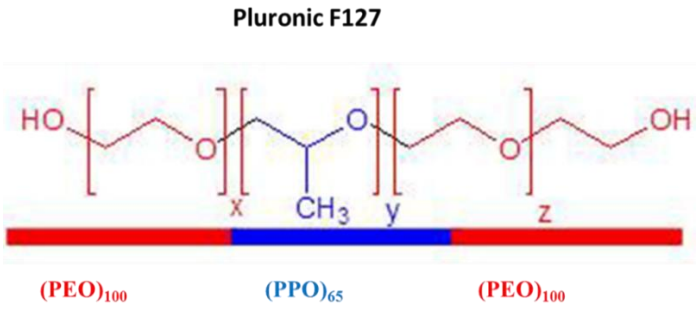

Scheme 3. 1 Illustration of the chemical composition of Pluronic F127

Coating plate with 100% gelatin is capable of making the PEO long chain anchor to the surface but allows the PPO short chain to extend into the air without the long flexible part usually observed (Scheme 3.2), and thereby might account for the poor protein adsorption

on this surface.[182] Therefore, the CA value was lowest on this surface, and protein adsorption was not observed. These surfaces response could lead to generation of aggregates with different sizes.

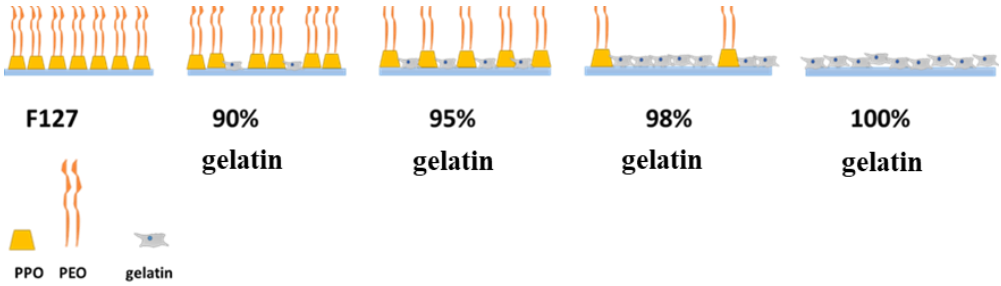

Scheme 3. 2 Illustration of the hypothesis of the molecular composition and chain morphology on SOP surface coating with a variation of F127 and gelatin percent in the solution

3.5.2 PPO block of F127 toward air and gelatin dominating the TCP plate when coating TCP plates

When the F127 solution was used to coat adhesive plates, i.e. to a hydrophilic surface, it is likely that the hydrophilic blocks were attached to the plate surface, and the hydrophobic block was toward air, i.e. in contact with the cells (Scheme 3.3). Such hydrophobic surfaces can adsorb proteins and lead to cell attachment. Nevertheless, the degree of protein adsorption was poor because the PPO block does not readily adsorb protein. For that reason, the adhesive properties of the TCP property were likely to support the ATR-FTIR spectra displaying low peak intensity related to Pluronic F127. Furthermore, the contact angle results showed more wettability when the surfaces were coated with F127, indicating that the PEO segment attached to surface and PPO sigment become toward air. The PPO segments adsorbed proteins or PPO segments easily, which led to highly hydrophilic environment producing relatively high protein adsorption and lower CA value compared to uncoated TCP surfaces (Scheme 3.3). Coating with 100%

gelatin displayed incremental increases in the intensity of the gelatin spectrum, which likely formed semi-hydrophilic surfaces, which may increase the CA value compared with the F127 coating. This is consistent with other studies.[176,178,183,185]

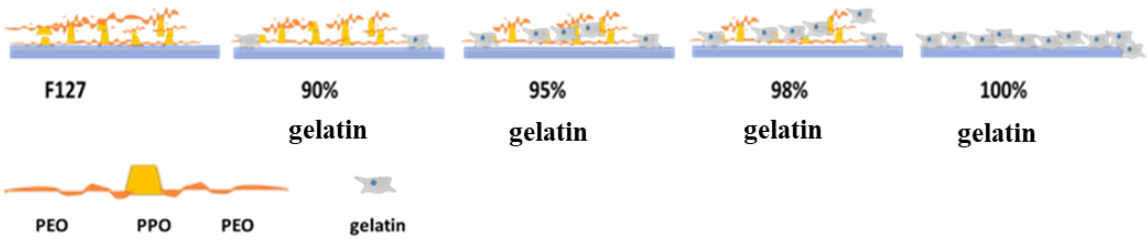

Scheme 3. 3 Illustration of the hypothesis of the molecular composition and chain morphology on TCP surface coating with a variation of F127 percent and gelatin percent in the solution

The data presented here suggest that coating solution can be used to manage cell attachment to the surface. Previous studies have proved that suspension surfaces coated with an F127 solution would prevent cell attachment[173,180,185]. Gelatin coating has previously been shown to generate a 2D monolayer.[75,180] Therefore, mixing gelatin solution and F127 may oppose gelatin's behaviour,[186] and explain the different environmental properties on the surface coated with varying percentages of F127 and gelatin. Coating with F127 solution and a mixture of F127-gelatin solutions modified culture surfaces to include highly hydrophobic lipid motifs and to limit cellular adhesion.

To date, there are few methods for conjugating protein or peptide ligands that address all of these concerns. The most promising methods so far have focused on decreasing the surface energy of the base material to which the ligand(s) of interest is immobilised.[173,187] This could reduce unwanted protein adsorption and consequently diminish nonspecific cell adhesion. Coating material with a non-ionic-hydrophilic polymer is an effective means of decreasing its surface energy. One such coating

substance is polyethylene oxide (PEO), which is well known for its ability to repel proteins and has been used to modify synthetic materials to provide them with a barrier to reduce protein adsorption.[180,188] Although producing such a PEO film at the material surface provides the necessary inert interface, it can be a challenge to modify the PEO chains further.

3.5.3 The stability of gelatin beads can be controlled precisely

Crosslinking of gelatin by GA results in the reaction of alpha-amine groups of lysine and hydroxylysine side groups with aldehydes[189]. Seldom, other groups for instance carboxyl, amide, imidazoyl or guanidine may be involved.[189,190] The amine groups present in gelatin are likely to react with aldehyde group in GA producing the relatively labile Schiff's base or aldimine (Scheme 3.4). It has been investigated that crosslinking of gelatin with GA leads to higher stability of gelatin due to imide bridge formation on the GBs surfaces[191] The aldehyde is very reactive and usually used for crosslinking of gelatin beads.[192] According to previous studies,[193,194] the aldehyde can react with an amino group of proteins like gelatin even in the presence of water, forming Schiff's base. GA has two functional (aldehyde) groups which lead to a crosslinking reaction; the aldehyde groups from GA react with amino groups of gelatin and forming stable imine bridge, and hence the GBs become insoluble even in a hot environment.[195] Also, an investigation of the reactive amino acid with aldehyde gelatin can indicate the formation of intermediate alkanolamine linkages and resulting dehydration products. Schiff's base under alkaline pH can produce stable ketoamines.[196]

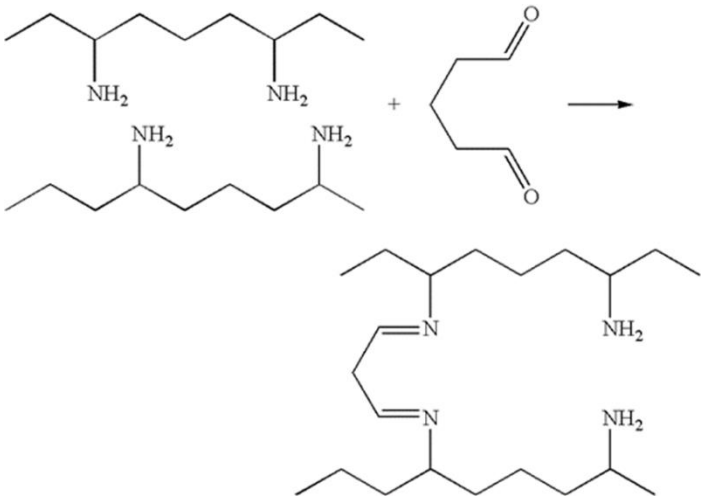

Scheme 3. 4 Crosslinking of gelatin by glutaraldehyde[188]

Generation of spherical gelatin beads requires crosslinking to decrease the solubility. GA is widely used to crosslink GBs through the formation of non-soluble networks on the beads surface. However, the use of crosslinker could lead to a toxic side effect from the remaining GA.[197] The crosslinking of GBs with GA can be done through a liquid phase or via gas phase. In this study, we used the gas phase. The crosslinked of GBs with vapour GA instead of using liquid crosslinking decreased the remaining amount of GA in gelatin beads, which would affect cell viability after the GBs are incorporated.

Crosslinking of GBs depends on the concentration of GA, which increases the number of the insoluble net on the surface of GBs and vice versa. This feature would be suitable to function as a microchannel inside PIs over a prolonged period. The 40 µm GBs displayed more swelling at 6-hCL than 30 µm at the same crosslinking time, likely due to the larger surface area leading to a greater number of unreacted amino groups. Thus, 40 µm GBs would swell more than another type. For that reason, 40 µm beads dissolved at 1-hCL and 3-hCL when treated with 5% GA.

3.6 Conclusions

Coating of surfaces with a mixture of F127 and gelatin solution altered the surface properties significantly. Previous studies have proved that F127-coated surfaces are protein resistant.[198,199] We have demonstrated for the first time that coating the surface with a mixture of F127 solution and gelatin solution can produce different ATR-FTIR spectra and a variety of CA values with different protein adsorption capacities. FTIR analysis showed that each surface had different spectra according to the type of the surface and the percentage of the mixture used for coating. Adsorption of PPO or PEO blockers of F127 on the substrate was the hydrophobicity dependent of the substrates. The CA values, and protein adsorption also agreed with FTIR results to prove that the coating with the high percentage of F127 led to lower contact angles and low protein anchored to surface.

GBs with diameters below 40 μm can be changed by crosslinking reaction with GA under gaseous phase to enhance swelling and stability over time. The swelling degree of the GBs can be controlled by GA concentration or reaction duration to be used for drug carrier and incorporated into cells. We have found that 5% GA with 6 h crosslinking is a better way to produces swelling GBs but not dissolve in short time with low GA effect by using vapour way rather than using liquid method for crosslinking of the GBs.

In the following chapters, the viability and function of PIs will be examined following the application of different coating solutions and incorporation of GB into PIs.

Chapter 4

Generation of Pseudoislets on different coating substrates

4.1 Introduction

Diabetes mellitus is one of the most common diseases globally and affects a significant number of the world's population. It has two major types: Type 1 and Type 2 diabetes mellitus (T1D and T2D respectively). T1D is characterised by the complete loss of beta cells as a consequence of the autoimmune destruction of beta cells in the pancreas,[4] which regulate insulin secretion and blood glucose homoeostasis. The islets of Langerhans are multicellular aggregates within the pancreas in which the beta cells sense changes in the blood glucose level and respond by secreting insulin.[4] The cells within the islets communicate with each other through calcium-dependent gap junctions.[21] The detrimental effects of uncontrolled blood glucose call for the development of therapeutic strategies that help in restoring insulin levels in a manner that mimics the physiological regulation of glucose.

The 3D spherical structure of the islets is crucial for their metabolic functions. Artificial reconstruction of isolated β-cells into islets of Langerhans through 3D cell aggregation has led to the generation of Pseudoislets (PIs). Although a useful model, the viability of PIs is reduced when cultured for prolonged periods of time.[75] Some of these PIs exhibit ultrastructural characteristics reminiscent of intact islets[153] and can secrete insulin in response to secretagogues with higher efficiency than monolayer cells. Hence, PIs are a perfect experimental model for studying pancreatic endocrine cell function in a 3D configuration, which mimics the islets of Langerhans.

To date, PIs have been generated on a variety of tissue culture plastics with varying success.[83] Manipulation of the substrate on which PIs are generated may assist in the generation of PIs of stable size and with enhanced viability and sustainability in comparison with traditional culture methods. Pluronic F127, a non-ionic triblock

copolymer of poly (ethylene oxide)-block-poly (propylene oxide)-block-poly (ethylene oxide) (PEO-b-PPO-b-PEO), is applied to coat the originally hydrophobic surface leading to an oil/water phase transfer.[186] Also, F127 is quite stable in culture media and displays excellent biocompatibility, and low toxicity.[186] Gelatin can be defined as heterogeneous water-soluble of hydrophobic proteins of high molecular weight present in collagen. The proteins are extracted by boiling skin, tendons, ligaments, and/or bones in water. Gelatin type A is derived from the acid-cured tissue while gelatin type B is derived from the lime-cured tissue. Collagen derived gelatin has biocompatible and biodegradable properties and is widely used in medical research.

4.2 Aim

This study sought to investigate the effect of coating tissue culture plates with varying ratios of F127 and gelatin with the view to optimising a protocol for the generation of PIs of stable size and prolonged viability, which display enhanced functionality in terms of insulin secretion.

4.3 Materials and Methods

4.3.1 Materials

Chemicals, plates types and reagents used in this chapter are listed in Chapter 2, Section 2.1.

4.3.2 PIs formation

PIs were generated on tissue culture plastic coated with different solutions as described in Chapter 2, Section 2.2.3. Static and dynamic formation of PIs were undertaken. Only the data of PIs generated through static culture and on SOP coating plates were presented in the chapter. The data of PIs formed assisted by shaking, and other types of plates were presented in the Appendix.

4.3.3 PI morphology characterisation

The morphology and size of the PIs were assessed as described in Chapter 2, Section 2.2.5.

4.3.4 PIs cell counting

A number of cells in PIs generated on surfaces coated with different coating solutions was counted by the method described in Chapter 2 Section 2.2.6.

4.3.5 Assessment of cell viability of PIs

Changes in the cellular viability of the cells were assessed using colourimetric MTT assay as outlined in Chapter 2, Section 2.2.7, and the CCK-8 assay as described in Chapter 2,

Section 2.2.8. The measurement of cytotoxicity of PIs by LDH assay was described in Chapter 2 Section 2.2.9.

4.3.6 Assessment of glucose-stimulated insulin secretion

PIs were primed with 1.1 mM glucose and then exposed to 16.7 mM glucose as outlined in Chapter 2, Section 2.2.10. Assessment of glucose-stimulated insulin secretion from the supernatants was assessed by ELISA as outlined in Chapter 2, Section 2.2.10.

4.3.7 Quantitative Polymerase Chain Reaction

The expression of Cx36, GLUT2 and Insulin mRNA were assessed by qPCR as described in Chapter 2, Section 2.2.11 Briefly, total RNA was extracted and a one-step qPCR reaction conducted as outlined in Section 2.2.12.

4.3.8 Immunological staining

The expression and localisation of Cx36, GLUT2 and Insulin protein was assessed by immunocytochemistry as outlined in Chapter 2, Section 2.2.13

4.3.9 Western blotting

The expression of Cx36, GLUT2 and Insulin were additionally assessed using Western blotting as described in Chapter 2, Section 2.2.14.

4.3.10 Oxygen expression

The expression of oxygen from PIs grown on different coating solutions and coating types were assessed using the PA2 probe, as described in Chapter 2, Section 2.2.15.

4.4 Results

4.4.1 Morphology of the PIs

Light microscopy was used to assess the morphology of BRIN-BD11 cells cultured on SOP with different coating solutions and at different seeding densities after day 3 and day 7. The coated surfaces with 90%, 95%, 98%, 100% gelatin were denoted as 90%, 95%, 98%, 100% respectively. The two negative controls, non-coated TCP and SOP were denoted as Adhesive and Uncoated respectively. The positive control, the ultra-low attachment plate was denoted as ULA. The 100% F127 coated was denoted as F127. As shown in Figure 4.1 and Figure 4.2, cells were grown on adhesive surfaces and uncoated surfaces, anchored to the surface and formed a 2D monolayer at day 3 and day 7 regardless of the starting seeding density. Furthermore, cells cultured on plates coated with 100% gelatin solution also formed a 2D monolayer. However, PIs were successfully generated using F127 as a coating solution (Figure 4.1 and Figure 4.2). In this instance though, there was little apparent difference between the seeding densities, and therefore, a combination of gelatin and F127 was used for further experiments as indicated in Figure 4.1 and Figure 4.2. PIs generated on 90% gelatin were larger than those generated in 95% gelatin, which in turn were larger than those generated in 98% gelatin. Furthermore, PIs generated in 98% gelatin appeared more homogeneous in size (Figure 4.1 and Figure 4.2). PIs generated on commercial ULA varied largely in size and morphology.

Figure 4.1 PI morphology with cell seeding density 8,000 cells/well grown on the substrates coating with different solutions.

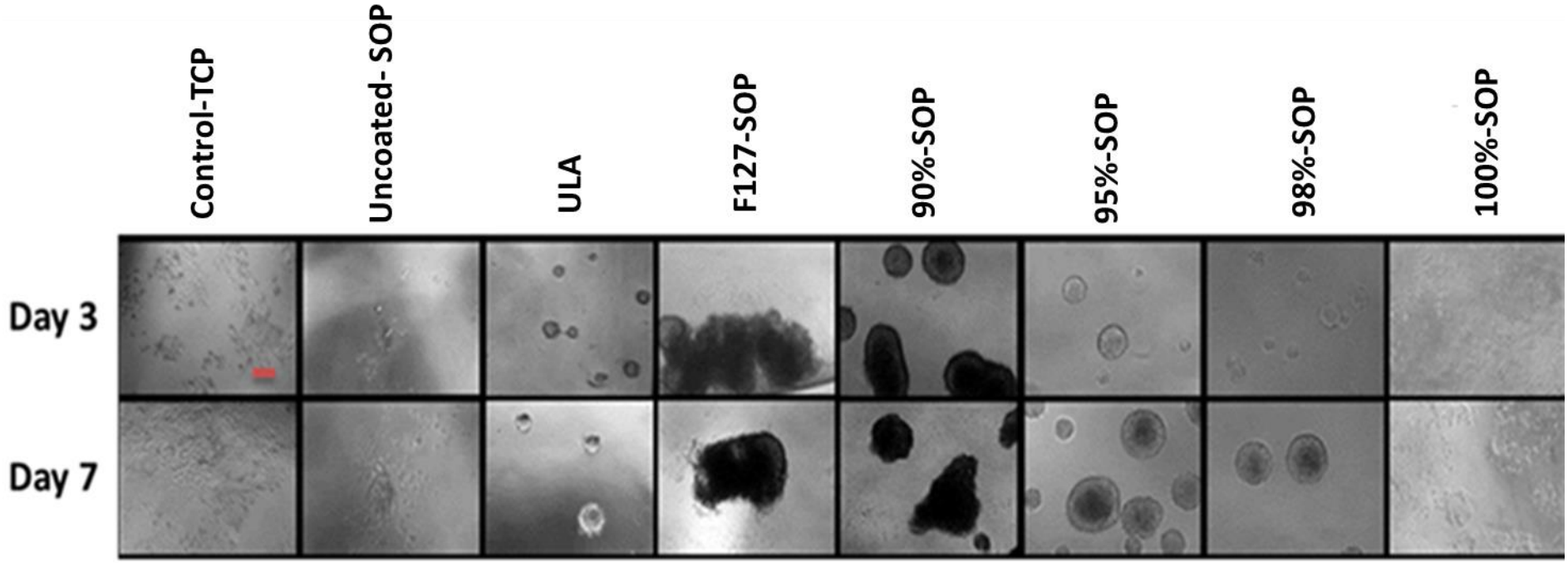

The effect of different coating solutions on the PI formation and morphology assessed by light microscopy (using a x10 objective) over 7 days culture. BRIN-BD11 cells were seeded at 8,000 cells/well. Scale bars = 200 µm.

Figure 4.2 PI morphology with cell seeding density 32,000 cells/well grown on the substrates coating with different coating solutions

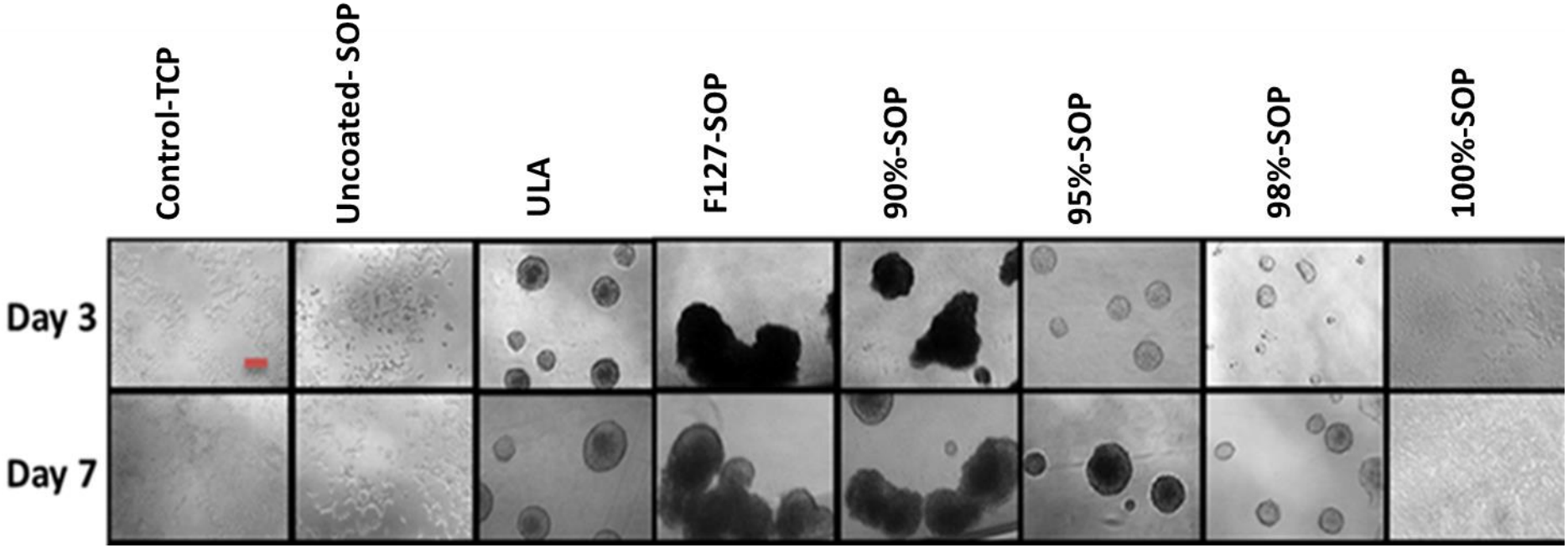

The effect of different coating solutions on the PI formation and morphology assessed by light microscopy (using a x10 objective) over 7 days culture. BRIN-BD11 cells were 32,000 cells/well. Scale bars = 200 µm.

4.4.2 Effect of coating solutions on the number of PIs

Cells were seeded onto 96 well plates treated with different coating solutions as indicated in Table 4.1 at two cell densities (8,000 cells/well and 32,000 cells/well). The number of PIs formed in each well varied significantly according to the coating solution used. Overall, the number of PIs generated in wells coated with a solution of F127 alone was the lowest (mean of 3-4 PIs). Furthermore, there was no obvious increase in the mean PI number between wells seeded at 8,000 cells/well and 32,000 cells/well (Table 4.1).

Table 4.1 Mean number of PIs per well at day 7

Type / Density	ULA	F127	90%	95%	98%
8,000 cells/well	30 ± 1	3 ± 1	8 ± 2	20 ± 3	30 ± 4
32,000 cells/well	45± 5	4 ± 1	10 ± 1	30 ± 4	38 ± 5

BRIN-BD11 cells were seeded at 8,000 cells/well, and 32,000 cells/well, and the effect of different coating solutions on the mean number of PIs formed in each well assessed. Data are presented as mean ± SD (n= 4).

4.4.3 Effect of coating solutions on PI diameter

The effect of the coating solution on the mean diameter of PIs was assessed after 3 and 7 days of culture and is shown in Figure 4.3 and Figure 4.4. In all instances, the largest PIs were observed when tissue culture plastic was coated with a solution of F127 alone. PIs grown on a solution of F127 alone were significantly larger ($P<0.0001$) than PIs generated on uncoated ultra-low attachment (ULA) plates regardless of seeding density or the number of days in culture (Figure 4.3 and Figure 4.4)

PIs generated on surfaces coated with a mixture of F127 and gelatin decreased in diameter as the percentage of gelatin increased. Again, this was independent of the starting seeding density or the number of days in culture (Figure 4.3 and Figure 4.4.). In the presence of 90% gelatin, the diameter of PIs was significantly greater than that of PIs grown on untreated ULA plates after 3 and 7 days in culture regardless of the starting seeding density was 8,000 cells/well ($P<0.001$; Figure 4.3A, B) or 32,000 cells/well ($P<0.01$; Figure 4.4A, B). Similar observations were recorded in the presence of 95% gelatin ($P<0.05$; Figure 4.3A, B). When the percentage of gelatin was increased to 98%, a significant difference in PI size over PIs grown on ULA plates was no longer observed (Figure 4.3 and Figure 4.4.).

Figure 4.3 Effect of the coating solutions on PI size for cell seeding density 8,000 cells/well.

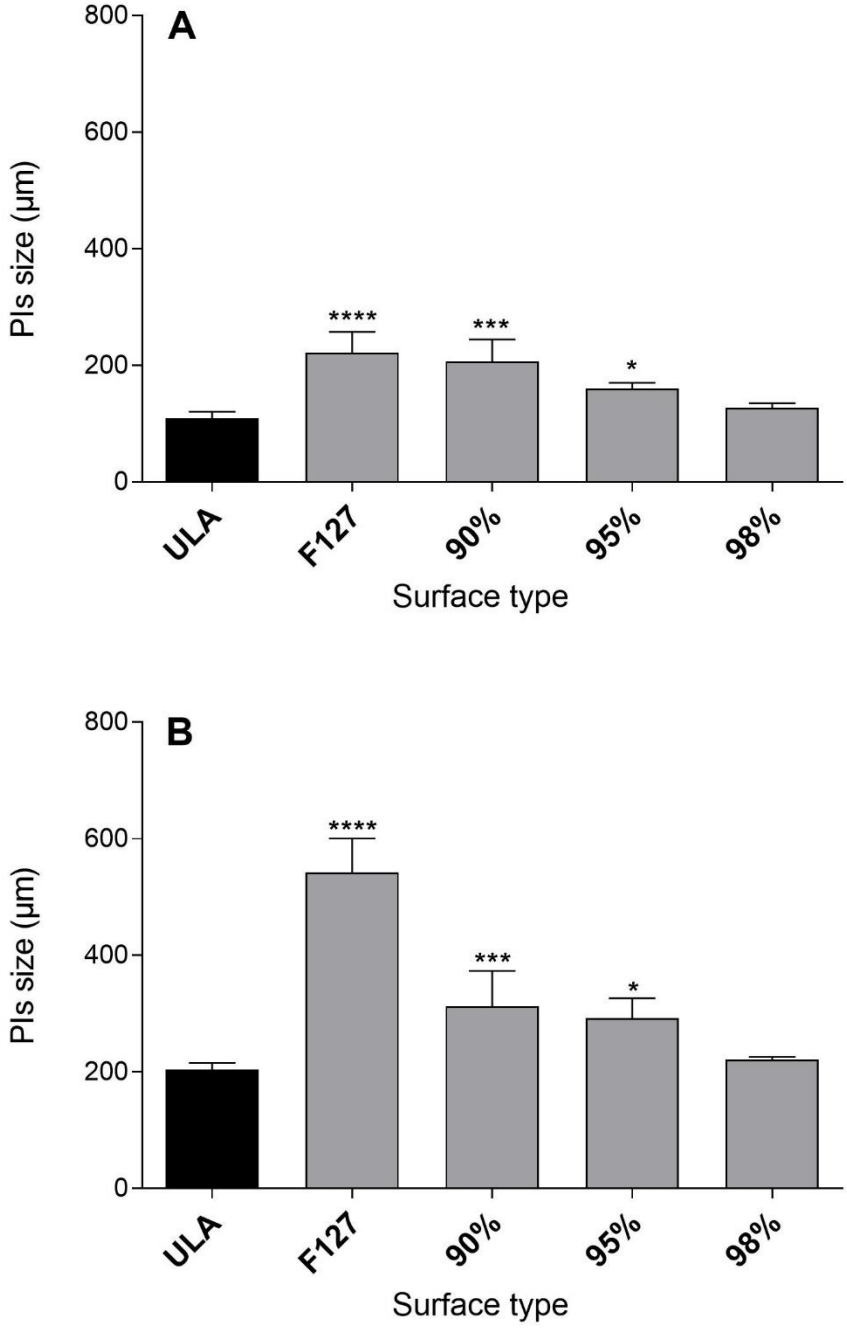

BRIN-BD11 cells were seeded at densities of 8,000 cells/well and the impact of the coating solution on PI size assessed after 3 days (**A**) and for 7 days (**B**). Data are presented as mean ± SD from 4-5 independent experiments conducted in triplicate. *P<0.05 ***P<0.001 and ****P<0.0001 compared with PIs generated on Ultra-low attachment (ULA) plates.

Figure 4.4 Effect of the coating solutions on PI size for cell seeding density 32,000 cells/well

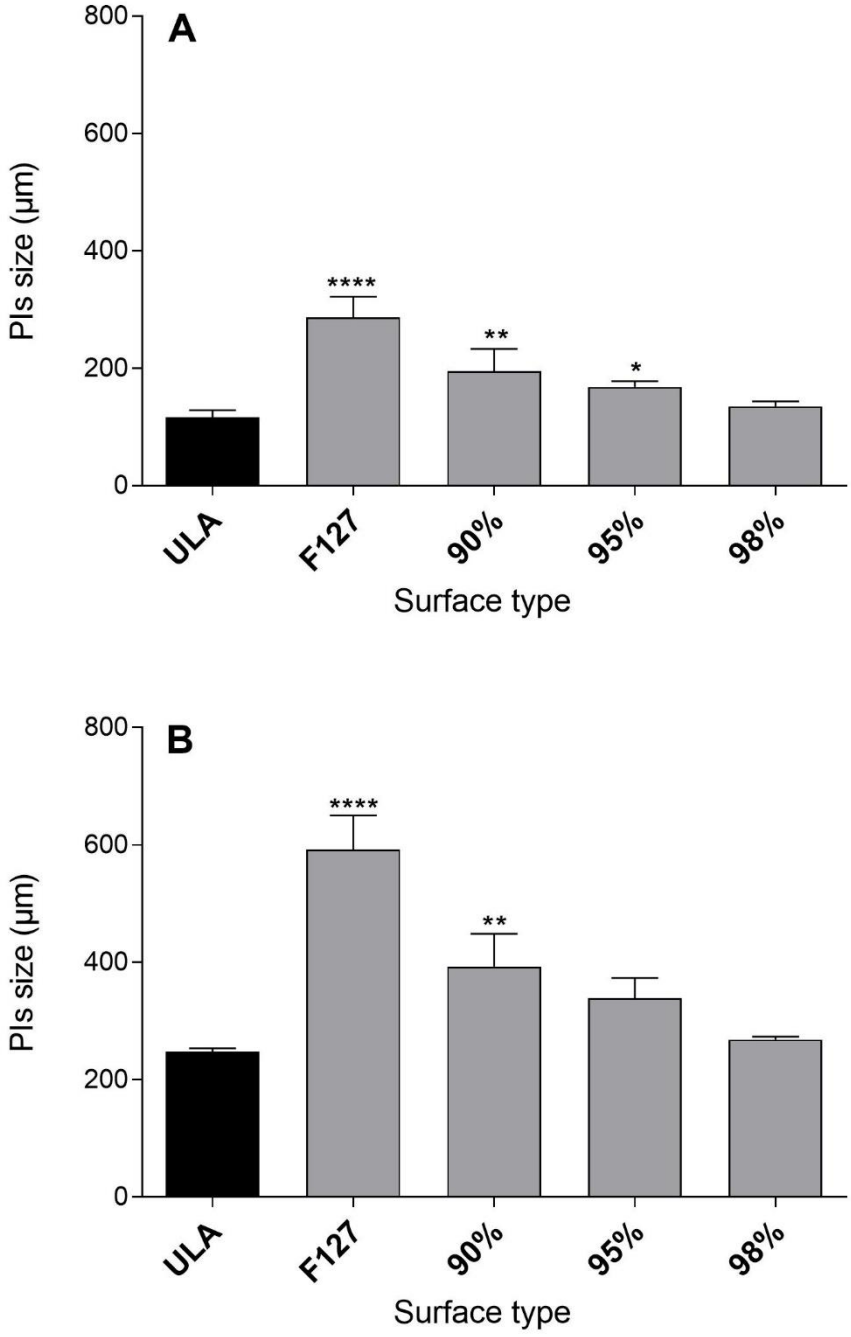

BRIN-BD11 cells were seeded at densities of 32,000 cells/well, and the impact of the coating solution on PI size assessed after 3 days (**A**) and for 7 days (**B**). Data are presented as mean ± SD from 4-5 independent experiments conducted in triplicate. *P<0.05 and **P<0.01 and ****P<0.0001 compared with PIs generated on Ultra-low attachment (ULA) plates.

4.4.4 Effect of coating solutions on the number of cells within PIs

The effect of the coating solution on the mean cell number of PIs was assessed after 3 and 7 days and is shown in Figure 4.5 and Figure 4.6. The number of cell growing on different surfaces was measured (after dissociation the PIs with HBSS free of calcium) using automated cell accounted with Trypan blue.

When the seeding density of 8,000 cells/well was used, a significant higher ($P<0.01$) in cell number was observed on the surface of an adhesive plate; and a significantly lower ($P<0.01$) in PIs formed on the surface coated with F127 at day 3 compared with cell number formed on ULA (Figure 4.5A). At day 7, the cell number was significantly higher ($P<0.0001$) on adhesive and uncoated ($P<0.01$) plates; and significantly lower ($P<0.01$) in the PIs formed in F127 coated plate comparing with that in the PIs generated on a ULA surface (Figure 4.5B).

When the seeding density of 32,000 cells/well (Figure 4.6) was used, the mean cell number of PIs was significantly lower ($P<0.01$) for cells proliferate on uncoated surfaces and surfaces coated with F127 than that of cells of PIs cultured on a ULA surface at day 3 (Figure 4.6A). While at day 7, the cell number of PIs was significantly higher ($P<0.0001$ and $P<0.05$) on adhesive uncoated and 100% gelatin plates. While significantly lower ($P<0.05$) cells number of PIs formed in F127 coated plate was observed comparing with cell numbers in the PIs generated on a ULA surface (Figure 4.6B).

Figure 4.5 Effect of the coating solution on PI cell number for cell seeding density 8,000 cells/well

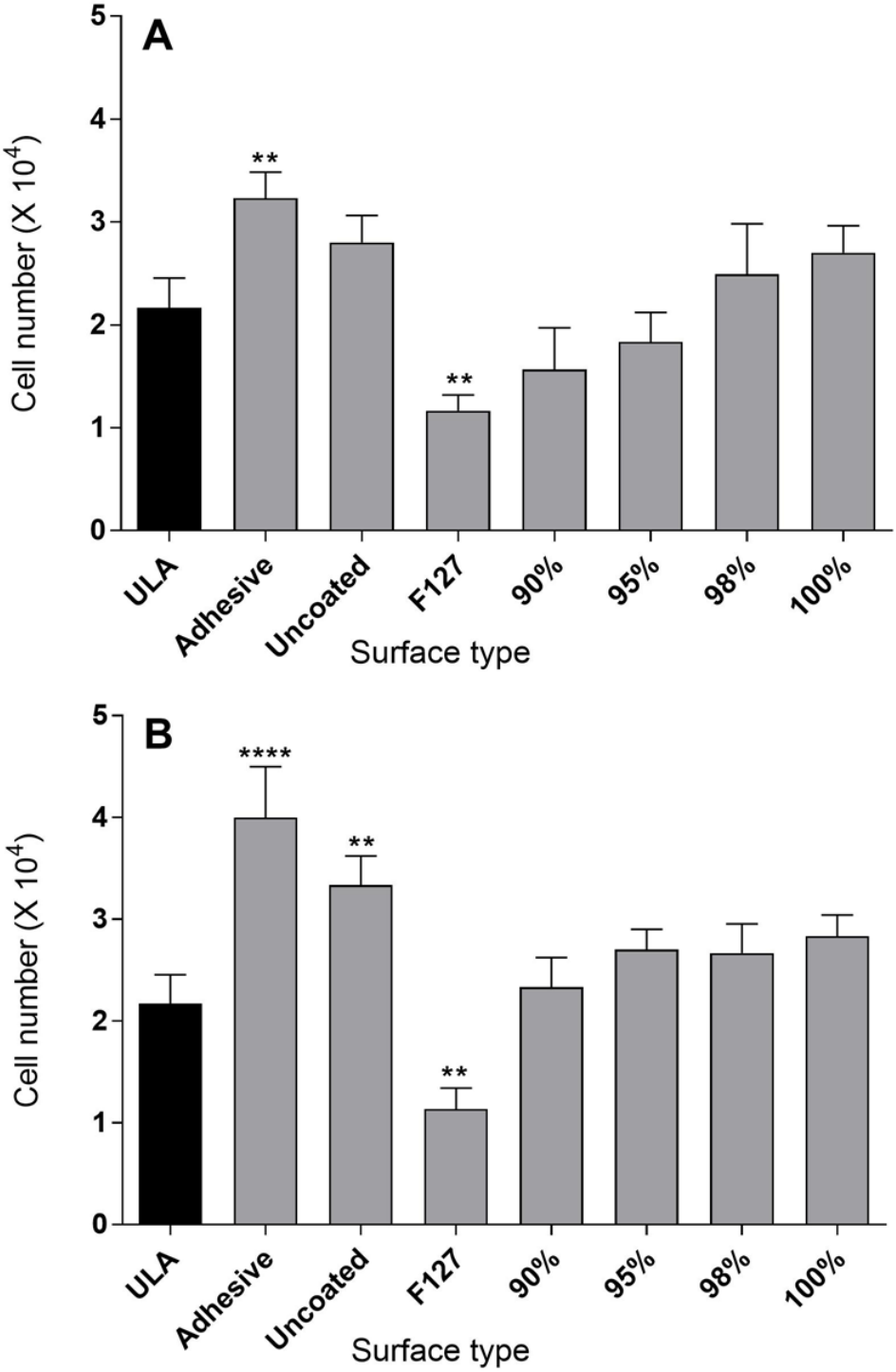

BRIN-BD11 cells were seeded at densities of 8,000 cells/well and the impact of the coating solution on cell numbers after 3 days (**A**) and for 7 days (**B**) using automated cell counter. Data are presented as mean ± SD from 3-4 independent experiments conducted in triplicate. **P<0.01 and ****P<0.0001 compared with cell number formed on ULA.

Figure 4.6 Effect of the coating solutions on PI cell number for cell seeding density 32,000 cells/well

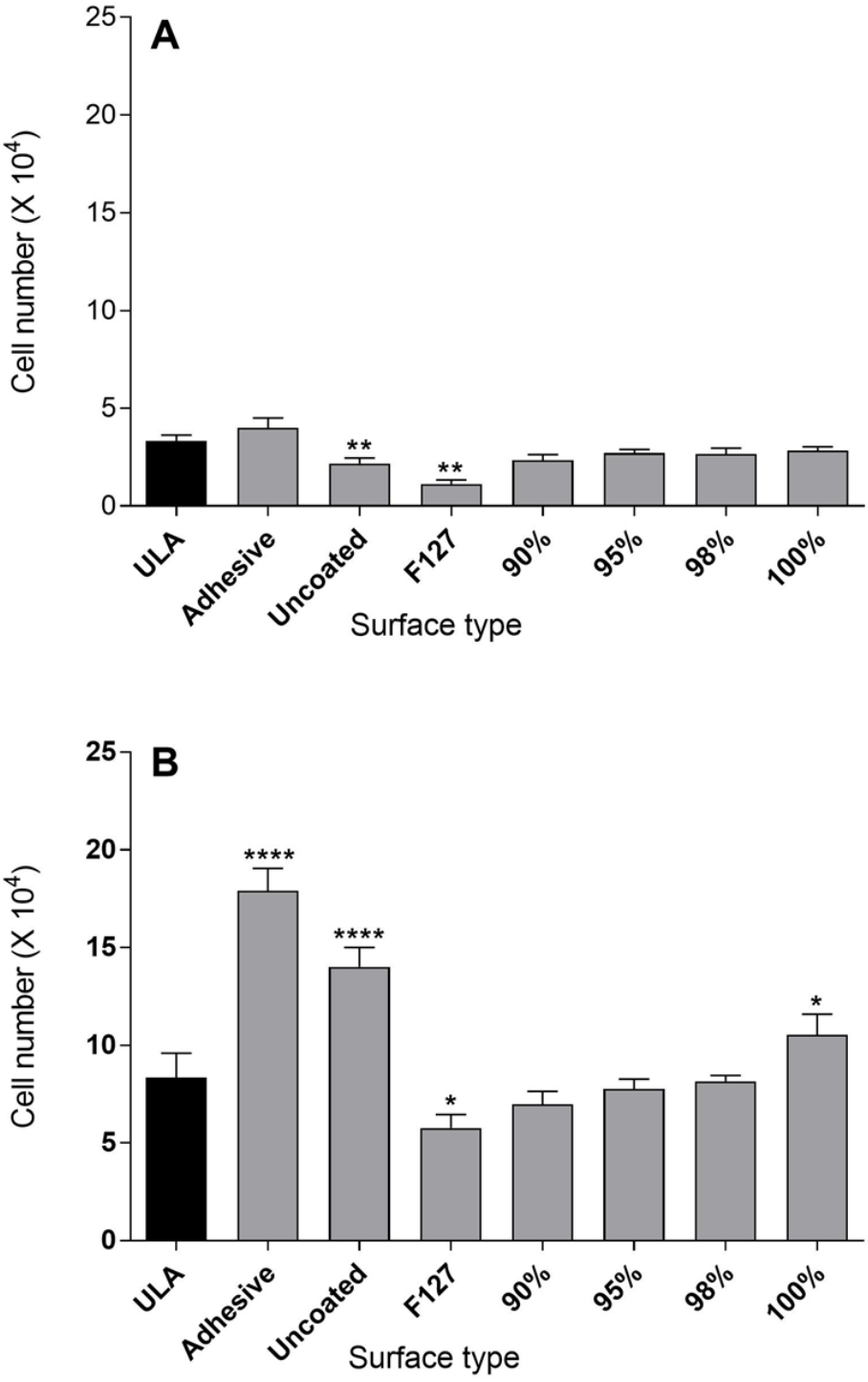

BRIN-BD11 cells were seeded at densities of 32,000 cells/well and the impact of the coating solution on cells numbers assessed after 3 days (**A**) and for 7 days (**B**) using automated cell counter. Data are presented as mean ± SD from 4-5 independent experiments conducted in triplicate. *P<0.05, **P<0.01 and ****P<0.0001 compared with cell number formed on ULA.

4.4.5 Effect of the coating solution on mitochondrial respiration of PIs (MTT assay)

The effect of the coating solutions on the mitochondrial respiration rate of PIs was assessed after 3 and 7 days and at different starting seeding densities for 8,000 cells/well (Figure 4.7) and for 32,000 cells/well (Figure 4.8) using MTT assay. The MTT assay was used as a surrogate for cellular proliferation on the basis that non-respiring mitochondria are reflective of poorly proliferating cells. MTT values in 8,000 cells/well were significantly higher ($P<0.01$-$P<0.0001$) in the cells grown on an adhesive, uncoated surfaces and 100% gelatine coated surface compared with those of cells grown on a ULA surface at day 3 and day 7 culture. (Figure 4.7).

For another cell seeding density (32,000 cells/well), MTT data at day 3 revealed that there were no significant differences on proliferation of cells on different surface types except cells proliferated ($P<0,05$) on surface coated with 98% gelatin comparing those of cells in PIs generated on a ULA surface at the same day. In the case of cells proliferation at day 7, MTT data was exhibited higher ($P<0.00l$- $P<0.0001$) proliferation rate in cells grown on an adhesive, uncoated surfaces and 100% gelatine than the proliferation of cells in PIs generated on a ULA surface. While MTT data showed lower values ($P<0.001$) in PIs formed in the F127 surface compared with PIs generated on a ULA surface (Figure 4.7B).

Figure 4.7 Effect of the coating solution on mitochondrial respiration of PIs (MTT assay) for cell seeding density 8,000 cells/well

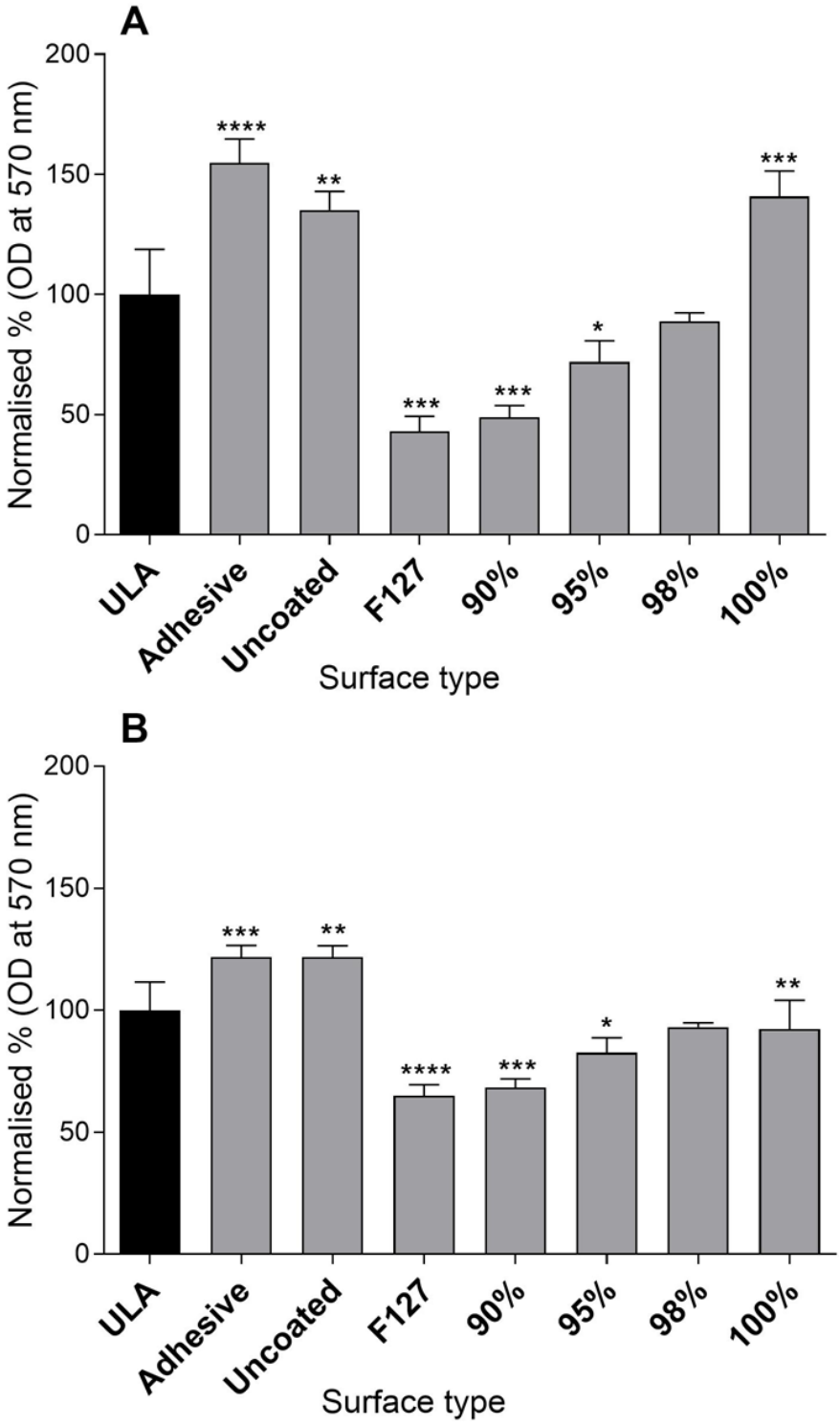

BRIN-BD11 cells were seeded at densities of 8,000 cells/well, and the impact of the coating solution on the proliferation of PIs assessed after 3 days (**A**) and for 7 days (**B**) using MTT assay. Data are presented as mean ± SD from 4-5 independent experiments conducted in triplicate. *P<0.05, **P<0.01, ***P<0.001, and ****P<0.0001 compared with the viability of cells grown on a ULA surface

Figure 4.8 Effect of the coating solution on mitochondrial respiration of PIs (MTT assay) for cell seeding density 32,000 cells/well

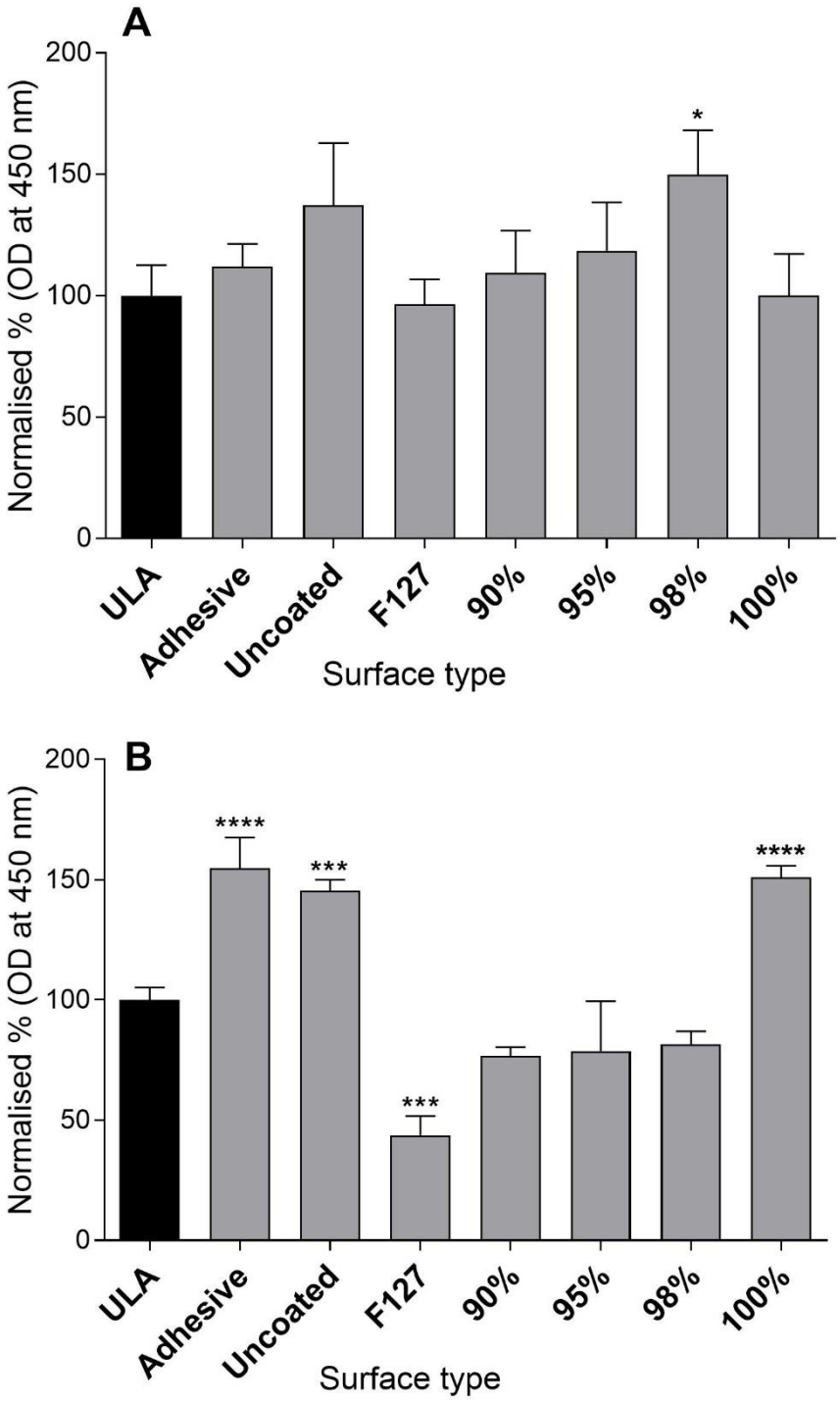

BRIN-BD11 cells were seeded at densities of 32,000 cells/well, and the impact of the coating solution on the proliferation of PIs assessed after 3 days (**A**) and for 7 days (**B**) using MTT assay. Data are presented as mean ± SD from 4-5 independent experiments conducted in triplicate. *P<0.05, ***P<0.01 ****P<0.0001 compared with the viability of cells grown on a ULA surface.

4.4.6 Effect of the coatng solution on the proliferative rate of PIs (CCK-8 assay)

The effect of the coating solution on the proliferative rate of cells within PIs was assessed after 3 and 7 days in culture for cell seeding density 8,000 cells/well (Figure 4.9) and for cell seeding density 32,000 cells/well (Figure 4.10). The proliferative rate of cells seeded at an initial density of 8,000 cells/well did not show much difference on different surfaces after 3 days in culture except for cells grown on 98% and 100% gelatin coated surface (Figure 4.9A). They showed higher proliferation rate than cells grown on a ULA surface. After 7 days culture, the proliferation rate significantly increased ($P<0.05$) on cells cultured on adhesive surfaces. On the other hand, CCK-8 results displayed significant reduction ($P<0.001$) in the proliferative rate for PIs generated on F127 coated surface when compared with cells grown on a ULA surface (Figure 4.9B).

When an initial seeding density of 32,000 cells/well was used, the proliferative rate of cells seeded did not show much difference on different surfaces after 3 days in culture except for the proliferation rate for cells in PIs grown on 98% gelatin coated surface (($P<0.05$) in comparing with proliferation rate of cells in PIs formed on a ULA surface (Figure 4.10A). After 7 days culture, the proliferation rate significantly increased ($P<0.05$) comparing with proliferation rate of cells in PIs formed on a ULA surface. On the other hand, CCK-8 results displayed significant increase ($P<0.001$-$P<0.0001$) for cells grown on the surfaces of adhesive, uncoated and 100% gelatin coated while the proliferation rate significantly reduced ($P<0.001$) in PIs formed on F127 surface when compared with PIs formed on a ULA surface (Figure 4.10B).

Figure 4.9 Proliferation (CCK-8 assay) of PIs generated on surfaces coated with different coating solutions for cell seeding density 8,000cells/well

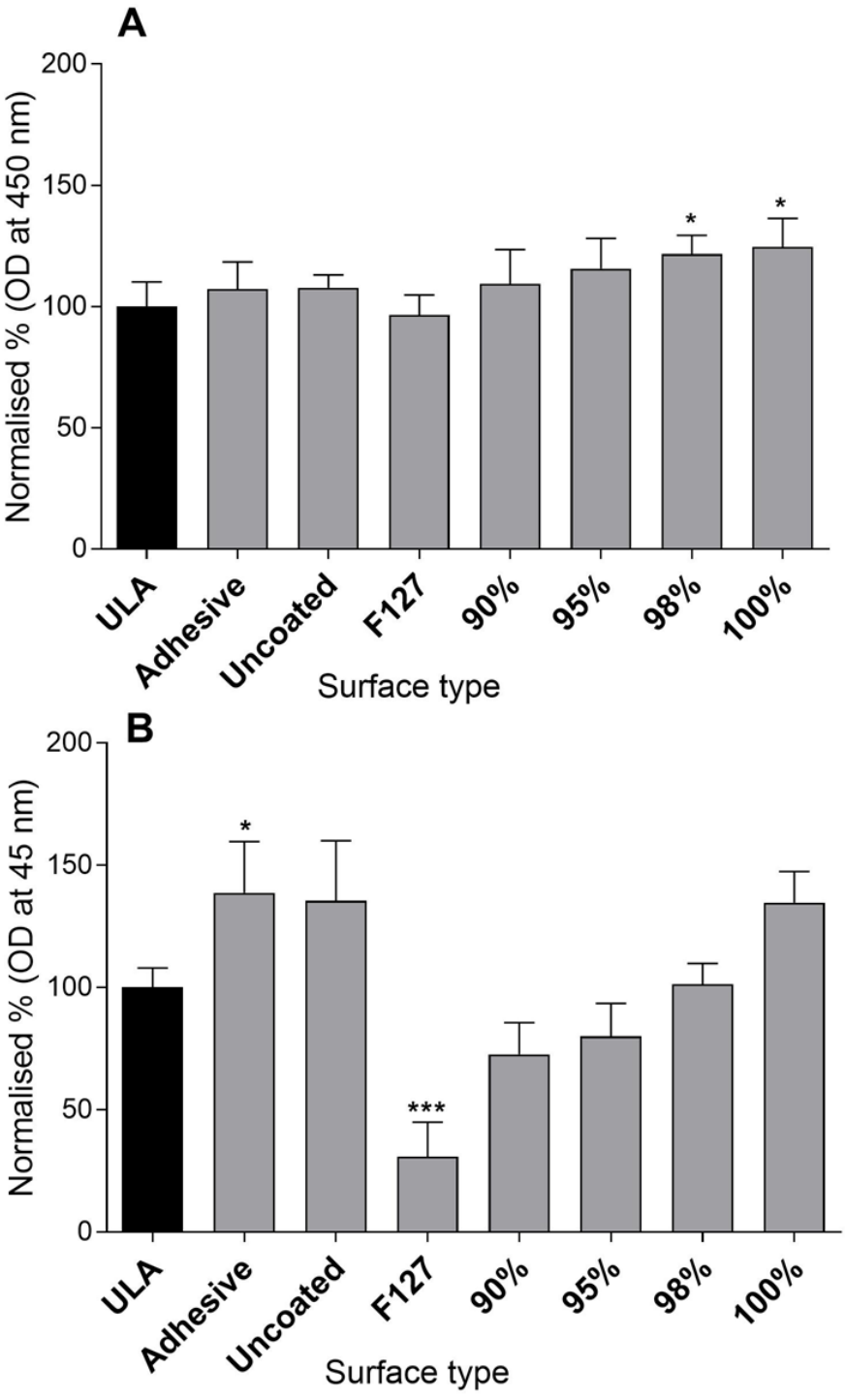

BRIN-BD11 cells were seeded at densities of 8,000 cells/well, and the impact of the coating solution on the proliferation of PIs assessed after 3 days (**A**) and for 7 days (**B**) using CCK-8 assay. Data are presented as mean ± SD from 4-5 independent experiments conducted in triplicate. *P<0.05,**P<0.01, and ****P<0.0001 compared with cells proliferated on ULA.

Figure 4.10 Proliferation of PIs generated on surfaces coated with different coating solutions for cell seeding density 32,000 cells/well

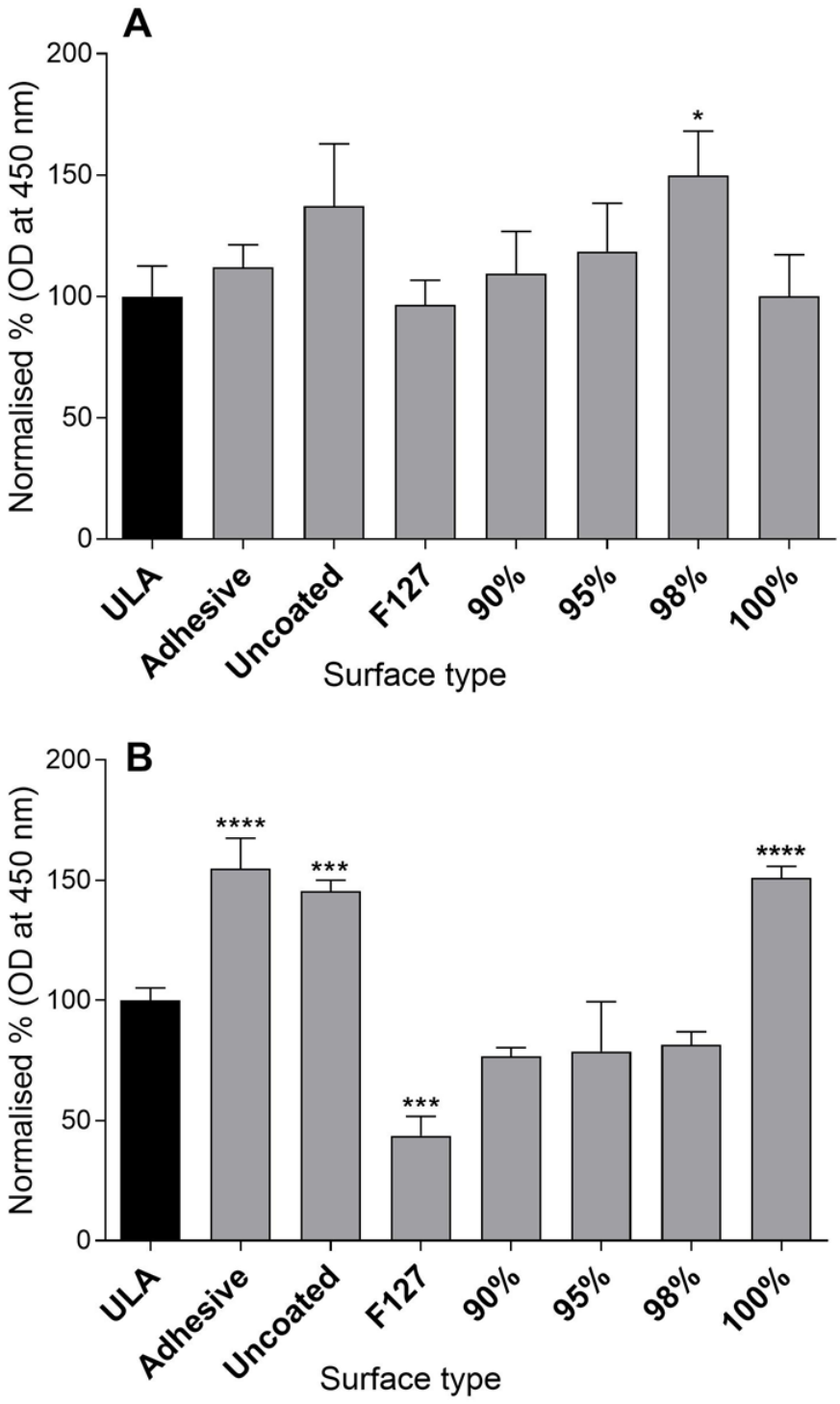

BRIN-BD11 cells were seeded at densities of 32,000 cells/well, and the impact of the coating solution on the proliferation of PIs assessed after 3 days (**A**) and for 7 days (**B**) using CCK-8 assay. Data are presented as mean ± SD from 3-4 independent experiments conducted in triplicate. *P<0.05, ***P<0.001, and ****P<0.0001 compared with cells proliferated on ULA.

4.4.7 Effect of coating solution on glucose-stimulated insulin secretion from PIs

The effect of the coating solution on glucose-stimulated insulin secretion (GSIS) from PIs was assessed after 7 days and is shown in Figure 4.11. At a starting seeding density of 8,000 cells/well, GSIS in response to 16.7 mM glucose was significantly decrease ($P<0.01$ and 0.0001) in all instances except PIs formed on surfaces coated 95% gelatin and 98% gelatin which showed non-significant increases in GSIS when compared with GSIS of PIs formed on ULA surfaces (Figure 4.11A). A similar effect was observed with a starting seeding density of 32,000 cells/well. However, in this instance, PIs generated on PIs formed on surfaces coated 95% and 98% gelatin showed increase in the GSIS but not reach to the significant different (Figure 4.11B) when compared with GSIS of PIs formed on ULA surface.

Figure 4.11 Effect of coating solution on glucose-stimulated insulin secretion of PIs

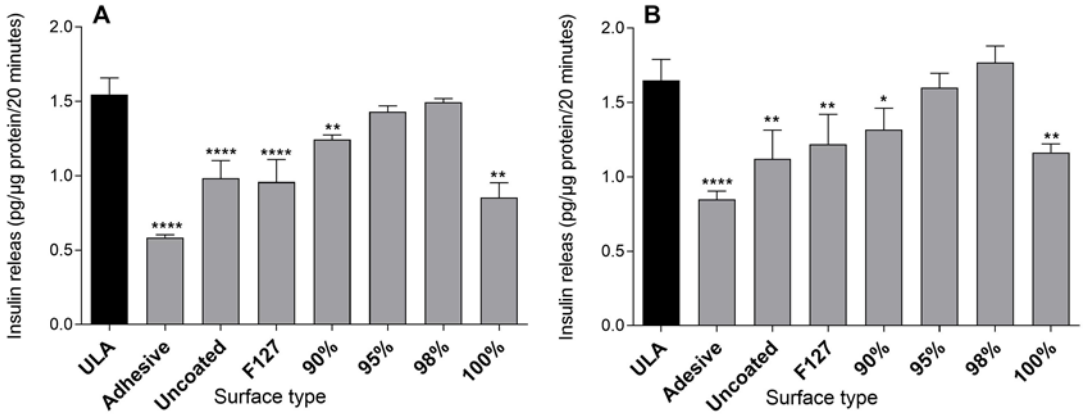

GSIS in response to 16.7 mM glucose was measured by ELISA after 7 days culture. PIs were generated from two different seeding densities: 8,000 cells/well **(A)** and 32,000 cells/well **(B).** Data are presented as mean ± SD (N=6 assayed in duplicate) *P<0.05, **P<0.01 and ****P<0.0001 compared with PIs were formed on ULA plate.

4.4.8 Effect of coating solution on the mRNA expression of Connexin 36, GLUT2 and insulin in PIs

The generation of PIs on tissue culture plastic coated with different solutions resulted in differential expression of Cx36, GLUT2 and insulin mRNA as shown in Figure 4.12. The mRNA expression of Cx36 (Figure 4.12A), GLUT2 (Figure 4.12B) or Insulin (Figure 4.12C) varied according to coating types. mRNA was significantly reduced ($P<0.001$ $P<0.01$) in PIs cultured on the surface coating with F127 solution alone or cells were grown on the plate coating with 100% gelatin when compared with PIs-formed on a ULA surface. This study displayed that the coating of 98% gelatin to grow PIs showed a significant improvement ($P<0.01$) in gene expression of Cx36 compared with that of PIs formed on a ULA surface (Figure 4.12A). Furthermore, PIs grown on the surface coating with the solution of 90%, and 95% gelatin resulted in an increase mRNA of Cx36 but did not reach a significant level as shown in Figure 4.12A. GLUT2 and insulin gene mRNA results showed an increase in PIs grown on 98% gelatin coated surface without significance but showed a significant decrease on PIs grown on the uncoated surface or coated with F127 or 100% gelatin ($P <0.01$-$P<0.0001$) (Figure 4.12B, C), when compared with PIs, formed on a ULA surface.

Figure 4.12 Effect of coating solutions on mRNA expressions of Connexin 36, GLUT2 and insulin in PIs

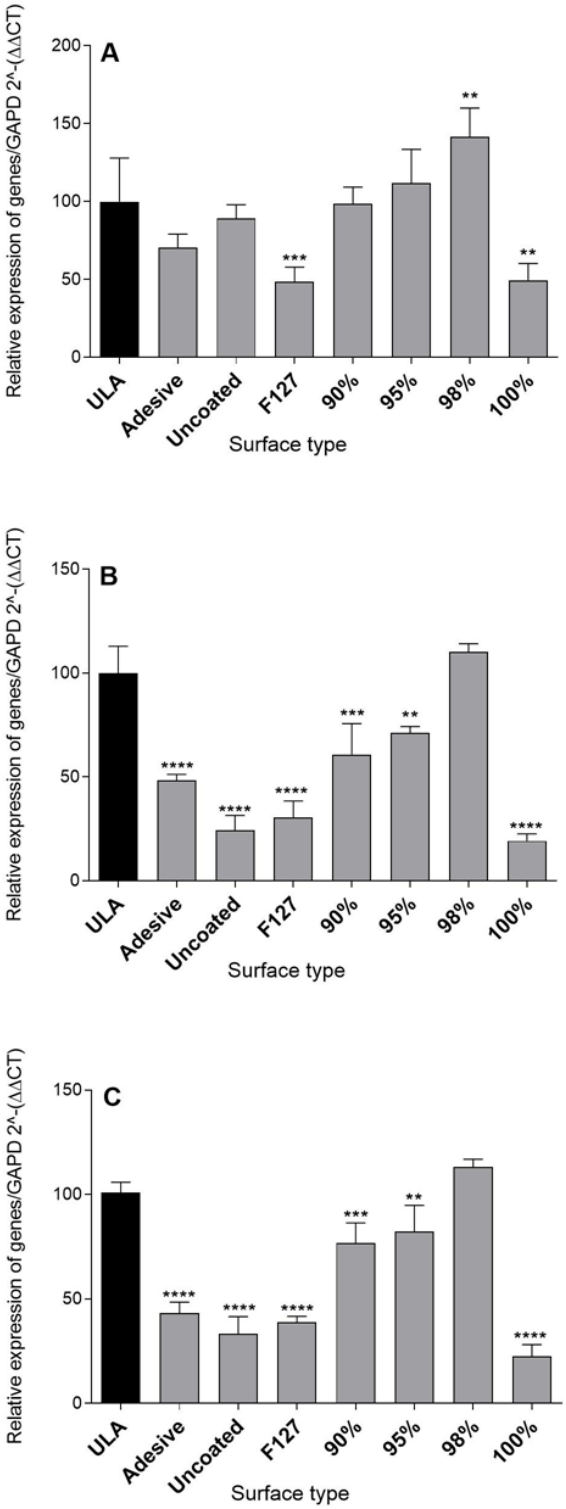

The effect of the coating solutions on the mRNA expression of Cx36 (A), GLUT2 (B) and insulin (C) of the PIs were assessed by qPCR after PIs in culture for 7 days. Data are presented as the mean ± standard deviation (SD) with n=4. **P<0.01, ***P<0.001 and ****P<0.0001 compared with PIs were formed on ULA plate.

4.4.9 Connexin 36 staining in PIs grown on substrates coating with different coating solutions

To assess the expression and localisation of Cx36 a key gap junction protein essential in the maintenance of cell-cell communication between beta cells, immunocytochemistry using an antibody against Cx36 was performed (Figure 4.13). Cells cultured in the presence of 100% gelatin formed a monolayer and shown no enhancement in Cx36 staining over cells grown on an adhesive surface (Figure 4.13 and Figure 4.14). However, in all other instances, the culture of cells as PIs on tissue culture plastic treated with various coating solutions significantly enhanced Cx36 staining ($P<0.001 – 0.0001$; Figure 4.14). Over that of cells grown on an adhesive surface. PIs generated on a coating solution of 98% gelatin showed the highest expression of Cx36.

Figure 4.13 Connexin 36 staining in PIs cultured on substrates coated with different coating solutions

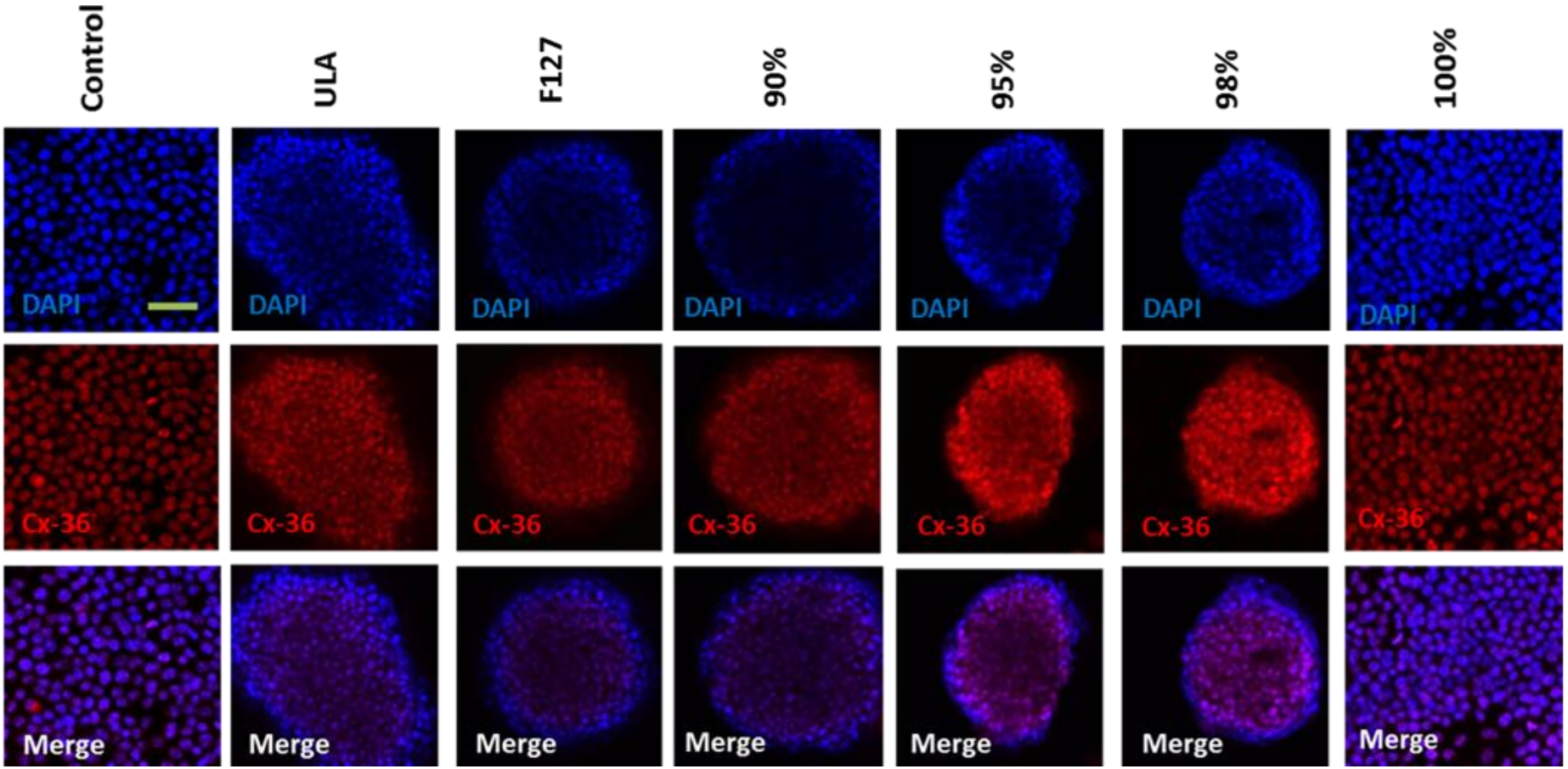

The effect of the coating solution on Cx36 staining after 7 days of culture was assessed by immunocytochemistry using confocal microscopy. Microscope magnification used was a 40X objective. Scale bars = 100 µm.

Figure 4.14 Connexin 36 expression in PIs grown on substrates coated with different coating solutions

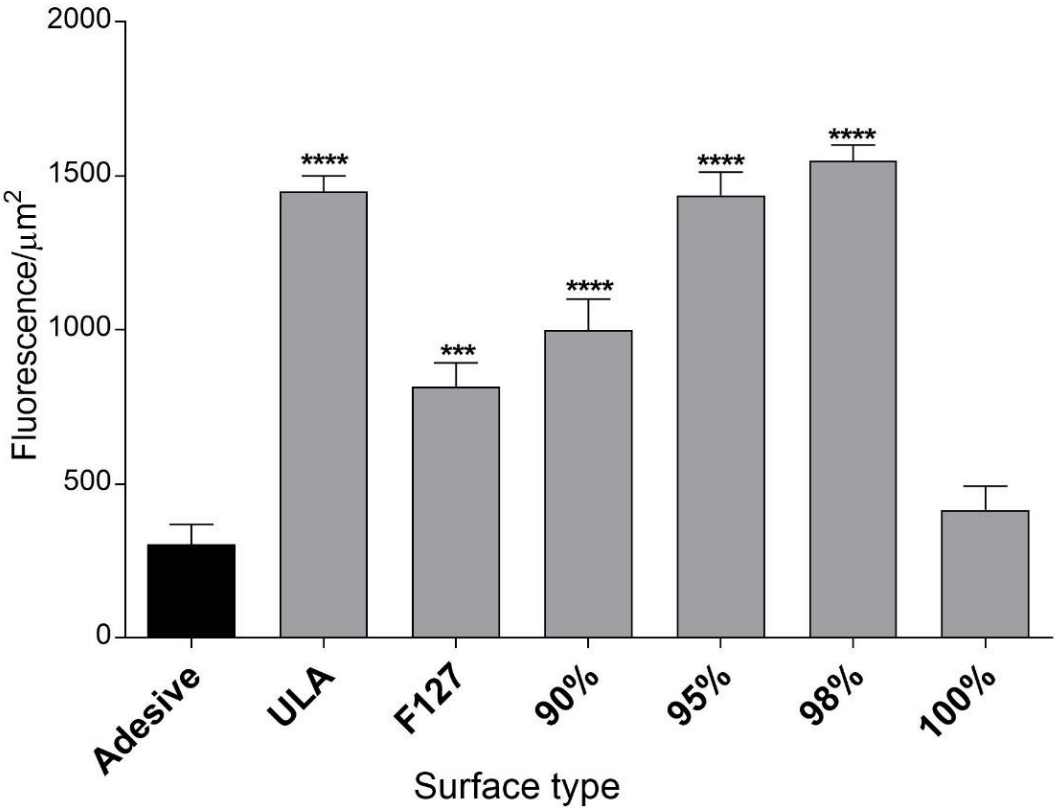

Semi quantified measurement of Cx36 stained images by using ImageJ software. Data are presented as mean ± SD from 4-5 independent experiments conducted in triplicate. ***P<0.001 and ****P<0.0001 compared with adhesive control.

4.4.10 GLUT2 staining in PIs cultured on a substrate coated with different coating solutions

To assess the expression and localization of the glucose transporter GLUT2, immunocytochemistry using an antibody against GLUT2 was performed (Figure 4.15). Cells cultured in the presence of 100% gelatin showed no enhancement in GLUT2 staining over cells grown on an adhesive surface (Figure 4.15 and Figure 4.16). However, in all other instances, the culture of cells as PIs on tissue culture plastic treated with various coating solutions significantly enhanced GLUT2 staining (P<0.01 – 0.0001;

Figure 4.16). Over that of cells grown on an adhesive surface. PIs generated on a coating solution of 98% gelatin showed the highest expression of GLUT2.

Figure 4.15 GLUT2 staining in PIs cultured on the substrates coated with different coating solutions

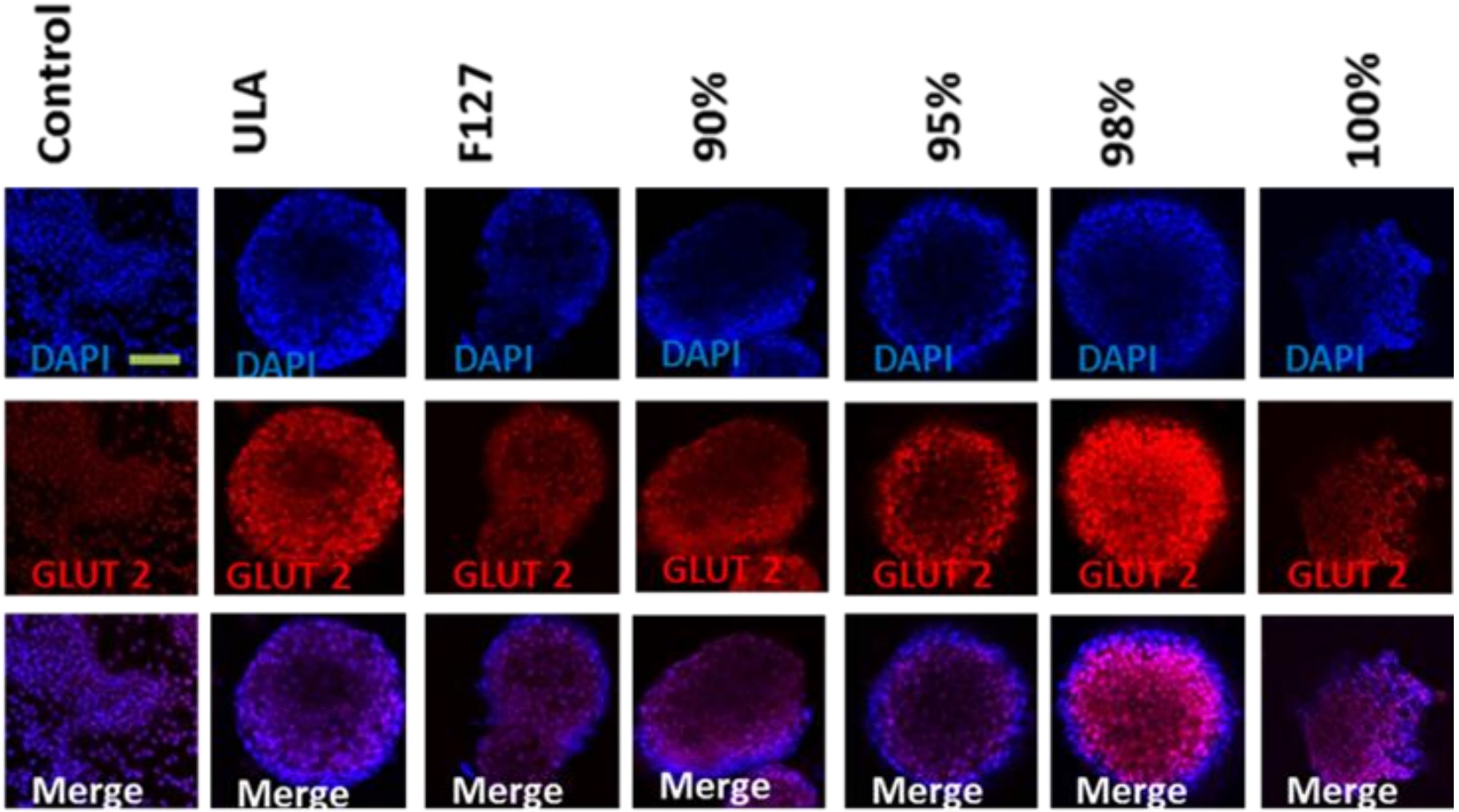

The effect of the coating solution on GLUT2 staining after 7 days of culture was assessed by immunocytochemistry using confocal microscopy quantified using ImageJ. Microscope magnification used was a 40X objective. Scale bars = 100 µm

Figure 4.16 GLUT2 expression in PIs cultured on the substrates coated with different coating solutions

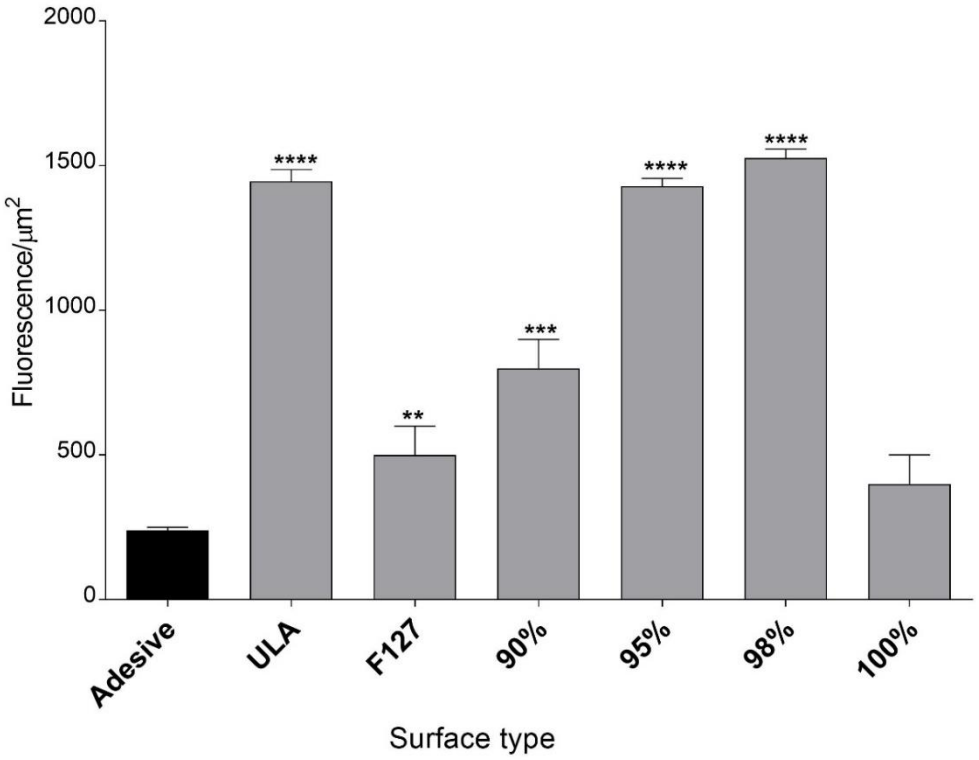

Semi quantified measurement of GLUT2 staining images by using ImageJ. Data are presented as mean ± SD from 4-5 independent experiments conducted in triplicate. **P<0.01, ***P<0.001 and ****P<0.0001 compared with adhesive control.

4.4.11 Insulin staining in PIs cultured on substrates coated with different coating solutions

To assess the expression and localization of insulin, immunocytochemistry using an antibody against insulin was performed (Figure 4.17). In all instances, the culture of cells as PIs on tissue culture plastic treated with various coating solutions significantly enhanced insulin staining (P<0.01 – 0.0001; Figure 4.17 and 4.18B) over that of cells grown on an adhesive surface. PIs generated on the substrate with a coating solution of 98% gelatin or on ULA plates showed the highest, and comparable increased expression of insulin.

Figure 4.17 Insulin staining in PIs cultured on the substrates coated with different coating solutions

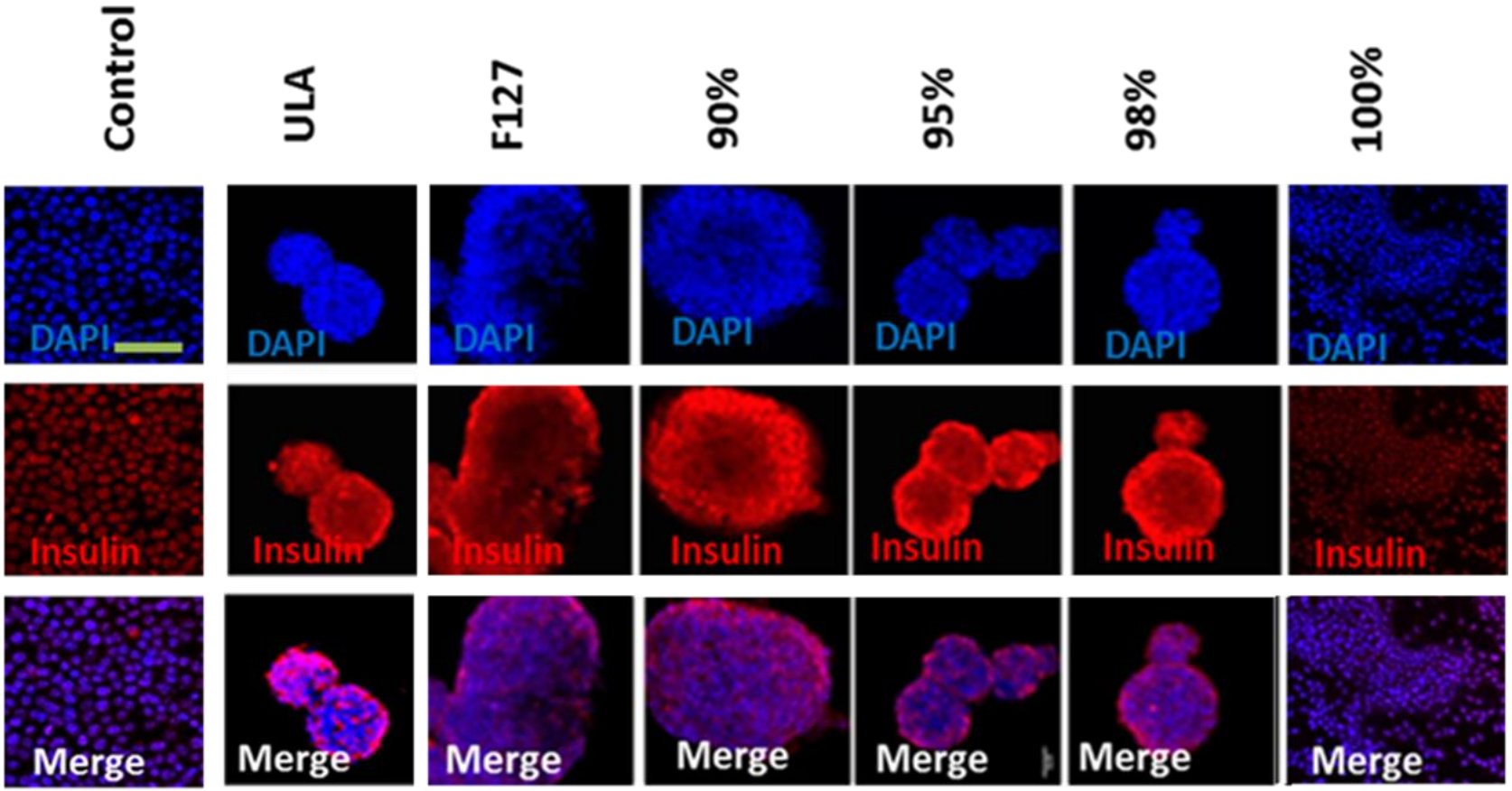

The effect of the coating solution on insulin staining after 7 days of culture was assessed by immunocytochemistry using confocal microscopy. Microscope magnification used was a 40X objective. Scale bars = 100 µm.

Figure 4.18 Insulin expression in PIs cultured on the substrates coated with different coating solutions

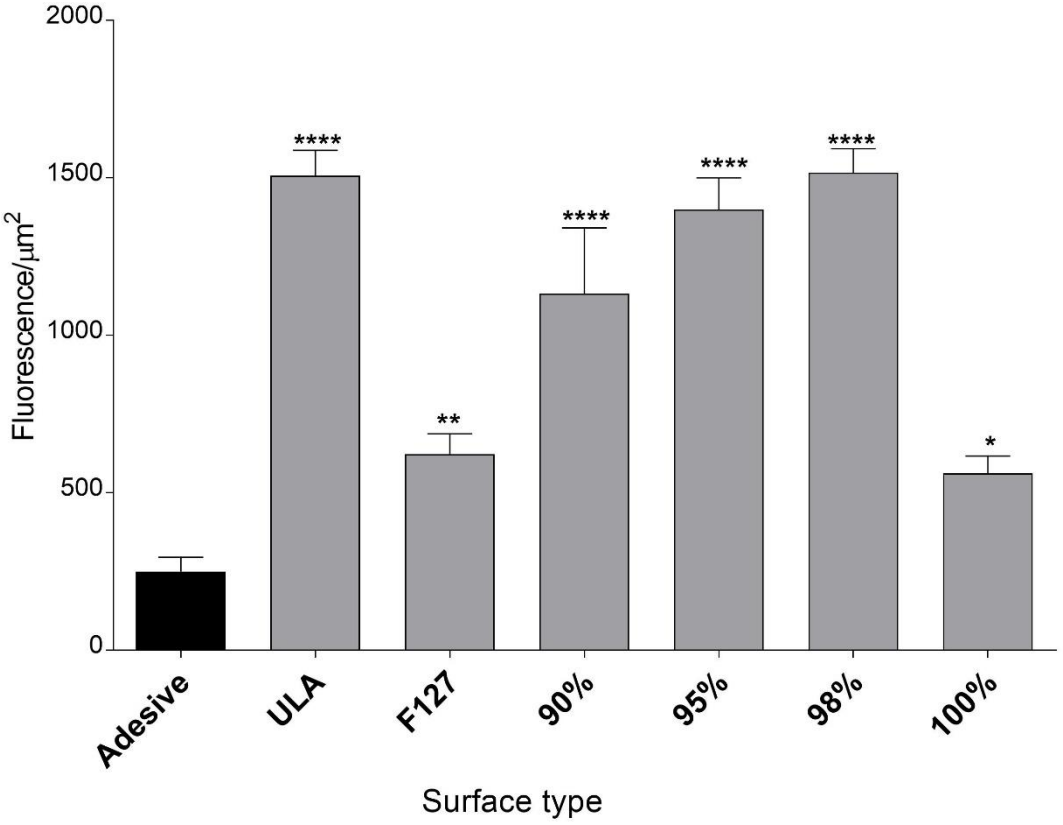

Semi quantified measurement of Insulin staining images by using ImageJ software. Data are presented as mean ± SD from 4-5 independent experiments conducted in triplicate. *P<0.05, **P<0.01 and ****P<0.0001 compared with adhesive control.

4.4.12 Western blotting analysis of connexin 36 expressions in PIs generated on different coating solutions

To further validate the expression levels of Cx36 following generation of PIs on different coating solutions, Western blot analysis was performed as shown in Figure 4.19. In all instances, Cx36 expression was higher ($P<0.0001$) than that of cells grown on an adhesive surface (control). Consistent with observations from immunocytochemistry experiments, Cx36 expression was highest in PIs generated on a solution of 98% gelatin (Figure 4.19B)

Figure 4.19 Western blotting analysis of Connexin 36 expression in PIs generated on different coating solutions

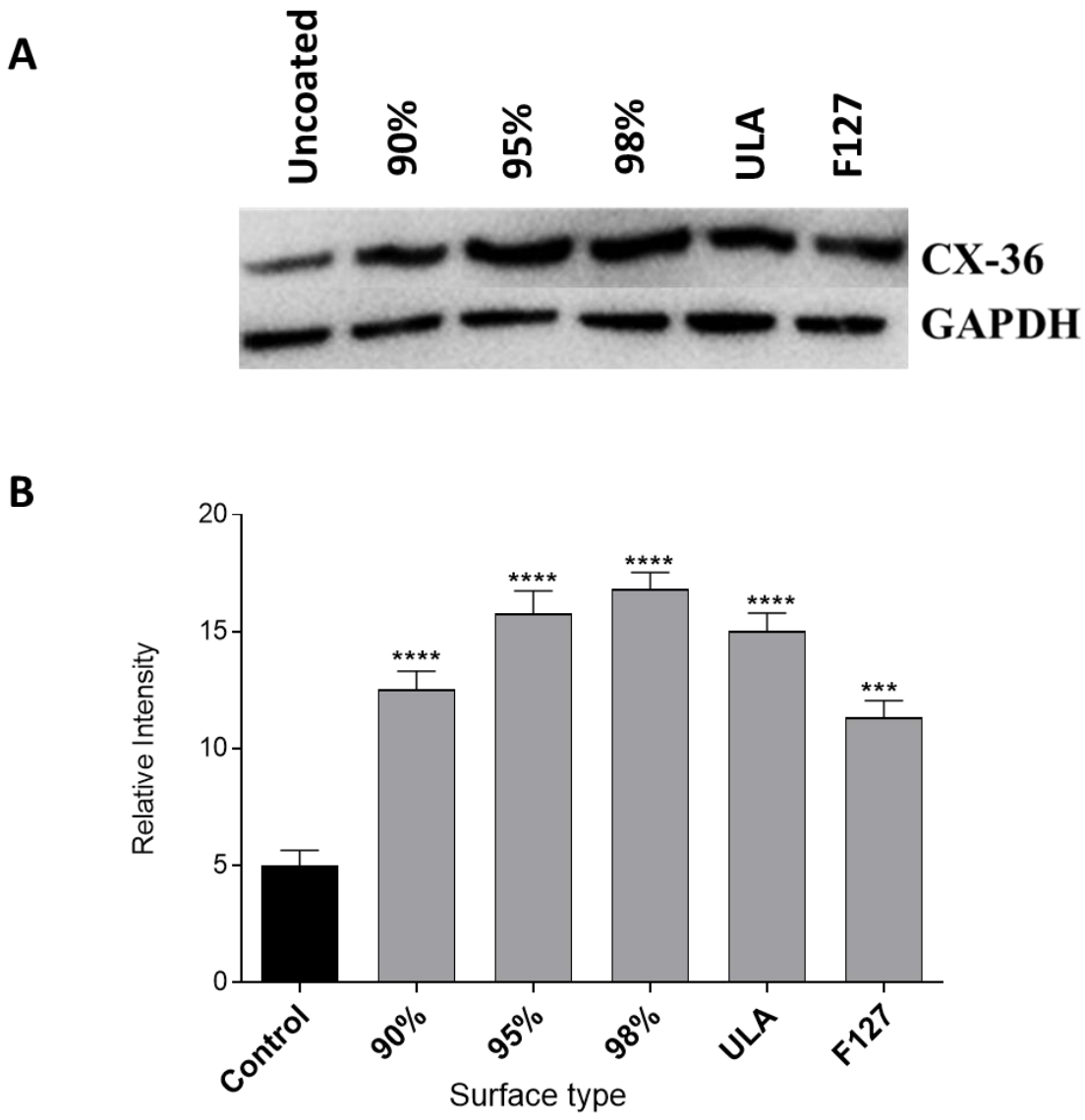

Western blotting was conducted to assess the expression of Cx36 in PIs generated on different coating solutions. Images representative of 4 independent experiments are shown in (A). Western blotting images were quantified using Alphaview software and expression levels relative to the loading control presented in (B). Data represented as mean ± SD (N= 4). ***P<0.001 and ****P<0.001 compared with Adhesive (controls).

4.4.13 Western blotting analysis of GLUT2 expression in PIs generated on substrates coated with different coating solutions

To validate the expression levels of GLUT2 following generation of PIs on different coating solutions, western blot analysis was performed as shown in Figure 4.20. In all instances, GLUT2 expression was higher ($P<0.001$ - 0.0001) than that of cells grown on an adhesive surface (control). Consistent with observations from immunocytochemistry experiments, GLUT2 expression was highest in PIs generated on a solution of 98% gelatin (Figure 4.20B). Additionally, the expression levels in PIs generated on ULA plates was comparable with that of PIs generated in a solution of 98% gelatin (Figure 4.20B).

Figure 4.20 Western blotting analysis of GLUT2 expression in PIs generated on substrates coated with different coating solutions

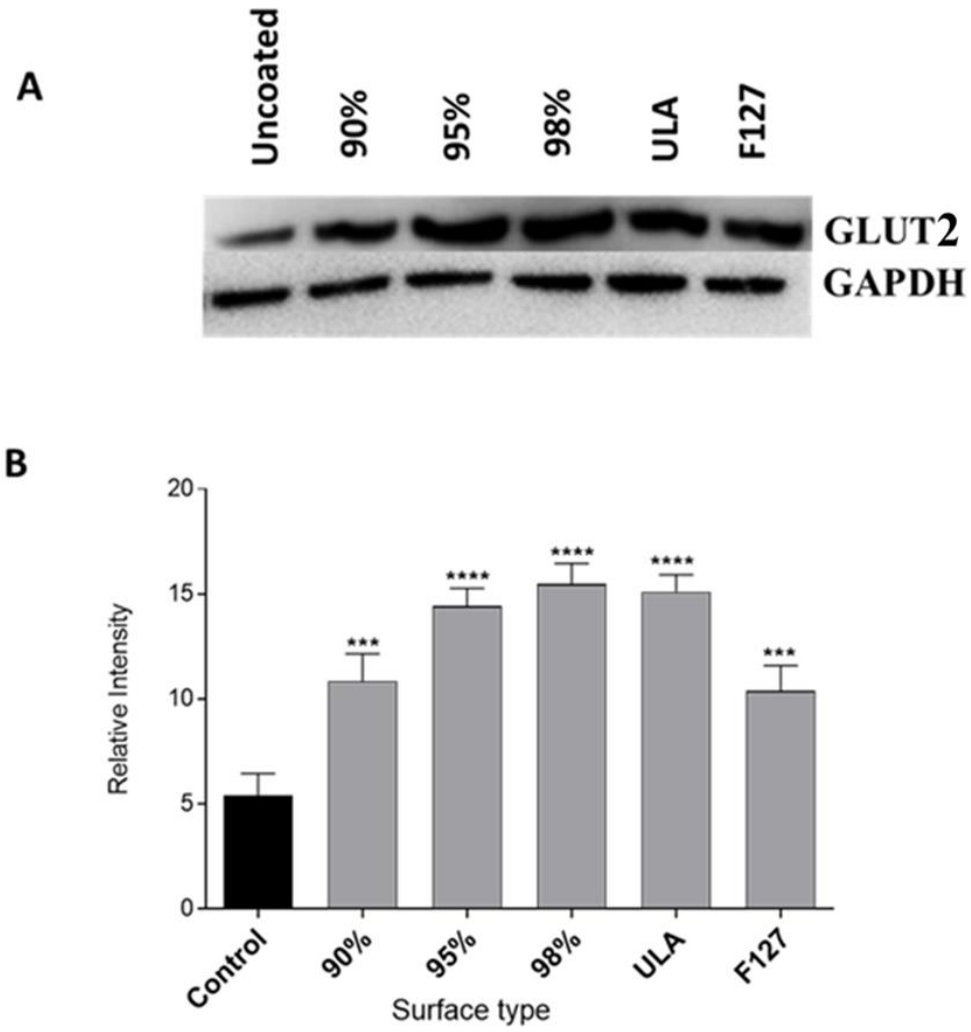

Western blotting was conducted to assess the expression of GLUT2 in PIs generated on the substrates coated with different coating solutions for 7 days. Images representative of 4 independent experiments are shown in (A). Western blotting images were quantified using Alphaview software and expression levels relative to the loading control presented in (B). Data represented as mean ± SD (N= 4). ***P<0.001 and ****P<0.001 compared with Adhesive (controls).

4.4.14 Western blotting analysis of insulin expression in PIs generated on different coating solutions.

Finally, to validate the expression levels of insulin following generation of PIs on different coating solutions, Western blot analysis was performed as shown in Figure 4.21. In all instances, insulin expression was higher ($P<0.001$ - 0.0001) than that of cells grown on an adhesive surface (control). Consistent with findings from immunocytochemistry experiments, PIs generated on a coating solution of 98% gelatin or on ULA plates showed the highest and comparable increases in the expression of insulin. (Figure 4.21B)

Figure 4.21 Western blotting analysis of insulin expression in PIs generated on different coating solutions

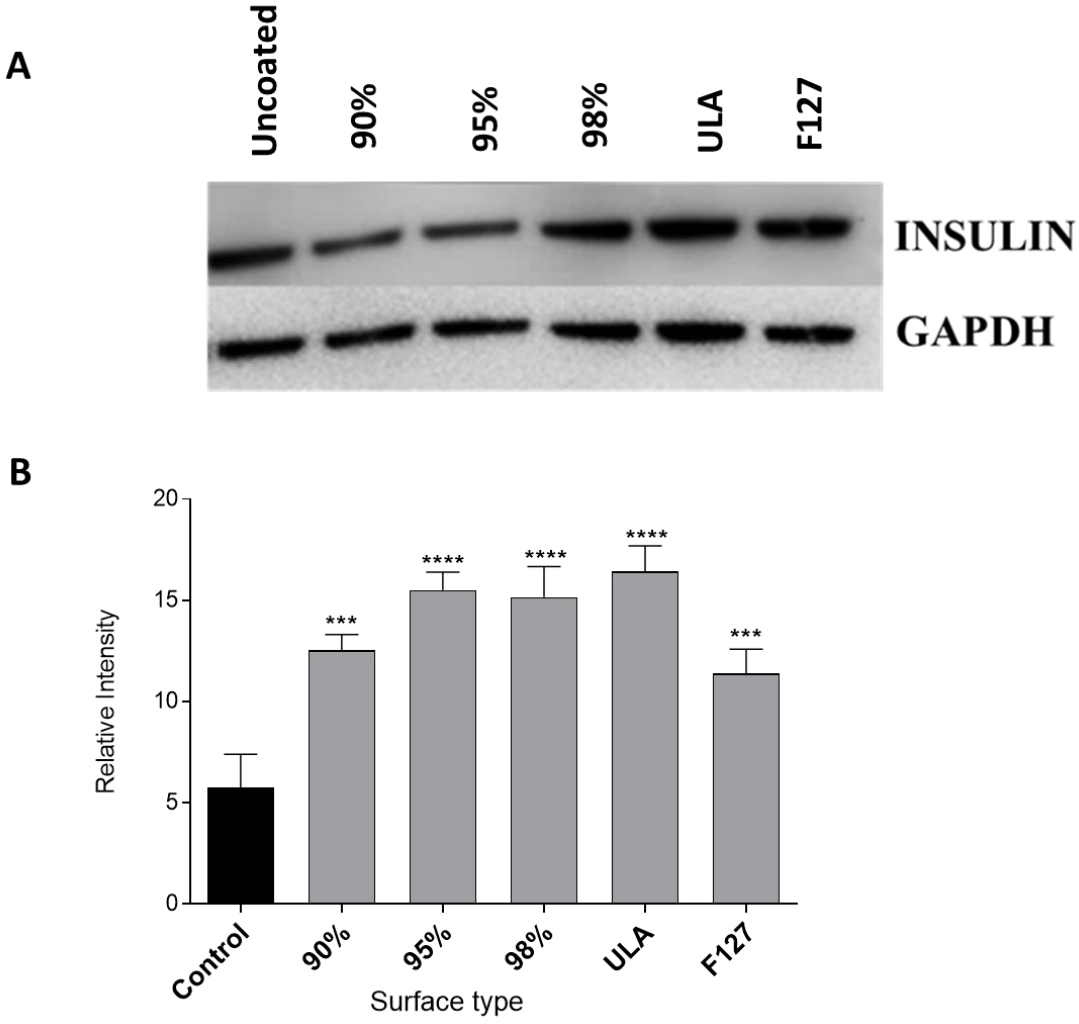

Western blotting was conducted to assess the expression of Insulin in PIs generated on different coating solutions. Images representative of 4 independent experiments are shown in **(A)**. Western blotting images were quantified using Alphaview software and expression levels relative to the loading control presented in **(B)**. Data represented as mean ± SD (N= 4). ***P<0.001 and ****P<0.001 compared with Adhesive (controls)

4.4.15 Effect of the coating solution on oxygen distribution in PIs grown on substrates coated different coating solutions

To assess the O_2 distribution within PIs generated on various coating solutions, the oxygen-sensitive poly(9,9-dioctylfluorene) (PFO) fluorophore was used in conjunction with a nanosensor to allow measurement of intracellular O_2 using a ratiometric intensity model. BRIN-BD11 cells were loaded with (reference/antennae dye-poly (9,9-diheptylfluorene-alt-9,9-di-P-tolyl-9H-fluorene) (PA2 probe).[200]

Figure 4.22A, B referred to O_2 distribution measured on a steady state luminescent spectrometer. The concentration of O_2 was high in PI grown on substrates coated with F127, 90% gelatin and ULA plates after 3 days culture. However, after 7 days culture, O_2 concentrations were higher in PIs generated on substrates coated with 95% gelatin or ULA plates (Figure 4.22A, B).

Figure 4.22 Oxygen distribution through the PIs at day 3 and day 7 culturing

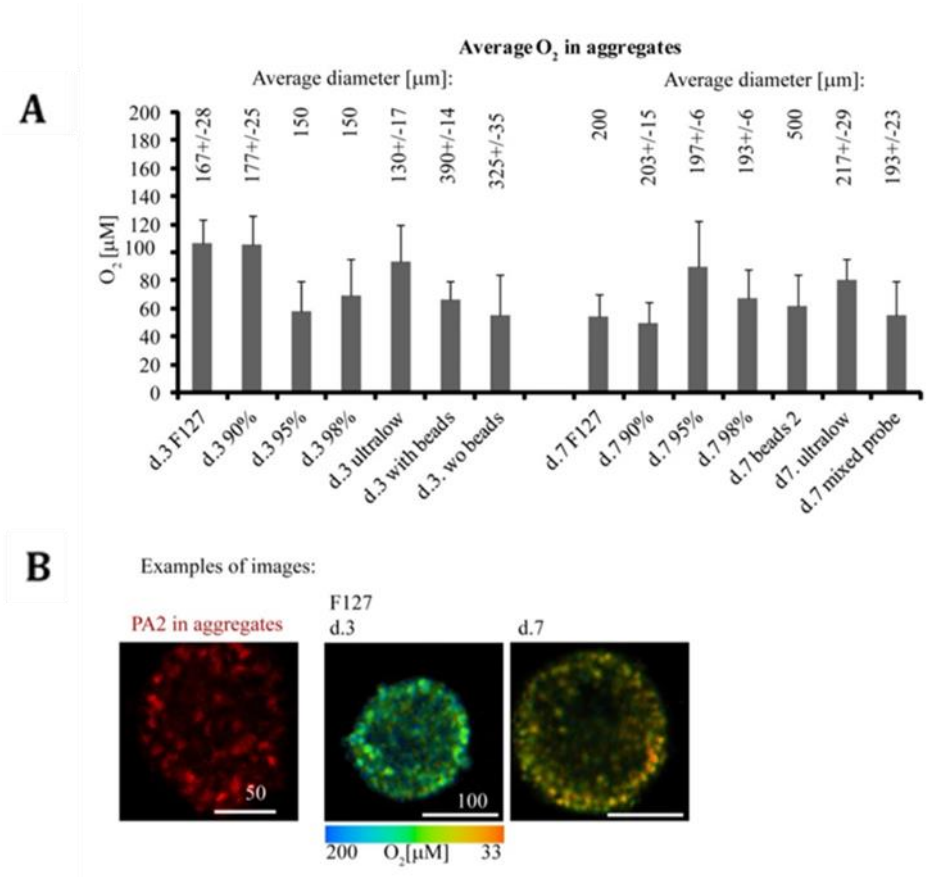

Average oxygen distribution within PIs generated by various coating solutions was measured using the oxygen sensitive probe (PA2). A: quantitative measurement of oxygen distribution in PIs at day 3 and day 7 culture. B: Live images for PIs stained with PA2 at day 3 and day 7 culture for PIs grown on F127 coated substrates.

4.5 Discussion

Different methodologies have been used to generate PIs from isolated beta cells in an attempt to mimic pancreatic islets in terms of cell-cell communication and physiological insulin secretion. The most important obstacle in such research is central necrosis of the PIs after approximately 7 days in culture. Several methods have been used to generate PIs. The most common and convenient protocol for PIs generation involves the use of ultra-low attachment (ULA) tissue culture plastic in suspension culture. However, it leads to the formation of PIs heterogeneous in size and often displaying central necrosis,[154,202]. The current study, therefore, aimed to produce PIs of homogeneous size, improved viability and enhanced functionality by altering the substrates chemistry on which PIs were formed. Series of coating mixture solutions have been designed, which systematically changed the hydrophobicity of the substrate and led to larger suspended PIs than those from ULA plates. Interestingly, some of the large PIs exhibited better or similar biofunction and cell viability than smaller size PIs, which offered a convenient tool to alter the cell arrangement in PIs and investigate the relation of physical properties of PIs to their biofunctions.

4.5.1 The effect of generation of different PIs' sizes on cell numbers

Previous work has shown that MIN6 PIs generated on ULA plates had an average diameter of 100-150 μm and comprised 3,000–4,000 cells per PI.[20,75] Consistently,

PIs of 150-200 μm were observed in this study when BRIN-BD11 cells were cultured on ULA 24 well plates with 32,000 cells per well as seeding density. However, the average number of cells per PI was significantly lower than those previous reports, likely reflecting the difference in cell lines used and surface area; because they use MIN6 cell line to compare insulin release from MIN6 pseudoislets and islets of Langerhans.[75] When PIs were generated on SOP plates coated with F127 and the mixture of F127 and gelatin, all PIs had sizes larger than 235 μm, the average size of PIs formed on ULA plates. PIs formed on a substrate coated with pure F127 were extremely large (up to 600 μm). A coating solution comprising gelatin alone was unable to generate suspended PIs suitable for experimental use. However, PIs grown on substrate coating with solutions containing both F127 and gelatin components reduced PI size than compared to that on F127 coated plate, a trend which was inversely proportionate to gelatin concentration. The higher F127 percentage, the higher the PIs sizes were. PIs grown on a coating containing 98% and 95% gelatin had comparable size and cell number to those generated on ULA. However, these PIs had a larger size than those from ULA. By 7 days culture, PIs from 98% gelatin coated plates reached the size of 268 ± 10 μm in comparison to ULA counterpart of 235 ±30 μm. Importantly, populations of these PIs were more uniform in size than PIs grown

on ULA plates. The larger PIs' size led to smaller numbers of total PIs when having the same seeding density.[75,171,203]

4.5.2 The cell viability and biofunction of different PIs' sizes

The current investigation, therefore, sought to determine the viability/proliferative rate of cells within PIs after 3 and 7 days in culture to determine if any coating substrate used could prolong the viability of larger PIs in culture. Both MTT and CCK-8 assays revealed that PIs generated on F127 performed poorly in terms of viability/proliferation, a finding that is conducive with other studies. Prior work has shown that large PI size was associated with poor oxygen and nutrient diffusion, eventually leading to reductions in proliferation and cell death in the central region.[34,204] Interestedly it is found that after 3 and 7 day culture, PIs generated on the plates coated with a solution coated 98% gelatin performed very well on both assays with the comparable cell viability data to PIs generated on ULA, which had smaller PI size. Furthermore, PIs generated on plates coated with a 98% gelatin solution displayed the same level of insulin release in GSIS and Western blotting assays and 14% higher expression in mRNA assay than PIs formed on ULA plates. This is the first time to reveal larger PIs can achieve similar or higher biofunction in comparison to smaller PIs.

4.5.3 The possible mechanisms underlying generation of different PIs' sizes

The primary mechanism by which PIs display enhanced functionality over monolayers is through the establishment or restoration of calcium-dependent gap junction signalling.[115] In islets, cell-cell contact is largely facilitated by E-cadherin,[20,75,96] which has previously been shown to be upregulated following configuration of cells as PIs.[75] Communication between beta cells is regulated by Cx36.[205] Which is also upregulated following configuration of cells as PIs.[204] Thus, regulation of beta cells' spatial arrangement and packing density during the PIs' formation through the substrate property may have an impact to the expression of E-cadherin and connexin on beta cells. The outcomes in the current study where the larger PIs exhibited similar or better biofunctions to smaller counterparts may be ascribed to the better cellular arrangement of beta cells in the PIs. The mRNA of Cx36 expression for PIs generated on plates coated with 98% gelatin was displayed increased by ~41% comparing with mRNA of Cx36 for PIs formed on ULA plate, (control); the PIs grown on 90% and 95% coating plates showed slight lower Cx36 expression by around 6-12% than PIs generated on ULA plates. Furthermore, the Western blot analysis for Cx36, GLUT2 and insulin expersions dispayed significan increase ($P<0.001$-0.0001) in PIs formed on 98% coated plate comapred with that formed on adhesive surface. However, the the comparison for Western bloting bands in insulin was hard to find out the

differences, the semiquantative revealed improvement in the PIs grown on surfaces coated with 98% gelatin. The discrepancy needs to be investiged further.

4.5.4 The application of series of coating solution

The amphiphilic polymer, F127, has been used to the modify surface properties of, for example, glass, polyethylene and polystyrene.[206] Olea *et al.* have indicated that mixing F127 with a hydrophobic polymer such as alkylphenol leads to the formation of micelle structures with stable, large cellular aggregates due to the effect of the length of the PPO in the F127 which anchors to the substrate leaving the PEO chain dangling in the solution (air).[207] Consistent with these observations, the culture of BRIN-BD11 cells on suspension plate coated with F127 generated large PIs in the current study most probably due to the strong protein expelling capacity of PEO.

Previously, it has been shown that the coating of tissue culture plastic with a 1% gelatin solution resulted in the generation of PIs using the MIN6 cell line.[20] However, in the current study, a pure gelatin solution coating suspension plate enhanced BRIN-BD11 cell adhesion into a dense monolayer. This discrepancy might be due to the different cell lines and the types of culture plate used. Mixing of F127 and gelatin in the coating solution with different ratios of the two components enabled us to generate PIs with different size and internal cell arrangement and investigate the correlation of

physical properties of PIs and the biofunctions in a systematic way. In such a way, we can produce large PIs with improved cell viability and insulin production. Yang *et al*. have investigated the effect of different types of coating chemicals on PIs' formation and their gene expression and insulin formation from beta cells.[83] The advantages of the coating solutions developed in this study are their biocompatibility of the components and the consistency without the interfering from coating chemical effect. Furthermore, the coating effect is substrate sensitive, which offer more variables to fine tune PIs' configuration and in turn biofunction.

It has been confirmed by that smaller PIs is better for oxygen diffusion. Also, the cell-cell configuration has established to play an essential role for small diffusion molecules such as oxygen,[20] which is consistent of the results obtained in this study. We found that PIs formed on 95%, 98% gelatin coated and ULA surfaces facilitated more oxygen diffusion than other types.

4.6 Conclusion

Culture substrate influences the generation of PIs' physical properties and biofunctions. PIs generated on SOP plates coating with the mixture solution of F127 and gelatin at different ratios exhibited significantly larger size than the PIs produced

on ULA plates. The lower the percentage of gelatin in the coating mixture, the higher the size of PIs. 95-98% gelatin coating solution produced more homogenous PIs compared with PI sizes formed on ULA. PIs formed on 98% gelatin coated plates had larger PIs sizes of 268 ± 10 μm against PIs sizes of 235 ± 30 μm formed on ULA at day 7 culture. The similar cell viability/proliferation, insulin production between the two types of PIs have been demonstrated. Western blotting and mRNA analysis further revealed that PIs formed on 98% gelatin coated plates expressed higher Cx36, GLUT2 in comparison to the PIs from other types of coated substrates and PIs from ULA. The systematical change of coating solution for suspension culture plates demonstrates a valuable tool to study PIs' internal structure and biofunction.

Chapter 5

Incorporation of gelatin beads into Pseudoislets and assessment of cellular viability

5.1 Introduction

Central necrosis or apoptosis hampers the formation of functional cell aggregates from islet cells (Pseudoislets (PIs)) after approximately 7 days in culture. This is largely driven by the lack of nutrient and oxygen diffusion to the core of the PIs. Cellular viability and growth of the cells drop off dramatically, and insulin concentrations in the culture medium decline.[75,90,94] It has been reported that PIs with 150 μm are superior to lager PIs (>300 μm) in viability, *in vitro* functional assays and transplantation outcomes. MacGregor *et al.* [208] have found that smaller PIs were 20% more viable, consumed twice as much oxygen and released more than double the amount of insulin.[209] It has been confirmed for years that mammalian cells rely on oxygen and nutrients for their survival and the natural diffusion limits of these vital chemicals are approximately 100 to 200 μm. Thus, blood vessels are essential for larger and multicellular organisms to grow beyond 200 μm in diameter naturally.[210] Based on this principle; it is easy to understand that the reduction of PI size is a good strategy to increase the viability of PIs. Alternatively, if we can generate 'vents' in the centre of PIs allowing nutrients and oxygen to enter, block the centre for cell residence, or deliver anti-necrosis or anti-apoptosis drugs to the centre of PIs, the cell viability of larger PIs may increase.

Gelatin is a natural polymer commonly used in the biomedical and biotechnology fields and is biocompatible. Moreover, it has been found that gelatin is a good candidate for preparation of microspheres and microcapsules due to the ability to control drug release easily.[210] The highly hydrophilic properties of gelatin lend itself to drug absorption and then drug release. Drug release can be controlled via several means such as diffusion through a rate-controlling membrane, osmosis, ion exchange or degradation of gelatin or a part of gelatin,[211] which can be controlled by either varying gelatin molecular weight, or via the extent of material crosslinking.[212]

Furthermore, the incorporation of gelatin beads (GBs) into vascular tissue (human smooth muscle) achieves improvements in the delivery of growth factors.[213] GBs can be used for sustained release of antibiotics, drugs, vaccines and hormones.[214] For instance, by taking the advantages of bead characterisation beyond basic benefits, the beads might provide a large surface area and possess an easier estimation of diffusion and mass transfer behaviour. The main advantages of using crosslinked GBs for incorporation into cell aggregates is that they are biocompatible, biodegradable and have a low degree of toxicity when dissolved.[214] Many factors affect fabrication of GBs such as the method of crosslinking and the sizes of GBs. Large GBs enable drugs delivery to a site over a long period. Additionally, drugs can be released slowly or in

a controlled manner by diffusion from carrier-GBs or by decomposition of the carrier itself.[182,214–219]

IL-10 produced primarily by monocytes, has a pleiotropic effect in inflammation and plays a role in the regulation of immunity through down-regulation of gene expression of Th1 cytokines and co-stimulatory molecules on macrophages. In addition, IL-10 helps in beta cells maintenance and proliferation through regulating of immune and autoimmune responses.[218] It also has the ability to block NF-kappa and controls JAK-STAT signalling pathway.[218] IL-10 has two receptors; IL-10R1 and IL-10R2. The mRNA of IL-10R1 participates in all IL-10 responsive cells, while IL-10R2 found in the most tissues and cells tested such as human alpha and beta cells and isolated INS-1E cells. IL-10, IL-13 and IL-4 are positively correlated with glucagon-stimulated C-peptide levels in human beta cells.[220] The mechanism by which IL-10 helps the secretion of pro-inflammatory molecules is still unclear. IL-10 has been found to have a positive effect on BRIN-BD11 PIs which is likely to indicate that this cell line has IL-10R.[221] This receptor has been proved by one of our colleques in the Guy Hilton research centre.[221] Some studies indicated that IL-10 deficiency in mice limits autoimmune pathology.[222] IL-10 enhances beta survival, proliferation, antibody formation and reduction of the pro-inflammatory potential like TNF-α.[211] Previous

studies have proved that the potential of anti-inflammatory cytokines as therapeutic targets in type 1 diabetes. Adoptive transfer of immunomodulatory cells preferentially secreting anti-inflammatory cytokines, which might result from the role of pro-inflammatory mediators such as macrophage and regulatory T-cells can be used to a reduction in incidents of T1DM and T2DM.[223,224]

Il-1β is a cytokine that is produced by the activation of macrophage as inactive pro-protein molecule which converts into an active form by the enzyme caspase 1. IL-1β acts as a mediator of the inflammatory response and plays a role in many cellular activities; like apoptosis, proliferation and differentiation.[220] Several studies on pancreatic islets and diabetes showed an increase in the concentration of pro-inflammatory cytokines such as INF-γ, TNF-α and IL-1β. The pro-inflammatory cytokines which are secreted from activated macrophages invade the pancreas. A deficiency in regulation of pro-inflammatory cytokine production will lead to the development of autoimmune disease such as T1DM.[225] Therefore, increased levels of the cytokines are responsible for beta destruction in T1DM.[225] Some researchers founded that using IL-1β triggered apoptosis in pancreatic beta cells lines and islets.[226] In addition, pro-inflammatory cytokines have been reported to produces

apoptosis in beta cell and primary cells.[225] In this study, anti-IL-1β, will use to decrease the action of IL-1β.

Based on the above, IL-10 and anti-IL-1β could be effective anti-inflammatory drug candidates for the fabrication of large PIs in order to reduce the inflammation-induced cell death in the centre and help to enhance PI biofunctionalities.

5.2 Aim

In this Chapter, we aim to resolve the issue of central necrosis within PIs through the incorporation of micrometre scale GBs, which may promote the construction of microchannel networks within PIs to help nutrient and oxygen transfer.[13] Furthermore, the potential use of GBs as drug carriers to deliver drugs including anti-necrosis and anti-inflammation drugs in a sustained manner to PIs is investigated.

In this study, we try to incorporate GBs into PIs after loading with IL-10, which will be released in the central region of the PIs aiming to prevent or delay apoptosis and inflammation in the centre of PIs. The effect of this corporation on the proliferation and cytotoxicity in the term of LDH assay and the ability of these PIs to produce insulin after stimulation with glucose will be investigated. Similarly, we try to load

anti-IL-1β into GBs and then incorporate the GBs into PIs in order to find out the effect of anti-pro-inflammatory drugs to the increase PIs' biofunctionality.

5.3 Materials

Chemicals, IL-10, anti-IL-1β, gelatin type A and reagents used in this Chapter are listed in Chapter 2, Section 2.1.

5.4 Methods

5.4.1 Generation and characterisation of GBs

Generation, separation, washing and characterisation of GBs from gelatin type A using water/oil emulsion are described in Chapter 2, Section 2.2.19 and Chapter 3 Section 3.4.4.

5.4.2 Incorporation of GBs into PIs

The incorporation of GBs into PIs via static and agitated manners using different pellet formation methods is described in Chapter 2 Section 2.2.20.

5.4.3 Loading and assessment of the mock drug release

The loading and assessment of the mock cytokine release from GBs are described Chapter 2 Section 2.2.22.

5.4.4 Loading IL-10, anti-IL-1β to GBs

The various concentrations of IL-10 and anti-IL-1β were assessed using CCK-8 assay to find out the best concentration which can be used for loading into GBs. The test procedure was described in Chapter 2 Section 2.2.21. The method of cytokines loaded to GBs was described in Chapter 2 Section 2.2.23.

5.4.5 Measuring PI cellular viability after incorporated with GBs by MTT assay

After incorporation GBs loaded with IL-10 or anti-IL-1β into PIs, the PIs' mitochondrial respiration was measured by MTT assay as described in Chapter 2 Section 2.2.7.

5.4.6 Measuring PI cellular viability using CCK-8

The proliferation of PIs after incorporation with GBs was measured by CCK assay, which is clarified in Chapter 2 Section 2.2.8

5.4.7 Measuring cytotoxicity by LDH assay

The cytotoxicity of PIs after incorporation of GBs was assessed using LDH assay, which is described in Chapter 2 Section 2.2.9.

5.4.8 Glucose-stimulated insulin secretion

The effect of GBs loaded with IL-10 and anti-IL1β on the functionality of PIs in term of glucose-stimulated insulin secretion is detailed in Chapter 2 Section 2.2.11.

5.5 Results

5.5.1 Selection and incorporation of the mock drug to GBs

After multiple analysis (in Chapter 3), it was confirmed that 40 µm GBs formed with a GA vapour crosslinking reaction time of 6 hours was optimal. The swelling rate of these GBs was more stable than 30 µm GBs, and the larger size of the GBs offered more opportunity for loading of drugs. Thus, 40µm GBs were used in this Chapter exclusively.

Goat anti-mouse IgG (H+L) secondary antibody with Alexa Fluor 568 conjugation (Ab-dye 568) was selected as a mock drug to be incorporated into GBs at different concentrations, and the release profiles of the molecule were tested. Measurement of fluorescence intensity allowed for the determination of the released protein. The reason to select Ab-dye-568 as the mock drug was its molecular weight (150 kD), which was close to the molecular weight of the drugs we hoped to enhance PI viability.

GBs were loaded with the dye and incubated in PBS for 4 days at 37 °C. Confocal images of the GBs loaded with Ab-dye-568 are shown in Figure 5.1. The fluorescent intensity was directly proportional to the concentration of Ab-dye-568 loaded into GBs (Figure 5.1). In addition, after 4 days' incubation, the fluorescence intensity in

GBs was still strong, indicating that the current drug incorporation method can sustain the drug within the GBs.

Figure 5.1 Fluorescence images of 40µm GBs incorporating Ab-dye 568 with culturing for 4 days

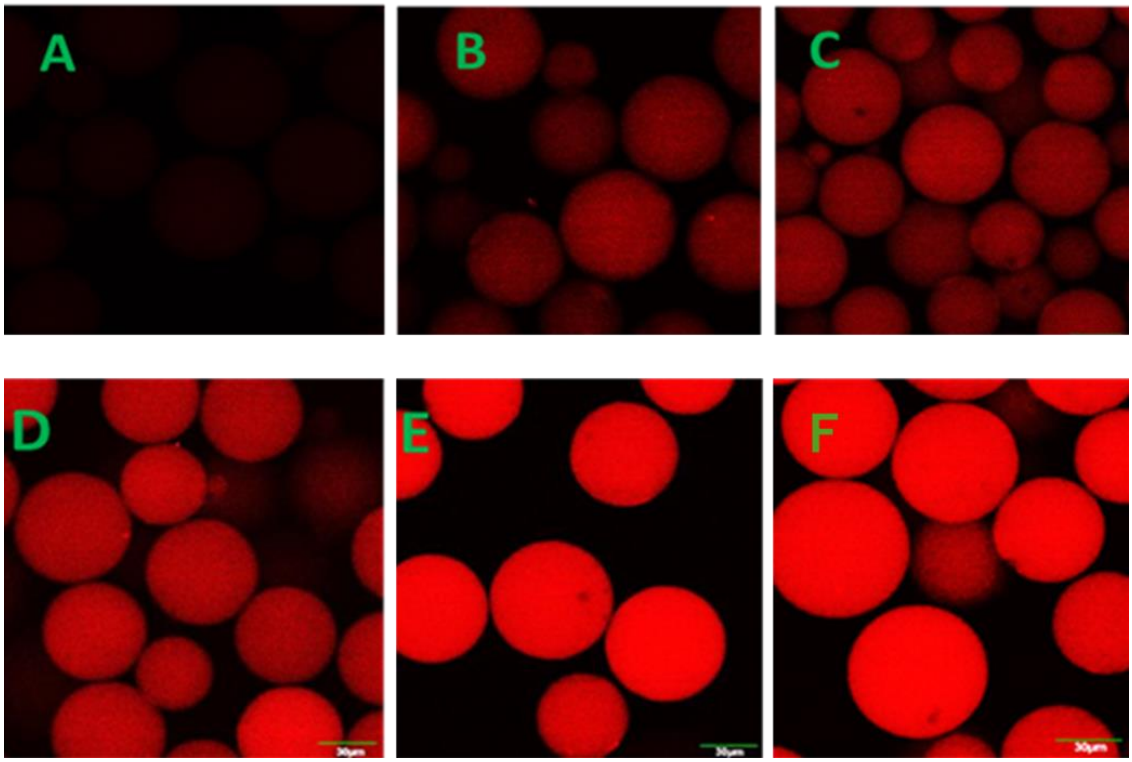

GBs were freeze dried for 2 hours then were loaded with mock drug (Ab-dye 568). The dye loaded GBs were incubated within PBS for 4 days at 37 °C. Confocal images showed the incorporation of dye into the beads with (A) 0 µg/mL; (B) 0.65 µg/mL; (C) 1.25 µg/mL; (D) 2.5 µg/mL; (E) 5 µg/mL and (F) 10 µg/mL. Images representative of 4 independent experiments performed in triplicate using a 40X objective; scale bar=50 µm

5.5.1.1 Assessment of Ab-dye 568 release from GBs

The release of Ab-dye 568 from GBs was assessed quantitatively at different culture time points for GBs loaded with different dye concentrations in order to evaluate the effect of incubation time and dye concentration on the fluorescence release rate and capacity of the GBs to retain dye at 37 °C (Figure 5.2).

The release was significantly elevated from day 2, with peak fluorescence observed at day 4, regardless of initial incorporation concentration ($P < 0.01$-0.0001) compared with control (dye released at day 1). By day 7, fluorescence fell back towards control levels.

Figure 5.2 Effect of incubation time and loading concentration of Ab-dye 568 on the dye release from GBs

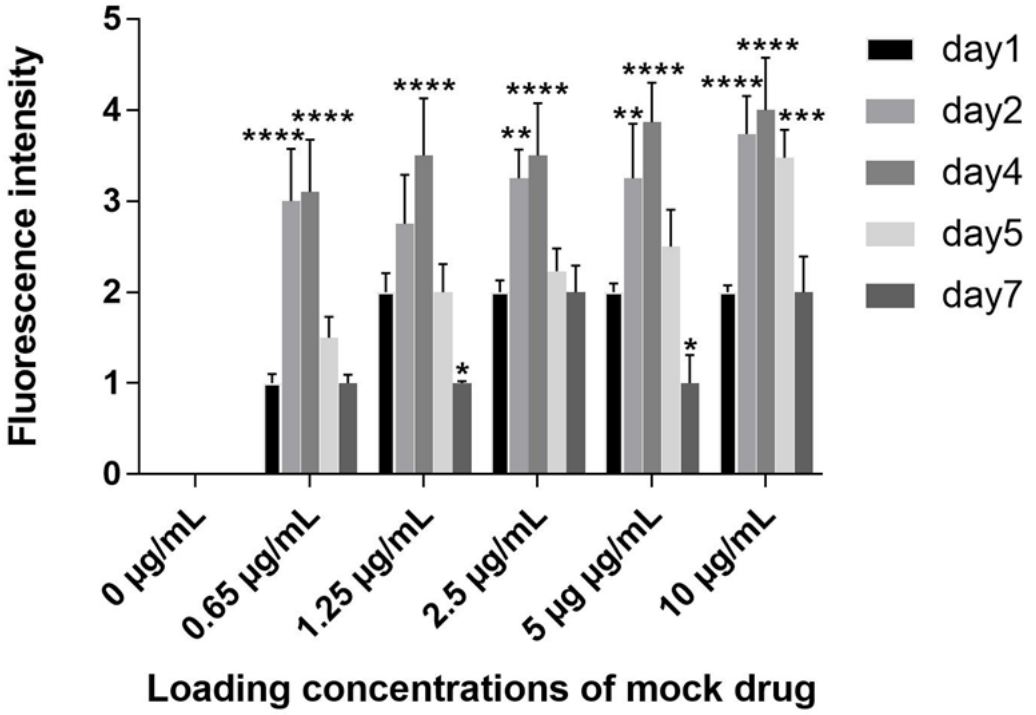

Quantitative measurement of fluorescence is released from GBs to PBS from day 1 to day 7 of incubation at 37 °C. Data are presented as mean ± SD from 3-4 independent experiments conducted in triplicate. *P<0.05, **P<0.01, ***P<0.001 and ****P<0.0001 compared with fluorescence of control (dye released at day 1).

5.5.2 Assessment of the GBs incorporation methods into PI

Different methods have been tried to incorporate GBs into the centre of PIs in order to form voids in the PIs, or to block cell residence in the centre, which allowed gas and nutrient molecules to be diffused to PIs from media within the 100-200 μm distance.

5.5.2.1 Via using flat bottom ULA plate

The first method used to incorporate GBs into PIs was using ULA flat bottom plate plus the shaking of the plate, which aimed to form aggregations of cells and force GBs

to the inner side of the aggregates. Figure 5.3A shows that this method was an inappropriate means of incorporation of GBs into the centre of PIs. This method also produced huge suspension aggregations. After 1, 3 and 7 days' culture, both aggregations with and without GBs did not show compact cell aggregations as exhibited in Figure 5.3A.

The assessment of the cellular viability of the aggregates incorporated with GBs showed that the proliferation of the cells was significantly increased ($P<0.001$) after 3 days and 7 days of culture compared with the proliferation of the aggregation free GBs (control after 1 day culture). An interesting phenomenon was that the incorporation of GBs into the cells increased the cell viability (MTT assay) of cells (Figure 5.3B).

Figure 5.3 Effect of incorporating GBs into PIs by using ULA suspension plates with shaking

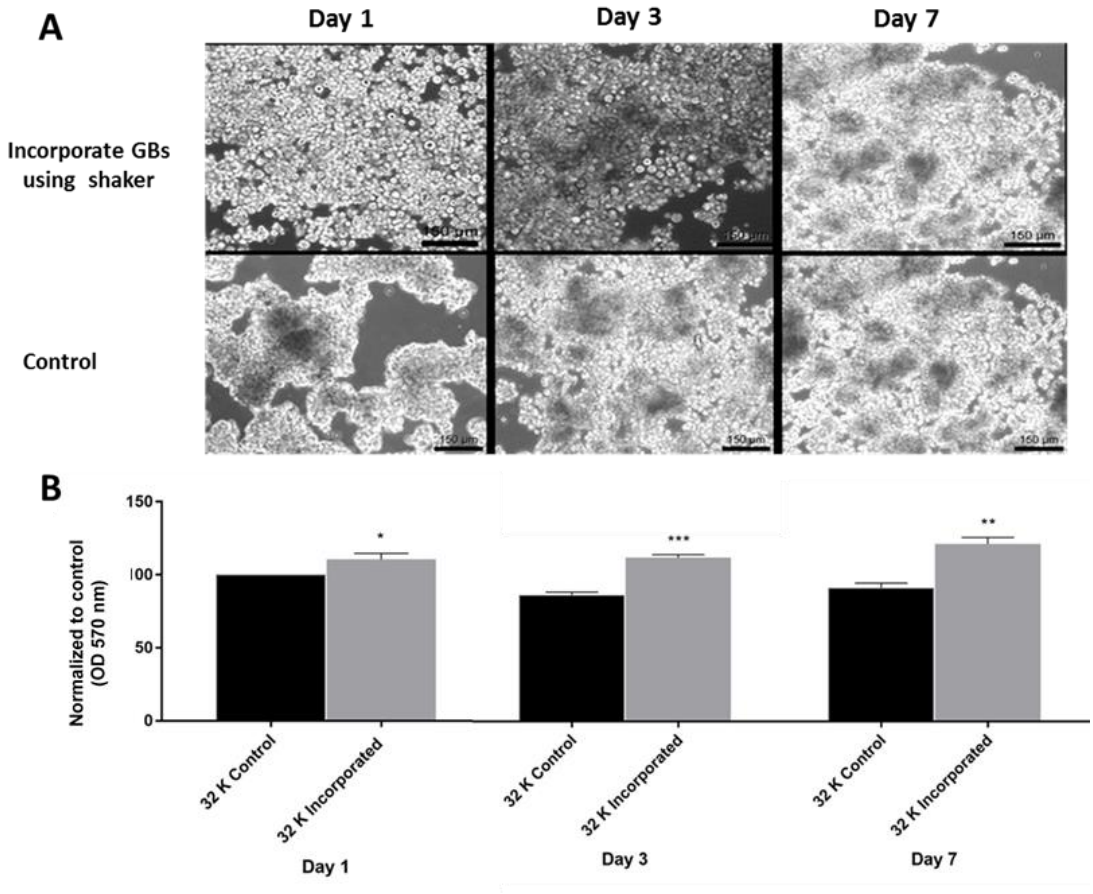

A: Live images of BRIN-BD11 PIs generated at cell seeding density of 32,000 cells/well using the ULA plate flat bottom. B: The impact of GBs on PIs proliferations assessed after 3 days and 7 days using MTT assay. Data are presented as mean ± SD from 3-4 independent experiments conducted in triplicate. *P<0.05, **P<0.01, ***P<0.001 compared with PIs without GBs (control) using a 10X objective; scale bar = 150 µm

5.5.2.2 Via using Eppendorf tube

The second method to incorporate GBs into the PIs used Eppendorf tubes. This method was also found to be inappropriate for the incorporation of GBs into PIs. Figure 5.4A

showed that the beta cells did not form clear PIs in a spherical shape; also not all PIs were incorporated with GBs

MTT assay was used to assess the proliferation of aggregates. The MTT assay results showed that the cell proliferation was significantly decreased ($P<0.001$) at 7 days culturing compared with the proliferation of the cells in PIs free of GBs after day 1 culture (control). Similar to incorporation using ULA method, the presence of GBs resulted in improvements in the cell viability of the PIs after 1, 3 and 7 days culture comparing with control (PIs free of GBs) as shown in Figure 5.4B.

Figure 5.4 Effect of incorporation GBs into PIs by Eppendorf tube method on cell viability

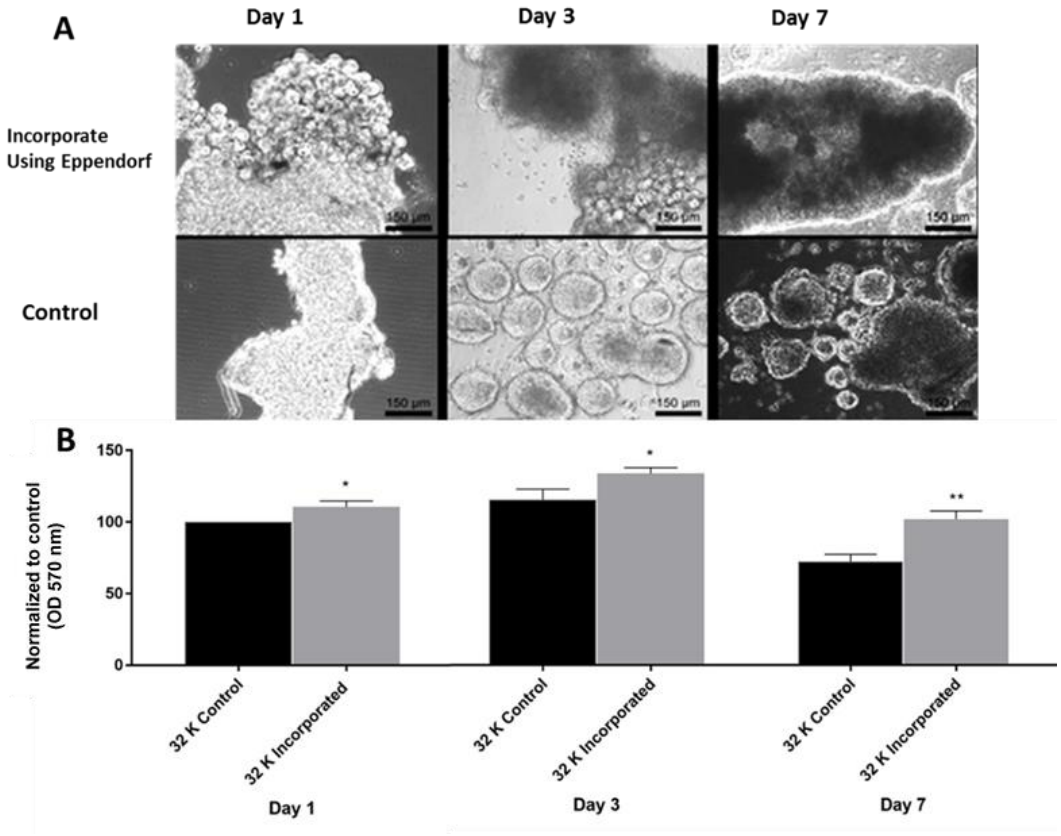

A: Live images of BRIN-BD11 PIs formed in Eppendorf tube at cell seeding density of 32,000 cells/well. B: The impact of GBs on PIs proliferations using Eppendorf tube and assessed after 1 day, 3 days and 7 days using MTT assay. Data are presented as mean ± SD from 3-4 independent experiments conducted in triplicate. *P<0.05, **P<0.01, compared with control (PIs free of GBs) using a 10X objective; scale bar = 150 µm.

5.5.2.3 Via using round bottom ULA plate

Figure 5.5A represents the PIs incorporating GBs using ULA round bottom 96 well plate. This method showed that GBs have successfully incorporated in the centre of PIs and the PIs exhibited symmetric spheroid morphology. Many GBs were stable in PIs after 7 days culture.

MTT assay was used for a quantitative assessment of the cell viability within the PIs. The MTT assay results showed that proliferation of the cells of PIs incorporating with GBs increased about 25% after 7 days culture compared with PIs without GBs as shown in Figure 5.5B.

Figure 5.5 Effect of incorporating GBs into PIs using round bottom ULA plate on cell viability

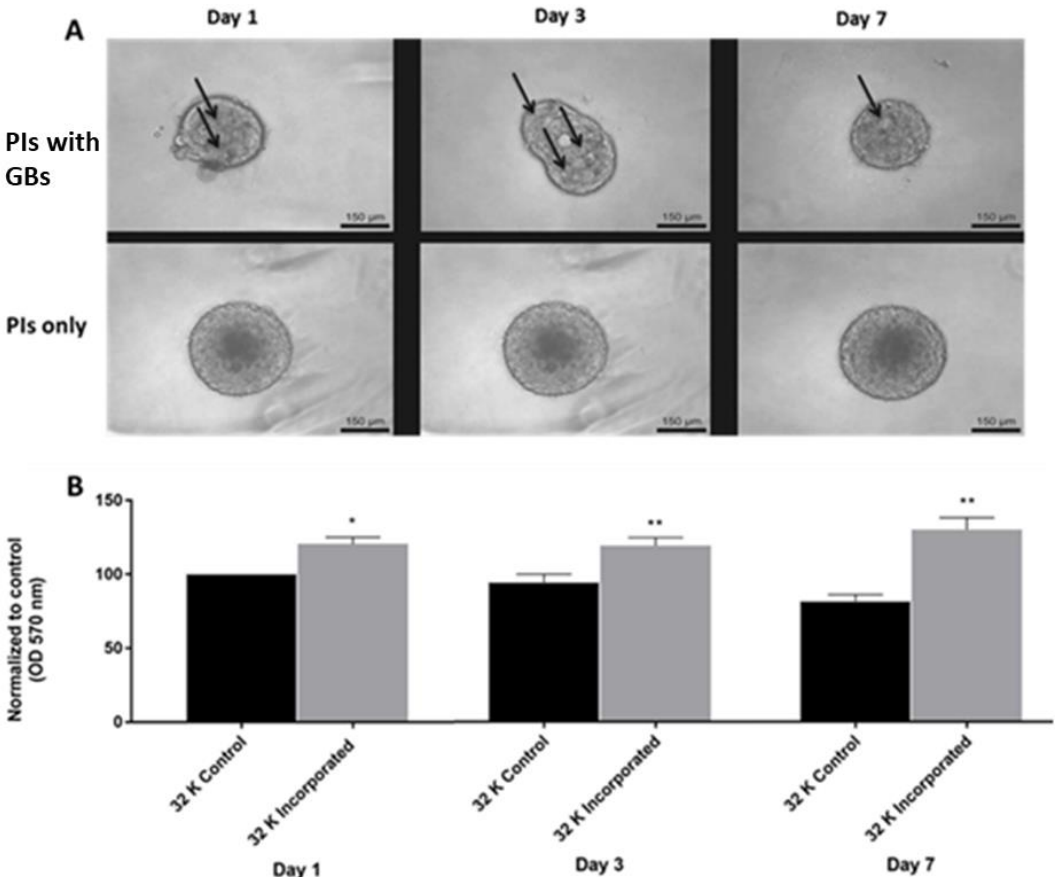

A: Live images of BRIN-BD11 PIs generated in ULA bottom round plate at cell seeding density of 32,000 cells/well. B: the impact of GBs on PIs proliferations using ULA round bottom plate round bottom and assessed after 1, 3 and 7 days culture using MTT assay. Data are presented as mean ± SD from 4-5 independent experiments conducted in triplicate. *P<0.05, **P<0.01, compared with control (PIs free of GBs) using a 10X objective; scale bar = 150 µm.

5.5.3 The effect GB incorporation on PIs' size and morphology

In order to investigate the impact of incorporating GBs into large and small PIs sizes, ULA round bottom plates were used to produce PIs with two seeding densities, 32,000 cells/well and 64,000 cells/well. Incorporation of 25-30 GBs into PIs for 32,000 cells/well and 50-60 GBs into PIs for 64,000 cells/well were performed (Figure 5.6).

Figure 5.6 Live images of PIs with GBs incorporation and cultured for 7 days

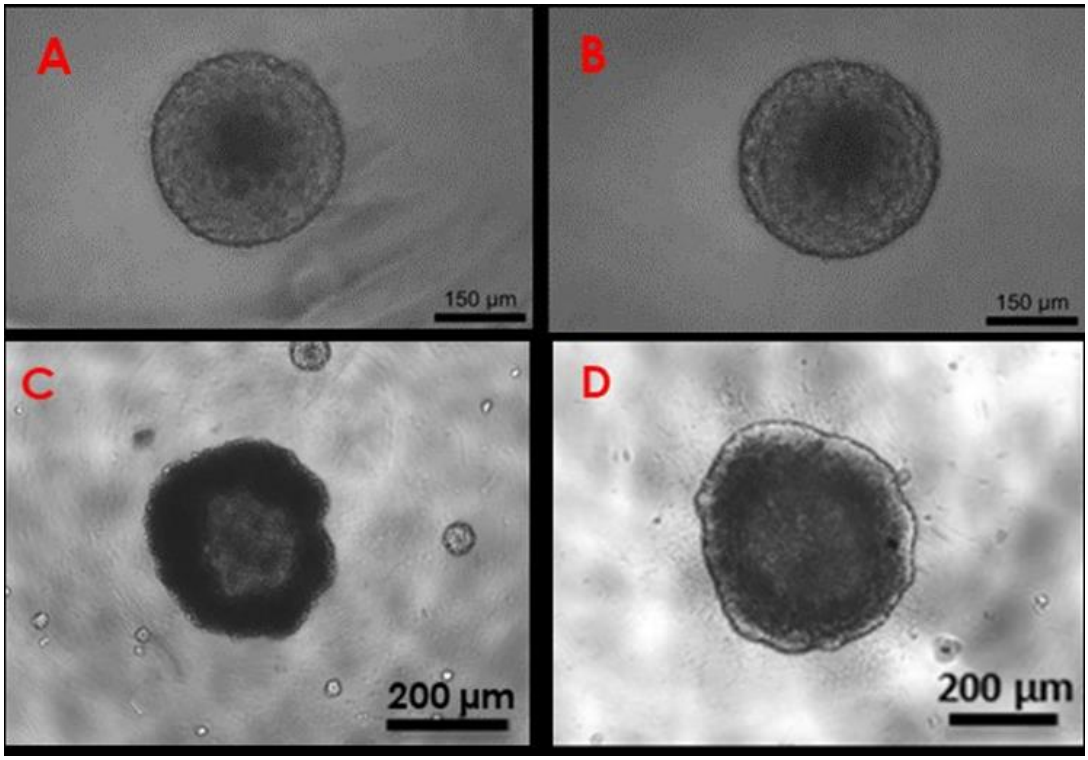

Live images of BRIN-BD11 PIs generated with cell seeding densities 32,000 cells/well free of GBs (A); 32,000 cells/well with GBs (B); 64,000 cells/well free of GBs (C); 64,000 cells/well with GBs (D) using a 20X objective; Scale bar is 150 µm for A, B and 200 µm for C, D

The size of these PIs with and without GBs was quantified using ImageJ after day 1, 3 and 7 in culture. The sizes of PIs were significantly increased ($P<0.01$) after 3 days

and 7 days of culturing for the PIs with GBs comparing with PI free of GBs (control) for cell seeding densities (32,000 cells/well); while for another cell seeding density (64,000 cells/well) there was a significant increase ($P<0.05$) for PIs incorporation of beads only at day 7 compared with PIs with control (Figure 5.7).

Figure 5.7 Effect of the cell density and GBs on PIs size

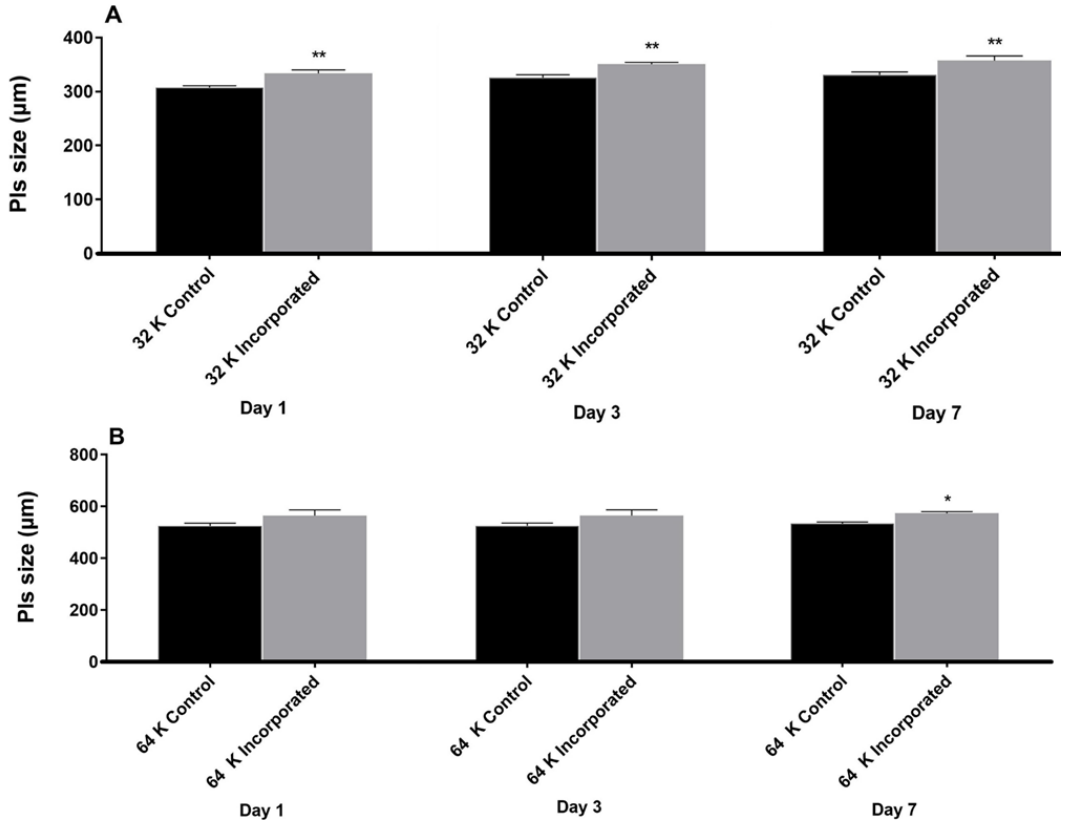

BRIN-BD11 cells were seeded at densities of 32,000 cells/well (A) 64,000 cells/well (B) and the impact of cell seeding density on PI size assessed after 1, 3, 7 days in the presence ('incorporated') or absence of GBs. Data are presented as mean ± SD from 3 independent experiments conducted in triplicate. *$P<0.05$ and **$P<0.01$ compared with control (PIs free of GBs).

5.5.4 The effect of coated GBs on the cell viability of PIs

The effect of coated GBs on the cell viability of PIs was assessed after 7 days culture (Figure 5.8A). Incorporation of GBs coated with fetal bovine serum (FBS), or fibronectin (FN) did not affect the proliferative rate of PIs. However, GBs coated with inactivated FBS showed a small improvement in proliferation ($P<0.05$; Figure 5.8B) comparing with control (PIs only) by using MTT assay.

Figure 5.8 Effect of GB coating on the proliferation of PIs incorporating with the GBs

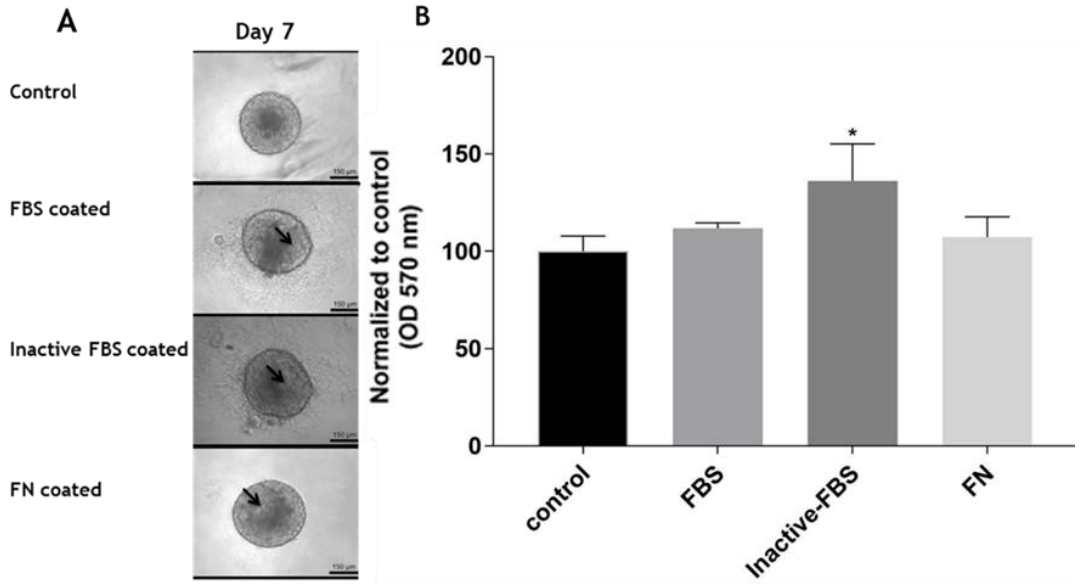

A: Live images of BRIN-BD11 PIs seeded at 32,000 cells/well and incorporating GBs. B: the impact of coated GBs on PIs proliferations assessed after 7 days culture using MTT assay. Data are presented as mean ± SD from 3-4 independent experiments conducted in triplicate. FN refers to fibronectin. *$P<0.05$, compared with control (PIs free of GBs). Scale bar = 150 µm.

5.5.5 Assessment of the activity of PIs after loaded with anti-inflammatory drugs

IL-10 is a regulatory cytokine which inhibits antigen presentation and subsequent pro-inflammatory release. This cytokine has been used as a potent anti-inflammatory agent in various biological applications.[216] IL-1β is a potent pro-inflammatory cytokine which is essential for host-defence responses to infection and injury.[212] So, incorporating IL-10 and anti-IL-1β agents inside of PIs and achieving sustained release of the agents in PIs could delay the inflammation of cells and improve the biological functionality of PIs.

5.5.5.1 The effect of IL-10 concentrations on the cell viability of PIs

IL-10 solutions at different concentrations in culture media were used to assess the optimized concentration for PIs' viability. The proliferation of PIs at day 7 culture was measured using CCK-8 assay (Figure 5.9A, B). The CCK-8 assay results showed that IL-10 concentrations between 10 ng/mL and 1000 ng/mL significantly increased ($P<0.05$-0.0001) the proliferation of the PIs. Also, it can be seen that the PIs cultured with 100 ng/mL of IL-10 in the media had the highest viability ($P<0.0001$) (Figure 5.9 B).

Figure 5.9 Effect of different concentrations of IL-10 on the cell viability

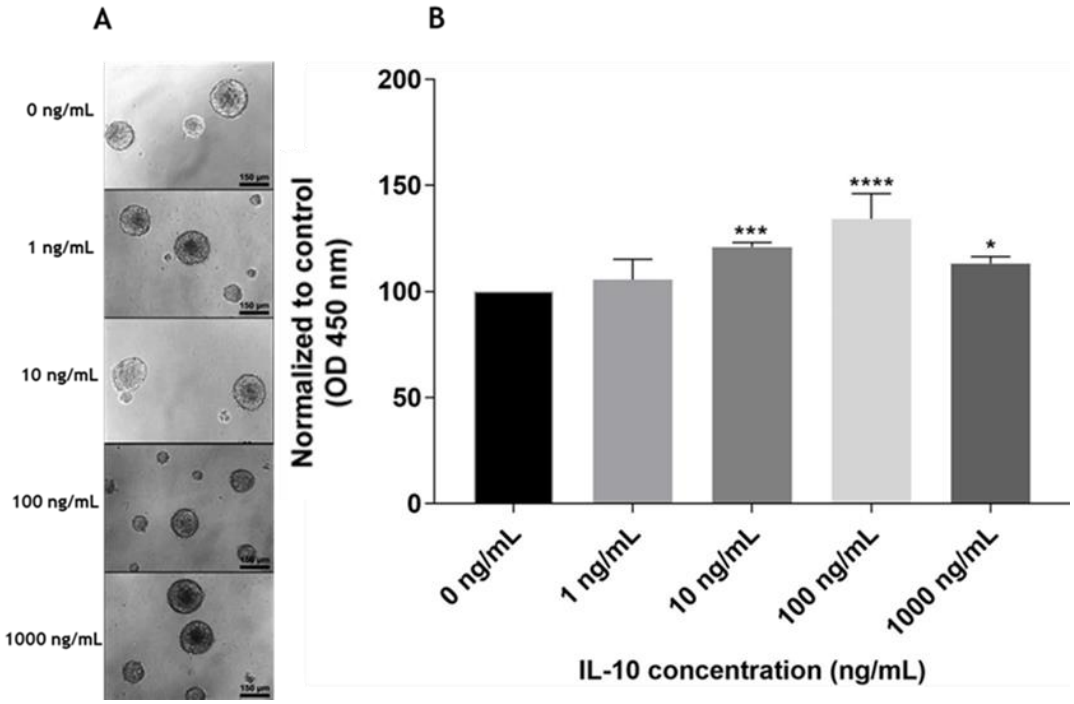

A: live image of BRIN-BD11 PIs generated at cell seeding densities of 32,000 cells/well. B: the impact of the GBs loading with IL-10 of different concentrations on the proliferation of PIs after 7 days culturing using CCK-8 assay. Data are presented as mean ± SD from 3-4 independent experiments conducted in triplicate. *P<0.05, ***P<0.001 and ****P<0.0001 compared with control (PIs with 0 ng/mL of IL-10). Scale bar = 150 µm

5.5.5.2 The effect of anti- IL-1β concentrations on the cell viability of PIs

Anti-IL-1β solutions at different concentrations in culture media were used to assess the optimized concentration for PIs' viability. The proliferation of PIs at day 7 culture was measured using CCK-8 assay. The CCK-8 assay results displayed that anti-IL-1β concentrations between 0 µg/mL and 1000 µg/mL significantly increased (P<0.0001)

the proliferation (cell viability) of the PIs. Also, it was seen that the PIs mixed with 100 ng/mL of IL-10 had the highest (P<0.0001) proliferation as shown in Figure 5.10B.

Figure 5.10 Effect of anti-IL-1β concentrations on the cell viability of PIs

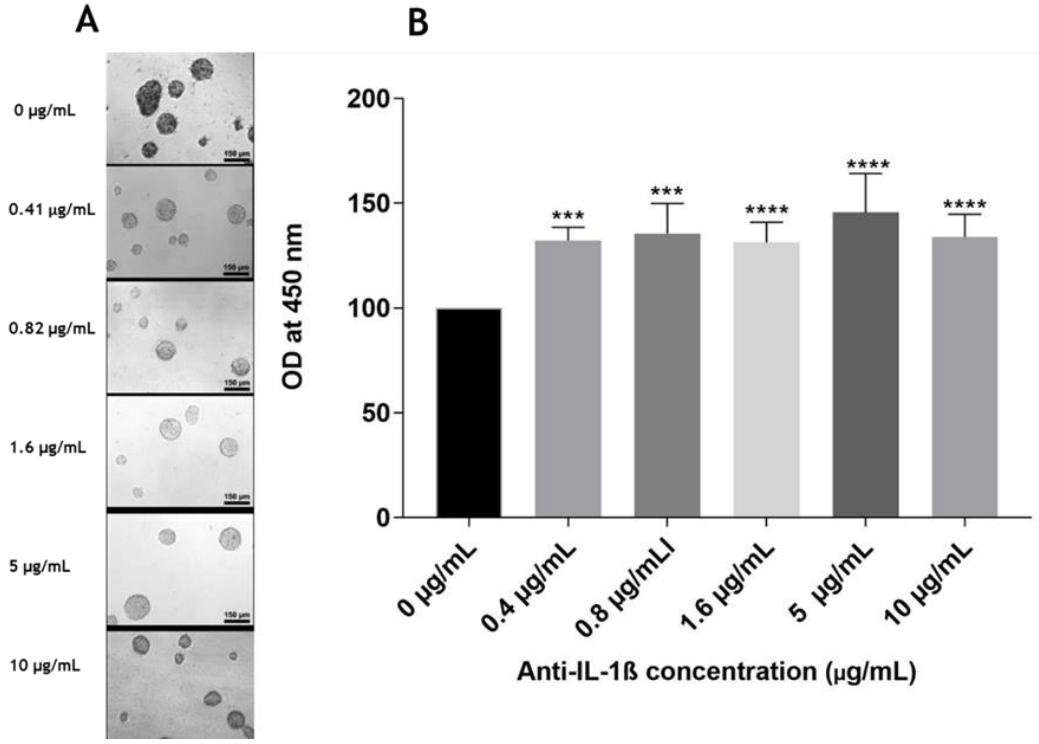

A: live images of BRIN-BD11 PIs generated at cell seeding densities of 32,000 cells/well. B: the impact of the GBs with anti-IL-1β in different concentrations on the proliferation of PIs after 7 days culturing using CCK-8 assay. Data are presented as mean ± SD from 4-5 independent experiments conducted in triplicate. ***P<0.001 and ****P<0.0001 compared with control (PIs with 0 µg/mL anti-IL-1β).

5.5.6 Assessment of the functionality of PIs incorporated with GBs loaded IL-10 and anti-IL-1β

5.5.6.1 Assessment using CCK-8 assay

5.5.6.1.1 GBs loaded with IL-10

After a study of the dose effect of IL-10 on the cell's viability, the GBs were loaded with the best effective dose, 100 ng/mL IL-10, and then incorporated into PIs. The cell proliferation of PIs was estimated by using CCK-8 assay after 7 days of culture. The results showed that the proliferation of PIs with cell seeding density 32,000 cells/well significantly increased ($P<0.05$-0.0001) after 3 7 days in culture. Furthermore, the incorporation of GBs without loading IL-10 showed a significantly improved ($P<0.05$-0.01) proliferation of the PIs after 3 days and 7 days in the culture comparing with proliferation of PIs only (control). The PIs incorporating GBs only or with GBs loaded with IL-10 showed a significant increase ($P<0.05$ and $P<0.01$) in proliferation, at 3 days and 7 days in comparison with control (PIs only) as shown in Figure 5.11A. Furthermore, the incorporation of GBs without loading IL-10 showed the same trend with significantly improved (0.0001) proliferation of the PIs after 3 days and 7 days.

Figure 5.11B shows the effect of GBs loaded IL-10 and incorporated into PIs at cell seeding density 64,000 cells/well on the proliferation. The PIs were assessed by using CCK-8 assay during 7 days culture. The activity of cells within PIs which were incorporated with GBs loaded with IL-10 was significantly increased ($P<0.05$-0.0001) after 3 and 7 days in the culture (comparing with the activities of the control (PIs free of GBs) as shown in Figure 5.11B. Whereas the proliferation of PIs significantly was increased ($P<0.05$-0.01) when the PIs incorporated with GBs only. So using IL-10 to be sustained release in the central of PIs could improve the cell viability in PIs cultures with cells seeding density of 64,000 cells/well.

Figure 5.11 Effect of GBs loaded with IL-10 on the proliferation of PI cells

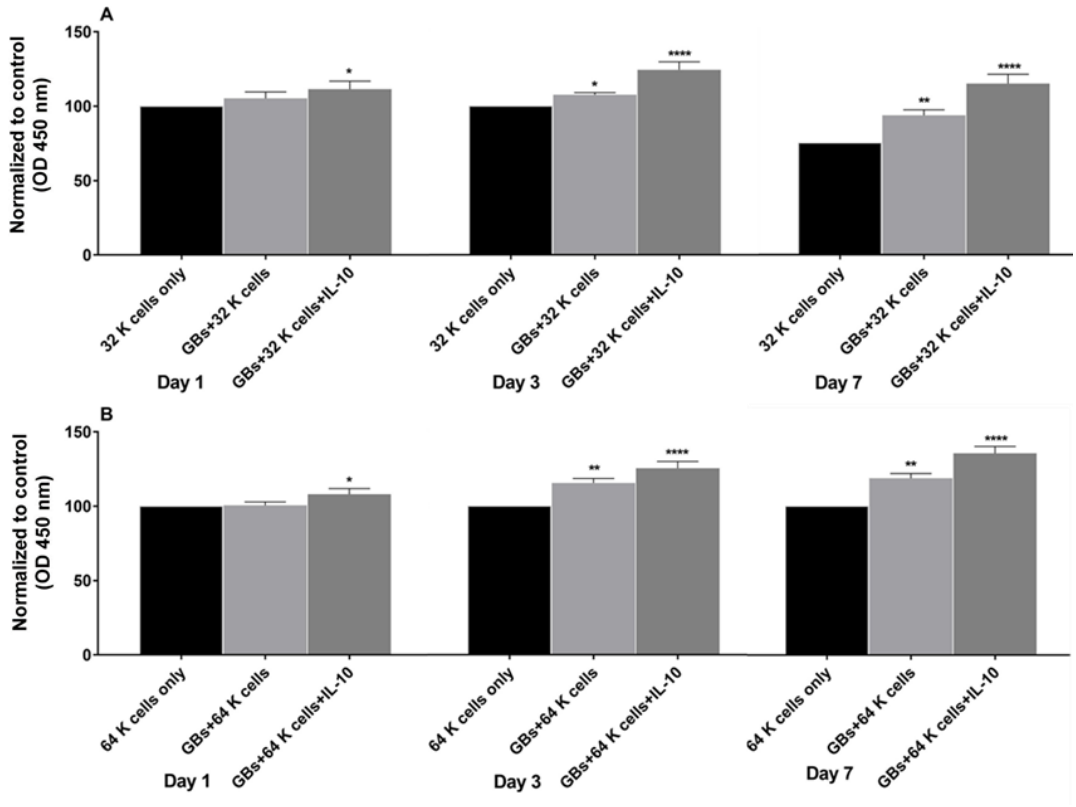

A: Cell seeding density 32,000 cells/well. B: Cell seeding density 64,000 cells/well. Data are presented as mean ± SD from 4-5 independent experiments conducted in triplicate. *P<0.05, **P<0.01 and ****P<0.0001 compared with control (PIs only)

5.5.6.1.2 GBs loaded with anti-IL-1β

After determination, the best dose of anti-IL-1β to be loaded in GBs was found as 5 µg/mL. Then, the GBs loaded with 5 µg/mL anti-IL-1β were incorporated into PIs. The cell viability of PIs was estimated by using CCK-8 assay during 7 days culture. The results showed that the cell viability of PIs with cell seeding density of 32,000 cells/well without GBs did not change at day 3, but reduced at day 7 culture. The cell viability of PIs incorporating with GBs loaded with anti-IL-1β was significantly

increased ($P<0.0001$) in comparison with control as shown Figure 5.12A. Furthermore, the PIs incorporated with GBs without anti-IL-1β also showed significant improvements in the proliferation of the PIs after 7 days culture in PIs with cell seeding density of 32,000 cells/well as shown in Figure 5.12A.

Figure 5.12B shows the effect of loading anti-IL-1β into GBs which were incorporated into PIs with cell seeding density of 64,000 cells/well on cell viability. The cell viability of the PIs was assessed by using CCK-8 assay during 7 days culture. The activity of cells within PIs which incorporated with GBs loaded with anti-IL-1β was significantly increased ($P<0.05$) after 1 day, 3 days ($P<0.0001$) and at 7 days ($P<0.0001$) comparing with that of control (PIs only) (Figure 5.12B). Whereas the cell viability of PIs significantly increased ($P<0.01$-0.001) at day 3 and day 7 culture respectively when incorporated with GBs without anti-IL-1β. So using anti-IL-1β loaded GBs which sustained release in the central of PIs would improve the cell viability in PIs with cell seeding density of 64,000 cells/well as shown in Figure 5.12B.

Figure 5.12 Effect of anti-IL-1β within GBs on the proliferation of PI cells

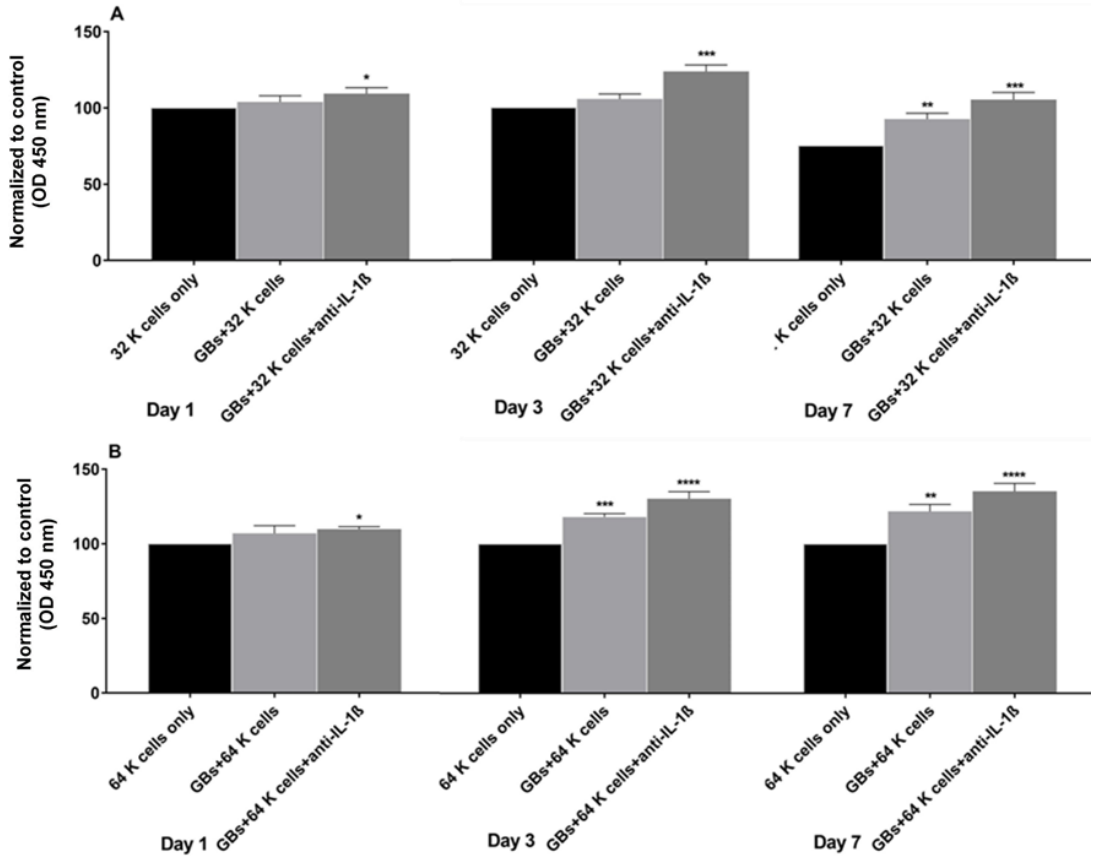

A: Cell seeding density 32,000 cells/well. B: Cell seeding density 64,000 cells/well. Data are presented as mean ± SD from 4-5 independent experiments conducted in triplicate. * P<0.05, **P<0.01, ***P<0.001 and ****P<0.0001 compared with control (PIs only).

5.5.6.2 Assessment of cellular LDH release

The cellular LDH release was used to measure the integrity of cellular membranes, which is elevated during cell death or cell apoptosis in PIs.[156] Four experimental groups have been examined: PIs only, PIs incorporating GBs, PIs incorporating GBs loaded with anti-inflammatory cytokines, PIs cultured with free anti-inflammatory cytokines in culture media.

5.5.6.2.1 PIs incorporating GBs loaded with IL-10

The cellular LDH released from PIs seeded at 32,000 cells/well was investigated at day 7, and the results are shown in Figure 5.13A. PIs generated significance ($P<0.01$ and $P<0.001$) lower LDH values, when incorporated with GBs or GBs loaded with IL-10 compared with PIs only group (control) after 7 days in culture as shown in Figure 5.13A. While adding IL-10 directly in media for PI culture did not show a significant decrease the LDH release compared with PIs only group (control) after 7 days in culture as shown in Figure 5.13A

The same trend was observed for the cellular LDH released from PIs seeding at 64,000 cells/well at day 7, and the results are shown in Figure 5.13B. PIs generated significance ($P<0.05$ and $P<0.001$) lower LDH values when PIs incorporated with GBs or GBs loaded with IL-10 compared with PIs only group ((control) after 7 days in culture. Therefore, using GBs and GBs loaded with IL-10 decreased the cytotoxicity in the term of cellular LDH release.(213). Also for large PIs (64,000 cells/well, adding anti-IL-10 directly to media did not show a significant decrease the LDH release compared with PIs only group (control) after 7 days in culture as shown in Figure 5.13B.

Figure 5.13 Cellular LDH release in PIs incorporating the GBs loaded with IL-10 at day 7

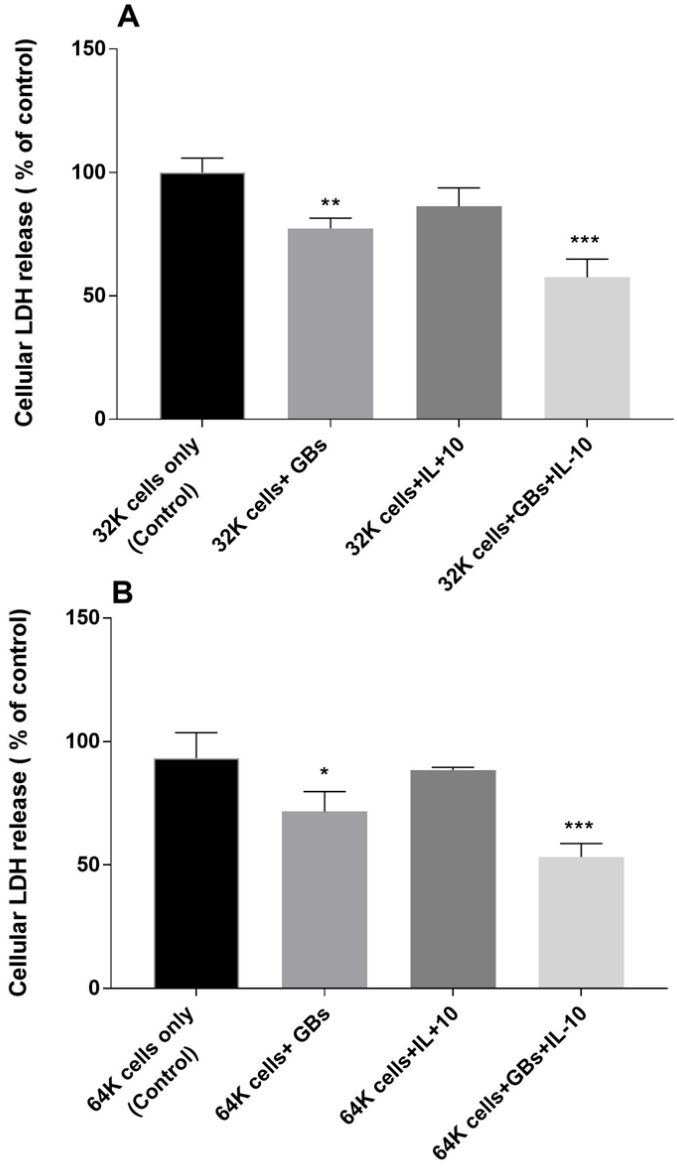

A: Cell seeding density 32,000 cells/well. B: Cell seeding density 64,000 cells/well. Data are presented as mean ± SD from 4 Independent experiments conducted in triplicate. *P<0.05 and ***P<0.001 compared with control (PIs only).

5.5.6.2.2 PIs incorporating GBs loaded with anti-IL-1β

The cellular LDH released from PIs seeded at 32,000 cells/well was investigated at day 7, and the results are shown in Figure 5.14A. PIs generated significance ($P<0.01$ - $P<0.0001$) lower LDH values when incorporated with GBs, or GBs loaded with anti-IL-1β compared with PIs only (control) after 7 days in culture shown in Figure 5.14A. But adding anti-IL-1β directly to media did not show a significant decrease in the LDH release compared with LDH release from PIs only group (control) after 7 days in culture Figure 5.14A.

On the same trend was observed the cellular LDH released from PIs seeded at 64,000 cells/well was investigated at day 7, and the results are shown in Figure 5.14B. PIs generated significance ($P<0.01$ - $P<0.0001$) lower LDH values when PIs incorporated with GBs or GBs loaded with anti-IL-1β compared with PIs only (control) after 7 days in culture. Therefore, using GBs and GBs loaded with anti-IL-1β significance ($P<0.01$ - $P<0.0001$) decreased the cytotoxicity in the term of cellular LDH release compared with PIs only (control) after 7 days in culture. Also. adding anti-IL-1β directly to media was revealed a significant decrease ($P<0.01$) in the LDH release compared with LDH data of PIs only group (control) after 7 days in culture (Figure 5.14B).

Figure 5.14 Cellular LDH release in PIs incorporating the GBs loaded with anti-IL-1β at day 7

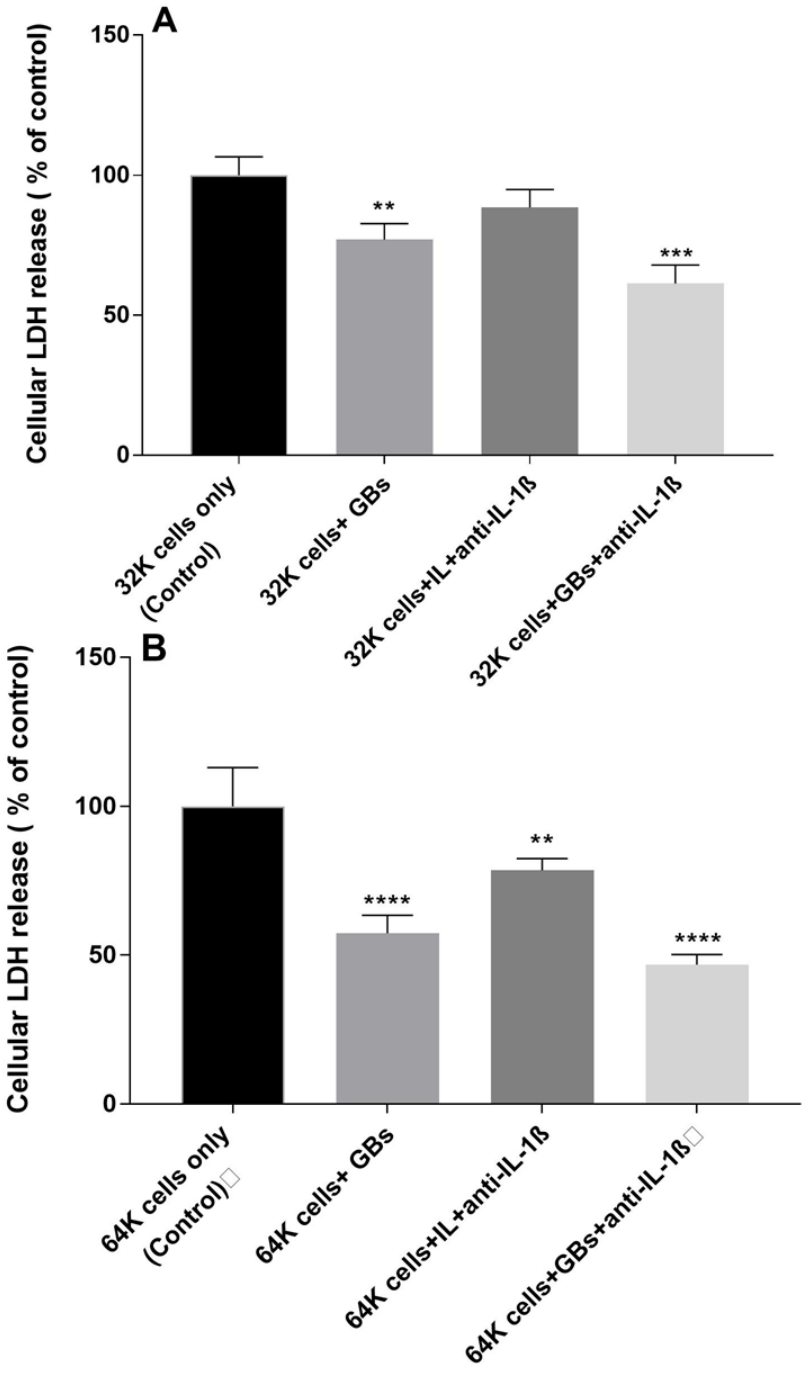

A: Cell seeding density 32,000 cells/well. B: Cell seeding density 64,000 cells/well. Data are presented as mean ± SD from 4 independent experiments conducted in triplicate. *P<0.01 and ***P<0.001 compared with control (PIs only)

5.5.6.3 Assessment of GSIS release

5.5.6.3.1 GBs loaded with IL-10

GSIS of PIs seeded at 32,000 cells/well with and without incorporation of GBs loaded with recombinant IL-10 was assessed. As shown in Figure 5.15, PIs culturing with free IL-10 in media or PIs incorporated with GBs or PIs incorporated with GBs loaded with IL-10 showed significant increases ($P<0.01$-0.001) in GSIS comparing with PIs only (control) at day 7 in culture. Therefore, the addition of GBs and IL-10 into PIs improved the functionality of PIs regarding GSIS.

Figure 5.15 Effect of incorporating GBs loaded with IL-10 into PIs on GSIS

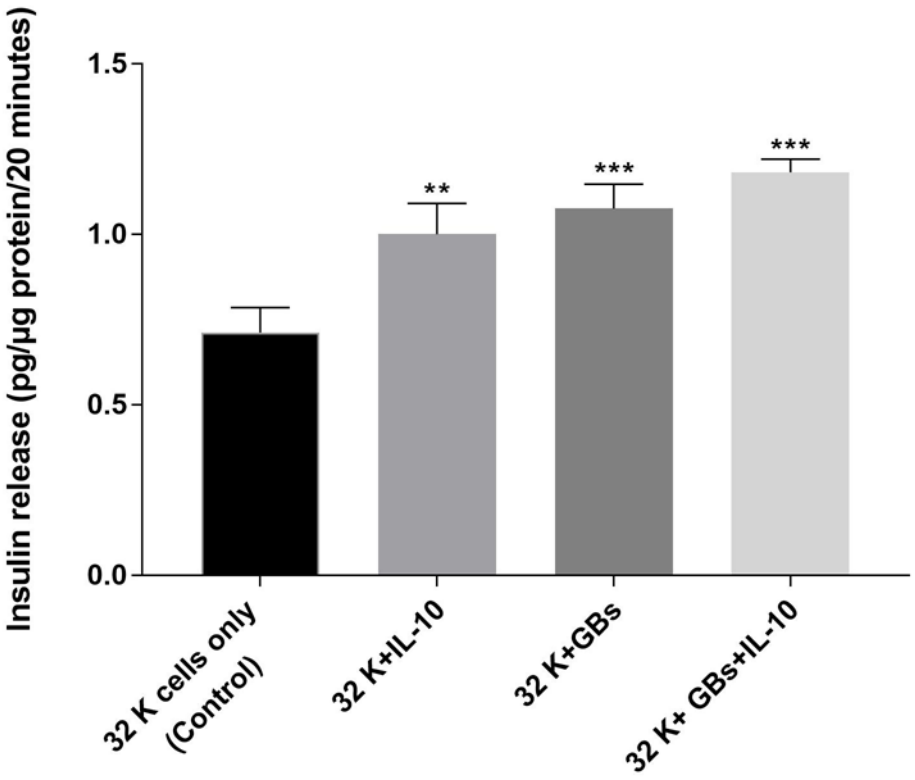

BRIN-BD11 cells were seeded at 32,000 cells/well and allowed to form PIs over a one-week period. Cells were exposed to recombinant IL-10 (100 ng/mL) alone, GBs alone, or GBs loaded with recombinant IL-10. Data are presented as mean ± SD from 3 Independent experiments conducted in triplicate. **P<0.01 and ***P<0.001 compared with control (PIs only).

5.5.6.3.2 GBs loaded with anti-IL-1β

GSIS of PIs seeded at 32,000 cells/well with and without incorporation of GBs loaded with recombinant anti-IL-1β was assessed. As shown in Figure 5.16, PIs culturing with free IL-10 in media and PIs incorporated with GBs loaded with anti-IL-1β showed significant increases ($P<0.01$-0.001) in GSIS comparing with PIs only (control) at day 7 in culture. Therefore, the addition of GBs and anti-IL-1β into PIs improved the functionality of PIs in term of GSIS assay.

Figure 5.16 Effect of incorporating GBs loaded with anti-IL-1β into PIs on GSIS

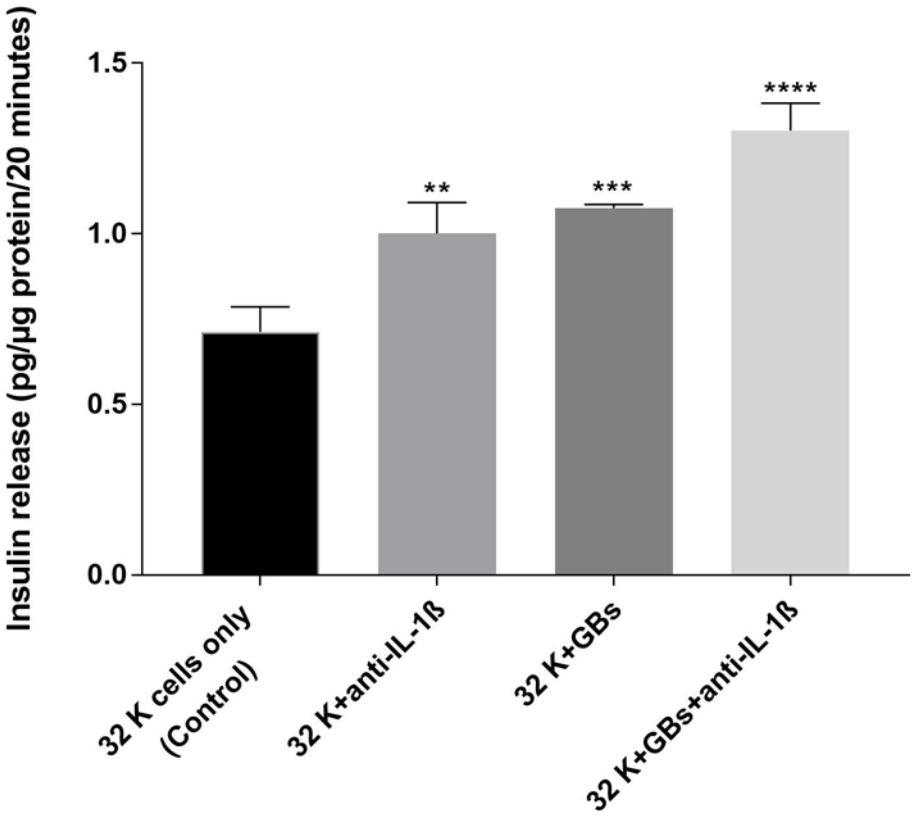

BRIN-BD11 cells were seeded at 32,000 cells per well and allowed to form PIs over a one-week period. Cells were exposed to anti-IL-1β alone, incorporated with GBs alone, or GBs loaded with anti-IL-1β. Data are presented as mean ± SD from 3 Independent experiments conducted in triplicate. **P<0.01, ***P<0.001 and ****P<0.0001 compared with control (PIs only).

5.6 Discussion

Although varied approaches have been used to generate PIs from cell suspensions, most of these approaches involve the use of suspension surfaces,[27,83] which are often associated with central necrosis.[17,18] In this Chapter, we aimed to improve the central necrosis of large PIs to ensure high cellular viability and good functionality regarding glucose-stimulated insulin secretion. Two approaches were employed: firstly, GBs were incorporated into PIs to create the vent or reduce cell residence in the centre of PIs; secondly, GBs were loaded with anti-inflammation or anti-necrosis agents to enhance cell survival.

Multiple assays confirmed that the GBs could be incorporated into PIs to produce voids within PIs, evidenced by the higher cell viability and insulin production. Synergistic use of GBs loaded with anti-inflammatory drugs further improved the cell viability and PIs' functionality.

5.6.1 Incorporation of GBs into PIs improved cell viability

The incorporation of GBs into PIs resulted in enhanced cell viability of PIs regardless of the seeding density used. This may arise due to the creation of a void following the dissolution of the GBs resulting in a morphological arrangement that enabled the efficient and easy exchange of gases and nutrients from the media to the cells. It was

exhibited that PIs with GBs incorporated formed larger structures without an increase in cell number. This again was likely due to the space created by the GBs. This arrangement of cells with 'pockets' where the GBs were present, was likely to significantly improve nutrient and oxygen diffusion to the centre of the PI and may account for the improvements in viability observed here and elsewhere.[214,215] Incorporating GBs to large PIs has special benefit and interests because this method can create a better gas and nutrient exchange environment to overcome the 200 μm diffusion limit.[4]

5.6.2 The synergetic effect of incorporating GBs loaded with anti-inflammatory cytokines on the cellular activities of PIs

To investigate the protective effects of anti-inflammatory cytokines on the cellular activities of PIs, both IL-10 and anti-IL-1β were loaded into GBs and compared with cytokines added to culture media in free form and also, to GBs only. Adding both IL-10 and anti-IL-1β to culture media increased PIs' viability. The viability of PIs increased by only 15% for cell seeding density of 32,000 cells/well and 11% for cell seeding density of 64,000 when IL-10 was added directly to culture media comparing with PIs only (control) at day 7. Similarly, adding anti-IL-1β directly to media slightly improved the viability of PIs in terms of the CCK-8 assay (at day 7) by 14% for 32,000

cells/well and 13% for 64 cells/well at the same day (day 7) comparing with control (PIs with free of GBs).

The sustained release of the anti-inflammatory drug from GBs showed the enhancement of the PIs functionality. The release of IL-10 increased cell viability by 60% at a cell seeding density of 32,000 cells/well and 35% at a cell seeding density of 64,000 cells/well for PIs with GBs loaded with IL-10 compared with control at day 7. Also, the viability was elevated by 35% at a cell seeding density of 32,000 cells/well and 40% at al cell seeding density of 64,000 cells/well for PIs with GBs loaded with anti-IL-1β compared with control at day 7.

The cytokines in free form placed in cell culture environment have short activity time due to degradation by proteinases released from the cultured cells. The incorporation of GBs loaded with cytokines into PIs apparently protected the cytokines from degradative processes and sustained the slow release of cytokines from GBs ensuring prolonged anti-apoptotic or anti-necrosis. Both cell viability assay and insulin production assay revealed the synergetic effect when the anti-inflammatory cytokines were loaded into GBs, and the GBs were incorporated into PIs in comparison to the incorporation of GBs only or using free cytokines.

5.6.3 The possible working mechanisms of IL-10 and anti- IL-1β loaded GBs in PIs

The improvement of the cellular activities of the PIs by GBs and further improvement by the GBs loaded with IL-10, and anti-IL-1β gave us the opportunity to study the main cause that reduced PIs' functionality during the prolonged culture.

It is well known that IL-10 is derived from macrophages and TH2 cells and exerts anti-inflammatory effects by inhibiting IL-12 and other pro-inflammatory macrophage cytokines (such as IL-1, IL-6, IL-8 and TNFα) via increasing macrophage production of IL-1 receptor antagonist and by inhibiting the generation of oxygen and nitrogen free radicals by the macrophage.[216,217] On the other hand, IL-1β works as a pro-inflammatory cytokine with cells displaying elevated levels of the cytokine under inflammatory challenge.[212]) Importantly, IL-1β is centrally driven by beta cell apoptosis in type 1 diabetes. In the current study, anti-IL-1β was employed to inhibit the action of IL-1β as an anti-inflammatory drug. According to the observation of Rubartelli and colleagues,[218] the cellular IL-1β is localised in intracellular vesicles and secreted by an intracellular membrane. It is elevated under stress condition,[233,234] but can be redirected to the extracellular space following inappropriate secretion. They proved that IL-1β could be blocked by using methylamine and low temperature.[219] The anti-IL-1β possibly delays or prevents cell signals from reaching to localised

cellular IL-1β, and the pro-inflammatory cytokine would delay from being secreted. In this study, we applied IL-10 or anti-IL-1β to PIs and improved PIs' activities. These observations indicate that inflammatory reactions or cell stress in PIs due to low oxygen level might be the main cause of PIs' lower cell viability and functionality after the prolonged culture. Hence, effective and sustained delivering of anti-inflammatory agents to PIs will be an effective strategy to enhance PIs' activities.

5.6.4 Multiple assessment techniques

In this study, multiple assays have been used to assess the enhancement effect of GBs. It is found that measurement of LDH is a feasible and sensitive assay alongside cell viability and GSIS assay.

Through using a sustained release of IL-10, the cellular LDH release from PIs with GBs loaded with IL-10 displayed a significant decrease in the ratio between cellular LDH release at day 7 culture and day 1 from a 3-fold against control to a 1.25-fold for PIs with GBs loaded with IL-10. This was consistent with results obtained from the cell viability, which was higher in PIs with GBs loaded with IL-10. Additionally, the LDH release was consistent with the results of mitochondrial and membrane activity assessed by CCK-8 that showed decreasing at day 7 culture due to some degree of

hypoxia in the central region of PIs which also the changes in the cellular integrity.[150] The enhancement outcome of PIs with GBs in GSIS was consistent with LDH and cell viability assays.

The cellular LDH released from the PIs showed a decline when GBs loaded with IL-10 were incorporated into the PIs regardless of the seeding density used. Similar data was contained with the use of anti-IL-1β. Ultimately, the viability and functionality of PIs over a one-week culture were improved with insulin production increased by 1.5-fold when IL-10 was loaded onto GBs and by 1.6-fold when anti-1L-1β was loaded onto the GBs over a one-week culture period.

5.6.5 The effect of dose and type of anti-inflammatory cytokines

Two types of anti-inflammation cytokines have been included into GBs. For IL-10, 100 ng/mL was used for GB loading and then incorporated into PIs. It caused an increase in the viability by 62% compared with control (PI free of IL-10). While loading of 5 μg/mL of anti-IL-1β into GBs and incorporating to PIs has elevated the viability by 35% comparing with PIs free of anti-IL-1β. The direct comparison of the effect of IL-10 and anti-IL-1β cytokine on the enhancement of PIs' activities is difficult from this study. The molecular weight and the total loaded mass of the two

cytokines to GBs were different. Further investigation is required to define the working pathway, and more candidate cytokine for GB loading should be undertaken.

5.7 Conclusion

The incorporation of GBs into the centre of PIs was successfully fabricated in this study. Thus GBs facilitated the creation of voids or blocked from being located in the centre of PIs. The proliferation of PIs significantly increased by incorporation of GBs into PIs. This was confirmed by both MTT and CCK-8 assays for large and small PIs.

Adding free anti-inflammatory drugs directly to the media showed an improvement in the functionality of PIs compared with PIs free of cytokines regardless. However, the improvement of the free anti-inflammation agents in the culture media was lower than the effect by incorporating GBs loaded with these agents into PIs. Both cell viability assay and GSIS assay showed that incorporating GBs only to PIs improve the PIs' performance. The sustained release of anti-inflammatory drug from GBs showed even higher enhancement of PIs' functionality, indicating a synergetic effect. The benefit from the release of both IL-10 and anti-IL-1β for the PIs were manifested as the rise of the cellular activities, decreasing of cellular LDH release, and eventually, the elevated amount of insulin released.

The cellular LDH activity was decreased by ~30-50% after incorporated PIs with GBs loaded with IL-10 comparing with PIs free of IL-10 at cell seeding densities of 32,000 cells/well and 64,000 cells/well over a one-week culture. Also, it was seen that cellular LDH activity declined by ~30% compared with PIs free of IL-10 at cell seeding density of 64,000 cells/well over a one-week culture. The results of the cellular LDH level could relate to the improvement in the viability of PIs with GBs loaded with IL-10. The increase in cell viability went up to 35% with sustained released of IL-10 from PIs. Similarly, the results of cellular LDH released from PIs incorporating with GBs loaded with anti-1L-1β showed improvements in the functionality of PIs in terms of decreasing LDH release. There was no clear difference in the effect of IL-10 and anti-IL-1β in the current study.

The functionality of PIs over a one-week culture was increased and indicating that the production of insulin from incorporated PIs was increased by ~1.5-fold when IL-10 loaded in GBs and by ~1.6-fold when anti-1L-1β loaded to the GBs. Overall, the inclusion of anti-inflammatory or anti-apoptotic agents bound to GBs appears to be an effective strategy to enhance cell survival and improve the functionality of PIs.

Chapter 6

General discussion, conclusions, and future directions

6.1 Overall discussion

Type 1 diabetes mellitus is a metabolic disorder characterised by hyperglycaemia due to death or loss of pancreatic beta cells. It is caused mainly by autoimmune destruction of insulin-producing beta cells, which leads to the development of macro and microvascular complications. The current treatment is exogenous insulin therapy. The key disadvantage of insulin treatment is that injected insulin does not generate a physiologically representative feedback mechanism. External monitoring of glucose levels by patients is required. Therefore, research into a new method of treatment is needed.

Cell therapy and pancreatic transplantation are alternative treatments for T1DM. Implantation of functional pancreatic tissue or cells may re-build the glucose-insulin feedback loop and maintain steady blood glucose levels. However, this type of treatment has faced a limitation due to immune rejection and insufficient supply. Therefore, mimicking islet through formation or generation of pseudoislets (PIs) *in vitro* could be used for insulin production or *in vivo* transplantation. In addition to other problems, the central necrosis of the PIs after the prolonged culture is still the main challenge. This project has studied two new techniques to battle this challenge;

controlling PIs'physical properties by substrate coating chemistry and incorporating gelatin beads into PIs to reduce inflammatory reaction.

6.1.1 Rational design of coating solutions to change substrate properties

A most convenient technique to generate a large number of PIs is through suspension culture. Although commercially available culture plates including bacterial Petri dishes and ultra-low attachment (ULA) culture plates could generate PIs, the formed PIs do still not possess optimal biofunctionality. Furthermore, these plates do not allow for a systematic study on the relation of the physical properties of PIs and their biofunctionality.

A series of coating solutions for suspension plates have been designed and produced in this study to control the physical properties of the substrate of suspension plates, which can influence PIs' physical properties. With the change of the ratio of gelatin type, A solution and F127 solution in the coating solutions and coating plates' chemistry, the use of adhesion or suspension plate, various substrate properties of suspension plates have been generated. ATR-FTIR spectra, surface protein adsorption and CA assessment, revealed the differences, which aided understanding of the effect

of the chemical coating of the substrate on the size of cell aggregates [28,144] and the corresponding mechanisms governing this.

It was confirmed that using amphiphilic chemicals, such as F127, in mixture coating solution can tailor the substrate properties. A better coating solution could be used for PIs generation leading to the production of small and homogenous sized PIs in large numbers from each batch culture.

6.1.2 Relationship of PI biofunctions to the surface properties of culture plates

Because of the limitation of using ULA plates or bacterial Petri dishes for production of PIs,[148,227] a series of coating solutions have been applied to different culture plates aiming to fabricate PIs with high homogeneity, small sizes and large numbers, enabling improvements in PI viability and functionality through their physical properties.

Coating SOP plates with F127 caused changes in the surface properties [228] through increasing the hydrophobicity of the surface which could cause cells to adhere to each other in densely packed cell aggregates.[207] The current study has proved that coating of SOP with F127 formed large sized PIs when culturing beta cells. Using gelatin type

A solution for coating SOP plates led to the formation of a 2D cell sheet over a one-week culture period. Thus, we expect that using a mixture of F127 solution and gelatin solution to coat SOP can induce beta cells into different cell aggregation structures, enabling manipulation of PI size and cell packing properties. The underlying mechanisms could be that increase of gelatin content in the coating solution tuned the overall hydrophilicity of coated substrates due to gelatin's medium hydrophilicity. The mixture coating solutions produced distinct changes of chemical and physical properties to SOP plates but not to TCP plates. The degree changes to SGP were between SOP and TCP substrates. This was mainly caused by the interaction of the amphiphilic F127 with the hydrophilicity of the original substrate.

The crucial investigation in this study was to determine the relationship between viability/proliferation rate of cells within the PIs to the coating solutions used. Therefore, the coating of the substrate can be optimised to produce homogeneous and relatively larger PIs, which would maintain prolonged biofunction in culture. Both MTT and CCK-8 assays for measuring proliferation, immunostaining of key cell-cell adhesion molecules and receptors, oxygen-consuming assay, PCR and protein expression of key genes and proteins in insulin production have been undertaken. The

outcomes of these assays revealed a consistent relationship between substrate coating and function.

It was confirmed that large PIs associated with poor central oxygen and nutrient diffusion lead to reductions in cellular proliferation.[34,204] The novel finding in this study was that 98% gelatin in mixture with F127 generated small PIs with a high proliferative rate at 3 and 7 days culture. Moreover, the immunohistochemistry staining for the PIs generated by 95%, and 98% gelatin in mixture with F127 showed more mRNA and protein expression for Cx36, GLUT2 and insulin. The expression of GLUT2 was the highest in PIs grown on a coating solution of 98% gelatin by the Western blotting. Thus it is easily understood that PIs grown on a coating solution of 98% gelatin in combination with F127 generated more insulin in GSIS assay. Altogether, the primary glucose sensor in the beta cells was significantly enhanced by the optimised configuration of cells in the PIs in comparison to PIs formed on different coating substrates. Through the systematic change of the substrate chemistry and assessment of PIs physical and biochemical properties, a consistent trend was observed that small PIs with appropriate cell-cell package/contact was associated with higher proliferative rates and insulin production.[83]

Prior studies have demonstrated that the spherical 3D configuration of pancreatic islets is vital for the secretion of insulin and regulation of blood glucose levels.[34,73,229] Several studies have been investigated that 3D structure of PIs significantly stimulates insulin secretion in response to glucose and other stimulations.[83,230] Some researchers have shown that different coating types led to varied gene expression and GSIS outcome from pancreatic beta cells.[83] The initial mechanism by which PIs exhibit enhanced functionality over monolayers is through formation or rebuilding of calcium-dependent gap junction signalling.[115] In native islets, cell to cell communication facilitated by E-cadherin is upregulated following PI formation.[75] In the beta cells, the regulation or stimulation is achieved by Cx36[75] which is also upregulated following configuration of cells as PIs.[75,240] These mechanisms have been observed and confirmed in the current study, where all PIs showed improved expression of Cx36 at both the mRNA and protein level in comparison with cells grown as an adhesive monolayer. The new coating formula allowed us to compare and select optimal conditions for the generation of PIs.

6.1.3 The distribution and detection of oxygen in PIs

Prior studies[208] have been shown that the oxygen distribution to the cells within the PIs using an oxygen probe system is greater in small PIs (45-55 μm). Besides, higher

viability, lower cell death and better insulin release were observed compared with medium sizes (130-160 μm) and large (200-240 μm) PIs. In the current study, a new type of nano-oxygen sensor has been incorporated into PIs to detect the oxygen distribution non-destructively, and consuming rate among PIs formed under the substrates with different coating solutions. The results showed that PIs cultured on a substrate coated with 95%, 98% gelatin and ULA plates increased oxygen distribution within PIs compared with other types of PIs. This method could be explored further to study the cellular activities within PIs.

6.1.4 Effect of incorporation of GBs into PIs

The functionality of PIs has shown an improvement in terms of cell viability after incorporation of GBs. The reasons behind could be resulting from the GBs' functioning as microchannels or voids inside of PIs, which helped the diffusion of small molecules between media and cells in PIs. It is found that the way to fabricate microchannel networks in cellular spheroid could be effective for cells that required a high supply of nutrients and oxygen in PIs. Besides, the microfabrication methodology of GBs might help the innovation of micro-sensors or micro-regulator or micro-carriers, which comprise cells and other materials.

The generation of GBs from gelatin using W/O emulsion was a feasible technique to form microchannel/voids in PIs when incorporating the GBs to PIs. The GBs are water-soluble, so they have to be crosslinked to become water insoluble. The reaction of alpha-amino groups of lysine and hydroxylysine side groups with aldehydes in GA at gas phase produced better biocompatible GBs in comparison to using liquid phase GA reaction. Furthermore, other groups have used other ways for crosslinking of gelatin. For instance, dextran dialdehyde carboxyl, amide, imidazoyl or guanidine may be involved.[189,241] The protocol established in this study, in which 6 hours crosslinking under 5% GA vapour was taken for 40 μm GBs, has demonstrated better outcomes in terms of generating stable but swollen GBs for PIs. Incorporation of GBs into PIs showed improvements in the proliferation of PIs for both small and large sized PIs. The of PIs viability in term of CCK-8 elevated by 17-25% after incorporation with GBs. Other biofunctions of PIs have also been shown being changed in this study such as decreasing of cellular LDH release, and enhancements in insulin production.

6.1.5 Synergetic effect of incorporating anti-inflammatory cytokines loaded GBs into PIs

The incorporation of GBs loaded with anti-inflammatory cytokines (IL-10 and anti-IL-1β) further enhanced the viability of PIs. The cell viability measured via CCK-8

assay was significantly increased in these PIs and LDH release was reduced. IL-10 acts as an anti-inflammatory agent that is derived from macrophage and TH2 cells exerting anti-inflammatory effects by inhibiting IL-12 and other pro-inflammatory agents. For normal growth, there is a regulation of the inflammatory cytokines including IL-1β, TNFα, IL-6, IL-15, IL-17 and IL-18, and anti-inflammatory cytokines such as IL-4, IL-10 and IL-13,[242] which act by increasing macrophage production of IL-1 receptor antagonist and by inhibiting the generation of oxygen and nitrogen free radicals by macrophages. Loading of IL-10 can act as an anti-inflammatory drug for any inflammation formed in the centre of PIs, which leads to a reduction of the cellular toxicity. So, the viability of PIs for cell seeding density 32,000 cells/well increased by 25% when incorporated with GBs free of IL-10 and increased by ~60% when beads loaded with IL-10 and increased by 35% when beads loaded with anti-IL-1β. The results were consistent with others who added IL-10 to rat islets inducing its activity.[232]

Il-1β works a potent pro-anti-inflammatory cytokine produced by cells of the innate immune system. It has been suggested that the mechanisms of IL-1β are part of a continuum of secretion in response to the strength of the inflammatory stimulus. Thereby the IL-1β release is in response to extracellular stimuli, which increases

inflammatory response.[227] Therefore, a slow release of anti-IL-1β into PIs should be capable of prolonging the viability of cells through inhibiting the release of IL-1β during apoptosis and necrosis. Similar to the action of IL-10, the viability of PIs for cell seeding density 64,000 cells/well increased by 17% when incorporated with GBs and the proliferation elevated by ~35-60% when beads loaded with IL-10 or anti-IL-1β comparing with PIs free of GBs and free of drugs. Also, the results obtained in this study showed an increase in the viability, an increase of GSIS and decreasing in the cellular LDH release after incorporated with GBs loaded with anti-IL-1β.

6.2 Overall conclusion

In summary, the substrate of culture plates influences the physical and biological properties of the PIs. The culture of substrates has a crucial role in the production of BRIN-BD11 PIs. A mixture of F127 solution and gelatin type A solution systematically affected surface properties and PIs. The surfaces coated with a variation of the ratio of Pluronic F127 and Gelatin type A generated different ATR-FTIR spectra and CA values. Furthermore, protein adsorption on treated surfaces was also dependent on the coating used. These complimentary results support each other. The higher the F127 content, the more the hydrophilic surface was, which generated larger sized PIs and lower CA values of the substrate.

The coating of SOP surfaces with a pure F127 solution or gelatin solution led to large/dense cell aggregates or cell sheets; while the mixture solution containing 95-98% gelatin produced homogenous and small PIs. Furthermore, it was revealed that PIs formed on 98% gelatin solution coated plates had the lowest PIs sizes (268 ± 10 μm) and high viability/proliferation through CCK-8 and MTT assays. Western blotting assays and higher expression in mRNA assay than smaller PIs formed on ULA plates. So, the expression of the protein using western blotting techniques showed higher expressions for Cx36. GLUT2 and insulin by 12%, 2% and 1% respectively for PIs generated on 98% gelatin surfaces comparing with these formed on ULA surface. On the same trend have been seen the mRNA assays for the PIs formed on 98% gelatin showed more of mRNA by 41% for Cx36, 10% for GLUT2 and 7% for insulin in comparison to PIs generated on ULA plates. Also, the diffusion of oxygen through PIs demonstrated more in PIs produced on 98% gelatin coated substrate. Such distinct coating-effect did not occur on PIs grown on coated TCP plates. The changes on SGP nd PIs grown on coated SGP were between SOP and TCP substrates. These findings were attributed to different interactions of the amphiphilic F127 with different hydrophilicity of the original substrate

Water/Oil emulsion techniques have successfully generated large quantity GBs in short reaction times. The degree of GB swelling can be optimized by crosslinking via different concentrations and reaction duration with GA. Under 5% GA vapour, 6 hour crosslinking reaction duration can stabilise GBs and maintain appropriate swelling capacity for GBs. The proliferation of PIs was significantly increased by incorporation of 40 μm GBs into PIs, which led to improvements in the cellular viability. This had been confirmed by both MTT and CCK-8 assay for large and small size PIs.

GBs loaded with anti-inflammatory cytokines, IL-10 and anti-IL-1β, had revealed a synergetic effect in the improvement of the proliferation/viability of PIs regardless of the cell seeding density used. LDH release from the PIs was decreased dramatically by ~1.5-fold for PIs with cell seeding density 32,000 cells/well and by ~1.6-fold for cell seeding density 64,000 cells/well. Finally, the level of GSIS was elevated after anti-inflammatory sustained released into PIs via using GBs as drugs carrier rather than helping create microchannels into PIs.

In summary, a large number of *in vitro* and *in vivo* model system are exciting to enable the find out the efficacy of new techniques which could be used for novel therapies. Although each way for re-aggregation of pancreatic beta cells suffers from central

necrosis after a few days, the incorporation of GBs into PIs might be a suitable technique to improve their biofunctionality. The application of these models for *in vitro* or *in vivo* insulin production still needs further investigation. The reasons behind come from the limitation of the lifespan of the PIs and most cell lines such as BRIN-BD11 are from electrofusion with insulinoma cell lines, which cannot be used for transplantation.

6.3 Future perspectives

The work described in this study has raised some approaches for future work, which could help in the treatment of diabetes. The solutions for the treatment of suspension culture surfaces to generate small sized PIs from mixing of the two solutions composed of F127 with gelatin did not fix on the substrate permanently. The coating could lose or dissolute in the media. So further studies are needed to find out the best way to stabilise the coating for long-term cell culture.

The use of large size GBs for incorporating into PIs could be investigated, for instance, GBs as large as 80 μm could be used, which have more space to carry more anti-inflammatory drugs into PIs.

The further study of the dose and type of anti-inflammatory drugs loaded on to GBs and then into PIs is also warranted. Anti-apoptosis and anti-necrosis drugs with longer and more sustained release patterns and with more efficient loading should also be investigated.

Future study is required to investigate reactive oxygen species in the PIs produced on different coating substrates and the associated effect on insulin release.

References

1. Cabrera O, Berman DM, Kenyon NS, Ricordi C, Berggren PO, Caicedo A. The unique cytoarchitecture of human pancreatic islets has implications for islet cell function. Proceedings of the National Academy of Sciences of the United States of America. 2006 Feb 14;103(7):2334-9.

2 Drake R, Vogl AW, Mitchell AW. Gray's Anatomy for Students E-Book Elsevier Health Sciences; 2009 Apr 4.

3. Jørgensen MC, Ahnfelt-Rønne J, Hald J, Madsen OD, Serup P, Hecksher-Sørensen J. An illustrated review of early pancreas development in the mouse. Endocrine reviews. 2007 Oct;28(6):685-705.

4. Eberhard D, Lammert E. The pancreatic beta-cell in the islet and organ community. Curr Opin Genet Dev. 2009 Oct;19(5):469–75.

5. Witt H, Apte MV, Keim V, Wilson JS. Chronic Pancreatitis: Challenges and Advances in Pathogenesis, Genetics, Diagnosis, and Therapy. Gastroenterology. 2007 Apr 1;132(4):1557–73.

6. FRCPA BYBsMSPMBcM, PhD(Melbourne) JWHBs. Wheater's Functional Histology: A Text and Colour Atlas. 4 edition. Edinburgh: Churchill Livingstone; 2000. 424 p.

7. Nobukini T, Thomas G. The mTOR/S6K signalling pathway: the role of the TSC1/2 tumour suppressor complex and the proto-oncogene Rheb. Novartis Found Symp. 2004;262:148-154; discussion 154-159, 265–8.

8. Wojtusciszyn A, Armanet M, Morel P, Berney T, Bosco D. Insulin secretion from human beta cells is heterogeneous and dependent on cell-to-cell contacts. Diabetologia. 2008 Oct 1;51(10):1843.

9. Drucker DJ. The role of gut hormones in glucose homeostasis. J Clin Invest. 2007 Jan;117(1):24–32.

10. Trimble ER, Halban PA, Wollheim CB, Renold AE. Functional differences between rat islets of ventral and dorsal pancreatic origin. J Clin Invest. 1982 Feb;69(2):405–13.

11. Ishihara H, Maechler P, Gjinovci A, Herrera P-L, Wollheim CB. Islet β-cell secretion determines glucagon release from neighbouring α-cells. Nat Cell Biol. 2003 Mar 17;5(4):ncb951.

12. Hills CE, Brunskill NJ. Intracellular signalling by C-peptide. Exp Diabetes Res. 2008;2008:635158.

13. Carroll RJ, Hammer RE, Chan SJ, Swift HH, Rubenstein AH, Steiner DF. A mutant human proinsulin is secreted from islets of Langerhans in increased amounts via an unregulated pathway. Proc Natl Acad Sci U S A. 1988 Dec;85(23):8943–7.

14. Yoon S, Kim J, Musen G, Renshaw PF, Hwang J, Bolo NR, Kim JE, Simonson DC, Weinger K, Ryan CM, Lyoo IK. Prefronto-temporal white matter microstructural alterations 20 years after the diagnosis of type 1 diabetes mellitus. Pediatric diabetes. 2017 Sep 20.

15. González-Sánchez JL, Serrano-Ríos M. Molecular basis of insulin action. Drug News Perspect. 2007 Oct;20(8):527–31.

16. Holt RI, Cockram C, Flyvbjerg A, Goldstein BJ, editors. Textbook of diabetes. John Wiley & Sons; 2017 Mar 6.

17. Prentki M, Tornheim K, Corkey BE. Signal transduction mechanisms in nutrient-induced insulin secretion. Diabetologia. 1997 Jul;40 Suppl 2:S32-41.

18. Roscioni SS, Migliorini A, Gegg M, Lickert H. Impact of islet architecture on β-cell heterogeneity, plasticity and function. Nat Rev Endocrinol. 2016 Sep 2;12(12):nrendo.2016.147.

19. Tripathy JP, Thakur JS, Jeet G, Chawla S, Jain S, Pal A, Prasad R, Saran R. Prevalence and risk factors of diabetes in a large community-based study in North India: results from a STEPS survey in Punjab, India. Diabetology & metabolic syndrome. 2017 Dec;9(1):8.

20. Hauge-Evans AC, Squires PE, Persaud SJ, Jones PM. Pancreatic beta-cell-to-beta-cell interactions are required for integrated responses to nutrient stimuli:

enhanced Ca2+ and insulin secretory responses of MIN6 pseudoislets. Diabetes. 1999 Jul;48(7):1402–8.

21. Luther MJ, Hauge-Evans A, Souza KL, Jörns A, Lenzen S, Persaud SJ, Jones PM. MIN6 β-cell–β-cell interactions influence insulin secretory responses to nutrients and non-nutrients. Biochemical and biophysical research communications. 2006 Apr 28;343(1):99-104.

22. Stützer I, Esterházy D, Stoffel M. The pancreatic beta cell surface proteome. Diabetologia. 2012 Jul 1;55(7):1877–89.

23. Hellman B, Idahl LA, Lernmark A, Sehlin J, Täljedal IB. The pancreatic beta-cell recognition of insulin secretagogues. Effects of calcium and sodium on glucose metabolism and insulin release. Biochem J. 1974 Jan;138(1):33–45.

24. Bavamian S, Klee P, Britan A, Populaire C, Caille D, Cancela J, *et al.* Islet-cell-to-cell communication as basis for normal insulin secretion. Diabetes Obes Metab. 2007 Nov;9 Suppl 2:118–32.

25. Wollheim CB, Sharp GW. Regulation of insulin release by calcium. Physiol Rev. 1981 Oct 1;61(4):914–73.

26. Van Loon LJ, Kruijshoop M, Verhagen H, Saris WH, Wagenmakers AJ. Ingestion of protein hydrolysate and amino acid–carbohydrate mixtures increases postexercise plasma insulin responses in men. The Journal of nutrition. 2000 Oct 1;130(10):2508-13.

27. Randle PJ. Regulatory interactions between lipids and carbohydrates: the glucose fatty acid cycle after 35 years. Diabetes/Metabolism Research and Reviews. 1998 Dec 1;14(4):263-83.

28. Tsang W-G, Zheng T, Wang Y, Tang J, Rind HB, Francki A, *et al.* Generation of functional islet-like clusters after monolayer culture and intracapsular aggregation of adult human pancreatic islet tissue. Transplantation. 2007 Mar 27;83(6):685–93.

29. Sweet IR, Cook DL, DeJulio E, Wallen AR, Khalil G, Callis J, *et al.* Regulation of ATP/ADP in pancreatic islets. Diabetes. 2004 Feb;53(2):401–9.

30. Wiederkehr A, Szanda G, Akhmedov D, Mataki C, Heizmann CW, Schoonjans K, *et al.* Mitochondrial matrix calcium is an activating signal for hormone secretion. Cell Metab. 2011 May 4;13(5):601–11.

31. Hopcroft DW, Mason DR, Scott RS. Structure-function relationships in pancreatic islets: support for intraislet modulation of insulin secretion. Endocrinology. 1985 Nov;117(5):2073–80.

32. Rorsman P, Renström E. Insulin granule dynamics in pancreatic beta cells. Diabetologia. 2003 Aug;46(8):1029–45.

33. Krassas GE, Tzotzas T, Papazisis K, Pazaitou-Panayiotou K, Boboridis K. The efficacy of somatostatin analogues in the treatment of diabetic retinopathy and thyroid eye disease. Clin Ophthalmol Auckl NZ. 2007 Sep;1(3):209–15.

34. Kelly C, Flatt PR, McClenaghan NH. Cell-to-cell communication and cellular environment alter the somatostatin status of delta cells. Biochem Biophys Res Commun. 2010 Aug 20;399(2):162–6.

35. Halban PA, Wollheim CB, Blondel B, Meda P, Niesor EN, Mintz DH. The possible importance of contact between pancreatic islet cells for the control of insulin release. Endocrinology. 1982 Jul;111(1):86–94.

36. King H, Aubert RE, Herman WH. Global Burden of Diabetes, 1995–2025: Prevalence, numerical estimates, and projections. Diabetes Care. 1998 Sep 1;21(9):1414–31.

37. Deshpande AD, Harris-Hayes M, Schootman M. Epidemiology of Diabetes and Diabetes-Related Complications. Phys Ther. 2008 Nov;88(11):1254–64.

38. Naemiratch B, Manderson L. Lay Explanations of Type 2 Diabetes in Bangkok, Thailand. Anthropol Med. 2007 Apr 1;14(1):83–94.

39. Association AD. Diagnosis and Classification of Diabetes Mellitus. Diabetes Care. 2010 Jan 1;33(Supplement 1):S62–9.

40. Nathan DM. The Diabetes Control and Complications Trial/Epidemiology of Diabetes Interventions and Complications Study at 30 Years: Overview. Diabetes Care. 2014 Jan;37(1):9–16.

41. Alberti KG, Zimmet PZ. Definition, diagnosis and classification of diabetes mellitus and its complications. Part 1: diagnosis and classification of diabetes mellitus provisional report of a WHO consultation. Diabet Med J Br Diabet Assoc. 1998 Jul;15(7):539–53.

42. Atkinson MA, Eisenbarth GS, Michels AW. Type 1 diabetes. The Lancet. 2014 Jan 4;383(9911):69–82.

43. Boggi U, Signori S, Vistoli F, Amorese G, Consani G, De Lio N, *et al.* Current Perspectives on Laparoscopic Robot-Assisted Pancreas and Pancreas-Kidney Transplantation. Rev Diabet Stud RDS. 2011;8(1):28–34.

44. Ehnert S, Glanemann M, Schmitt A, Vogt S, Shanny N, Nussler NC, *et al.* The possible use of stem cells in regenerative medicine: dream or reality? Langenbecks Arch Surg. 2009 Nov;394(6):985–97.

45. Bassi R, Fiorina P. Impact of islet transplantation on diabetes complications and quality of life. Curr Diab Rep. 2011 Oct;11(5):355–63.

46. Shapiro AMJ, Lakey JRT, Ryan EA, Korbutt GS, Toth E, Warnock GL, *et al.* Islet Transplantation in Seven Patients with Type 1 Diabetes Mellitus Using a Glucocorticoid-Free Immunosuppressive Regimen. N Engl J Med. 2000 Jul 27;343(4):230–8.

47. Paget M, Murray H, Bailey CJ, Downing R. Human islet isolation: semi-automated and manual methods. Diab Vasc Dis Res. 2007 Mar 1;4(1):7–12.

48. Wieczorek G, Pospischil A, Perentes E. A comparative immunohistochemical study of pancreatic islets in laboratory animals (rats, dogs, minipigs, nonhuman primates). Exp Toxicol Pathol Off J Ges Toxikol Pathol. 1998 Jun;50(3):151–72.

49. Steiner DJ, Kim A, Miller K, Hara M. Pancreatic islet plasticity: interspecies comparison of islet architecture and composition. Islets. 2010 Jun;2(3):135–45.

50. Sujatha SR, Pulimood A, Gunasekaran S. Comparative immunocytochemistry of isolated rat & monkey pancreatic islet cell types. Indian J Med Res. 2004 Jan;119(1):38–44.

51. O'Brien TD, Hayden DW, Johnson KH, Fletcher TF. Immunohistochemical morphometry of pancreatic endocrine cells in diabetic, normoglycaemic glucose-intolerant and normal cats. J Comp Pathol. 1986 Jul;96(4):357–69.

52. Reddy SN, Bibby NJ, Elliott RB. Cellular distribution of insulin, glucagon, pancreatic polypeptide hormone and somatostatin in the fetal and adult pancreas of the guinea pig: a comparative immunohistochemical study. Eur J Cell Biol. 1985 Sep;38(2):301–5.

53. Guidoux R, Möhren G, Peters G. The effect of dilution on the suppressible and the nonsuppressible insulin-like activity of rat serum. Naunyn Schmiedebergs Arch Pharmacol. 1974 Dec 1;282(4):421–32.

54. Kojima N, Takeuchi S, Sakai Y. Rapid aggregation of heterogeneous cells and multiple-sized microspheres in methylcellulose medium. Biomaterials. 2012 Jun;33(18):4508–14.

55. Kojima N, Takeuchi S, Sakai Y. Establishment of self-organization system in rapidly formed multicellular heterospheroids. Biomaterials. 2011 Sep;32(26):6059–67.

56. Korbutt GS, Elliott JF, Ao Z, Smith DK, Warnock GL, Rajotte RV. Large scale isolation, growth, and function of porcine neonatal islet cells. J Clin Invest. 1996 May 1;97(9):2119–29.

57. Schröder D, Wegner U, Besch W, Zühlke H. Characterization of pseudo-islets formed from pancreatic islet cell suspensions of neonatal rats. Mol Cell Endocrinol. 1983 Oct;32(2–3):179–93.

58. Kuo CY, Herrod HG, Burghen GA. Formation of pseudoislets from human pancreatic cultures. Pancreas. 1992;7(3):320–5.

59. Farkas G, Joó F. Simple and Reliable Conditions for Routine, Long-Term Culturing of Fetal Human Pancreatic Tissue Fragments. Diabetes. 1984 Dec 1;33(12):1165–8.

60. McCluskey JT, Hamid M, Guo-Parke H, McClenaghan NH, Gomis R, Flatt PR. Development and functional characterization of insulin-releasing human

pancreatic beta cell lines produced by electrofusion. J Biol Chem. 2011 Jun 24;286(25):21982–92.

61. Radvanyi F, Christgau S, Baekkeskov S, Jolicoeur C, Hanahan D. Pancreatic beta cells cultured from individual preneoplastic foci in a multistage tumorigenesis pathway: a potentially general technique for isolating physiologically representative cell lines. Mol Cell Biol. 1993 Jul;13(7):4223–32.

62. Brereton H, Carvell MJ, Persaud SJ, Jones PM. Islet α-cells do not influence insulin secretion from β-cells through cell–cell contact. Endocrine. 2007 Feb 1;31(1):61-5.

63. Kelly C, Parke HG, McCluskey JT, Flatt PR, McClenaghan NH. The role of glucagon- and somatostatin-secreting cells in the regulation of insulin release and beta-cell function in heterotypic pseudoislets. Diabetes Metab Res Rev. 2010 Oct;26(7):525–33.

64. Halban PA, Powers SL, George KL, Bonner-Weir S. Altered differentiated cell surface properties of transformed (RINm5F) compared with native adult rat pancreatic B cells. Endocrinology. 1988 Jul;123(1):113–9.

65. Nikolova G, Jabs N, Konstantinova I, Domogatskaya A, Tryggvason K, Sorokin L, *et al.* The vascular basement membrane: a niche for insulin gene expression and Beta cell proliferation. Dev Cell. 2006 Mar;10(3):397–405.

66. Foty RA, Pfleger CM, Forgacs G, Steinberg MS. Surface tensions of embryonic tissues predict their mutual envelopment behavior. Dev Camb Engl. 1996 May;122(5):1611–20.

67. Napolitano AP, Chai P, Dean DM, Morgan JR. Dynamics of the self-assembly of complex cellular aggregates on micromolded nonadhesive hydrogels. Tissue Eng. 2007 Aug;13(8):2087–94.

68. Pece S, Chiariello M, Murga C, Gutkind JS. Activation of the protein kinase Akt/PKB by the formation of E-cadherin-mediated cell-cell junctions. Evidence for the association of phosphatidylinositol 3-kinase with the E-cadherin adhesion complex. J Biol Chem. 1999 Jul 2;274(27):19347–51.

69. Liu J, Liu S, Chen Y, Zhao X, Lu Y, Cheng J. Functionalized self-assembling peptide improves INS-1 β-cell function and proliferation via the integrin/FAK/ERK/cyclin pathway. Int J Nanomedicine. 2015 May 13;10:3519–31.

70. Kelm JM, Timmins NE, Brown CJ, Fussenegger M, Nielsen LK. Method for generation of homogeneous multicellular tumor spheroids applicable to a wide variety of cell types. Biotechnol Bioeng. 2003 Jul 20;83(2):173–80.

71. Lin R-Z, Lin R-Z, Chang H-Y. Recent advances in three-dimensional multicellular spheroid culture for biomedical research. Biotechnol J. 2008 Oct;3(9–10):1172–84.

72. Cavallari G, Zuellig RA, Lehmann R, Weber M, Moritz W. Rat pancreatic islet size standardization by the 'hanging drop' technique. Transplant Proc. 2007 Aug;39(6):2018–20.

73. Tung Y-C, Hsiao AY, Allen SG, Torisawa Y, Ho M, Takayama S. High-throughput 3D spheroid culture and drug testing using a 384 hanging drop array. Analyst. 2011 Jan 18;136(3):473–8.

74. Asghar W, Shafiee H, Chen P, Tasoglu S, Guven S, Gurkan UA, Demirci U. In vitro three-dimensional cancer culture models. InCancer Targeted Drug Delivery 2013 (pp. 635-665). Springer New York.

75. Kelly C, Guo H, McCluskey JT, Flatt PR, McClenaghan NH. Comparison of insulin release from MIN6 pseudoislets and pancreatic islets of Langerhans reveals importance of homotypic cell interactions. Pancreas. 2010 Oct;39(7):1016–23.

76. Sionov RV, Finesilver G, Sapozhnikov L, Soroker A, Zlotkin-Rivkin E, Saad Y, *et al.* Beta Cells Secrete Significant and Regulated Levels of Insulin for Long Periods when Seeded onto Acellular Micro-Scaffolds. Tissue Eng Part A. 2015 Sep 29;21(21–22):2691–702.

77. Zhi Z, Liu B, Jones PM, Pickup JC. Polysaccharide Multilayer Nanoencapsulation of Insulin-Producing β-Cells Grown as Pseudoislets for

Potential Cellular Delivery of Insulin. Biomacromolecules. 2010 Mar 8;11(3):610–6.

78. Hilderink J, Spijker S, Carlotti F, Lange L, Engelse M, van Blitterswijk C, *et al.* Controlled aggregation of primary human pancreatic islet cells leads to glucose-responsive pseudoislets comparable to native islets. J Cell Mol Med. 2015 Aug 1;19(8):1836–46.

79. Li Y, Kniss DA, Lasky LC, Yang S-T. Culturing and differentiation of murine embryonic stem cells in a three-dimensional fibrous matrix. Cytotechnology. 2003 Jan;41(1):23–35.

80. Hamid M, McCluskey JT, McClenaghan NH, Flatt PR. Culture and Function of Electrofusion-Derived Clonal Insulin-Secreting Cells Immobilized on Solid and Macroporous Microcarrier Beads. Biosci Rep. 2000 Jun 1;20(3):167–76.

81. Lin H-Y, Tsai C-C, Chen L-L, Chiou S-H, Wang Y-J, Hung S-C. Fibronectin and laminin promote differentiation of human mesenchymal stem cells into insulin producing cells through activating Akt and ERK. J Biomed Sci. 2010 Jul 12;17(1):56.

82. Lehmann R, Zuellig RA, Kugelmeier P, Baenninger PB, Moritz W, Perren A, *et al.* Superiority of small islets in human islet transplantation. Diabetes. 2007 Mar;56(3):594–603.

83. Yang K-C, Wu C-C, Yang S-H, Chiu C-C, Sumi S, Lee H-S. Investigating the suspension culture on aggregation and function of mouse pancreatic β-cells. J Biomed Mater Res A. 2013 Aug;101(8):2273–82.

84. Fischer AH, Jacobson KA, Rose J, Zeller R. Hematoxylin and eosin staining of tissue and cell sections. CSH Protoc. 2008 May 1;2008:pdb.prot4986.

85. Kelly C, McClenaghan NH, Flatt PR. Role of islet structure and cellular interactions in the control of insulin secretion. Islets. 2011 Apr;3(2):41–7.

86. Coons AH, Leduc EH, Connolly JM. Studies on antibody production. J exp med. 1955 jul 1;102(1):49–60.

87. Hopcroft DW, Mason DR, Scott RS. Insulin secretion from perifused rat pancreatic pseudoislets. Vitro Cell Dev Biol J Tissue Cult Assoc. 1985 Aug;21(8):421–7.

88. Rogers GJ, Hodgkin MN, Squires PE. E-cadherin and cell adhesion: a role in architecture and function in the pancreatic islet. Cell Physiol Biochem Int J Exp Cell Physiol Biochem Pharmacol. 2007;20(6):987–94.

89. Zhi Z, Liu B, Jones PM, Pickup JC. Polysaccharide multilayer nanoencapsulation of insulin-producing beta-cells grown as pseudoislets for potential cellular delivery of insulin. Biomacromolecules. 2010 Mar 8;11(3):610–6.

90. Irani V, Guy AJ, Andrew D, Beeson JG, Ramsland PA, Richards JS. Molecular properties of human IgG subclasses and their implications for designing therapeutic monoclonal antibodies against infectious diseases. Mol Immunol. 2015 Oct 1;67(2, Part A):171–82.

91. Ramos-Vara JA. Principles and methods of immunohistochemistry. Methods Mol Biol Clifton NJ. 2011;691:83–96.

92. Whiteside G, Munglani R. TUNEL, Hoechst and immunohistochemistry triple-labelling: an improved method for detection of apoptosis in tissue sections—an update. Brain Res Protoc. 1998 Sep 1;3(1):52–3.

93. Luther MJ, Hauge-Evans A, Souza KLA, Jörns A, Lenzen S, Persaud SJ, *et al.* MIN6 beta-cell-beta-cell interactions influence insulin secretory responses to nutrients and non-nutrients. Biochem Biophys Res Commun. 2006 Apr 28;343(1):99–104.

94. Mendelsohn AD, Nyitray C, Sena M, Desai TA. Size-controlled Insulin Secreting Cell Clusters. Acta Biomater. 2012 Dec;8(12):4278–84.

95. Chapter 1: Methods for Determining Serum Insulin. Acta Med Scand. 1965 Jan 12;179(S441):13–34.

96. Polonsky KS, Herold KC, Gilden JL, Bergenstal RM, Fang VS, Moossa AR, et al. Glucose counterregulation in patients after pancreatectomy. Comparison with other clinical forms of diabetes. Diabetes. 1984 Nov;33(11):1112–9.

97. Kuzuya H, Blix PM, Horwitz DL, Rubenstein AH, Steiner DF, Binder C, et al. Heterogeneity of circulating C-peptide. J Clin Endocrinol Metab. 1977 May;44(5):952–62

98. Yalow RS, Berson SA. Assay of Plasma Insulin in Human Subjects by Immunological Methods. Nature. 1959 Nov;184(4699):1648–9.

99. Albano JD, Ekins RP, Maritz G, Turner RC. A sensitive, precise radioimmunoassay of serum insulin relying on charcoal separation of bound and free hormone moieties. Acta Endocrinol (Copenh). 1972 Jul;70(3):487–509.

100. Webster HV, Bone AJ, Webster KA, Wilkin TJ. Comparison of an enzyme-linked immunosorbent assay (ELISA) with a radioimmunoassay (RIA) for the measurement of rat insulin. J Immunol Methods. 1990 Nov 6;134(1):95–100.

101. Farino ZJ, Morgenstern TJ, Vallaghe J, Gregor N, Donthamsetti P, Harris PE, Pierre N, Freyberg R, Charrier-Savournin F, Javitch JA, Freyberg Z. Development of a rapid insulin assay by homogenous time-resolved fluorescence. PloS one. 2016 Feb 5;11(2):e0148684.

102. Tsai A-C, Liu Y, Yuan X, Ma T. Compaction, fusion, and functional activation of three-dimensional human mesenchymal stem cell aggregate. Tissue Eng Part A. 2015 May;21(9–10):1705–19.

103. Liu X. Engineering beta-cell spheroids for type i diabetes treatment (Doctoral dissertation, Clemson University).

104. Hilderink J, Spijker S, Carlotti F, Lange L, Engelse M, van Blitterswijk C, *et al.* Controlled aggregation of primary human pancreatic islet cells leads to glucose-responsive pseudoislets comparable to native islets. J Cell Mol Med. 2015 Aug;19(8):1836–46.

105. Hellerström C, Andersson A, Gunnarsson R. Regeneration of islet cells. Acta Endocrinol Suppl (Copenh). 1976;205:145–60.

106. Marrif HI, Al-Sunousi SI. Pancreatic β cell mass death. Frontiers in pharmacology. 2016;7.

107. Valamehr B, Jonas SJ, Polleux J, Qiao R, Guo S, Gschweng EH, *et al.* Hydrophobic surfaces for enhanced differentiation of embryonic stem cell-derived embryoid bodies. Proc Natl Acad Sci. 2008 Sep 23;105(38):14459–64.

108. Halban PA, Powers SL, George KL, Bonner-Weir S. Spontaneous reassociation of dispersed adult rat pancreatic islet cells into aggregates with three-dimensional architecture typical of native islets. Diabetes. 1987 Jul;36(7):783–90.

109 Persaud SJ, Arden C, Bergsten P, Bone AJ, Brown J, Dunmore S, *et al.* Pseudoislets as primary islet replacements for research. Islets. 2010 Jul 1;2(4):236–9.

110. Green AD, Vasu S, McClenaghan NH, Flatt PR. Pseudoislet formation enhances gene expression, insulin secretion and cytoprotective mechanisms of clonal human insulin-secreting 1.1B4 cells. Pflüg Arch - Eur J Physiol. 2015 Oct 1;467(10):2219–28.

111 Carlessi R, Keane KN, Mamotte C, Newsholme P. Nutrient regulation of β-cell function: what do islet cell/animal studies tell us?. European journal of clinical nutrition. 2017 Jul;71(7):890.

112. Arous C, Wehrle-Haller B. Role and impact of the extracellular matrix on integrin-mediated pancreatic β-cell functions. Biol Cell. 2017 Jun;109(6):223–37.

113 Geron E, Boura-Halfon S, Schejter ED, Shilo B-Z. The Edges of Pancreatic Islet β Cells Constitute Adhesive and Signaling Microdomains. Cell Rep. 2015 Jan 13.

114. Gan WJ, Zavortink M, Ludick C, Templin R, Webb R, Webb R, *et al.* Cell polarity defines three distinct domains in pancreatic β-cells. J Cell Sci. 2017 01;130(1):143–51.

115. Meda P. Protein-mediated interactions of pancreatic islet cells. Scientifica. 2013 Jan 8;2013.

116. Heino J. The collagen receptor integrins have distinct ligand recognition and signaling functions. Matrix Biol J Int Soc Matrix Biol. 2000 Aug;19(4):319–23.

117. Lin H-Y, Tsai C-C, Chen L-L, Chiou S-H, Wang Y-J, Hung S-C. Fibronectin and laminin promote differentiation of human mesenchymal stem cells into insulin producing cells through activating Akt and ERK. J Biomed Sci. 2010 Jul 12;17(1):56.

118. Hughes CS, Postovit LM, Lajoie GA. Matrigel: A complex protein mixture required for optimal growth of cell culture. PROTEOMICS. 2010 May 1;10(9):1886–90.

119. Carré A, Lacarrière V. How Substrate Properties Control Cell Adhesion. A Physical–Chemical Approach. J Adhes Sci Technol. 2010 Jan 1;24(5):815–30.

120. Alberts B, Johnson A, Lewis J, Raff M, Roberts K, Walter P. Cell-Cell Adhesion. 2002.

121. Wesslén B, Kober M, Freij-Larsson C, Ljungh Å, Paulsson M. Protein adsorption of poly (ether methane) surfaces modified by amphiphilic and hydrophilic polymers. Biomaterials. 1994 Mar 1;15(4):278-84.

122. Sanchez Dominguez M, Maillard E, Krafft MP, Sigrist S, Belcourt A. Prevention of Adhesion and Promotion of Pseudoislets Formation from a β-Cell Line by Fluorocarbon Emulsions. ChemBioChem. 2006 Aug 4;7(8):1160–3.

123. Amiji M, Park K. Prevention of protein adsorption and platelet adhesion on surfaces by PEO/PPO/PEO triblock copolymers. Biomaterials. 1992 Jan 1;13(10):682–92.

124. Beyer D, Knoll W, Ringsdorf H, Wang J-H, Timmons RB, Sluka P. Reduced protein adsorption on plastics via direct plasma deposition of triethylene glycol monoallyl ether. J Biomed Mater Res. 1997 Aug 1;36(2):181–9.

125. Noh H, Vogler EA. Volumetric interpretation of protein adsorption: competition from mixtures and the Vroman effect. Biomaterials. 2007 Jan;28(3):405–22.

126. Gooch NW, Hlady V. Two surface gradients of polyethylene glycol for a reduction in protein adsorption. Surf Innov. 2015 Sep;3(3):172–80.

127. Mason MN, Mahoney MJ. Inhibition of Gamma-Secretase Activity Promotes Differentiation of Embryonic Pancreatic Precursor Cells into Functional Islet-like Clusters in Poly(Ethylene Glycol) Hydrogel Culture. Tissue Eng Part A. 2010 Aug;16(8):2593–603.

128. Fale PLV, Chan KLA. Preventing damage of germanium optical material in attenuated total reflection-Fourier transform infrared (ATR-FTIR) studies of living cells. Vib Spectrosc. 2017 Jul 1;91:59–67.

129. Beecher JF, Frihart CR. X-ray photoelectron spectroscopy for characterization of wood surfaces in adhesion studies. Wood Adhes 2005 Novemb 2-4 2005 San Diego Calif USA Madison

130. Lynge M, Westen R van der, Postma A, Städler B. Polydopamine—a nature-inspired polymer coating for biomedical science. Nanoscale. 2011;3(12):4916–28.

131. Yuan Y, Lee TR. Contact Angle and Wetting Properties. In: Surface Science Techniques [Internet]. Springer, Berlin, Heidelberg; 2013 [cited 2018 Jan 18]. p. 3–34.

132. Perelaer J, Hendriks CE, Laat AWM de, Schubert US. One-step inkjet printing of conductive silver tracks on polymer substrates. Nanotechnology. 2009;20(16):165303.

133. EL-Mahdy G, Abdel-Reheem M, M.EL-Roudi O, Atta A, Issa Z, Al-Lohedan H. Assessment of Salt and Acid Droplets Evaporations on the Corrosion Mechanism of Aluminum. Vol. 10. 2015. 6392 p.

134. Kota AK, Mabry JM, Tuteja A. Superoleophobic surfaces: design criteria and recent studies. Surf Innov. 2013 Jun 1;1(2):71–83.

135. Yang S, Jin X, Liu K, Jiang L. Nanoparticles assembly-induced special wettability for bio-inspired materials. Particuology. 2013 Aug 1;11(4):361–70.

136. Celia E, Darmanin T, Taffin de Givenchy E, Amigoni S, Guittard F. Recent advances in designing superhydrophobic surfaces. J Colloid Interface Sci. 2013 Jul 15;402:1–18.

137. Yuan Y, Lee TR. Contact angle and wetting properties. InSurface science techniques 2013 (pp. 3-34). Springer Berlin Heidelberg.

138. Gomes DJC, de Souza NC, Silva JR. Using a monocular optical microscope to assemble a wetting contact angle analyser. Measurement. 2013 Nov 1;46(9):3623–7.

139. Cuijpers VMJI, Walboomers XF, Jansen JA. Scanning electron microscopy stereoimaging for three-dimensional visualization and analysis of cells in tissue-engineered constructs: technical note. Tissue Eng Part C Methods. 2011 Jun;17(6):663–8.

140. Williams DB, Carter CB. The transmission electron microscope. InTransmission electron microscopy 1996 (pp. 3-17). Springer, Boston, MA.

141. Variola F. Atomic force microscopy in biomaterials surface science. Phys Chem Chem Phys. 2015 Jan 21;17(5):2950–9.

142. A Nguyen U, Squaglia N, Boge A, Fung PA. The Simple Western [trade]: a gel-free, blot-free, hands-free Western blotting reinvention. Nature Methods. 2011 Nov 1;8(11)..

143. Barbes L, Radulescu C, Stihi C. ATR - FTIR spectrometry characterisation of polymeric materials. Vol. 66. 2014.

144. Iwanaga K, Yabuta T, Kakemi M, Morimoto K, Tabata Y, Ikada Y. Usefulness of microspheres composed of gelatin with various cross-linking density. J Microencapsul. 2003 Dec;20(6):767–76.

145 Nakase H, Okazaki K, Tabata Y, Ozeki M, Watanabe N, Ohana M, Uose S, Uchida K, Nishi T, Mastuura M, Tamaki H. New cytokine delivery system using gelatin microspheres containing interleukin-10 for experimental inflammatory bowel disease. Journal of Pharmacology and Experimental Therapeutics. 2002 Apr 1;301(1):59-65..

146. Ramachandran K, Williams SJ, Huang H-H, Novikova L, Stehno-Bittel L. Engineering islets for improved performance by optimized reaggregation in a micromold. Tissue Eng Part A. 2013 Mar;19(5–6):604–12.

147. Hamaguchi K, Utsunomiya N, Takaki R, Yoshimatsu H, Sakata T. Cellular interaction between mouse pancreatic alpha-cell and beta-cell lines: possible contact-dependent inhibition of insulin secretion. Exp Biol Med Maywood NJ. 2003 Nov;228(10):1227–33.

148. Charnley M, Textor M, Khademhosseini A, Lutolf MP. Integration column: microwell arrays for mammalian cell culture. Integr Biol Quant Biosci Nano Macro. 2009 Dec;1(11–12):625–34.

149. Lee LH, Peerani R, Ungrin M, Joshi C, Kumacheva E, Zandstra P. Micropatterning of human embryonic stem cells dissects the mesoderm and endoderm lineages. Stem Cell Res. 2009 Mar;2(2):155–62.

150. Nguyen D, Sa S, Pegan JD, Rich B, Xiang G, McCloskey KE, *et al.* Tunable shrink-induced honeycomb microwell arrays for uniform embryoid bodies. Lab Chip. 2009 Dec 7;9(23):3338–44.

151. Pipeleers D, Veld PI, Maes E, Van De Winkel M. Glucose-Induced Insulin Release Depends on Functional Cooperation between Islet Cells. Proc Natl Acad Sci U S A. 1982;79(23):7322–5.

152. Guo-Parke H, McCluskey JT, Kelly C, Hamid M, McClenaghan NH, Flatt PR. Configuration of electrofusion-derived human insulin-secreting cell line as

pseudoislets enhances functionality and therapeutic utility. J Endocrinol. 2012 Sep 1;214(3):257–65.

153. Shinohara M, Kimura H, Montagne K, Komori K, Fujii T, Sakai Y. Combination of microwell structures and direct oxygenation enables efficient and size-regulated aggregate formation of an insulin-secreting pancreatic β-cell line. Biotechnol Prog. 2014 Jan 1;30(1):178–87.

154. IIchihara Y, Utoh R, Yamada M, Shimizu T, Uchigata Y. Size effect of engineered islets prepared using microfabricated wells on islet cell function and arrangement. Heliyon. 2016 Jan 6;2(6):e00129.

155. Vazquez-Zapien GJ, Mata-Miranda MM, Sanchez-Monroy V, Delgado-Macuil RJ, Perez-Ishiwara DG, Rojas-Lopez M. FTIR spectroscopic and molecular analysis during differentiation of pluripotent stem cells to pancreatic cells. Stem cells international. 2016 Aug 29;2016

156. León-Bermúdez A-Y, Salazar R. Synthesis and characterization of the polystyrene - asphaltene graft copolymer by ft-ir spectroscopy. Ctf - Cienc Tecnol Futuro. 2008 Dec;3(4):157–67.

157. Kaniappan K, Latha S. Certain investigations on the formulation and characterization of polystyrene/poly(methyl methacrylate) blends. Int J ChemTech Res. 2011 Apr 1;3:708–15.

158. Kong J, Yu S. Fourier transform infrared spectroscopic analysis of protein secondary structures. Acta Biochim Biophys Sin. 2007 Aug;39(8):549–59.

159. Pelton JT, McLean LR. Spectroscopic methods for analysis of protein secondary structure. Anal Biochem. 2000 Jan 15;277(2):167–76.

160. Hashim DM, Man YBC, Norakasha R, Shuhaimi M, Salmah Y, Syahariza ZA. Potential use of Fourier transform infrared spectroscopy for differentiation of bovine and porcine gelatins. Food Chem. 2010 Feb;118(3):856–60.

161. Muyonga J, Cole CGB, Duodu G. Fourier transform infrared (FTIR) spectroscopic study of acid soluble collagen and gelatin from skins and bones

of young and adult Nile perch (Lates niloticus). Food Chem. 2004 Jul 1;86:325–32.

162. Sun Y, Liu H, Wang X, Kong X, Zhang H. Optical Spectroscopy and Visible Upconversion Studies of YVO4:Er3+ Nanocrystals Synthesized by a Hydrothermal Process. Chem Mater. 2006 May 1;18(11):2726–32.

163. Basak S, Nanda J, Banerjee A. A new aromatic amino acid based organogel for oil spill recovery. J Mater Chem. 2012 May 22;22(23):11658–64.

164. Innocenzi P, Malfatti L, Piccinini M, Marcelli A. Evaporation-Induced Crystallization of Pluronic F127 Studied in Situ by Time-Resolved Infrared Spectroscopy. J Phys Chem A. 2009 Dec 1;114:304–8.

165. Guo null, Liu null, Wang null, Chen null. Conformational Structure of Triblock Copolymers by FT-Raman and FTIR Spectroscopy. J Colloid Interface Sci. 1999 Jan 15;209(2):368–73.

166. Stolnik S, Daudali B, Arien A, Whetstone J, Heald CR, Garnett MC, *et al.* The effect of surface coverage and conformation of poly(ethylene oxide) (PEO) chains of poloxamer 407 on the biological fate of model colloidal drug carriers. Biochim Biophys Acta BBA - Biomembr. 2001 Oct 1;1514(2):261–79.

167. Abelson JN, Simon MI, Wetzel R. Amyloid, prions, and other protein aggregates. Academic Press; 1999 Sep 22.

168 Berthold A, Cremer K, Kreuter JS. Preparation and characterization of chitosan microspheres as drug carrier for prednisolone sodium phosphate as model for anti-inflammatory drugs. Journal of Controlled Release. 1996 Mar 1;39(1):17-25.

169. Ogata T, Park KY, Seno M, Kojima I. Reversal of streptozotocin-induced hyperglycemia by transplantation of pseudoislets consisting of beta cells derived from ductal cells. Endocr J. 2004 Jun;51(3):381–6.

170. Roderigo-Milne H, Hauge-Evans AC, Persaud SJ, Jones PM. Differential expression of insulin genes 1 and 2 in MIN6 cells and pseudoislets. Biochem Biophys Res Commun. 2002 Aug 23;296(3):589–95.

171. Lock LT, Laychock SG, Tzanakakis ES. Pseudoislets in stirred-suspension culture exhibit enhanced cell survival, propagation and insulin secretion. J Biotechnol. 2011 Feb 10;151(3):278–86.

172. Hayes PA, Vahur S, Leito I. ATR-FTIR spectroscopy and quantitative multivariate analysis of paints and coating materials. Spectrochim Acta A Mol Biomol Spectrosc. 2014 Dec 10;133:207–13.

173. Sarkar B, Venugopal V, Tsianou M, Alexandridis P. Adsorption of Pluronic block copolymers on silica nanoparticles. Colloids Surf Physicochem Eng Asp. 2013 Apr 5;422:155–64.

174. Guruvenket S, Rao GM, Komath M, Raichur AM. Plasma surface modification of polystyrene and polyethylene. Appl Surf Sci. 2004 Sep 15;236(1):278–84.

175. Liou Y-B, Tsay R-Y. Adsorption of PEO–PPO–PEO triblock copolymers on a gold surface. J Taiwan Inst Chem Eng. 2011 May 1;42(3):533–40.

176 Burns NL, Holmberg K, Brink C. Influence of Surface Charge on Protein Adsorption at an Amphoteric Surface: Effects of Varying Acid to Base Ratio. J Colloid Interface Sci. 1996 Mar 1;178(1):116–22.

177. VandeVondele S, Vörös J, Hubbell JA. RGD-grafted poly-L-lysine-graft-(polyethylene glycol) copolymers block non-specific protein adsorption while promoting cell adhesion. Biotechnol Bioeng. 2003 Jun 30;82(7):784–90.

178. Rabe M, Verdes D, Seeger S. Understanding protein adsorption phenomena at solid surfaces. Adv Colloid Interface Sci. 2011 Feb 17;162(1):87–106.

179. Dewez J-L, Schneider Y-J, Rouxhet PG. Coupled influence of substratum hydrophilicity and surfactant on epithelial cell adhesion. J Biomed Mater Res. 1996 Mar 1;30(3):373–83.

180. Wu Z, Guo C, Liang S, Zhang H, Wang L, Sun H, *et al.* A pluronic F127 coating strategy to produce stable up-conversion NaYF4 :Yb,Er(Tm) nanoparticles in culture media for bioimaging. J Mater Chem. 2012;22(35):18596–602.

181. Nejadnik MR, van der Mei HC, Norde W, Busscher HJ. Bacterial adhesion and growth on a polymer brush-coating. Biomaterials. 2008 Oct;29(30):4117–21.

182. Van Vlierberghe S, Vanderleyden E, Boterberg V, Dubruel P. gelatin Functionalization of Biomaterial Surfaces: Strategies for Immobilization and Visualization. Polymers. 2011 Jan 5;3(1):114–30.

183. Wesslén B, Kober M, Freij-Larsson C, Ljungh Å, Paulsson M. Protein adsorption of poly(ether urethane) surfaces modified by amphiphilic and hydrophilic polymers. Biomaterials. 1994;15(4):278–84.

184. Neff JA, Caldwell KD, Tresco PA. A novel method for surface modification to promote cell attachment to hydrophobic substrates. J Biomed Mater Res. 1998 Jun 15;40(4):511–9.

185. Karolewicz B, Gajda M, Pluta J, Górniak A. The effect of Pluronic F127 on the physicochemical properties and dissolution profile of lovastatin solid dispersions. J Therm Anal Calorim. 2016 Mar 1;123(3):2283–90.

186. Tatini D, Tempesti P, Ridi F, Fratini E, Bonini M, Baglioni P. Pluronic/gelatin composites for controlled release of actives. Colloids Surf B Biointerfaces. 2015 Nov 1;135:400–7.

187. Tao SL, Popat KC, Norman JJ, Desai TA. Surface Modification of SU-8 for Enhanced Biofunctionality and Nonfouling Properties. Langmuir. 2008 Mar 1;24(6):2631–6.

188. Drelich J, Chibowski E, Meng DD, Terpilowski K. Hydrophilic and superhydrophilic surfaces and materials. Soft Matter. 2011 Oct 18;7(21):9804–28.

189. Schacht E, Nobels M, Vansteenkiste S, Demeester J, Franssen J, Lemahieu A. Some aspects of the crosslinking of gelatin by dextran dialdehydes. Polym Gels Netw. 1993 Jan 1;1(4):213–24.

190. Pérez OE, Wargon V, M.R. Pilosof A. Gelation and structural characteristics of incompatible whey proteins/hydroxypropylmethylcellulose mixtures. Food Hydrocoll. 2006 Oct 1;20(7):966–74.

191. Davis NR, Anwar RA. Mechanism of formation of desmosine and isodesmosine cross-links of elastin. J Am Chem Soc. 1970 Jun 1;92(12):3778–82.

192. Perez RA, Del Valle S, Altankov G, Ginebra M-P. Porous hydroxyapatite and gelatin/hydroxyapatite microspheres obtained by calcium phosphate cement emulsion. J Biomed Mater Res B Appl Biomater. 2011 Apr 1;97B(1):156–66.

193. Kim K-J, Lee S-B, Han N-W. Kinetics of crosslinking reaction of PVA membrane with glutaraldehyde. Korean J Chem Eng. 1994 Jan 1;11(1):41–7.

194. Distantina S, Rochmadi R, Fahrurrozi M, Wiratni W. Preparation and Characterization of Glutaraldehyde-Crosslinked Kappa Carrageenan Hydrogel. Eng J Eng J. 2013 Jan 17;17(3):57–66.

195. Matsuda S, Iwata H, Se N, Ikada Y. Bioadhesion of gelatin films crosslinked with glutaraldehyde. J Biomed Mater Res. 1999 Apr;45(1):20–7.

196. Mntarot ation, Hydrolysis, and Rearrangement Reactions of Glycosylamines [Internet]. [cited 2017 Sep 5]. Available from: http://cyber.sci-hub.cc/MTAuMTAyMS9qbzAxMTAzYTAxOQ==/isbell1958.pdf

197. Esposito E, Cortesi R, Nastruzzi C. gelatin microspheres: influence of preparation parameters and thermal treatment on chemico-physical and biopharmaceutical properties. Biomaterials. 1996 Oct 1;17(20):2009–20.

198. Mori Y, Nagaoka S, Takiuchi H, Kikuchi T, Noguchi N, Tanzawa H, *et al.* A new antithrombogenic material with long polyethyleneoxide chains. Trans - Am Soc Artif Intern Organs. 1982;28:459–63.

199. Lee J, Martic PA, Tan JS. Protein adsorption on pluronic copolymer-coated polystyrene particles. J Colloid Interface Sci. 1989 Aug 1;131(1):252–66.

200. Agrawal CM, Ray RB. Biodegradable polymeric scaffolds for musculoskeletal tissue engineering. J Biomed Mater Res. 2001 May;55(2):141–50.

201. Dmitriev RI, Borisov SM, Kondrashina AV, Pakan JMP, Anilkumar U, Prehn JHM, *et al.* Imaging oxygen in neural cell and tissue models by means of

anionic cell-permeable phosphorescent nanoparticles. Cell Mol Life Sci CMLS. 2015 Jan;72(2):367–81.

202. Wang H, Boerman OC, Sariibrahimoglu K, Li Y, Jansen JA, Leeuwenburgh SCG. Comparison of micro- vs. nanostructured colloidal gelatin gels for sustained delivery of osteogenic proteins: Bone morphogenetic protein-2 and alkaline phosphatase. Biomaterials. 2012 Nov;33(33):8695–703.

203. Del Buffa S, Bonini M, Ridi F, Severi M, Losi P, Volpi S, *et al.* Design and characterization of a composite material based on Sr(II)-loaded clay nanotubes included within a biopolymer matrix. J Colloid Interface Sci. 2015 Jun 15;448:501–7.

204. Reers C, Hauge-Evans AC, Morgan NG, Wilcox A, Persaud SJ, Jones PM. Down-regulation of proliferation does not affect the secretory function of transformed β-cell lines regardless of their anatomical configuration. Islets. 2011 May 1;3(3):80-8.

205. Charpantier E, Cancela J, Meda P. Beta cells preferentially exchange cationic molecules via connexin 36 gap junction channels. Diabetologia. 2007 Nov 1;50(11):2332–41.

206. Yokoyama S, Matsui TS, Deguchi S. Microcontact Peeling as a New Method for Cell Micropatterning. PLOS ONE. 2014 Jul 25;9(7):e102735.

207. ANDRÉS F OL, HÉCTOR C, LUIS E, BETSABE A. Solubilization of p-alkylphenols in Pluronics F-68 and F-127 micelles: Partition coefficients and effect of solute on the aggregate structure. Journal of the Chilean Chemical Society. 2014 Jul;59(2):2451-4.

208. MacGregor RR, Williams SJ, Tong PY, Kover K, Moore WV, Stehno-Bittel L. Small rat islets are superior to large islets in in vitro function and in transplantation outcomes. Am J Physiol - Endocrinol Metab. 2006 May 1;290(5):E771–9.

209. Carmeliet P, Jain RK. Angiogenesis in cancer and other diseases. Nature. 2000 Sep 14;407(6801):249–57.

210. Nezhadi SH, Choong PFM, Lotfipour F, Dass CR. gelatin-based delivery systems for cancer gene therapy. J Drug Target. 2009 Dec;17(10):731–8.

211. Shi M, Kretlow JD, Spicer PP, Tabata Y, Demian N, Wong ME, *et al.* Antibiotic-Releasing Porous Polymethylmethacrylate/gelatin/Antibiotic Constructs for Craniofacial Tissue Engineering. J Control Release Off J Control Release Soc. 2011 May 30;152(1):196–205.

212. Tabata Y, Ikada Y. Protein release from gelatin matrices. Adv Drug Deliv Rev. 1998 May 4;31(3):287–301.

213. Strobel HA, Dikina AD, Levi K, Solorio LD, Alsberg E, Rolle MW. Cellular Self-Assembly with Microsphere Incorporation for Growth Factor Delivery Within Engineered Vascular Tissue Rings. Tissue Eng Part A. 2017 Feb;23(3–4):143–55.

214. Nakase H, Okazaki K, Tabata Y, Chiba T. Biodegradable microspheres targeting mucosal immune-regulating cells: New approach for treatment of inflammatory bowel disease. J Gastroenterol. 2003 Apr 1;38 Suppl 15:59–62.

215. Kawaguchi H. Functional polymer microspheres. Progress in polymer science. 2000 Oct 31;25(8):1171-210.

216. Nezhadi SH, Choong PF, Lotfipour F, Dass CR. gelatin-based delivery systems for cancer gene therapy. Journal of drug targeting. 2009 Dec 1;17(10):731-8.

217. Nakase H, Okazaki K, Tabata Y, Ozeki M, Watanabe N, Ohana M, *et al.* New Cytokine Delivery System Using gelatin Microspheres Containing Interleukin-10 for Experimental Inflammatory Bowel Disease. J Pharmacol Exp Ther. 2002 Apr 1;301(1):59–65.

218. Li M-C, He S-H. IL-10 and its related cytokines for treatment of inflammatory bowel disease. World J Gastroenterol. 2004 Mar 1;10(5):620–5.

219. Mosser DM, Zhang X. Interleukin-10: new perspectives on an old cytokine. Immunol Rev. 2008 Dec;226:205–18.

220. Pfleger C, Meierhoff G, Kolb H, Schloot NC. Association of T-cell reactivity with beta-cell function in recent onset type 1 diabetes patients. J Autoimmun. 2010 Mar;34(2):127–35.

221. Al-Azzawi B. A role for the human mesenchymal stem cell secretome in attenuation of cytokine-induced apoptosis in pancreatic beta cells, PhD thesis, Keele University, 2017).

222. Hunter CA, Ellis-Neyes LA, Slifer T, Kanaly S, Grünig G, Fort M, et al. IL-10 is required to prevent immune hyperactivity during infection with Trypanosoma cruzi. J Immunol Baltim Md 1950. 1997 Apr 1;158(7):3311–6.

223. Parsa R, Andresen P, Gillett A, Mia S, Zhang X-M, Mayans S, et al. Adoptive transfer of immunomodulatory M2 macrophages prevents type 1 diabetes in NOD mice. Diabetes. 2012 Nov;61(11):2881–92.

224. Mukherjee R, Chaturvedi P, Qin H-Y, Singh B. CD4+CD25+regulatory T cells generated in response to insulin B:9–23 peptide prevent adoptive transfer of diabetes by diabetogenic T cells. J Autoimmun. 2003 Nov 1;21(3):221–37.

225. Wang C, Guan Y, Yang J. Cytokines in the Progression of Pancreatic β-Cell Dysfunction. Int J Endocrinol. 2010; 2010:515136.

226. Zha J, Chi X, Yu X, Liu X, Liu D, Zhu J, et al. Interleukin-1β-Targeted Vaccine Improves Glucose Control and β-Cell Function in a Diabetic KK-Ay Mouse Model. PLOS ONE. 2016 May 6;11(5):e0154298.

227. Lopez-Castejon G, Brough D. Understanding the mechanism of IL-1β secretion. Cytokine Growth Factor Rev. 2011 Aug;22(4):189–95.

228. Sekine N, Cirulli V, Regazzi R, Brown LJ, Gine E, Tamarit-Rodriguez J, *et al.* Low lactate dehydrogenase and high mitochondrial glycerol phosphate dehydrogenase in pancreatic beta-cells. Potential role in nutrient sensing. J Biol Chem. 1994 Feb 18;269(7):4895–902.

229. Kojima N, Takeuchi S, Sakai Y. Fabrication of microchannel networks in multicellular spheroids. Sens Actuators B Chem. 2014 Jul 31;198(Supplement C):249–54.

230. Xu Y, Xie F, Qiu T, Xie L, Xing W, Cheng J. Rapid fabrication of a microdevice with concave microwells and its application in embryoid body formation. Biomicrofluidics. 2012 Feb 24;6(1):016504.

231. Breuck S, Baeyens L, Bouwens L. Expression and function of leukaemia inhibitory factor and its receptor in normal and regenerating rat pancreas. Diabetologia. 49(1):108–16.

232. Sandler S, Welsh N. Interleukin-10 Stimulates Rat Pancreatic Islets in Vitro, but Fails to Protect against Interleukin-1. Biochem Biophys Res Commun. 1993 Sep 15;195(2):859–65.

233. Rubartelli A, Cozzolino F, Talio M, Sitia R. A novel secretory pathway for interleukin-1 beta, a protein lacking a signal sequence. EMBO J. 1990 May;9(5):1503–10.

234. Andrei C, Dazzi C, Lotti L, Torrisi MR, Chimini G, Rubartelli A. The secretory route of the leaderless protein interleukin 1beta involves exocytosis of endolysosome-related vesicles. Mol Biol Cell. 1999 May;10(5):1463–75.

235. Wang H, Boerman OC, Sariibrahimoglu K, Li Y, Jansen JA, Leeuwenburgh SCG. Comparison of micro- vs. nanostructured colloidal gelatin gels for sustained delivery of osteogenic proteins: Bone morphogenetic protein-2 and alkaline phosphatase. Biomaterials. 2012 Nov 1;33(33):8695–703.

236. Yokoyama S, Matsui TS, Deguchi S. Microcontact Peeling as a New Method for Cell Micropatterning. PLOS ONE. 2014 Jul 25;9(7):e102735.

237. Wu Z, Jing S, Li Y, Gao Y, Yu S, Li Z, *et al.* The effects of SAHA on radiosensitivity in pancreatic cancer cells by inducing apoptosis and targeting RAD51. Biomed Pharmacother. 2017 May;89:705–10.

238. Persaud SJ, Arden C, Bergsten P, Bone AJ, Brown J, Dunmore S, *et al.* Pseudoislets as primary islet replacements for research: Report on a

symposium at King’s College London, London UK. Islets. 2010 Jul;2(4):236–9.

239. Guo S. Insulin Signaling, Resistance, and the Metabolic Syndrome: Insights from Mouse Models to Disease Mechanisms. J Endocrinol. 2014 Feb;220(2):T1–23.

240. Squires PE, Hauge-Evans AC, Persaud SJ, Jones PM. Synchronization of Ca(2+)-signals within insulin-secreting pseudoislets: effects of gap-junctional uncouplers. Cell Calcium. 2000 May;27(5):287–96.

241. Santoro M, Tatara AM, Mikos AG. gelatin carriers for drug and cell delivery in tissue engineering. J Control Release Off J Control Release Soc. 2014 Sep 28;190:210–8.

242. Wojdasiewicz P, Poniatowski ŁA, Szukiewicz D. The role of inflammatory and anti-inflammatory cytokines in the pathogenesis of osteoarthritis. Mediators Inflamm. 2014;2014:561459.

Appendix

Figure 1 The morphology of the BRIN-BD11 cells grown on treated TCP under static culture

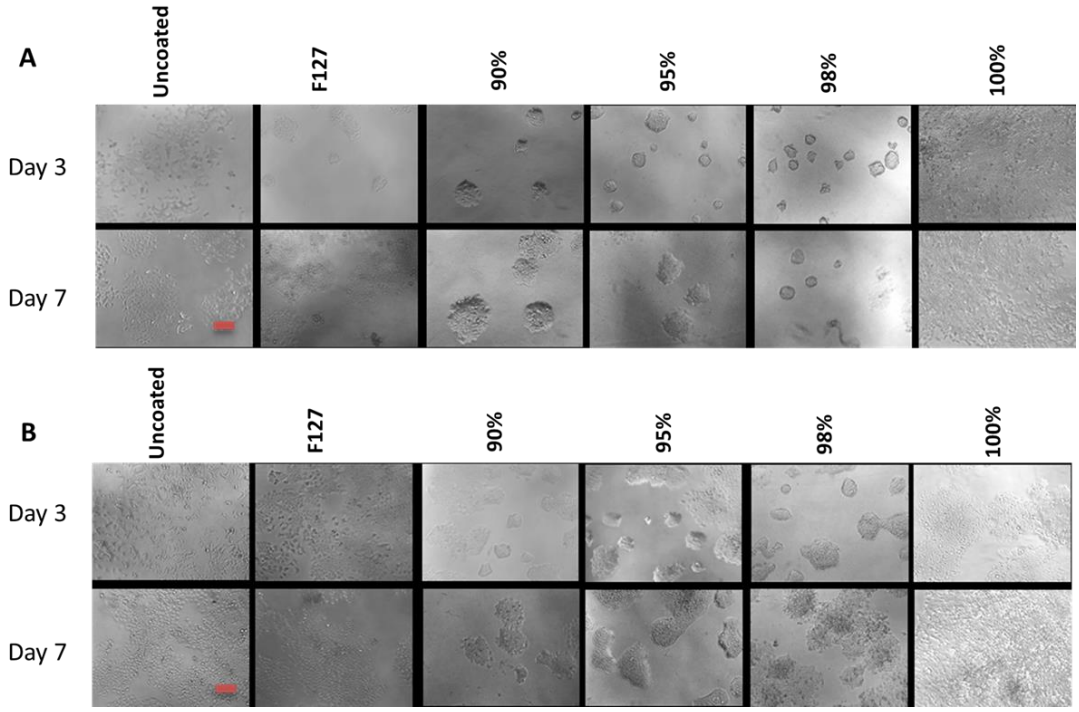

BRIN-BD11 were seeded at cell density 8,000 cell/well (A) and 32,000 cells/well (B) at day 3 and day 7. Cultivation of BRIN-BD11 formed anchor monolayer cells on the TCP, uncoated, coated with 100% gelatin, and F127 formed 2D cell sheets. Growing on TCP coating with mixture of F127-and gelatin solution formed aggregates anchored to the surface. The investigations of cell morphologies were assessed by light microscopy using a x10 objective. Scale bar 200 µm.

Figure 2 **The morphology of BRIN-BD11 cells grown on treated TCP under agitation state**

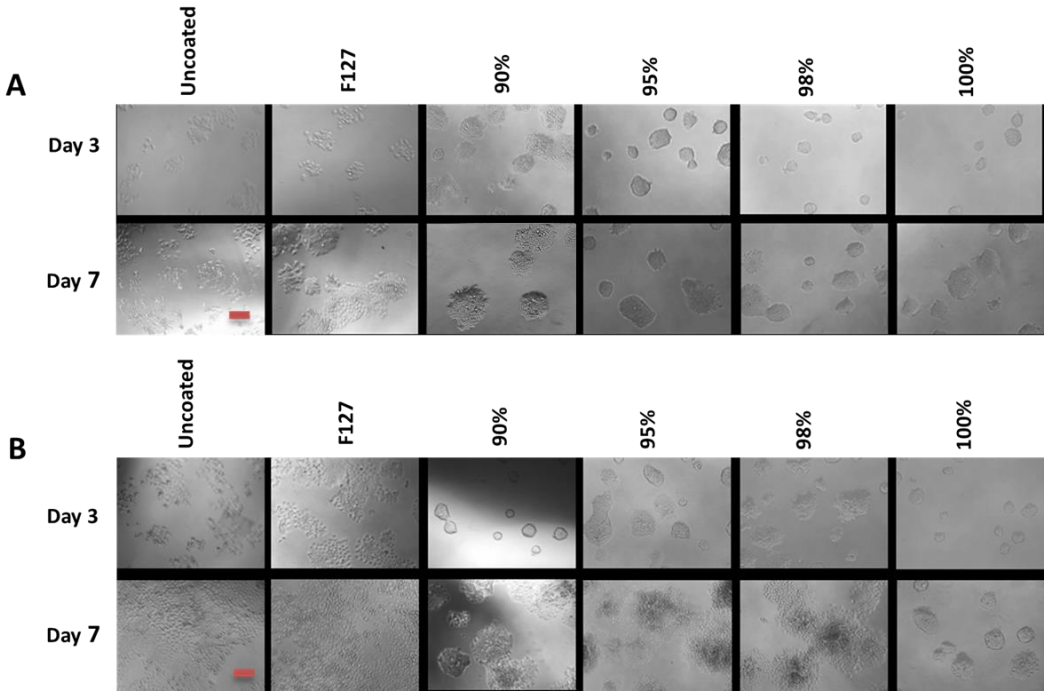

BRIN-BD11 were seeded at cell density 8,000 cell/well (A) and cell density 32,000 cells/well (B) at day 3 and day 7 using plate Shaker at 30 rotators/minute. Cultivation of BRIN-BD11 formed anchor monolayer cells (2D) on the TCP coated with F127. Growing on 100%-gelatin coating and mixture of F127-and gelatin coating TCP formed aggregates anchored to the surface. The investigations of cell morphologies were assessed by light microscopy using a x10 objective. Scale bar 200 µm

Figure 3 The morphology of BRIN-BD11 cells grown on treated SOP under static culture

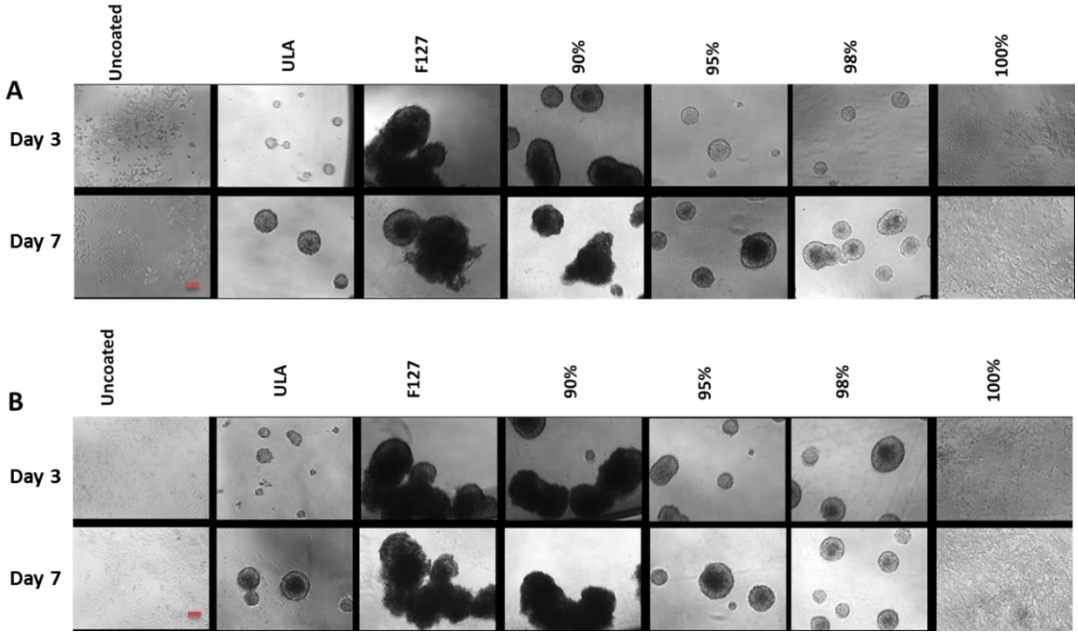

BRIN-BD11 cells were seeded at 8,000 cells/well **(A)** and 32,000 cells/well **(B)** at day 3 and day 7. Cultivation of BRIN-BD11 on suspension plate coated with different coating types which formed different PI morphologies under static culture. The PIs were assessed using light microscopy (x10 magnification) over 7 days using a x10 objective. Scale bar 200 µm

Figure 4 The morphology of BRIN_BD11 cells grown on treated SOP under agitation culture

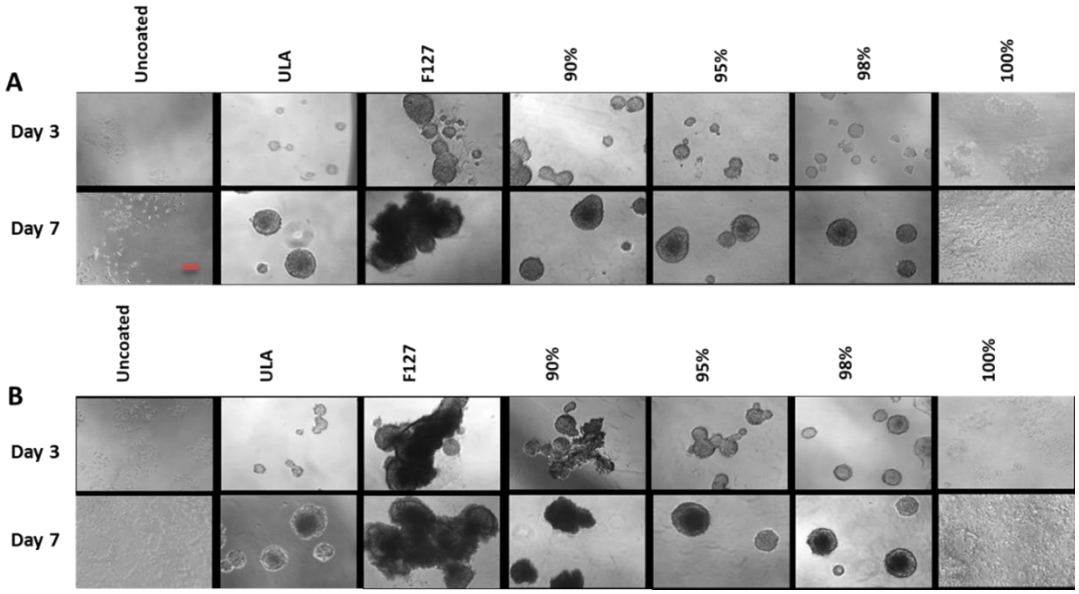

BRIN-BD11 cells were seeded at 8,000 cells/well **(A)** and 32,000 cells/well **(B)** at day 3 and day 7. Cultivation of BRIN-BD11 on SOP coated with different coating solution which formed different PI morphologies under agitation culture. The PIs were assessed using light microscopy (x10 magnification) over 7 days using a x10 objective. Scale bar 200 µm